The influence of beneficiation on the petrographic, geochemical & physical properties of metallurgical coal from the Soutpansberg Coalfield, South Africa

by

Mandy-Jane Tlou Sebola

A thesis submitted, in fulfilment of the requirements for the degree of Doctor of Philosophy in Geology in the Faculty of Science, University of the Witwatersrand, Johannesburg.

Supervisor: Professor Gillian R. Drennan, University of the Witwatersrand

Co-supervisor: Professor Nicola J. Wagner, University of Johannesburg

13 March 2023

Declaration

I declare that this dissertation is my own, unaided work. It is being submitted for the Degree of Doctor of Philosophy in the School of Geosciences, University of the Witwatersrand, Johannesburg. It has not been submitted before for any degree or examination at any other University.

_____

Mandy-Jane Tlou Sebola

_____13_____ Day of _____March_____ 2023

Abstract

The Soutpansberg Coalfield hosts South Africa's Hard Coking Coal (HCC) reserves, however it is relatively understudied and underdeveloped compared to other coalfields in the country. The Makhado Project, located within the central Tshipise sub-basin of the Soutpansberg Coalfield, is the current focus for the re-establishment of Hard Coking Coal production in South Africa by MC Mining Limited.

This study investigated the properties of a 10% ash metallurgical coal product derived from the beneficiation of a wide diameter drill core (LD57) from the Soutpansberg Coalfield, South Africa. The research was conducted in two parts. Part one of the research entailed testing of LD57 by means of drop shatter, dry tumble and wet tumble tests to estimate the breakage expected during the transportation, handling and processing of the coals. Float-sink testing was conducted to determine suitable washability conditions for the production of a primary metallurgical product of 10% ash content. The fine size fraction (1+0.25 mm) floats yielded the desired 10% ash metallurgical product hence, the fine size fraction floats were selected for further characterisation in terms of their petrographic and geochemical properties in Part two of the research. These fine-sized float samples were analysed for their petrographic composition, coal quality (proximate analyses and total sulphur), mineralogy (X-Ray Diffraction), trace element and rare earth element (REE) composition (X-Ray Fluorescence and Inductively Coupled Plasma Mass Spectrometry), and carbonization (Free Swelling Index) properties.

The breakage tests indicate partitioning of daughter particles will be predominantly into coarse particles, 60% on average. The washability analysis shows clean coal for the desired 10% ash metallurgical product could theoretically be obtained in the 1+0.25 mm size fraction of the Makhado seams, with yields up to 78% at 1.55-1.70 g/cm^3. Simple to moderate separation conditions at ± 0.10 NGM are predicted under these separation parameters.

The fine float samples (metallurgical product) are classified as Medium Rank Bituminous C coals (0.88 %RoV) and are highly vitrinitic in composition (97 vol% mmf). All 1+0.25 mm samples reported FSI values of 9. However, further beneficiation of these samples is necessary for minor reduction of the sulphur content, alkali content and phosphorus content to acceptable industry standards for metallurgical coal. Trace element and REE concentrations in the ashed fine float samples are highly enriched relative to the crustal abundance values. Furthermore, all but samples SU and SMU were found to be a promising source of REE as the total REE concentrations exceeded the 1000 ppm cut-off grade.

Dedication

To my parents, Mokgadi Kate Setjie and Dr Ramagwai Joseph Sebola.

Thank you for consistently being my biggest cheer leaders, I am forever grateful for you.

Acknowledgements

First and foremost, I thank my supervisors Professors Gillian Drennan and Nicola Wagner for nurturing me and seeing me through my academic development from undergrad through to post graduate level. I thank both of you for always motivating and pushing me, especially in what has been a very challenging period due to restrictions meant to manage the Covid-19 pandemic. Thank you for always leading by example and for always providing valuable input. Not many students are fortunate to be supervised by both great minds and compassionate supervisors.

The Council for Geoscience is acknowledged for providing financial support during the course of my PhD. The Phillip Vallentine Tobias Scholarship at the University of the Witwatersrand is also acknowledged for financial support during the study.

MC Mining is acknowledged for providing the coal studied in this research, as well as for providing the extensive data sets to support the study. I am especially thankful to John Sparrow whose enthusiasm and generosity made this research endeavour possible. Thank you for sharing your insights into the Soutpansberg Coalfield and enabling academic research into these coals. The coalfield will no longer be “forgotten”, thanks to your contribution. I thank Nthabiseng Masunyane for always taking me under her wing and guiding me during fieldwork.

Xavier Prevost (XMP consulting) and Walter Anderson (Hislop Anderson Commodities) are thanked for providing some reference material for South African metallurgical coals which is very difficult to come by.

I thank my fellow colleagues from the Coal Research Group for the invigorating biweekly coal meetings. I am thankful for all the friendships that have sustained me throughout this journey, especially during my “peak hermit seasons”. Eiríkur, takk fyrir þinn endalausa stuðning hvað varðar nám mitt og drauma, ég elska þig svo mikið!

Praise be to אל ראי.

Contents

List of Figures

List of Tables

Abbreviations and acronyms

CoAL	Coal of Africa Limited
CREE	Critical rare earth elements
CRI	Coke Reactivity Index
CRM	Certified Reference Materials
CRM	Critical Raw Materials
CSN	Crucible swelling number
CSR	Coke Strength After Reaction
DMRE	Department of Mineral Resources and Energy
DMS	Dense medium separation
FGX	Fuhe Ganfa Xuan mei
FSI	Free swelling index
HCC	Hard coking coal
HMS	Heavy medium separation
HREE	Heavy rare earth elements
ICCP	International Committee for Coal and Organic Petrology
ICP-MS	Inductively Coupled Plasma Mass Spectrometry
IEA	International Energy Agency
LREE	Light rare earth elements
MCM/MC Mining	Metallurgical Coal Mining Limited
MKB	Main Karoo Basin
MREE	Medium rare earth elements
MREY	Medium rare earth elements including yttrium
Mtpa	Million tonnes per annum
NDM	Near-density material
NGM	Near-gravity material
PCI	Pulverized coal for injection
RC	Reflux classifiers
REE	Rare earth elements
REY	Rare earth elements including yttrium
REY+Sc	Rare earth elements including yttrium and scandium
SACS	South African Committee for Stratigraphy
SHCC	Semi-hard coking coal

SIP1	Strategic Integrated Projects
SSCC	Semi-soft coking coal
TBS	Teetered bed separators
XRD	X-Ray Diffraction
XRF	X-Ray Fluorescence
XRT	X-ray transmission

Sample nomenclature

LD57	Large diameter drill core W649LD57
LD58	Large diameter drill core W649LD58
LD88	Large diameter drill core T648LD88
LD89	Large diameter drill core T648LD89
SU	Seam Upper
SMU	Seam Middle Upper
P2	Parting 2
SML	Seam Middle Lower
P3	Parting 3
SBU	Seam Bottom Upper
SBM	Seam Bottom Middle
SBL	Seam Bottom Lower

Chapter 1: Introduction

1.1. Premise for the study

The Republic of South Africa is endowed with vast coal reserves most of which have been mined commercially from the Main Karoo Basin (MKB) since 1857. As a result, the properties of these coals have been extensively studied to optimise their extraction and use. Almost all the coal mined in South Africa is of thermal quality and is primarily (77%) used to generate electricity (Minerals Council, 2018). In contrast, approximately 1% of coal mined in South Africa is of coking/metallurgical quality (Peatfield, 2003; Prévost, 2013; IEA, 2017). Metallurgical coal is mined locally from a few mines: the Grootegeluk Coal Mine (≈ 2.5 Mtpa) in the Waterberg Coalfield. Metallurgical coal is mined locally from a few mines: the Grootegeluk Coal Mine (≈ 2.5 Mtpa) in the Waterberg Coalfield; and to a far smaller extent from selected seams in the MKB: Witbank, Ermelo, Klip River, Vryheid and Utrecht coalfields, as well as the Nongoma (artisanal), Somkhele and Kangwane coalfields (Figure 1.1).

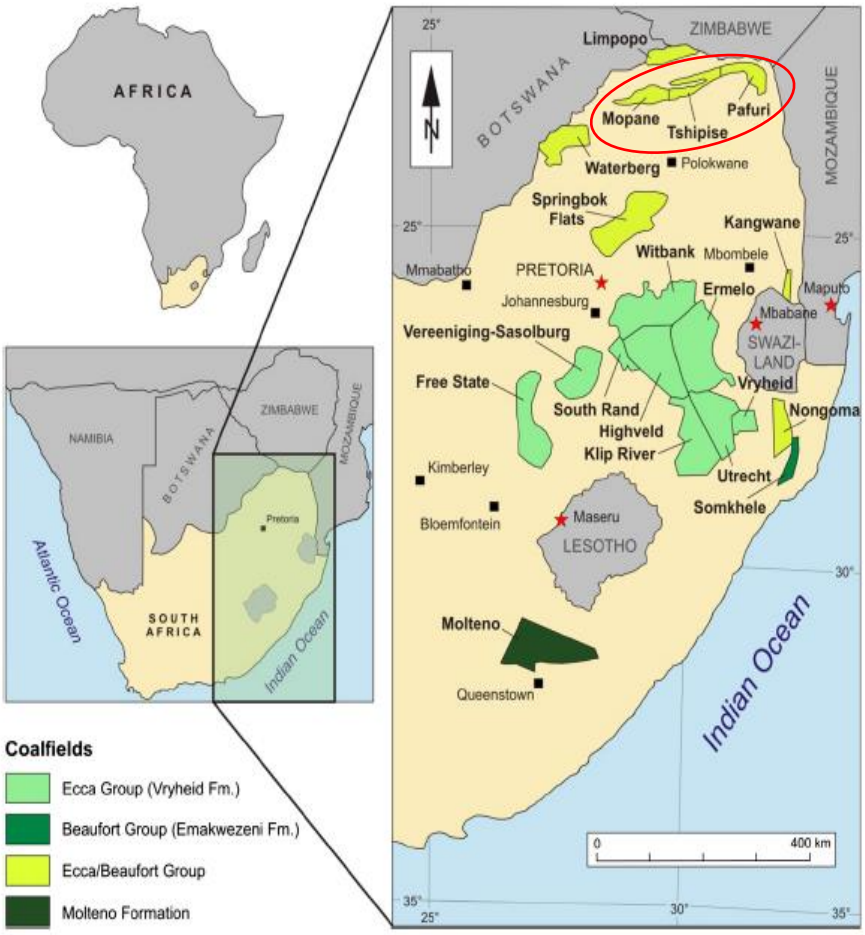

Figure 1.1. Distribution of South African coalfields (Hancox and Götz, 2014). The Mopane, Tshipise and Pafuri sub-basins constitute the Soutpansberg Coalfield.

Metallurgical coal is defined as “coal that, when heated in the absence of air, will melt, vesiculate and harden into a spongelike mass of almost pure carbon, referred to as coke” (Suárez-Ruiz and Crelling, 2008, p. 174). Several categories of metallurgical coal exist, namely: hard coking coal (HCC), semi-hard coking coal (SHCC), semi-soft coking coal (SSCC) and pulverized coal for injection (PCI) (BHP, 2021). Metallurgical coal is a key component in the conversion of metallic ores into steel and ferroalloys whereby the coke releases carbon monoxide and heat when heated in the furnace, allowing the iron to melt while the impurities are removed through flux minerals such as limestone (Suárez-Ruiz and Crelling, 2008).

According to the International Energy Agency (IEA), the global consumption of metallurgical coal in 2020 declined by 3% due to setbacks related to the Covid-19 pandemic. It is estimated that the global consumption of metallurgical coal in 2021 recovered marginally by 0.5%, i.e., from 1101 Mt to 1106 Mt (IEA, 2021). However, high energy prices and slow economic growth resulted in a 2.7% decline in the consumption of metallurgical coal in 2022 (IEA, 2022).

Despite the negative perceptions of coal use associated with climate change, investment into metallurgical coal projects is on the rise (IEA, 2020). South Africa is amongst several countries which have received major investment for export-oriented coal mining. It is estimated that approximately 2 Mtpa of metallurgical coal will be exported from new mining projects, whilst an additional 2 Mtpa will be produced from a combination of thermal and metallurgical coal projects. Metallurgical Coal Mining`s (MCM or MC Mining) Makhado project is counted amongst these major investments.

MC Mining, formerly Coal of Africa Limited (CoAL), is a South African and Australian based mining company that develops and mines coking and thermal coal assets (MC Mining, 2018). The Makhado Project is situated in the Tshipise sub-basin within the Soutpansberg Coalfield, where significant deposits of metallurgical coal were discovered in the 19th century (Sparrow, 2012; Mdungazi, 2019). In 1984, extensive exploration projects were primarily initiated by ISCOR (now ArcelorMittal South Africa), culminating in the development of the Tshikondeni Mine in the eastern sector of the coalfield (Pafuri sub-basin). Despite renewed exploration work by RioTinto and Kwezi in 2002, and later by MC Mining, the Soutpansberg Coalfield has been dubbed as the “forgotten basin” due to its resources remaining largely untapped. The Tshikondeni Mine ceased operations in October 2014 (Sparrow, 2012: Exxaro, 2019). Consequently, the scarcity of metallurgical coal production in South Africa has led to annual imports worth 4-billion Rand to supplement the demand in the South African iron and steel industry (Minerals Council, 2018).

MC Mining aims to meet the demand for HCC through the development of its Makhado Project situated in the Tshipise sub-basin. The project will make MC Mining, “the only significant

producer of prime HCC in South Africa" as stated by MC Mining (2018). The coals in this region have proven HCC properties (Sparrow, 2012; MC Mining, 2021). Phase 1 of the Makhado Project is expected to produce 540000 tonnes of HCC production, as well as 570 000 tonnes of thermal coal by-product over a 9-year life of mine commencing in 2022 (MC Mining, 2021). As part of Phase 1 Development at the Makhado Project, four large diameter boreholes were drilled in late November-December 2018 for the purpose of conducting coal strength tests and beneficiation tests. The primary aim of these tests was to estimate the particle size distribution and optimal size and density parameters required to produce a primary 10% ash metallurgical product. .

The Makhado/Musina region has been identified as a special economic zone under the Strategic Integrated Projects (SIP1) in South Africa, which is focused on unlocking the minerals and metals belt in the Limpopo Province (CoAL, 2016; GOVZA, 2017; Mdungazi, 2019). Therefore, the development of the Makhado Project will play a vital role in alleviating the high demand for coking coal in South Africa and could inject revenue into the economy through increased local sales and international exports. In addition, local communities within the Makhado region stand to benefit from employment and educational opportunities (CoAL, 2016).

1.2. Research Aims and Objectives

Considering the limited research detailing the properties of the vitrinite-rich coal horizons in the Soutpansberg Coalfield, and in alignment with MC Mining's objectives, the aim of this research was to assess the properties of a 10% ash metallurgical coal product derived from the beneficiation of a wide diameter drill core. It was found that the fine float fraction (-1+0.25 mm) yielded the 10% ash metallurgical coal product hence, the -1+0.25 mm size fraction was further analysed for its petrographic and geochemical properties. A large diameter borehole obtained during the Phase 1 Development of the Makhado Project in 2018 was used to determine the beneficiation properties of the No. 6 seam. The key objectives of the study were achieved in two parts:

Part 1 objectives: The influence of coal properties on the breakage and washability characteristics of metallurgical coal

1. Study the friability and resultant breakage of samples from a large diameter drill core through drop shatter and tumbling tests. The results provided information regarding physical changes during transportation, handling and processing of the coal.
2. Determine the washability characteristics of the coal horizons in terms of their ash, total sulphur, particle size and density; Assess the effectiveness of gravity-based separation in achieving a primary metallurgical product of 10% ash content.

3. Evaluate the degree of difficulty in beneficiating the coal horizons using the near gravity material (NGM) parameter.

Part 2 objectives: Assessment of the petrographic and geochemical properties of the fine size float fraction

4. Characterise the 10% ash metallurgical coal product (-1+0.25 mm) by conducting detailed coal petrography and geochemistry. The geochemical characterisation led to an interest into the investigation of Makhado coals as a potential secondary source of rare earth elements, a research interest which has not been previously studied.

1.3. Thesis outline

The scope of work covered in this thesis is outlined as follows:

Chapter 1: Introduces the background, aims and objectives of the research.

Chapter 2: The literature review sets the context for South African metallurgical coal deposits and mining activity. Fundamental quality attributes of metallurgical coals are discussed in terms of their impact on beneficiation and technological use both locally and internationally.

Chapter 3: An overview of the regional geology of the Soutpansberg Coalfield and sub-basins are presented.

Chapter 4: The methods employed in the study are presented in two parts. The first part of the research entailed sampling of large diameter drill cores from the Makhado Project which were logged before being sent for friability and strength testing in terms of Drop shatter, dry tumbling and wet tumbling. This was followed by float-sink testing to determine the washability of the coal horizons. The washability results are presented in two parts (Chapters 6 and 7) due to the large dataset. The methods covered in part one of the research address the influence of physical properties of metallurgical coal on beneficiation. Methods conducted for the second part of the research entailed characterisation of the 10% ash metallurgical coal product (-1+0.25 mm) obtained from the float-sink testing in terms of their petrographic and geochemical properties post beneficiation.

Chapter 5: The drop shatter and tumbling results highlighting the breakage characteristics under dry and wet processing. This chapter forms part one of the research.

Chapter 6: Results and discussion on the gravity-based separation in order to identify optimal float yields and ash content, the ease of separation/washing. This chapter forms part one of the research.

Chapter 7: Results and discussion on the coal quality of the float fraction in terms of moisture, volatile matter and total sulphur content. This chapter forms part one of the research.

Chapter 8: Petrographic characterisation of the selected density fractions for 10% ash metallurgical coal product (-1+0.25 mm). This chapter forms part two of the research.

Chapter 9: Geochemical characterisation of selected density fractions for 10% ash metallurgical coal product (-1+0.25 mm). This chapter forms part two of the research.

Chapter 10: The major findings from each results chapter are discussed to address the objectives of the study. Recommendations to support further research are provided.

1.4. Publications

The data and findings from part two of this research (Chapter 8 and 9) were used to draft the manuscript titled, 'Petrographic and geochemical characteristics of beneficiated metallurgical coal from the No. 6 Seam, Tshipise Sub-basin, Soutpansberg Coalfield, South Africa'. The manuscript has been published in the 8th edition of The Southern African Institute of Mining and Metallurgy (SAIMM) Journal:

Sebola, M. J. T., Drennan, G. R., Wagner, N. J. (2022). Petrographic and geochemical characteristics of beneficiated metallurgical coal from the No. 6 Seam, Tshipise sub-basin, Soutpansberg coalfield, South Africa. Journal of the Southern African Institute of Mining and Metallurgy, 122, 461-472. DOI ID: http://dx.doi.org/10.17159/2411-9717/2061/2022

Chapter 2: Literature review

2.1. Introduction

The literature review provides background into the occurrence of metallurgical coal deposits in South Africa and their importance to the local and international mining value chain. Context into the Makhado Project is provided in terms of its pivotal role in the production of HCC for South Africa's steel industry. Factors pertaining to metallurgical coal and coke quality are discussed, as well as their impact on beneficiation and carbonization. Furthermore, research into South African coals as alternative sources for the extraction of rare earth elements is discussed.

2.2. Metallurgical coal deposits and production in South Africa

According to the Minerals Council (2018; 2021), coal mining in South Africa plays three pivotal roles (Minerals Council, 2018; 2021). Firstly, 77% of the country's energy requirements are met through coal-fired electricity. Secondly, the coal sector is ranked third in terms of providing employment, accounting for 92 230 jobs in 2019 (Minerals Council, 2021). Lastly, coal mining earned R27.9 billion in 2019, a major contribution towards economic growth. Consequently, coal is regarded as a strategic or critical mineral resource in South Africa (PWC, 2017; Dikgwatlhe, 2018).

Coal deposits of metallurgical quality are scarce in South Africa (Jeffrey, 2005a). The bulk of the coal deposits (≥90%) are of thermal quality, particularly in the MKB (Eberhard, 2011; Prévost, 2013). Here the coals are predominantly enriched with inertinite macerals, with lower proportions of vitrinite and liptinite. Anthracite in the MKB mostly occur in the KwaZulu-Natal coalfields (Utrecht, Klip River, Vryheid, Nongoma and Somkhele), as a result of regional metamorphism by post Karoo dolerite dike and sill intrusions (Barker, 1999). Mining of these resources was previously monopolized by ISCOR (ArcelorMittal) for the local metallurgical industry until the Grootegeluk Mine (1976) and Tshikondeni Mine were established to supply more coking coal (Barker, 1999). North of the MKB, major metallurgical coal deposits occur in the Waterberg, Soutpansberg and Tuli coalfields (Snyman, 1989; Hancox and Götz, 2014). Table 2.1. summarizes the localities of metallurgical coal seams that are currently exploited in South Africa, including those which have been historically mined. It is expected that the northern coalfields (Waterberg, Limpopo/Tuli and Soutpansberg coalfields) will become the hub of coal mining from 2033 as exploitable resources dwindle in the MKB (Prévost, 2017). This provides further opportunity to unlock metallurgical reserves, as well as more thermal coal reserves in the northern coalfield. Hence, an understanding of the coal and processing characteristics of these coals is vital (Jeffery, 2005b; Hancox and Götz, 2014; Prévost, 2017).

Some anthracite coal is mined from the KwaZulu-Natal coalfields as a cheaper alternative to the rare and expensive metallurgical coal (Anderson, 2020). This type of coal is referred to as metallurgical anthracite. The distinction between metallurgical coal/coking coal versus metallurgical anthracite is often used interchangeably in South African literature, making it difficult to differentiate between the two when reporting on these commodities. Furthermore, records of metallurgical coal production in South Africa and southern Africa (Zimbabwe and Mozambique) are difficult to obtain due to the very small production, compounded by company confidentiality (Anderson, 2020). Data provided by the South African Department of Mineral Resources and Energy (DMRE), and Minerals Council only provide a broad overview of coal production by tonnage, and specifications on the different coal products are rarely made.

Figure 2.1 illustrates the major trade routes for metallurgical coal, highlighting Australia as the leading exporter (52%), followed by the United States (14%), Canada (10%), Russia (9%) and Mongolia (9%) (IEA, 2020). Although the contribution of African countries to global metallurgical trade is omitted in Figure 2.1 (presumably due to its minor contribution compared to the major metallurgical coal exporters), it is estimated that 11 Mt of metallurgical coal was mined in Africa in 2018 (IEA, 2020). The bulk (~ 6 Mt) of this coal was produced by mining company Vale in the Moatize Basin of Mozambique (IEA, 2019; Vale, 2021). South Africa`s contribution to this figure was approximately 1 Mt (IEA, 2019).

Table 2.1. Coal deposits of metallurgical quality in South Africa summarized from Barker, 1999; Jeffery, 2005a; Wagner and Tlotleng, 2012; Kruger, 2013; Hancox and Götz, 2014; Anderson, 2020.

Coalfield	Seam	Metallurgical coal/product quality
Witbank	No.1 Seam	Low phosphorus metallurgical coal
	No. 2 Seam-basal 3 zones	Low ash metallurgical coal
	No. 5 Seam	Metallurgical coal of domestic, export & ferro-manganese industry quality
Ermelo	No metallurgical coal documented	
Highveld	No. 4 and 5 Seam	Metallurgical quality pending beneficiation at Kriel and Matla collieries
Klip River	Bottom Seam from the Indumeni, Northfield & Durban Navigation collieries	Good coking coal: Free swelling index > 6.5 & Roga > 60
Utrecht	The Coking, Alfred & Gus seams	Coking coal for ArcelorMittal in Newcastle is currently reclaimed from discard piles as mines are closed
Nongoma	M Seam	Metallurgical anthracite: low phosphorus content. 71-77% yield for a 10% ash, 6% volatile matter, 82–83% fixed carbon product
Somkhele	Seams B1, B2 and B3	Metallurgical anthracite: low sulphur & low phosphorus for the domestic ferroalloy & the export market
Vryheid	Alfred & Gus seams	Metallurgical anthracite for domestic market & secondary product for iron ore pelletising market in Brazil
Waterberg	Benches 2, 3, 4, 5, 9B &11	Benches 2, 3 & 4 are blended to produce a SSCC of 10% ash after beneficiation. Sold domestically, primarily to ArcelorMittal. Benches 9B &11 are blended to produce a metallurgical product for export
Soutpansberg	Mopane and Tshipise sub-basins: Upper, middle and bottom seams	HCC for ArcelorMittal and export market: Makhado Phase 1 currently underway
	Pafuri: Main seam	HCC previously produced at Tshikondeni: Free swelling index 9, 13.7% ash, 22.9% volatile matter
Limpopo (Tuli)	Bottom, Middle and Top seams	Higher grade coal than MKB containing a valuable percentage of South Africa's coking coal. On care and maintenance since 2013.

The iron and steel industry are the principal driver for the demand of metallurgical coal in South Africa and internationally. In South Africa, it is estimated that 30% of the local coal demand is for metallurgical coal use (Minerals Council, 2018). However, additional metallurgical coal imports to the value of 4 billion Rand per annum are required to supplement the demand (Minerals Council, 2018). The dependency on metallurgical coal imports is to a small degree mitigated by innovative processes such as Corex which allows non-coking coal to be directly used in the manufacture of steel instead of coking coal (Lu *et al*., 2013; Subba Rao and Gouricharan, 2016). Corex has been a supplementary method for many steel manufacturers globally (Cooke, 1994; Kernot, 2000). However, an advantageous solution for reducing the shortage of metallurgical coal in South Africa is through the development of the northern coalfields, which will benefit South Africa by decreasing dependency on metallurgical coal imports and position the country amongst key exporters of metallurgical coal (GOVZA, 2017; Mdungazi, 2019; MC Mining, 2021).

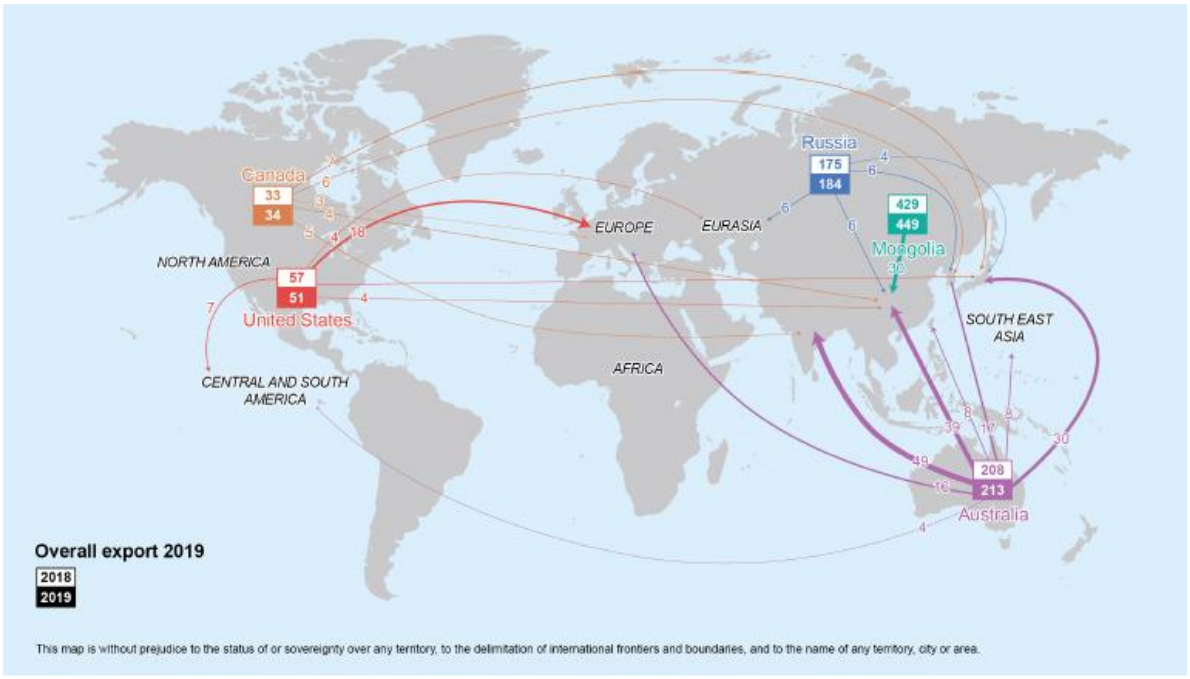

Figure 2.1. Key trade routes for metallurgical coal (Mt) trade in 2019 (IEA, 2020).

ArcelorMittal is the biggest manufacturer of steel and coke products in South Africa and consumes the bulk of both local and imported metallurgical coal. The steel giant produces 4.8 million tonnes of saleable steel products on an annual basis, which contribute to more than 61% of the steel used in South Africa (SAISI, 2013). It is estimated 5.7 million tonnes of crude steel was produced in 2019 (SAISI, 2022). ArcelorMittal operations are set up at Vanderbijlpark and Saldanha, which specialize in the production of flat steel products (SAISI, 2013; ArcelorMittal, 2021). The Newcastle and Vereeniging operations specialize in long steel products. In addition, a bar and rebar mill are operated in Maputo, Mozambique (SAISI, 2013; ArcelorMittal, 2021).

Carbonization, i.e., the conversion of metallurgical coal to commercial grade coke and chemical by-products is a major process conducted by ArcelorMittal (SAISI, 2013; ArcelorMittal, 2021). Two types of commercial grade coke are produced: 1) market coke, which is utilised by the ferroalloy industry; and 2) metallurgical coke for steel plants. Carbonization is conducted across several plants in Pretoria, Newcastle, Vanderbijlpark and Saldanha. The latter plant uses the Corex process to convert iron ore into steel (DOE, 2019). It is estimated that ArcelorMittal produces 226 000 tonnes of commercial grade coke from 332 000 tonnes of metallurgical coal annually (ArcelorMittal, 2021). The process yields 118 000 tonnes/year of coal tar which is further distilled into oil (naphthalene, creosote, carbon black) and pitch products (aluminium smelters, graphite electrodes, specialty carbon products, pavement coatings, refractories) (ArcelorMittal, 2021).

2.3. The impact of Covid-19 on the South African coal industry.

The outbreak of the Covid-19 pandemic and subsequent restriction measures resulted in a severe decline in the global coal demand in 2020, the largest drop since World War II. The decline was exacerbated by existing issues in the coal industry (IEA, 2020). Global metallurgical coal imports and exports declined by 29 Mt and 43 Mt, respectively, primarily due to low steel production (IEA, 2020). However, post pandemic recovery in the global steel industry increased metallurgical coal consumption by 1.3% in 2021 (IEA, 2021). The recovery was short lived due to rising energy prices (driven by the Russian invasion of Ukraine in 2022) and slow economic growth which resulted in a 2.7% decline in the consumption of metallurgical coal in 2022 (IEA, 2022). Overall, the global coal industry is seeing the divestment of thermal coal in favour of metallurgical projects becoming prevalent, as shown by recent acquisitions by mining giants such as BHP and Anglo American (IEA, 2020).

South Africa produced 247 Mt of coal in 2020 compared to 258 Mt in 2019 i.e., a 4.4% decline due to Covid-19 (IEA, 2021). The overall coal consumption in South Africa was lower between 2018 and 2020, primarily due to less expenditure by the construction sector resulting in a low demand for coal by the cement and brick industry (IEA, 2020). Ongoing challenges within the financial and operational management of the country's primary energy generator, Eskom, resulted in intermittent load shedding and therefore less coal consumption. Furthermore, coal trade was constrained by limited railway capacity which continues to limit exports (IEA, 2020; 2022).

Due to Covid-19, South Africa only produced 3.9 Mt of crude steel in 2020 compared to 6.2 Mt in the previous year. However, Post covid recovery yielded 5 Mt of crude steel production in 2021 (World Steel Association, 2021; 2022). A report by Anderson (2020) shows viability for the upgrading of several mines in the KwaZulu-Natal coalfields for the production of anthracite and metallurgical anthracite which will supply both the South African and international metallurgical markets. Despite the pandemic related challenges, MC Mining has reported favourable economic returns for its Makahdo Project during the second quarter of 2021 (MC Mining, 2021).

2.4. The Makhado HCC Project, South Africa

The Makhado Project is the flagship hard coking and thermal coal project belonging to MC Mining which is situated 36 km from the town of Makhado, Limpopo Province (Figure 2.2). It is centrally located within the Soutpansberg Coalfield, i.e. the Tshipise sub-basin. The geology of the region is discussed in Chapter 3.

Previous test work conducted by MC Mining on the Makhado coals and coke products indicate the following coal quality specifications (Sparrow, 2012):

- Free Swelling Index (FSI) values from 7.5 to 9 indicate SHCC to HCC quality
- Hot strength as measured by Coke Reactivity Index (CRI) with CO_2: 19.6
- Hot strength as measured by Coke Strength After Reaction (CSR) with CO_2: >60
- Cold strength as measured by Micum drum index:

  M40- an index of fissuring: 71.3%

  M10- an index of abrasion resistance: 7.5%

The Makhado Project has reported resources of 344.8 Mt mineable tonnes *in situ* and reserves of 188.3 Mt mineable tonnes *in situ* (de Klerk and Sparrow, 2015; Mostert, 2016; MC Mining, 2021). In order to generate capital and supply metallurgical coal to the market, the Makhado Project is expected to operate in two phases. Phase 1 will be carried out in the west pit and is expected to yield 3 Mtpa of run of mine (ROM) coal. MC Mining signed an offtake agreement in 2019 to provide ArcelorMittal with metallurgical coal from Phase 1 (MC Mining, 2019).

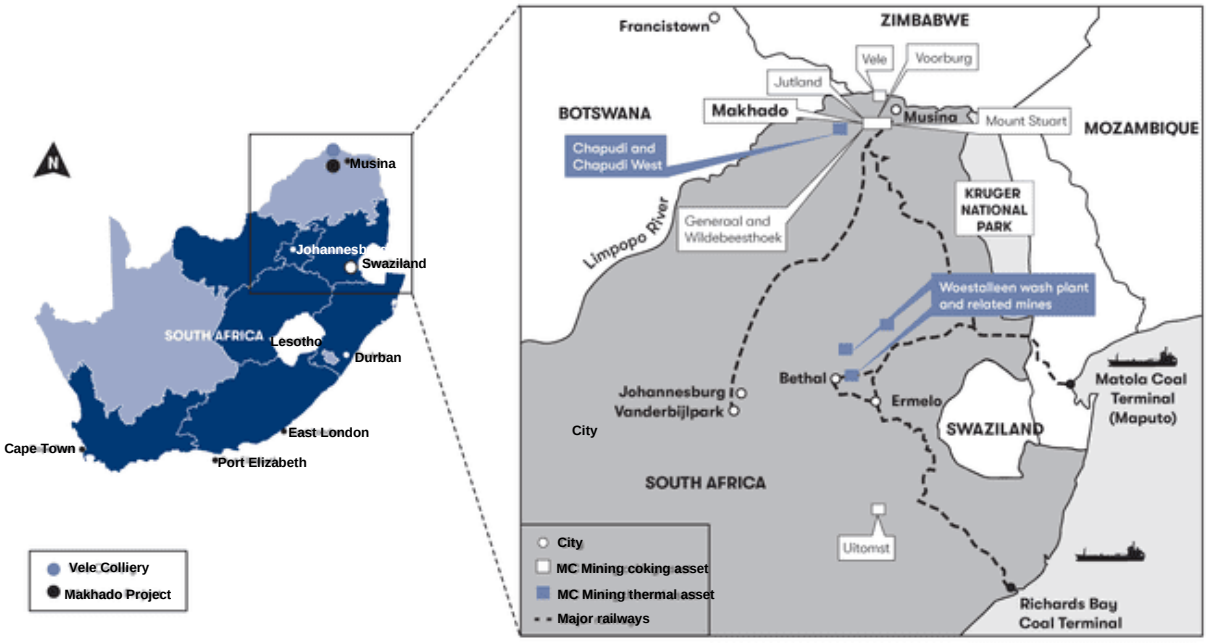

Figure 2.2. Location of the Makhado Project (MC Mining, 2019).

Phase 2 is expected to commence in 2022 and will be carried out in the east and central pits over a 29 year life of mine. Phase 2 is expected to produce ~4 Mtpa of ROM coal, from which ~1.2 Mtpa of saleable hard coking and export quality thermal coal will be processed. A new processing plant will be built onsite at the Makhado Project to process Phase 2 coals (MC Mining, 2019).

The Makhado coals will be mined by open cast method and beneficiation will be initially carried out at Vele Colliery (owned by MC Mining), 80 km northwest of Makhado (Figure 2.2). The Vele processing plant will be modified to process the Makhado Phase 1 coal and will include the incorporation of a new fines circuit comprising of a reflux classifier in series with the existing spiral plant, low density secondary wash plant and a froth flotation plant to capture the ultra-fine coal (MC Mining, 2019; Mostert, 2016). These modifications will allow simultaneous production of HCC and export quality thermal coal.

Metallurgical coal trends in the Soutpansberg Coalfield are generally characterised by a west-east increase in coal rank, coke strength after reaction CSR, and yield. Furthermore, the phosphorus content increases northwards (Sparrow, 2012).

2.5. Metallurgical coal quality

Coal is an organic sedimentary rock that is heterogeneous in composition, comprising predominantly of carbonaceous material and mineral matter in varying proportions (Diessel, 1992). The composition of coal determines the extent to which a desired product can be achieved. The carbonaceous material is preserved as discrete plant remains that are microscopically termed `macerals` (Falcon and Ham, 1988; Teichmüller, 1989). Mineral matter forms the inorganic component of coal and is often intricately bound within the macerals from the onset of peat formation in the coal forming environment (Ward, 2002). The intimate relationship between macerals and mineral matter is problematic from an economic point of view, because it necessitates beneficiation in order to liberate and concentrate the valuable carbonaceous material from the mineral matter (Holuszko and Grieve, 1990; Esterle, 2008). As a consequence, a good understanding of the inherent coal characteristics is vital in order to optimize the extraction, beneficiation and subsequent utilisation of coal within the bounds of sound health and environmental practice.

The desired outcome of metallurgical coal beneficiation is to concentrate macerals that possess caking properties, i.e., macerals that have the ability to fuse when heated in the absence of oxygen (Suárez-Ruiz and Crelling, 2008; Falcon, 2013; Schernikau, 2017; Wagner *et al*., 2018). Medium rank C/B bituminous coals that contain vitrinite showing maximum reflectance ($\%R_{max}$) values between 1.1% and 1.45%, possess caking properties (Lu *et al*., 2013). Vitrinite has good plasticity and swelling properties that allow it to produce excellent coke, whereas inertinite is nearly inert and does not soften on heating in coals of this rank (Wagner *et al*., 2018). Liptinite becomes extremely plastic and tends to produce tar (Falcon and Ham, 1988; Lett and Ruppel, 2004). Metallurgical coals are a calculated balance of reactive macerals (vitrinite and liptinite) versus inert macerals (inertinite) (Jordan, 2008). Despite the broad generalization of inertness attributed to the inertinite maceral group,

selected macerals have been found to be reactive, and therefore contribute towards coking strength in carbonization (Guerrero *et al*., 2013). Inertinites with reactive properties include semi-fusinite, macrinite and inertodetrinite (Kershaw and Taylor, 1992; Maroto-Valer *et al*.,1998; Thomas, 2012). As such, metallurgical coals derived from inertinite-rich coals of the MKB contain high proportions of inertinite macerals compared to coals derived from the Waterberg and Soutpansberg coalfields which are vitrinite-rich (Das, 2001; Wagner *et al*., 2018). Due to the scarcity of high-quality metallurgical coal deposits and the high cost of prime coking coal, various coals are often blended based on their petrographic compositions to produce suitable metallurgical coal products (Ekmann and Le, 2005).

Macerals vary in their physical properties such as density and hardness which allow them to be selectively concentrated during gravity-based beneficiation (Esterle, 2008). Macerals of the liptinite group are the least dense macerals and vary in density between 1.15 and 1.30 g/cm^3 compared to 1.22-1.40 g/cm^3 for vitrinite and, 1.36-1.74 g/cm^3 for inertinite (Crelling 1992 in Roux 2011). The density of the common types of minerals in coal (e.g., clay minerals, carbonates, quartz and sulphides) vary between 2.3 and 5.0 g/cm^3 (Franzidis,1992).

In a simplistic scenario (Figure 2.3) where a vitrinite-rich coal is beneficiated by gravity separation, a high amount of vitrinite will report to the float fraction, while denser inertinite

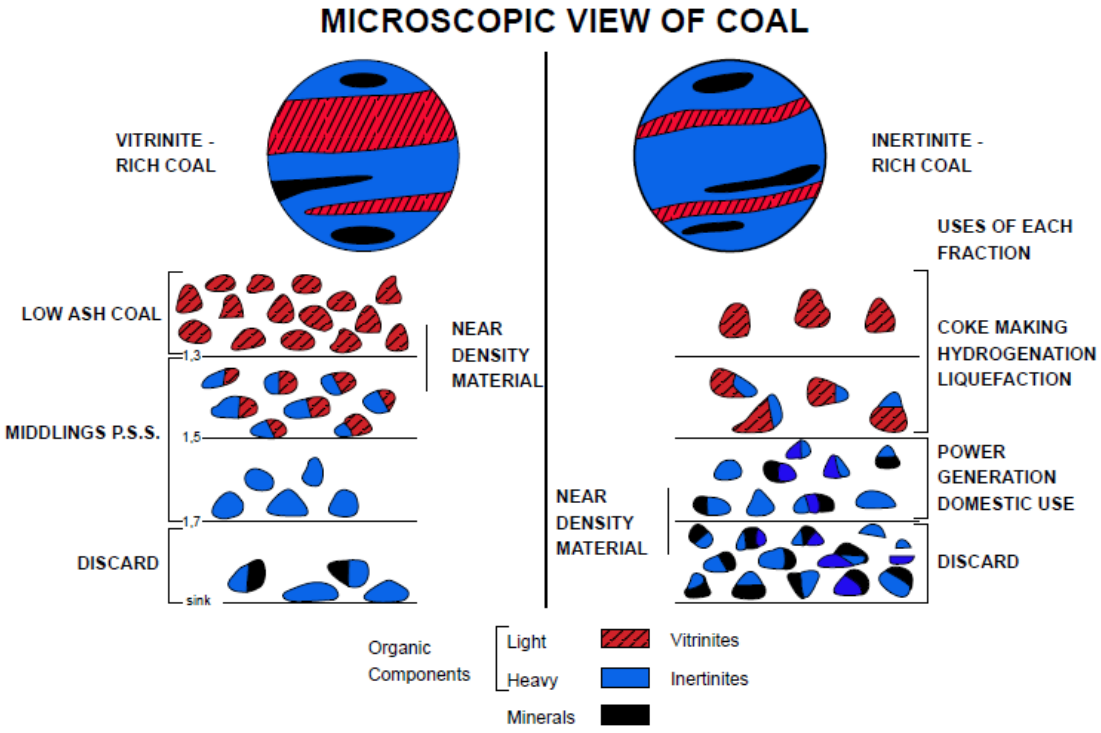

macerals, especially when associated with minerals, report to the middlings or discards.

Figure 2.3. Example of fractionation of macerals from a vitrinite-rich coal relative to an inertinite-rich coal during float-sink (Wagner *et al*., 2018).

Conversely, an inertinite-rich coal will yield higher amounts of middlings and or discards, with a low amount of vitrinite reporting to the low-density float yields. It is important to also consider the effect of intricately bound maceral-mineral matter associations on the achievable yields (King and Birtek, 1990).

The maceral-maceral, and maceral-mineral matter associations in coal are referred to as 'lithotypes' when characterised on a macroscopic scale (e.g., on outcrops or on drill cores during logging), or as 'microlithotypes' when determined using a petrographic microscope (Falcon and Falcon, 1987; Teichmüller, 1989). Microlithoypes are assemblages consisting of one, two or three groups of macerals. Minerals are considered in the assemblage when they occur in proportions < 20% by volume, or < 5% for sulphides (Hower, 2008: Suárez-Ruiz, and Crelling, 2008; Wagner *et al*., 2018). The relationship between lithotypes and microlithotypes are illustrated in Figure 2.4. Lithotypes in humic coals are coal layers that are ≥ 5 mm in thickness and can be differentiated based on lustre, fracture pattern, colour, streak, texture and the type of banding (Figure 2.4; Wagner *et al*., 2018).

Microlithotypes are petrographically characterised across a diameter of 50 µm in the field of view (Wagner *et al*., 2018). Where single maceral groups are identified in the field of view, it is termed a monomaceral. Bimacerals are designated where two maceral groups occur together in proportions > 95%. Three maceral groups occurring together in proportions > 95% are termed trimacerals. The term carbominerite is assigned when 20% (5% for sulphides) of the field of view comprises minerals. Minerite or rock is assigned when minerals occur in amounts > 60% (Wagner *et al*., 2018). Lithotypes and microlithotypes, therefore have a cumulative effect on the chemical, and physical properties of coal which in turn affect the coals behaviour during mining and beneficiation, as well as for various technological applications (Wagner *et al*., 2018). Metallurgical coals generally comprise ≥ 60% vitrite and clarite (monomacerals), vitrinertite (bimaceral), and trimacerals (Ghosh *et al*., 2020). The proportions of these constituents vary depending on the technological properties of the coal which are dependent on coal rank, chemical quality, and physical properties.

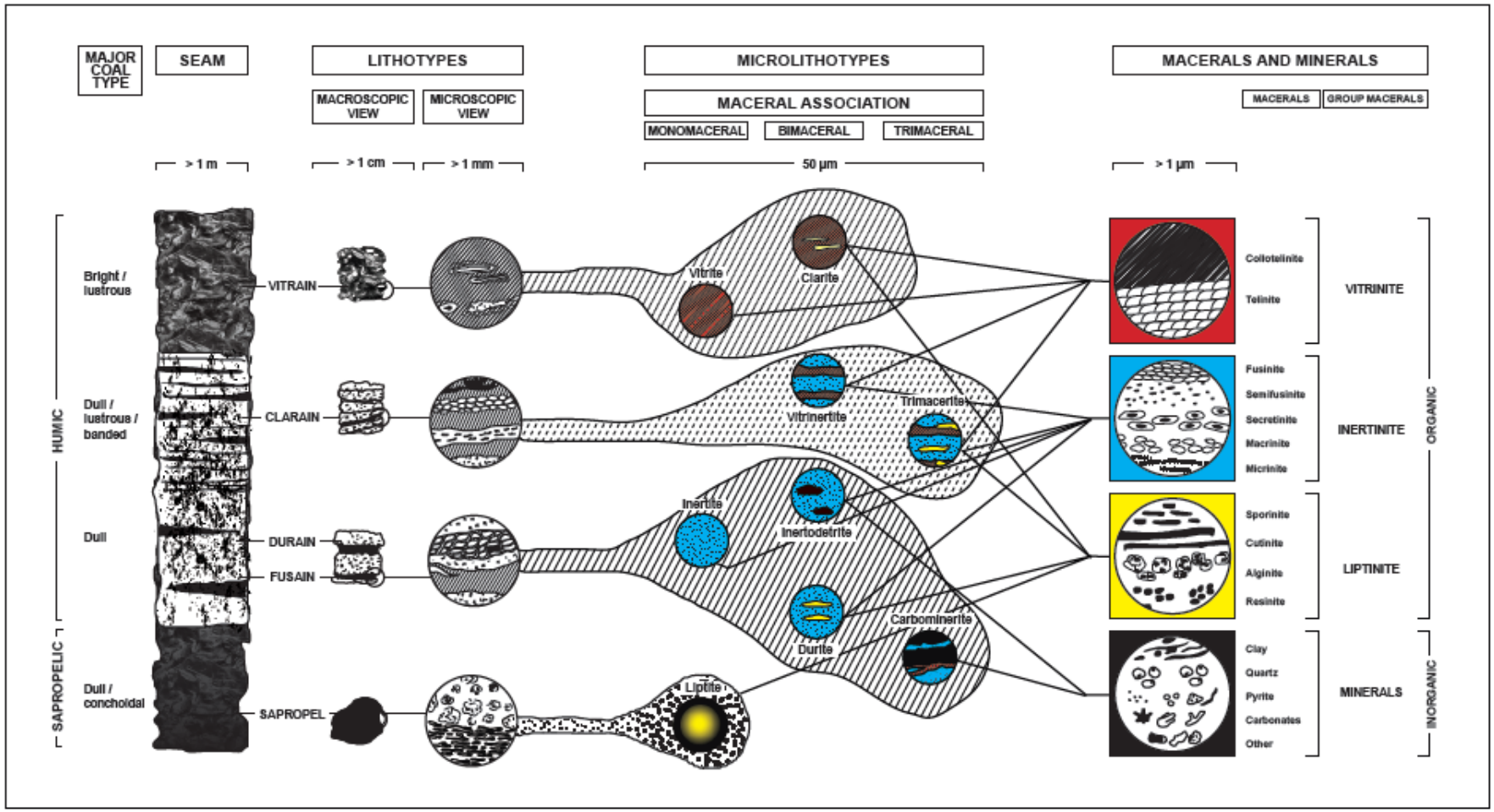

Figure 2.4. Relationship between macro and microscopic coal constituents (Wagner *et al*., 2018).

Metallurgical coal needs to be low in ash (mineral matter), ideally not exceeding 10% (Wagner *et al*., 2018). Coals containing high amounts of minerals that are inherently part of the coal/maceral structure (fixed ash) are difficult to beneficiate compared to minerals that occur as discrete particles within the coal (free ash) (Bhattacharya *et al*., 2016; Subba Rao and Gouricharan, 2016). Fixed ash originates from minerals that were either within the plant structure itself or deposited by wind or water during peatification (Wagner *et al*., 2018). These minerals are referred to as syngenetic minerals and tend to be very fine-sub microscopic or coarse grained (Lett and Ruppel, 2004; Ward, 2016). Free ash is a result of secondary or epigenetic minerals that are deposited or precipitated in openings within the coal structures such as veins and cavities (Ward, 2002; Ward, 2016).

Figure 2.5 shows that epigenetic minerals may be efficiently liberated from coal by gravity separation methods. Similarly, coarse grained syngenetic minerals are liberated with some ease compared to fine-grained syngenetic minerals that are embedded with the coal matrix. Generally crushing and milling to finer particle sizes increases the degree of liberation; however, some fine-grained syngenetic minerals cannot be completely removed by beneficiation (Wagner *et al*., 2018). For commercial purposes, the mineral matter that can be liberated by beneficiation is called adventitious while those that cannot be beneficiated are referred to as inherent minerals (Wagner *et al*., 2018).

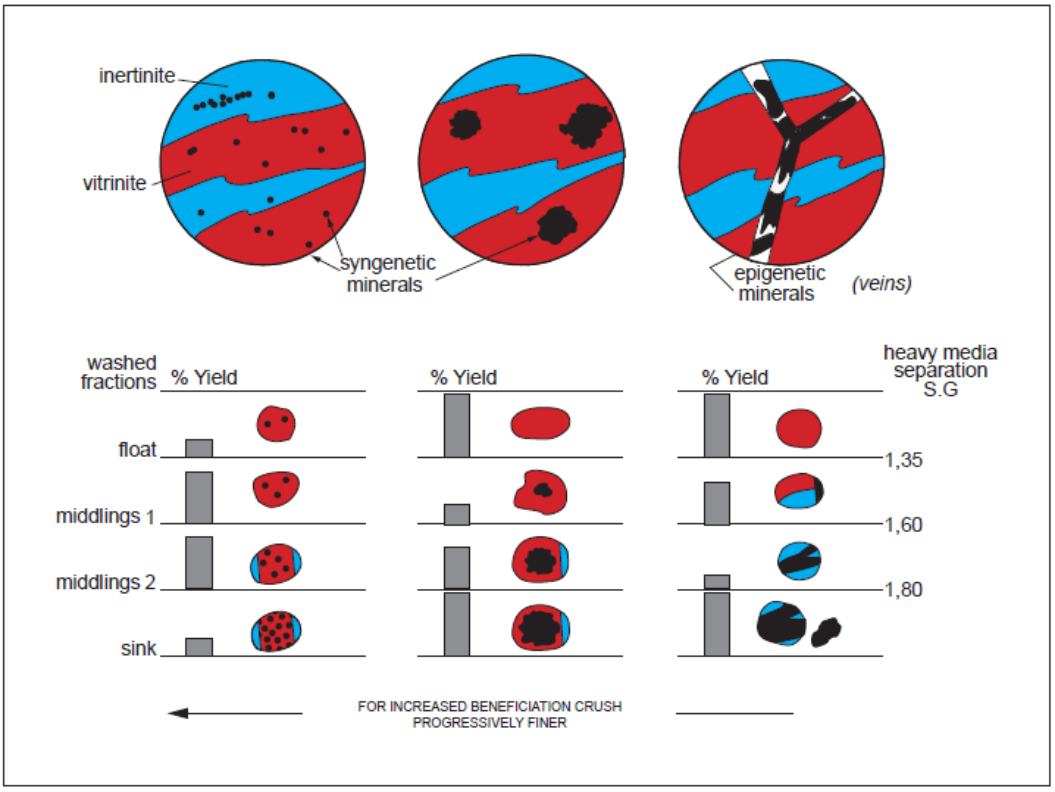

Figure 2.5. Liberation of syngenetic minerals compared to epigenetic minerals in coal (Wagner *et al*., 2018).

Mineral matter in coal broadly encompasses inorganic constituents such as dissolved salts, inorganic elements and amorphous or crystalline minerals (Vassilev and Vassileva, 1996). Dissolved salts occur in the pore structure, whereas inorganic elements are bound to the organic macerals. (Falcon and Snyman, 1986; Ward, 2002; Ribeiro *et al*., 2010). Deleterious mineral matter affecting the utilisation of metallurgical coals for coking include volatile matter, phosphorus, sulphur, alkalis and chlorine. Table 2.2 summarizes the role of these impurities in diminishing coke quality, decreasing productivity of the blast furnaces and lowering the quality of resultant steel output.

While several beneficiation studies have either detailed the washability of Tshikondeni coals (Pretorius, 2010; Powell, 2016), and others have incorporated samples from Tshikondeni Mine or undisclosed basins within the Soutpansberg (King and Birtek, 1990; Voges, 1991), no detailed study on the beneficiation characteristics of Makhado coals have been determined. Powell (2016) reported the typical HCC product specifications produced at Tshikondeni Mine through dense medium separation (DMS) and froth floatation yielded 60% product, with 14% ash (dry basis).

Table 2.2. Summary of deleterious effects of major quality parameters for metallurgical coal and coke.

Impurity	Source	Effects on coke and carbonization applications	References
Moisture	• Inherent coal moisture	• Decreases blast furnace temperature efficiency (heat capacity) and therefore low coking rate • Poor coke quality • Added cost of drying	Bertling, 1999; Lu *et al*., 2013; Schernikau, 2017
Volatile matter	• Gases bound to macerals and minerals	• Too high (>28%dmmf): high coke oven wall pressure, poor quality coke. Low coke yield during coal to coke conversion • Too low:(<23%dmmf): low coke oven wall pressure, weak coke	Speight, 2005; Lu *et al*., 2013; Schernikau, 2017
Phosphorus	• Phosphate bearing minerals such as apatite, goyazite, gorceixite	• Reduces steel strength • Leached as pollutant in coal waste	Vassilev and Vassileva, 1996; Ward *et al*., 1996; Lu *et al*., 2013; Schernikau, 2017
Sulphur	• Sulphide minerals such as pyrite • Organically bound sulphur in coal • Sulphates	• Decreases coke fluidity • Contributes to slag formation in blast furnace • Pollutant as H_2S and SO_2 • Reduces steel strength • Reports to liquid by products	Gluskoter, 1975; Vassilev and Vassileva, 1996; Bertling, 1999; Mochizuki *et al*., 2013, Lu *et al*., 2013; da Silva *et al*., 2017
Alkalis	• Inorganically bound as K_2O and Na_2O in coal • Introduced by water used to quench coke products	• Increase coke reactivity with CO_2 (CRI index) • Decrease coke strength (CSR index) • Accumulation causes corrosion, as well as crusting and clogging of blast furnace	Bertling, 1999; Sahajwalla *et al*., 2004. Bytnar and Burmistrz, 2013; Li *et al*., 2014; Chakravarty *et al*., 2020
Chlorine	• Organically bound to macerals, or present as mineral salts (NaCl, KCl, $CaCl_2$, $MgCl_2$)	• Causes corrosion of blast furnace when released as HCl • Decreases blast furnace heating rate	Yudovich and Ketris, 2006; Nomura, 2010; Tsubouchi *et al*.,2018; Mazurek *et al*., 2021

2.6. Beneficiation of metallurgical coal

Coal beneficiation is predominantly a physical sorting process that exploits the particle size, density and surface chemistry of coal in order to produce a relatively homogenous product that meets the end users' specifications in terms of energy yield, particle size, as well as compliance with environmental and health standards (Peatfield, 2003; Esterle, 2008; Subba Rao and Gouricharan, 2016; Kumar and Kumar, 2018). South African coals are typically difficult to wash as they contain high amounts of mineral matter, typically > 25% ash (King and Birtek, 1990; Franzidis, 1992).

Beneficiation is carried out at a coal preparation plant (Figure 2.6) entailing processes of size reduction, size classification, cleaning and waste disposal (Singh, 1987; Noble and Luttrell,

2015). These processes primarily exploit the differences in the physical properties of the organic material (low density) and mineral impurities (high density). Hence methods involving gravity separation, centrifugal action, surface tension, and magnetic separation are employed to beneficiate coal (Ozbayoglu, 2018; Kundu *et al*., 2021). The efficiency of these methods is dependent on the particle size of the coal; the smaller the particles, the more ineffective the physical properties become in beneficiating. Hence, other properties such as hydrophobicity and magnetism are used to facilitate beneficiation downstream (Thomas, 2012). As a result, processing plants consist of several unit operations or "circuits" that are designed to treat different particle sizes ranging from coarse (>10 mm), intermediate (10-1 mm), fine (1-0.15 mm), to ultra-fine (<0.15 mm) (Noble and Luttrell, 2015). From a financial and handling point of view, coarse coal particles are relatively easy to beneficiate compared to the finer coal particles which require more complex circuits (Ramudzwagi *et al*., 2020).

The first stage of beneficiation, namely size reduction, commences from the time coal is blasted and extracted. Further size reduction is achieved at the preparation plant by crushing and/or milling to finer sizes using machinery such as rotary breakers, impact mills, single or double crushers (Singh, 1987; Noble and Luttrell, 2015; Kundu *et al*., 2021). The coal is then sorted into different size fractions by means of stationary, vibrating, and cross flow screens as well as classifying cyclones at finer particle size (Singh, 1987; Noble and Luttrell, 2015; Ramudzwagi *et al*., 2020; Kundu *et al*., 2021). Further processing is focused on cleaning the coal. Commonly utilised coal cleaning equipment include, jigs, cyclones and conversion tables, froth floatation and heavy or dense medium separation (HMS or DMS). For coarser size fractions, the latter method utilises the density contrast between the coal and mineral matter in order to separate them using a heavy medium such as magnetite or sand (Singh, 1987; Noble and Luttrell, 2015; Ramudzwagi *et al*., 2020; Kundu *et al*., 2021). Ultra-fine coal particles are cleaned using froth floatation whereby the hydrophobic nature of coal is exploited in order to recover the low-density organic material by floating it to the surface, while the denser impurities sink (Singh, 1987; Noble and Luttrell, 2015; Kumar and Kumar, 2018; Ramudzwagi et al., 2020; Kundu et al., 2021).

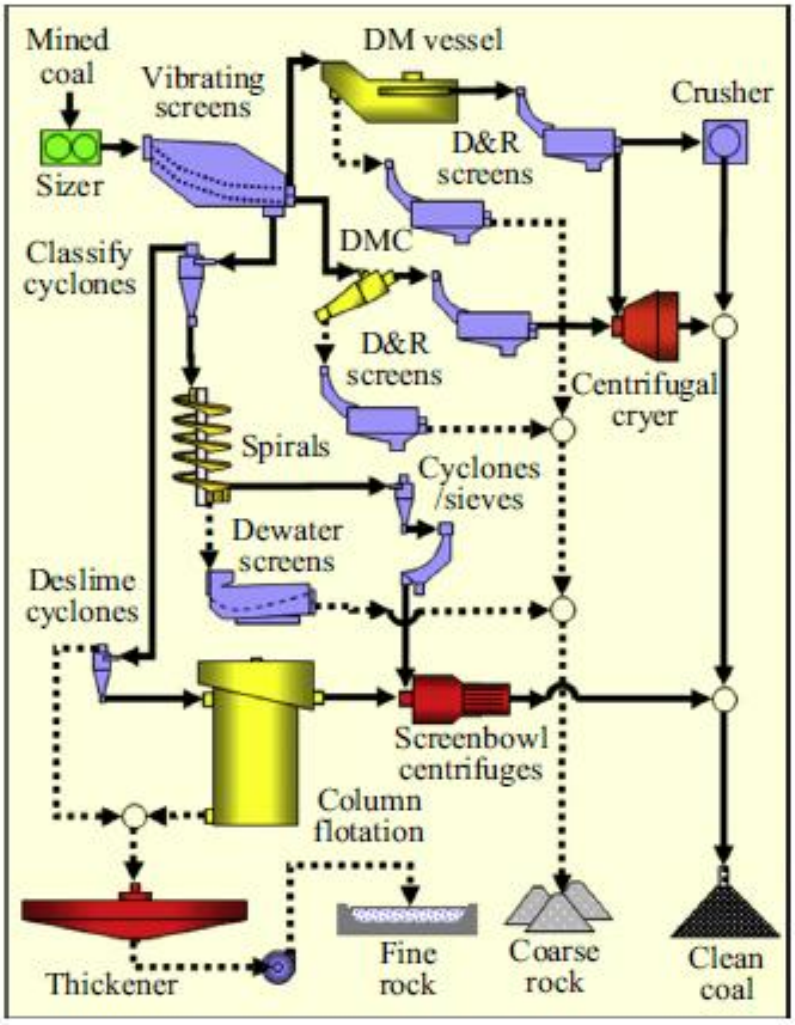

Figure 2.6. Typical coal beneficiation configuration at processing plants (Noble and Luttrell, 2015).

Since most coal cleaning processes are water-based they effectively increase the moisture content of the coal, especially at finer particle sizes. Screens, filters, centrifuges and thermal dryers achieve reduction of the additional moisture to an acceptable level (Noble and Luttrell, 2015; Ramudzwagi *et al*., 2020). Efficient water usage during beneficiation is important in water scarce regions, even more so in the northern coalfields of South Africa (Jeffrey, 2005b).

Dry beneficiation methods are more desirable due to the additional costs involved in drying wet coal, coupled with water scarcity. Testing of dry coal beneficiation technologies has been chiefly conducted by Coaltech Research Association (de Korte, 2010; 2013; 2014; 2015; Von Ketelhodt and Bergmann, 2010). These studies show that the Fuhe Ganfa Xuan mei (FGX) sorter, which translates to “compound dry type coal washer” and the X-ray transmission (XRT) sorter are capable of cleaning low quality coals at economically feasible rates in the short term. However, for long term coal processing, the use of dense medium beneficiation remains more profitable due to a higher product yield, albeit at the expense of the environment (de Korte

2010, de Korte, 2013; de Korte 2014; de Korte 2015). The studies also highlighted that the efficiency of the FGX and XRT sorters greatly depended on the physical, petrographic, and geochemical properties of coal. A comparison of the performance results of the FGX and XRT are contrasted in Table 2.3. Details of the experiment can be accessed in de Korte (2013).

Table 2.3. Beneficiation efficiency of the FGX sorter versus XRT sorter (de Korte, 2013).

Parameter	FGX	XRT
Feed % Ash	40.4	71.0
Product % Ash	31.9	59.5
Discard % Ash	60.2	81.4
Product Yield %	70.08	47.58
D_{50} cut-point RD	2.007	2.062
EPM (Ecart Probable Moyen)	0.2168	0.2878
Organic Efficiency %	86.8	79.4
Sink in float %	6.78	27.54
Float in Sink %	10.94	3.83
Total misplaced %	17.73	31.37
Near dense material (NGM) %	8.4	1.9

Bergh *et al.* (2013) discussed five levels of coal beneficiation that are typically conducted in South Africa (Figure 2.7). Metallurgical coals require fine-ultra fine coal beneficiation (level 4 and/or level 5) to produce low ash products (typically ± 10%), as well as to concentrate the fundamental coking component-vitrinite (de Korte, 2016). Full-scale or multiple-process beneficiation is utilised for level 4 and/or level 5 cleaning whereby several coal products are obtained from ultra-clean floats and middlings (Bergh *et al*., 2013). The middlings are mainly of export or local thermal quality while the floats are suitable for metallurgical purposes, usually after undergoing level 5 processing (Bergh *et al*., 2013).

Froth floatation was historically utilised during level 5 beneficiation by metallurgical coal mines in KwaZulu-Natal, the Waterberg and Soutpansberg, and later in the Witbank coalfields (Franzidis,1992; de Korte, 2001). de Korte (2016) advises the use of two-stage beneficiation employing Spirals or Teetered bed separators (TBS) or Reflux classifiers (RC) for the beneficiation of metallurgical coal specifically from the Waterberg and Limpopo coalfields. When Tshikondeni Mine was still operational, dense medium cyclones and froth floatation were utilised, the latter being particularly efficient at operating at the low-cut point densities required to produce low ash HCC from fine-ultrafine coals (Powell, 2016).

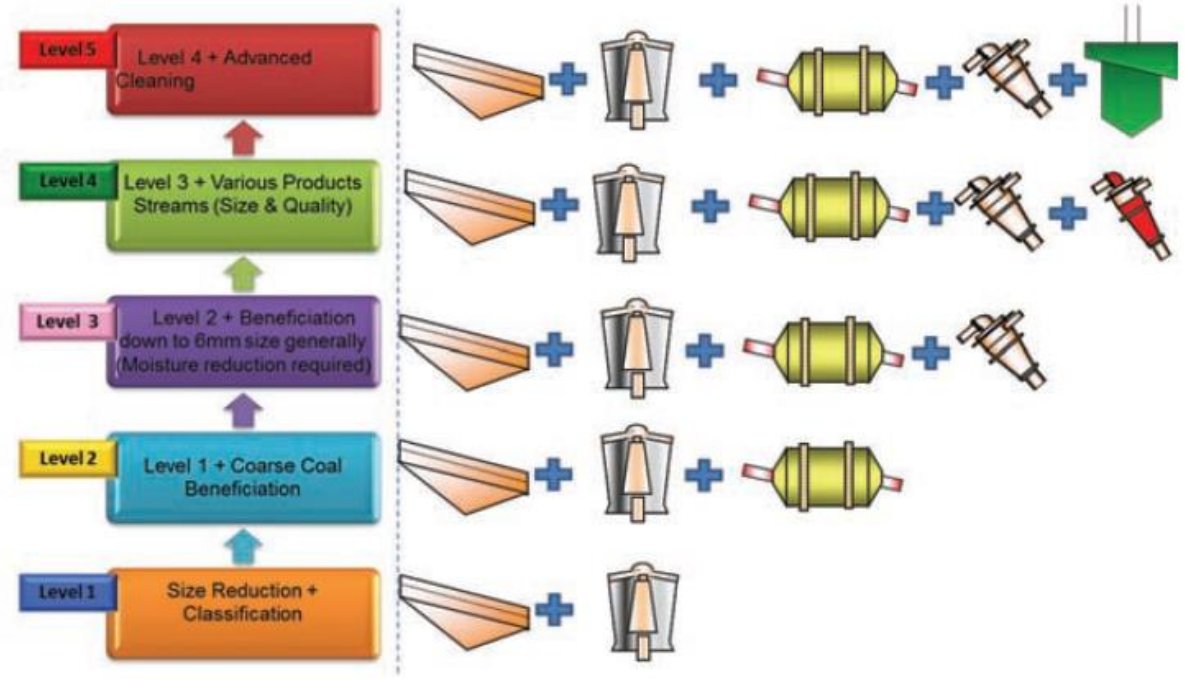

Figure 2.7. Levels of coal beneficiation (Bergh *et al*., 2013).

Mining companies carry out beneficiation test work to determine the quality of prospective coal resources and the best configuration of machinery to construct processing plants for the production of saleable coal products. This is achieved using washability data that is obtained from laboratory float-sink tests (Thomas, 2012; Subba Rao and Gouricharan, 2016). The process of the float-sink test and derived washability data are detailed in Chapter 4.

2.7. Methods for the determination of metallurgical coal quality

The mining industry utilises several conventional methods to assess the suitability of coal for metallurgical purposes by assessing the caking (plasticity) properties of coal. Depending on the objective, the tests described below are used in combination of simple and advanced tests.

Preliminary indicators of caking properties in coal may be inferred from chemical parameters obtained from conventional assays such as the Proximate and Ultimate analyses (Kruger, 2013). Metallurgical coals are generally characterised by relatively high volatile matter, carbon content and hydrogen (Lu *et al*., 2013).

Coal petrography (SANS/ISO 7404-1-6) is a powerful tool in the characterisation of metallurgical coals and coke (Jordan, 2008; Falcon, 2013). The use of maceral composition, coal rank and the level of vitrinite reflectance are particularly important petrographic parameters (Jordan, 2008; Lu *et al*., 2013; Wagner *et al*., 2018). Vitrinite reflectance can

further be expressed as vitrinoid type (v-type), which is a measure of the number of 0.1%R_{max} measurements. For example, the v-class V8 corresponds to reflectance measurements between 0.80 and 0.89% (Raaness and Gray, 1995). The v-type groups are important for coal blending whereby different coals constituting a blend can be identified to verify the suitability of the coal for coking.

The FSI or crucible swelling number (CSN) is a simple, rapid, and cost-effective technique that can be used to indicate whether coal has caking properties by measuring the extent to which the coal swells when heated in inert air (Speight, 2005). The test is carried out by heating coal and comparing the resultant coke button to standardized size profiles, according to ISO 501. The FSI procedure is detailed in Chapter 4. The FSI method is, however, limited by the subjectivity of the analyst in classifying the resultant cake buttons (Speight, 2005). Hence, more advanced and quantitative tests are commonly used to quantify the plasticity of coal in addition to the FSI test.

A similar method in the characterising the swelling properties of coal, is the Gray-King test (ISO 502). The quality, texture and shape of the coke residue in a glass tube is used to assess the degree of swelling and coke strength using the Gray-King Index (Lu *et al*., 2013; Mazumder, 2012). The Gray-King Index ranges from A to G9, the former indicating no coking properties, while the latter indicates excellent coking properties as summarized in Table 2.4.

A further step in characterising caking properties involves testing the mechanical strength (agglomerating) of coke buttons by means of the Roga test (ISO 335). The coal under investigation is combined with an anthracite standard and heated in inert air, producing a coke button akin to the FSI test (Kruger, 2013; Mazumder, 2012). However, the coke button is rotated in a drum to determine its strength, and the data is used to calculate the Roga Index (Speight, 2005). A broad correlation exists between the results of the FSI, Roga Index and Gray-King Index as shown in Table 2.4.

Table 2.4. Correlation between FSI vs Gray-King Index, and FSI vs Roga Index (Adapted from Speight, 2005, Mazumder, 2012; Kruger, 2013).

Free Swelling Index (FSI)	Gray-King Index	Free Swelling Index (FSI)	Roga Index
0-0.5 (Non-caking)	A-B (Non-caking coals)	0-0.5 (Non-caking)	0-5
1-4 (Weakly-Medium caking)	C-G2 (Very feebly-Medium caking)	1-2 (Weakly caking)	5-20
4.5-6 (Strongly caking)	F-G4 (Weakly-Medium caking)	2.5-4 (Medium caking)	20-45
6.5-8 (Strongly caking)	G3-G9 (Medium-Strongly caking)	>4 (Strongly caking)	>45
8.5-9 (Strongly caking)	G9+ (Very Strongly caking)		

The Giseler plastometer test (ASTM D-2639) indicates the coking performance (fluidity) when coal is heated slowly during carbonization. The various temperatures at which the coal changes from the solid state to fluid, until it cools into hard coke are recorded (Speight, 2005; Kumar *et al*., 2008; Mazumder, 2012).

It is important to note that caking properties are particularly susceptible to oxidation (Wang *et al*., 2003; Kus and Misz-Kennan, 2017). Consequently, coals exhibiting high oxygen contents may be indicative of poor or deteriorated caking properties (Sebola, 2015; Sebola, 2018). It is therefore of importance for metallurgical coal to be stored in airtight storage prior to testing and tested immediately after milling/preparation to avoid oxidation which will affect the test results (Speight, 2005).

2.8. Carbonization: the conversion of metallurgical coal to coke

Once metallurgical coal is mined and beneficiated to required specifications, it is converted to coke using coke ovens called batteries (Suárez-Ruiz and Crelling, 2008). The coke ovens are heated in inert air at ± 1000°C, using a thermal coal charge which causes the metallurgical coal to melt, swell and devolatilize into a hard, porous, carbon-rich mass referred to as coke or metallurgical coke (Lu *et al*., 2013). Tar residues are by products of this process and can be further processed to make chemicals (Kernot, 2000; Granda *et al*., 2014).

The conversion of iron ore into steel (Figure 2.8) is carried out in a blast furnace using coke and limestone. The latter melts during the process, acting as a chemical flux to purify the molten iron by trapping impurities. The former has several key functions summarized below (Kernot, 2000; Lu *et al*., 2013):

- Provide heat to drive the conversion process
- Release carbon monoxide gas to reduce the iron oxides into iron metal and carbon dioxide gas
- Remain in solid phase to support the burden
- Allow the molten iron, slag and gasses to pass through its permeable structure

Although alternative sources of heat and chemical reducing agents such as PCIs and biomass products can be substituted in the blast furnace, no other suitable material exists to efficiently facilitate the separation between the metal, slag and gases (Deiz *et al*., 2002; Suárez-Ruiz and Crelling, 2008; Duda and Fidalgo Valverde, 2021). Therefore, metallurgical coal remains a critical component in the conversion of iron ore coal to steel.

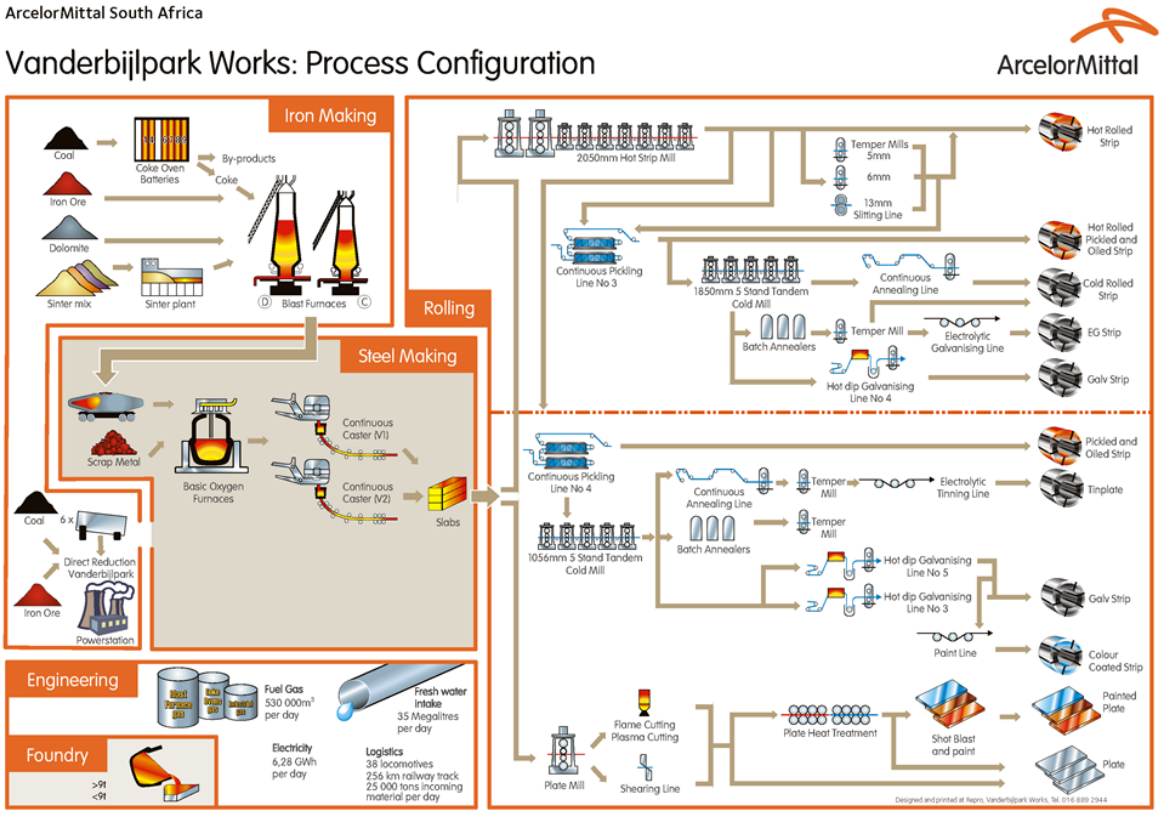

Figure 2.8. Example of coal to coke to steel conversion process carried out at ArcelorMittal`s Vanderbijlpark operation (ArcelorMittal, 2021).

Due to the ripple effect of metallurgical coal quality on the resultant coke and steel products, strict quality specifications are also enforced on coke products (Grigore *et al*., 2008; Jordan, 2008; Li *et al*., 2014). An example of quality parameters applicable to cokes, specifically for Europe is provided in Table 2.5.

Table 2.5. Blast furnace coke quality specifications (Deiz *et al*., 2002).

Chemical property	Chemical property European range
Moisture (wt.%)	1 –6
Volatile matter (wt.% db)	< 1.0
Ash (wt.% db)	8 –12
Sulphur (wt.% db)	0.5– 0.9
Phosphorus (wt.% db)	0.02– 0.06
Alkalis (wt.% db)	< 0.3

In addition to its commercial role in steelmaking, high value products are derived from the coke oven chars and gases released during the steel making process. These products include complex chemicals, carbon fibres, carbon nanostructures, hydrogen, coal-based adsorbents (Schobert and Song, 2002; Schweinfurth, 2009). Despite the strong public, corporate and scientific push for the world to rapidly transition away from coal use, the transition to renewable energy cannot occur without the use of metallurgical coal because it is a key ingredient in the manufacturing of the materials required to build renewable technologies. For example, metallurgical coal is a primary ingredient in the steelmaking process, and it is estimated that

770 kilograms of metallurgical coal is required to make one ton of steel (Ozbayoglu, 2018; York and Bell, 2019; BHP, 2021; Duda and Fidalgo Valverde, 2021). This steel is utilised in building the parts and infrastructure (blades, tower, generator, and foundation) required to generate clean energy. Furthermore, steel is largely used in the manufacture of household appliances, transport and construction. Hence, it is expected that metallurgical coal will remain in high demand until such time that an alternative carbon source that is equally or more efficient than metallurgical coal can be developed ((Diez *et al*., 2002; Matyjaszek *et al.,* 2018). Research into the use of green hydrogen, biomass, electrolysis and the use of carbon capture and storage (CCS) technology are underway in the European Union and South Africa in effort to reduce carbon dioxide emissions during the carbonization process (Ozga-Blashke, 2020; Trollip *et al*., 2022).

The importance of metallurgical coal as a key ingredient in the development of clean energy is further shown by its re-listing on the latest Critical Raw Materials (CRM) publication by the European Commission, (2020). This declaration ensures:

- Added investment into the development of additional metallurgical coal projects.
- Job security with the prospect of increasing employment opportunities
- Steady supply of metallurgical coal and associated by-products.
- The development of an innovative and low-emission economy.

These factors are critical to South Africa`s coal mining, iron and steel industries.

2.9. Coal as an economic source of rare earth elements

Rare earth elements (REE) are a group of 14 individual elements referred to as lanthanides comprising of La, Ce, Pr, Nd, Sm, Eu, Gd, Tb, Dy, Ho, Er, Tm, Yb and Lu (Thomas, 2012). Promethium (Pm) is omitted due to its extremely rare occurrence in nature, while yttrium (Y) and scandium (Sc) are included in the REE category due to similar chemical and physical properties (Van Gosen *et al*., 2014; Eterigho-Ikelegbe *et al*., 2021; Fu *et al*., 2022). The REE series is abbreviated ‘REY’ when Y is included, or ‘REY+Sc’ when Sc is included. The REE are geochemically grouped on the basis of their atomic number, electron arrangement, and chemical properties. Light REE (LREE) consist of: Sc, La, Ce, Pr, Nd and Sm. Medium REE (MREE/MREY) consist of: Eu, Gd, Tb, Dy and Y. Heavy REE (HREE) consist of: Ho, Er, Tm, Yb and Lu (Franus *et al*., 2015; Dai *et al*., 2016). Critical rare earth elements (CREE) considered to be of economic significance are Nd, Eu, Tb, Dy, Er and Y (Seredin, 2010).

Rare earth elements are traditionally concentrated and therefore exploited from deposits such as igneous rocks, carbonatites, alkaline granites or weathered soils (Dai *et al*., 2016). These

deposits typically host REE in the range 1000-5000 ppm (Eterigho-Ikelegbe *et al*., 2021). More than half of the world`s REE reserves occur in China and as a result, China dominates the global production and supply of REE (Van Gosen *et al*., 2014; Dai and Finkelman, 2018; Eterigho-Ikelegbe *et al*., 2021). China`s dominance in REE reserves, coupled with their restrictions on REE trade, as well as the high global demand for REE, has ignited significant efforts into the exploration and research for alternative unconventional REE sources (Eterigho-Ikelegbe *et al*., 2021).

Locally, a monazite rich vein deposit is mined for REY at the Steenkampskraal Monazite Mine situated in the Western Cape Province of South Africa. The mine has been operational since 1952, and boasts a high-grade deposit on average, 14.36%. More than half of the product yield is neodymium (Nd), with lesser amounts of dysprosium (Dy), praseodymium (Pr), terbium (Tb), gadolinium (Gd), cerium (Ce), and others (Steenkampskraal, 2021). Recent REE projects in South Africa include: 1) the Glenover Rare Earth Project (carbonatite deposit), 2) the Zandkopsdrift Rare Earths Project (carbonatite deposit), 3) the Naboomspruit pegmatite, 4) the Namaqua Sands heavy minerals tailings, 5) the Richards Bay heavy minerals tailings and, 6) the Phalabora Phospho-gypsum waste dumps (Harmer and Nex, 2016; Jellico, 2019; Galileoresources, 2021).

The scarcity and high demand for critical materials play a vital role for the transition and establishment of clean energy technologies, as well as for use in modern electronics (Van Gosen *et al*., 2014; Eterigho-Ikelegbe *et al.,* 2021; Fu *et al*., 2022). The importance of REE is further highlighted by their presence on the CRM list by the European Commission (2020). Coal and coal ash are recognized as alternative sources for the exploitation of REE. Eterigho-Ikelegbe *et al*. (2021) and others have noted that approximately 3147 open-source literature have been published between 1990 and the first half of 2021 on the subject matter of REE associated with coal.

REE in coal are present in the form of REE-bearing minerals, ion adsorbed REE on the surfaces of clay minerals, or occurring with the coal matrices (Zhang *et al*., 2017). Studies have shown that REE predominately show inorganic mode of occurrence whereby the REE are associated with mineral matter in the coal, typically in the sink/discard fractions (Wang *et al*., 2006; Weng-feng *et al*., 2009). Furthermore, greater heavy rare earth element (HREE) enrichment compared to light rare earth element (LREE) has been widely observed in coal and coal ashes (Eterigho-Ikelegbe *et al*., 2021; Fu *et al*., 2022). The occurrence of REE from various coal products and by-products across the coal value chain is summarized in Figure 2.9.

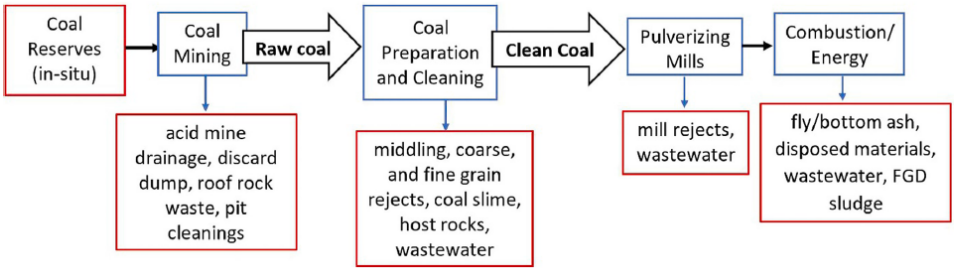

Figure 2.9. REE sources in the coal mining, preparation and utilisation value chain (Eterigho-Ikelegbe *et al*., 2021).

Seredin (2010) proposed the outlook coefficient (K_{outl}) as a rapid method for the preliminary evaluation of economic REE deposits. The outlook coefficient is based on the concentrations of REE in deposits and also considers the market demand for CREEs.

Dai *et al*. (2017) provided a revised criterion for the preliminary assessment of the REY in coal ash as economic raw materials. The revised outlook coefficient (C_{outl}) is defined as "the ratio of the relative amount of critical REY metals in the total REY to the relative amount of excessive REY" (Dai *et al*., 2017, pp 15), and is thus calculated:

$$C_{outl} = \frac{(Nd + Eu + Tb + Dy + Er + Y)/\Sigma REY}{(Ce + Ho + Tm + Yb + Lu)/\Sigma REY}$$

The overall percentage of critical elements in REY (REY_{def}) are plotted against the outlook coefficient on the REY_{def}, $_{rel}$-C_{outl} graph (Figure 2.10A) on which genetic comparison can be made relative to well-known and untraditional REY ores (Seredin 2010; Seredin and Dai, 2012).

The revised clusters are defined as follows (Dai *et al*., 2017):

- Cluster I-unpromising REY source: $C_{outl} < 0.7$
- Cluster II-promising REY source: $0.7 \leq C_{outl} \leq 1.9$
- Cluster III- highly promising REY source: $C_{outl} > 2.4$

In addition to the above C_{outl} criteria, the ΣREY must be ≥ 1000 ppm in order to meet the cut-off grade required for economic recovery, and can be illustrated on a C_{outl}, ΣREY graph as shown in Figure 2.10B (Dai *et al*., 2017). None the less the extraction of REE`s from coal and its by-products is currently limited to laboratory scale as, attempts at commercialisation are ongoing through continued global research efforts (Eterigho-Ikelegbe *et al*., 2021; Fu *et al*., 2022).

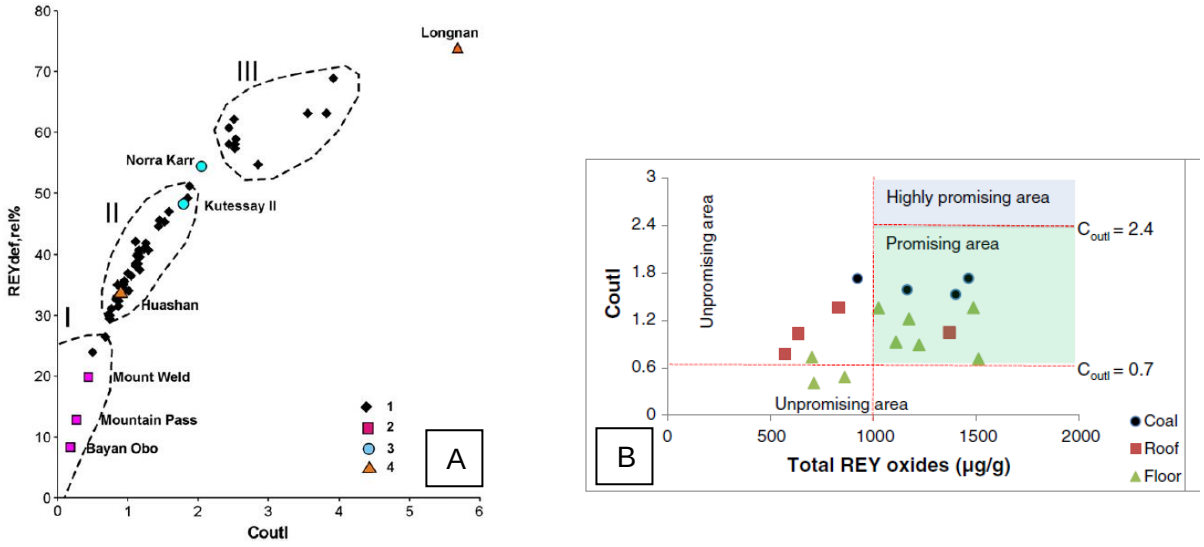

Figure 2.10. Graphic representations for the outlook coefficient. (A) The economic potential of REY sources are classified into cluster I unpromising, cluster II promising or cluster III, highly promising (Seredin and Dai 2012). (B) Revised representation of the outlook coefficient vs ΣREY adapted from Dai *et al*., (2017).

There are good grounds for the research into the economic development of REY from coal in South Africa given that the country has abundant coal deposits, discards and fly ash accumulated over centuries of mining and utilisation (Lloyd, 2000; DOE, 2001). It is estimated that just over 50 million tonnes of coal ash is produced annually in South Africa, yet only 5 million is reclaimed for use in various industries including cements, construction (road and buildings) and agriculture (SACAA, 2021). However, research into coal derived REY is relatively in its infancy compared to international efforts, with available literature being published on MKB coals. The total REY+ Sc in coal and coal ash from the Tutuka Power Station reported by Akinyemi *et al.* (2012) is 218.3 ppm and 517.17 ppm, respectively. While Eze *et al.* (2013) reported total REY+ Sc of 480.31 ppm in fly ash from Matla Power Station.

Wagner and Matiane (2018) reported total REY between 111.93 and 149.58 ppm in power station feedstock from the MKB, and total REY between 488.91 and 598.70 ppm in the ash products. Akdogan *et al*. (2019) reported average total REY content to be 280 ppm in ash from the four Upper coal seams of the Springs-Witbank Coalfield. Although the above-mentioned total REY concentrations are elevated (168.37 ppm) relative to the upper continental crust (UCC) and world hard coals (68.69 ppm), respectively, they do not qualify as economic promising sources as the ΣREY is less than prerequisite 1000 ppm proposed by Dai *et al*. (2017) at preliminary a level. ROM and discard coal samples from the Waterberg were found to have total REE content greater than 225 ppm, with kaolinite, pyrite, and hematite identified as the dominant host minerals (Harrar *et al*., 2022). Similar REY characterisation and research into the economic REY potential of coals in the Soutpansberg Coafield has not been investigated in the public domain.

Chapter 3: Geology of the Soutpansberg Coalfield

3.1. Introduction

The geological setting of the Soutpansberg Coalfield and its subsidiary basins is provided, with a focus on the Makhado Project located in the Tshipise sub-basin. The geological overview entails a summary of the stratigraphic units and general coal qualities in the region.

3.2. Background into exploration and mining activities

The Soutpansberg Coalfield is an intracratonic rift basin of Karoo-age located in the Limpopo Province of South Africa (Figure 3.1). Three sub-basins are demarcated in the Soutpansberg Coalfield, namely: the western (Mopane sub-basin), central (Tshipise sub-basin) and eastern (Pafuri sub-basin) basins (Snyman, 1998; Malaza, 2013). The Soutpansberg Coalfield is generally elongate, trending approximately 300 km WNW-NNE, which roughly parallels the neighbouring Tuli/Limpopo Coalfield (Malaza, 2013). The Makhado Project is situated 36 km north of the town of Makhado (previously Louis Trichardt) within the Tshipise sub-basin (Figure 3.1).

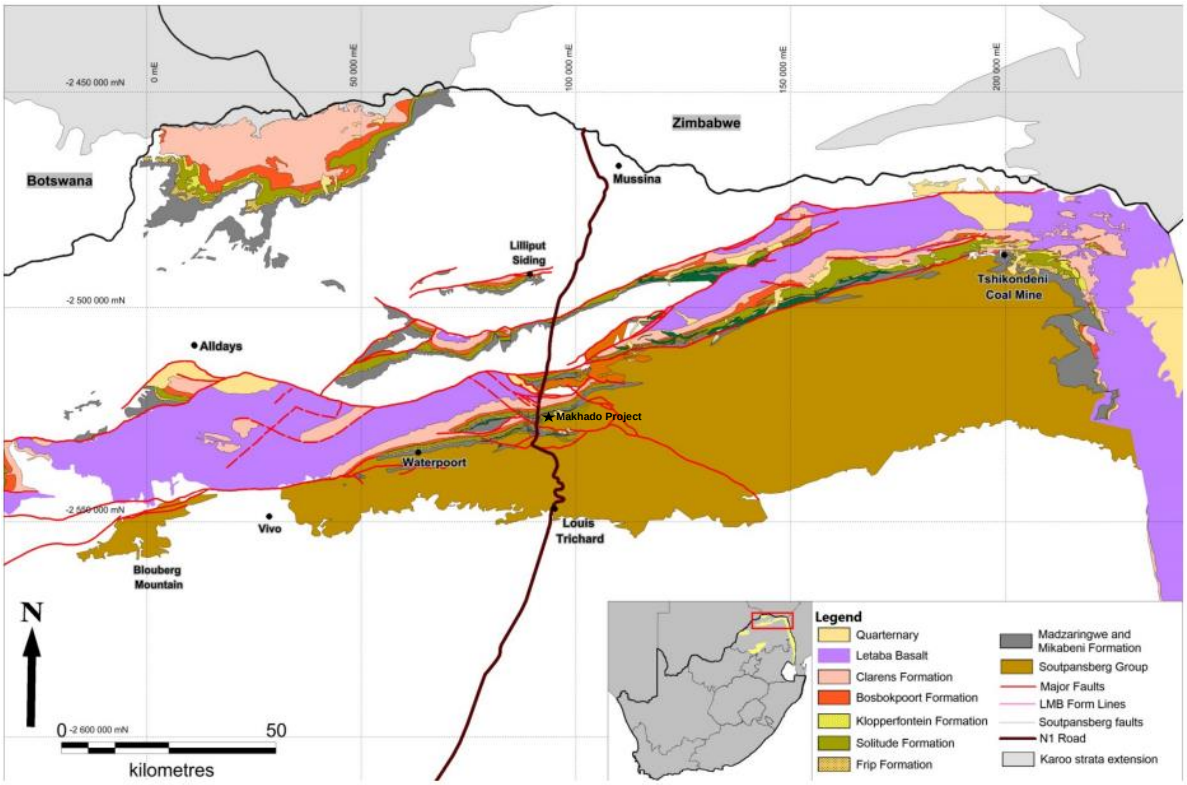

Figure 3.1 The Makhado Project is centrally located in the Tshipise sub-basin of the Soutpansberg Coalfield (modified after Luyt, 2017).

Coal deposits in the Soutpansberg Coalfield have been known since the 19th century (Sparrow, 2012). The Messina Transvaal Copper Company was the first to mine coal in the area between 1911 and 1918, supplying a total of 14488 tonnes of metallurgical coal from Lilliput Mine (Figure 3.1) to the local copper smelter in the Town of Musina (Sparrow, 2012; de Klerk and Sparrow, 2015; Mostert, 2016). After a lengthy hiatus, various companies, and parastatal entities such as the Fuels Research Foundation, the Council for Geosciences South Africa (formerly, the National Geological Survey), Department of Mines and ArcelorMittal South Africa (formerly, ISCOR), conducted exploration and tests on coals in the region during the period of 1947-1970 (Sparrow, 2012). ISCOR carried out an extensive exploration program throughout the Soutpansberg Coalfield in 1978 and 1979 which led to the development of the Tshikondeni Mine in 1984 (Hancox and Götz, 2014). Exxaro operated Tshikondeni Mine using traditional underground extraction methods (board and pillar), yielding 316000 tonnes per annum of prime coking coal primarily for ArcelorMittal's steel operation in Vanderbijlpark (Hancox and Götz, 2014). The only active coal mine in the Soutpansberg Coalfield, Tshikondeni Mine, unfortunately, closed its operation in 2014 due to increasing structural complexity affecting feasible mining (Exxaro, 2019).

Other exploration efforts that have been carried out in various parts of the Soutpansberg Coalfield since 1983 include: Trans Natal in the Mopane sub-basin; and Anglo American, Rio Tinto and Kwezi carried out extensive exploration on the Chapudi Project in the Tshipise sub-basin. Finally, in 2007 MC Mining acquired the vast exploration data from Rio Tinto to supplement their own exploration program (Hancox and Götz, 2014).

In the most recent review of South African coalfields, Hancox and Götz (2014) note that what is known of the geology of the Soutpansberg Coalfield is based on the classical works of McCourt and Brandl (1980), Van der Berg (1980), Brandl (1981), De Jager (1986), Sullivan (1995) and Thabo and Sullivan (2000). Hancox and Götz (2014) provide an updated overview on the exploration, geology, research and coal quality of the Soutpansberg Coalfield and its sub-basins. The reader is referred to Hancox and Götz (2014) for the overview of the Soutpansberg Coalfield and its relation to the MKB.

Recent academic research has attempted to provide greater insight into the tectonics, sedimentology and coal petrology of the region. Malaza (2013) investigated the sedimentological framework and coal forming environment in the Tshipise sub-basin and greater Soutpansberg Coalfield. Preliminary palynology findings by Cindi, (2014) support a model of coal deposition in fresh water. The extent of coal quality deterioration in several stockpiled coals in the Tshipise sub-basin were studied by Sebola (2015; 2018). Mphaphuli (2017) carried out a petrographic assessment on coal quality to identify variation arising due

to fault structures across the Tshipise sub-basin. Luyt (2017) conducted an in-depth chronological investigation into the tectonic regime influencing the deposition of Karoo strata within the Tshipise sub-basin. Localized studies utilising exploration drill holes around the Tshipise sub-basin (Mawila, 2019) and Pafuri sub-basin (Kataka *et al*., 2018; Mukatuni, 2019) have been conducted in effort to better characterise the sedimentology and coal deposits of the region. Notably, the lithostratigraphic nomenclature of the Tshidzi Formation (Bordy, 2018) and Clarens Formation (Bordy and Head, 2018) in the northern coalfields have been formalized to correlate to their counterparts in the MKB.

3.3. Stratigraphy

Deposition of the stratigraphic units of the Soutpansberg Coalfield is synonymous to those of the Karoo Supergroup in the MKB (Cadle *et al*., 1993). However, the Karoo-age strata in the Soutpansberg Coalfield were deposited in horst and graben structures (Catuneanu *et al*., 2005; Johnson *et al*, 2006). The sedimentary units of the Karoo Supergroup were deposited from the end of the Carboniferous period (300 Ma) to the mid Jurassic (183 Ma) and show evidence of transition from a glacial to arid climate (Cairncross, 2001).

The fault system in the Soutpansberg Coalfield are predominantly normal and likely post-Karoo in age (Brandl, 1981; Luyt, 2017). The major pre-Karoo faults affecting the Soutpansberg Coalfield trend parallel to the strike (SW-NE) of the Limpopo Mobile Belt (LMB) and are known as the Tshipise, Klein Tshipise and Bosbokpoort faults (Malaza, 2013). Unlike the stratigraphic units of the MKB, detailed studies of the lithological units of Karoo strata in the Soutpansberg Coalfield are understudied and as such informal nomenclature (i.e., not approved by the South African Committee for Stratigraphy, SACS) is largely used to name most of the strata (Snyman, 1998). Figure 3.2 shows the correlation between the stratigraphy of the Karoo Supergroup in the MKB and the Tshipise sub-basin, Soutpansberg Coalfield.

The trends in the metallurgical coal quality in the Soutpansberg Coalfield are generally characterised by a west-east increase in coal rank, coke strength after reaction (CSR), and yield. Volatile matter decreases west-east from 35% to 25%, and the phosphorus content increases northwards (Sparrow, 2012). Cindi (2014) determined that coal from the Makhado Project were ranked medium C bituminous while those from Tshikondeni Mine were ranked medium B bituminous. The coalfield is thickest in its northeast margin resulting in a higher geothermal gradient and thicker deposits (Snyman and Barclay, 1989; Cadle *et al*., 1993; O'Keefe *et al*., 2013). It is estimated that the geothermal gradient in the Soutpansberg Coalfield is in the range 60-80°C/km (Luyt, 2017).

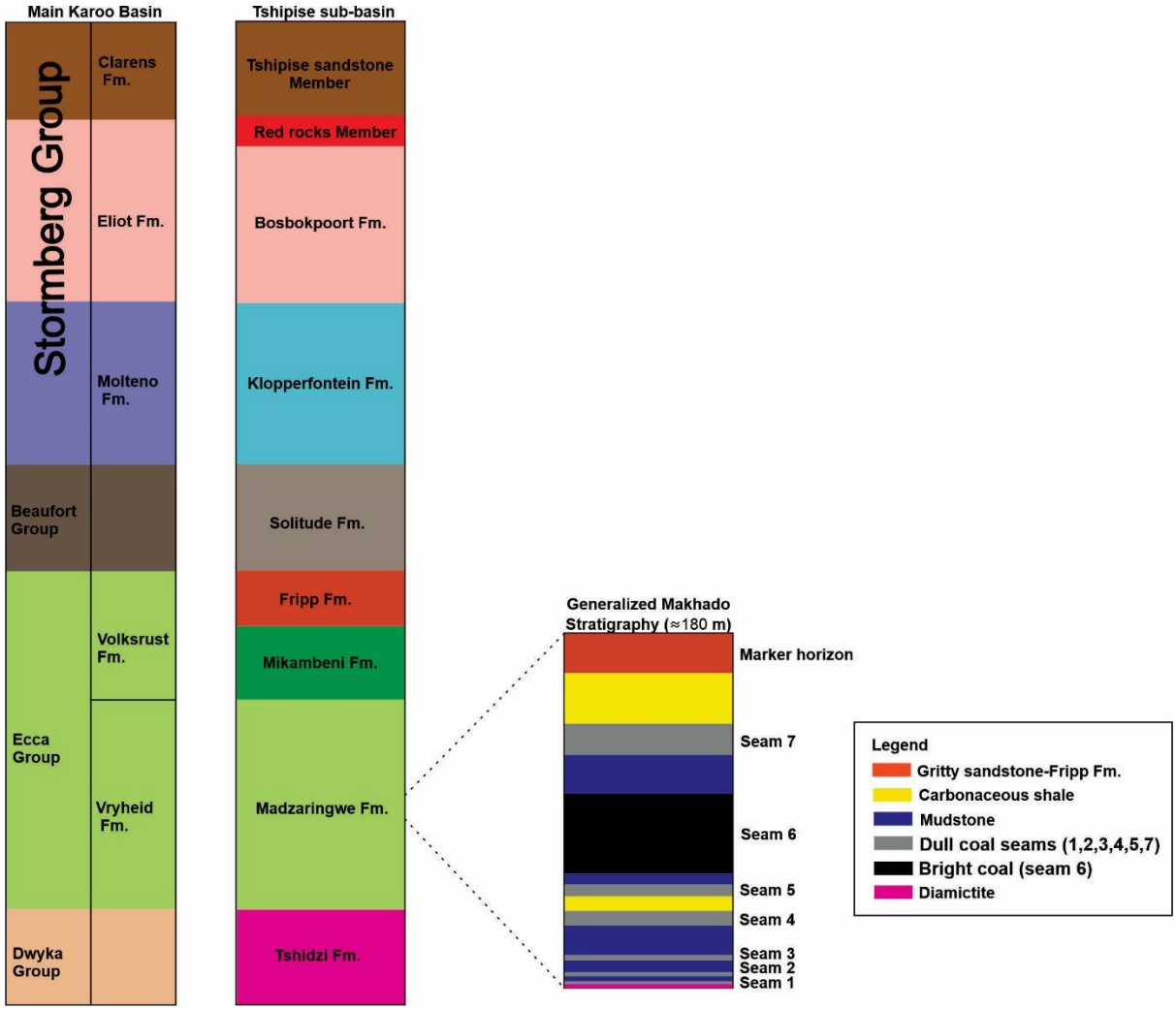

Figure 3.2. Stratigraphic correlation of the Karoo Supergroup in the Main Karoo Basin, with the Tshipise sub-basin, Soutpansberg Coalfield. Fm = Formation (Modified after Sparrow 2012; Luyt, 2017).

The major stratigraphic units constituting the Soutpansberg Coalfield are discussed below:

3.3.1. Tshidzi Formation

All glacial and fluvioglacial units in the northern coalfields are referred to as the Tshidzi Formation, which is the equivalent of the Dwyka Group in the MKB (Bordy, 2018). The Tshidzi Formation is named after Tshidzi Hill situated in the Tshipise sub-basin, and consists of diamictites, pebbly mudstones and breccias that directly overly the metaquarzites of the Soutpansberg Group and basement rocks of the Beitbridge Complex (Malaza, 2013). The Tshidzi Formation ranges in thickness from 5-20 m in the Tshipise sub-basin (Hancox and Götz, 2014).

3.3.2. Madzaringwe Formation

The Madzaringwe Formation is the equivalent of the coal-bearing Ecca Group in the MKB and is characterised by an upward coarsening sequence consisting of coal alternating with

carbonaceous mudstones and shales towards the base (Malaza *et al*., 2013). The economic coal seams occur within the Madzaringwe Formation.

3.3.3. Mikambeni Formation

The Mikambeni Formation is 20-150 m in thickness, consisting of shale, carbonaceous mudstone, and laminated sandstones. Thinly banded coal seams occur throughout the horizon, albeit not considered economic (Malaza *et al*., 2013).

3.3.4. Fripp Formation

The Fripp Formation is 110 m thick and laterally continuous unit, consisting of gritty feldspathic sandstones, interbedded with siltstone and mudstone. The units are characterised by trough cross beds, indicating deposition in braided streams (Malaza *et al*., 2013). Fossils encountered in the Fripp Formation are limited to *Dicroidium* imprints and worm burrows (*skolithos*) (Luyt, 2017).

3.3.5. Solitude Formation

The Solitude Formation marks the onset of deposition during the Triassic period. The unit is 170 m thick and comprises purple mudstones and grey shales. Chlorite-rich siltstones (green in appearance) occur higher in the sequence (Luyt, 2017). These rocks are floodplain deposits of extensive meandering streams (Malaza *et al.*, 2013).

3.3.6. Klopperfontein Formation

The Klopperfontein Formation is a 20 m thick unit consisting of coarse-grained feldspathic sandstones. The sandstones show cross-bedding, indicating deposition by braided streams (Malaza *et al*., 2013). The Klopperfontein Formation is the equivalent of the Molteno Formation of the MKB.

3.3.7. Bosbokpoort Formation

The Bosbokpoort Formation corresponds to the Elliot Formation in the MKB. The unit is 100m thick and consists of red mudstones and very fine-grained sandstones. The unit indicates deposition in oxidising conditions by meandering streams (Malaza *et al*., 2013).

3.3.8. Clarens Formation

The Clarens Formation in the Soutpansberg Coalfield and neighbouring Limpopo (Tuli) Coalfield was previously considered to consist of the basal Red Rocks Member and the overlying Tshipise Sandstone Member (McCourt and Brandl, 1980; Brandl, 2002). However, the Red Rocks Member is now considered the equivalent of the Elliot Formation in the MKB, while the Tshipise Sandstone Member correlates with the Clarens Formation (Bordy and

Head, 2018). The Clarens Formation in the Tshipise sub-basin reaches a maximum thickness of 150 m. The lithologies reflect SW to NE aeolian deposition and comprise fine to silty sandstones. Botanical findings in the Clarens Formation are limited to tree stems (Truter,1945 in Bordy and Head, 2018).

3.3.9. Letaba Formation and Jozini Formation

Sedimentation in the Karoo Basins ceased in the mid-Jurassic due to the extrusion of flood basalts from extensive dike and sill bodies, forming the Drakensburg Group Lavas (Tankard *et al*., 2009). The continental magmatism was due to a change from compressional to extensional tectonic regime which initiated the breakup of Gondwana from Pangea around 183 ± 1 Ma (Duncan *et al*.,1997; Cairncross, 2001).

The intrusive bodies of the Drakensburg Group caused some localised ugrades in coal rank, particularly in the KwaZulu-Natal coalfields whereby the heat imparted by contact metamorphism gave rise to anthracites (Snyman and Barclay, 1989). Similar upgrades in coal rank are uncommon in the Soutpansberg Coalfield (Sparrow, 2012).

The Letaba Formation and Jozini Formation are the extrusive equivalents of the Drakensburg lavas in the Soutpansberg Coalfield (Luyt, 2017). The Letaba Formation is characterised by basaltic lava, occurring with minor andesite and rhyolite flows and tuffs (Johnson *et al*., 2006). The Jozini Formation is composed of pink to reddish rhyolite. The dolerite sills are thickest in the Pafuri sub-basin, as well as in the vicinity of the Siloam Fault Zone within the Tshipise sub-basin (Luyt, 2017).

3.4. Sub-basins of the Soutpansberg Coalfield

3.4.1. The Mopane sub-basin

The Mopane sub-basin covers an area ~3640 km² on the western margin of the Soutpansberg Coalfield from the towns of Mopane to Waterpoort (Hancox and Götz, 2014; de Klerk and Sparrow, 2015; Mostert, 2016). The basalts of the Letaba Formation cover much of the area in the Mopane sub-basin, hence, outcrops of Karoo rocks are scarce in the area. The coal seams found in the area are sporadic and quite thin, ~1 m thick (Luyt, 2017).

Further studies in the area are needed to characterise the lithostratigraphy and coal qualities in the area.

3.4.2. The Tshipise sub-basin

The Tshipise sub-basin is centrally located within the Soutpansberg Coalfield and consists of eleven fault-controlled blocks namely, the Verlooren, Chaphudi West, Chapudi and Wildebeesthoek in the western margin (Sparrow, 2012; Luyt, 2017). The Mopane, Jutland, General, Makhado, Telema, and Overwinning are located centrally. The Solitude and Mount Stuart blocks lie on the eastern margin of the sub-basin (Figure 3.3).

Like the Mopane sub-basin, multi seam coals also occur in the Tshipise sub-basin. Hancox and Götz (2014) note the vitrinite content decreases with depth from 90 vol% to 80 vol% in both the Mopane and Tshipise sub-basins. Both coalfields host seven discrete coal seams alternating with carbonaceous mudstone. The Seam 6 or the No. 6 Seam in the Tshipise sub-basin has been identified as the primary economic target and is further divided into six distinct plies or horizons or seams (Figure 3.4): Seam Bottom lower (SBL), Seam Bottom Middle (SBM), Seam Bottom Upper (SBU), Seam Middle Lower (SML), Seam Middle Upper (SMU) and Seam Upper (SU) (Sparrow, 2012; de Klerk and Sparrow, 2015; Mostert, 2016). The No. 6 Seam is approximately 30-38 m thick, consisting of very brittle vitrinite-rich coal. The vitrinite content increases with depth (Luyt, 2017).

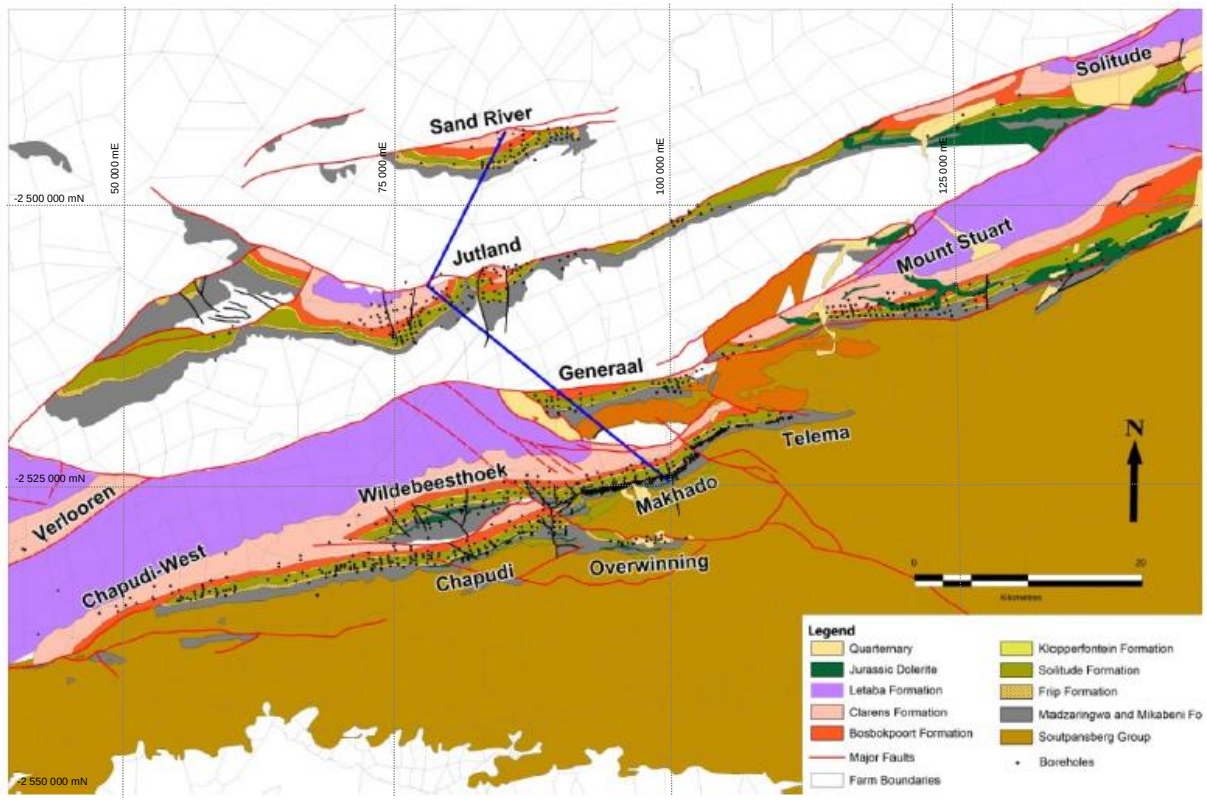

Figure 3.3. Half graben deposits across the Tshipise sub-basin (Luyt, 2013).

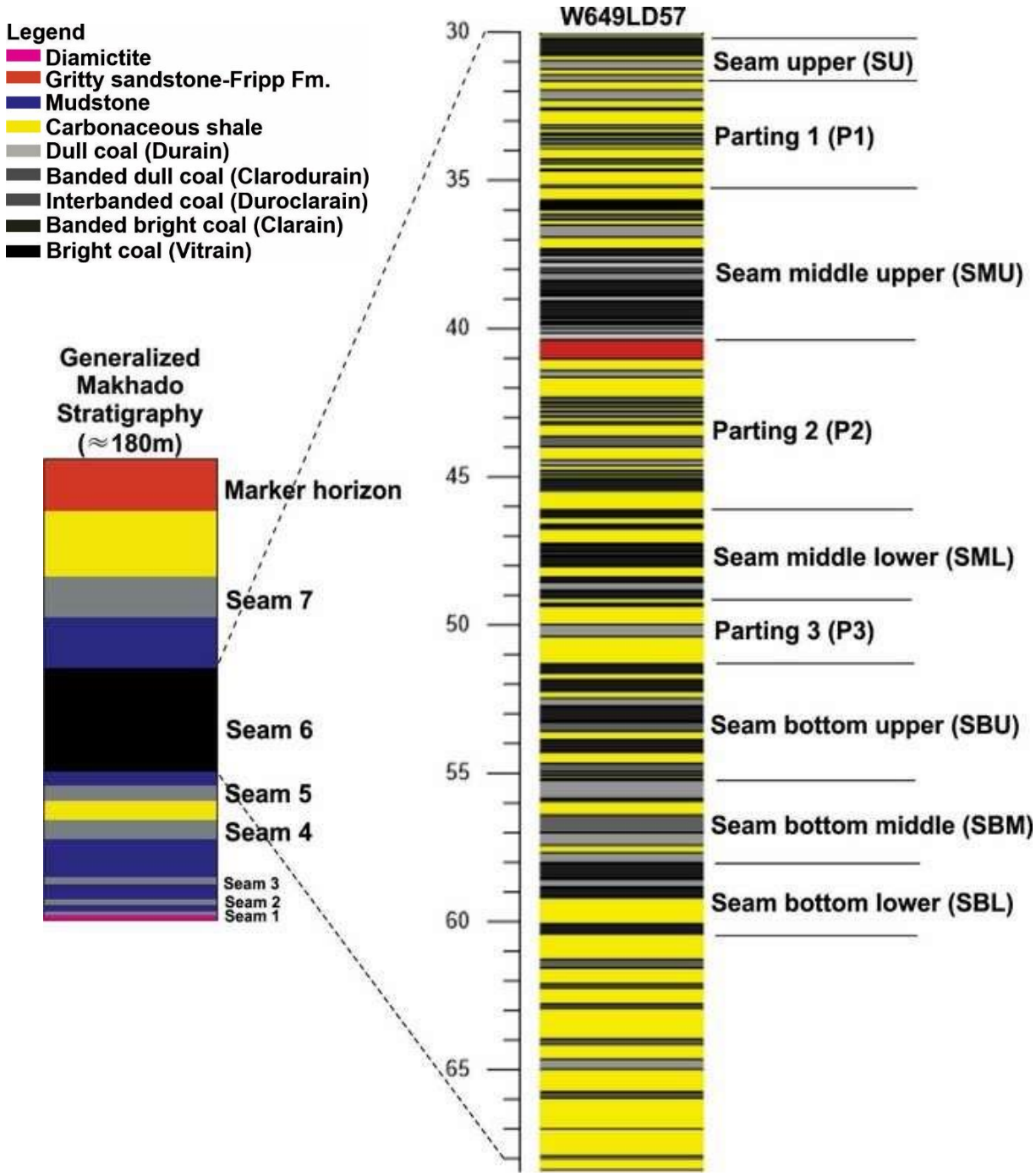

Figure 3.4. Economic coal horizons of the No. 6 Seam logged from a recent large diameter drill hole from the Makhado Project in the Tshipise sub-basin.

3.4.3. The Pafuri sub-basin

The Pafuri sub-basin occurs on the eastern arm of the Soutpansberg Coalfield. Unlike the preceding sub-basins which are characterised by seven discrete coal seams alternating with carbonaceous mudstone, the Pafuri sub-basin comprises two individual seams in the Madzaringwe Formation (Hancox and Götz, 2014). The upper seam is 3 m thick and was mined at Tshikondeni coal mine to produce HCC, while the 2 m thick lower seam was too high in phosphorus for metallurgical purposes (de Klerk and Sparrow, 2015; Mostert, 2016). Figure 3.5 shows the correlation between the coal seams across the Soutpansberg Coalfield.

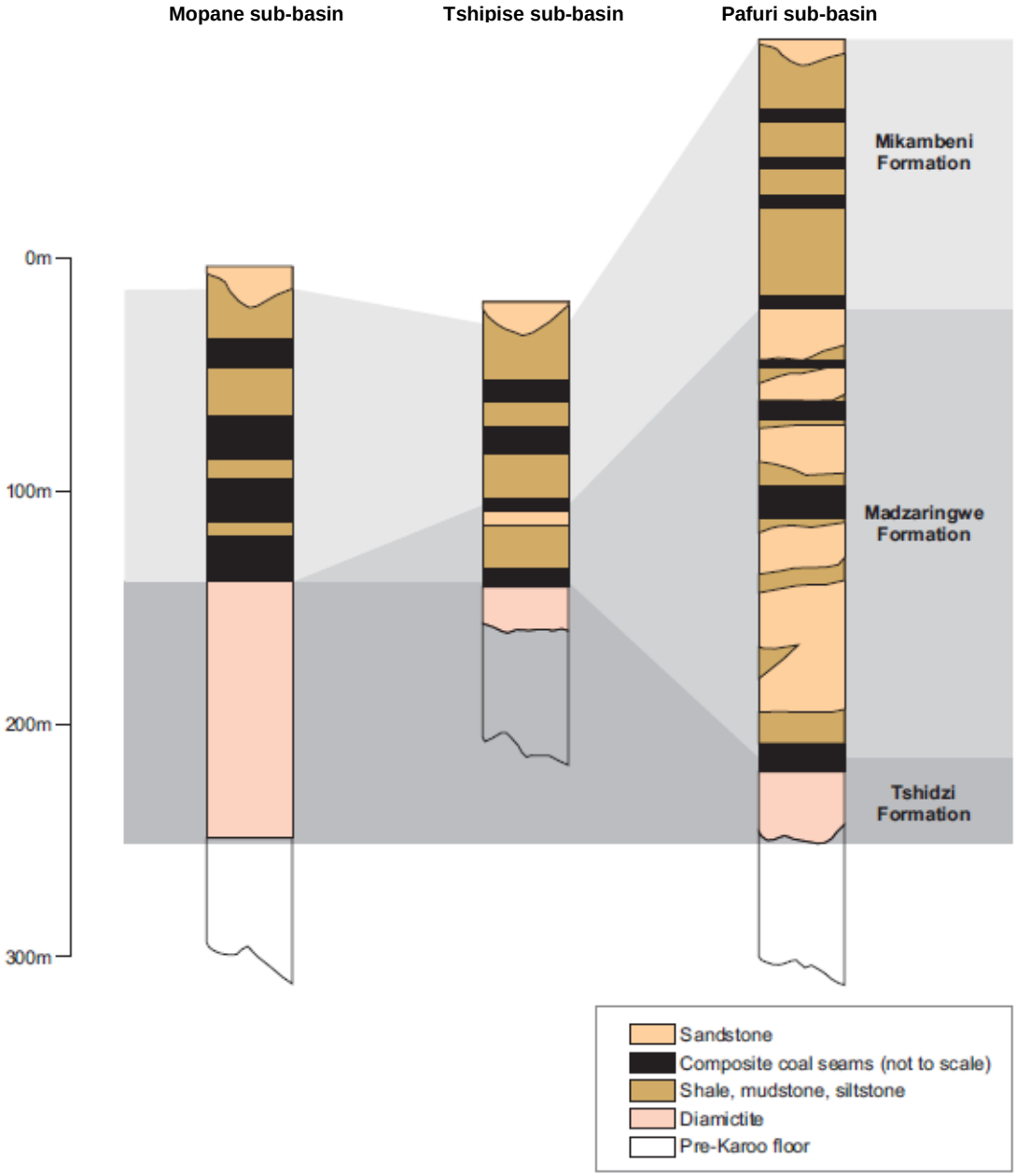

Figure 3.5. Generalized stratigraphic correlation across the Soutpansberg Coalfield (de Klerk and Sparrow, 2015).

Chapter 4: Methodology

4.1. Introduction

The scope of this study was conducted in two parts. Part 1 involved collection of the coal from the Makhado Project drill site in the Tshipise sub-basin, followed by strength testing and beneficiation test work. Part 2 of the study entailed petrographic and geochemical characterisation of selected samples obtained from the float-sink testing (-1+0.25 mm). The methods and analytical techniques conducted for this study are detailed herein.

4.2. Part 1: Drilling and Beneficiation test work

4.2.1. Background

A large dataset was obtained for Phase 1 Development in the west pit of the Makhado Project in the Tshipise sub-basin. The project development involved the drilling of four large diameter drill cores (160 mm) referred to as: T648LD88 (LD88), T648LD89 (LD89), W649LD58 (LD58) and W649LD57 (57), between November and December 2018. The locations of the borehole collars are omitted for confidentiality reasons. Strength testing and beneficiation test work was carried between December 2018 and August 2019. The drill cores intercepted the No.6 of the Madzaringwe Formation at an average depth of 30 m from surface as illustrated in Figure 4.1. The No. 6 Seam comprises the: Seam Upper (SU), Parting 1 (P1), Seam Middle Upper (SMU), Parting 2 (P2), Seam Middle Lower (SML), Parting 3 (P3), Seam Bottom Upper (SBU), Seam Bottom Middle (SBM), and Seam Bottom Lower (SBL).

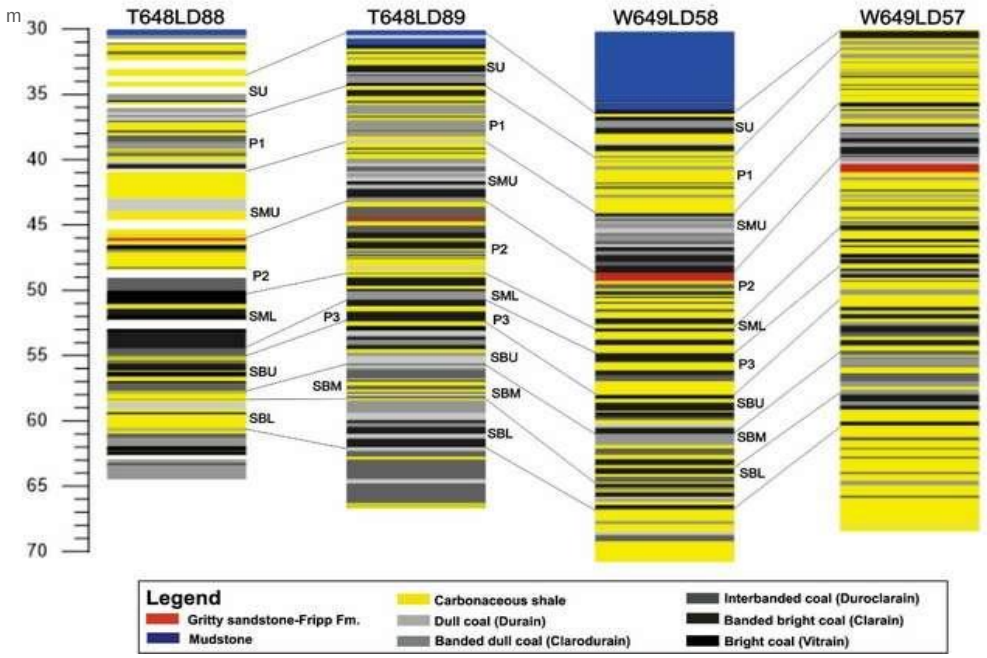

Figure 4.1. Correlation of the No. 6 Seam across drill cores from the Makhado Project, Phase 1. Seams = SU, SMU, SML, SBU, SBM and SBL. Partings = P1, P2 and P3.

The dataset for W649LD57, here on referred to as LD57, was selected as the primary focus for this research because both seams and partings were analysed and tested, affording a continuum into the vertical variations of the coal quality and beneficiation characteristics. Although large diameter drill cores are expensive to obtain and pose handling challenges, they are reliable in studying the breakage of coal in preparation for plant design (Hand, 2014).

Drill core LD57 was logged by MC Mining and sealed in bubble wrap to avoid oxidation and excess moisture gain. The seams and partings vary in thickness from 1 to 5 m, with SMU and P2 being the thickest. The photograph of LD57 (Figure 4.2) shows the horizons of the No. 6 Seam as light grey to dark grey in colour, the lighter grey Indicating zones of less coaly units. Zones with particularly friable coal during handling occur in the lowermost seams, SBU, SBM and SBL. The seams and partings were sampled in their entirety according to the intervals shown in Figure 4.1.

Previous test work entailing particle size distribution, bulk density determination and washability was conducted on a 60-tonne bulk sample from the west pit of the Makhado Project in 2011 (Mostert, 2016). The neighbouring Tshikondeni process plant was unsuccessful in yielding a 10% ash product because waste was incorporated into the coal during blasting and extraction of the sample (Mostert, 2016). Furthermore, the Tshikondeni plant was not reconfigured specifically to process the Makhado coals. The afore mentioned factors resulted in low yields (11-19%) and high ash (12-16%) product which were exacerbated by the fact that the west pit is known to have the lowest yields. Mostert (2016) further reports that the CAM Laboratory in Polokwane successfully upgraded the product obtained from the Tshikondeni test work to a 10% ash product. However, details of the washability characteristics are not publicly available. The use of a large diameter borehole in the current study avoided contamination of the seams and partings furthermore, the washability characteristics of the individual seams and partings were studied in detail including, assessment of the petrographic and geochemical properties post beneficiation.

Figure 4.2. Large diameter drill core W649LD57, courtesy of John Sparrow.

It must be noted that SBM is omitted from the Makhado resource estimate because it frequently consists of mudstone however, in some areas SBM contains enough coal to be included (Mostert, 2016). The partings are also not included as part of the resource estimate; however, they were sampled for academic interest.

Coal lithologies in the drill cores are interlaminated with [1]stone, predominantly carbonaceous shale and coaly shale. The carbonaceous shale tends to grade into silty mudstone at intervals, particularly in SU. A distinct marker horizon of gritty siltstone (20-66cm) characteristically occurs at the base of SMU, marking the onset of P2. The gritty siltstone is distinctly grey to white in colour and is feldspathic in composition.

The nomenclature of lithotypes occurring in the seams are defined in Table 4.1. In order of highest abundance, the seams comprise clarain, duroclarain, clarodurain and durain, with less vitrain as illustrated by the lithotype frequency graph (Figure 4.3A). Clarodurain and durain are slightly higher in the uppermost horizons (SMU> P2 >P1). Vitrain and clarain do not display any particular trend as they are more abundant in SML, SBU, SML and SBL (Figure 4.3A).

Table 4.1. Lithotype descriptions modified from Wagner *et al*. (2018).

Lithotype	%Bright bands	Description	MC Mining coal logging nomenclature	
Vitrain	>90%	Bright coal	CB	Bright Coal >80%
Clarain	60-90%	Banded bright coal	CMB	Coal mixed mainly Bright >60% <80%
Duroclarain	40-60%	Banded coal	CM	Coal mixed 40-60%
Clarodurain	10-40%	Banded dull coal	CMD	Coal mixed, mainly dull 20-40%
Durain	1-10%	Dull coal	CD	Coal Dull <20%
Fusain	<1%	Fibrous coal		

The major minerals observed in the drill cores are pyrite, siderite and calcite; albeit no mineral data was captured on the logs by MC Mining for SU, P1 and P3 (Figure 4.3B). Pyrite is the dominant mineral, and frequently occurs as disseminated specks (<2 mm) within the coal and stone layers. Pyrite also occurs as nodules typically 2-5mm in diameter, sometimes reaching up to 10mm at various intervals. Secondary mineralisation of pyrite was also observed along fractures in the drill core. Although abundant throughout, pyrite concentrates in the lowermost

[1] Stone in this study, collectively refers to carbonaceous shale, coaly shale, shaly coal, and mudstone. The latter is characterised by less than 10% carbonaceous matter, while the former lithologies are characterised by up to 60% inorganic constituents (Wagner *et al*., 2018).

seams. Similarly, siderite occurs in the form of specks or nodules. Carbonates are present throughout the drill core in the form of cleats, cross cutting veinlets and nodules.

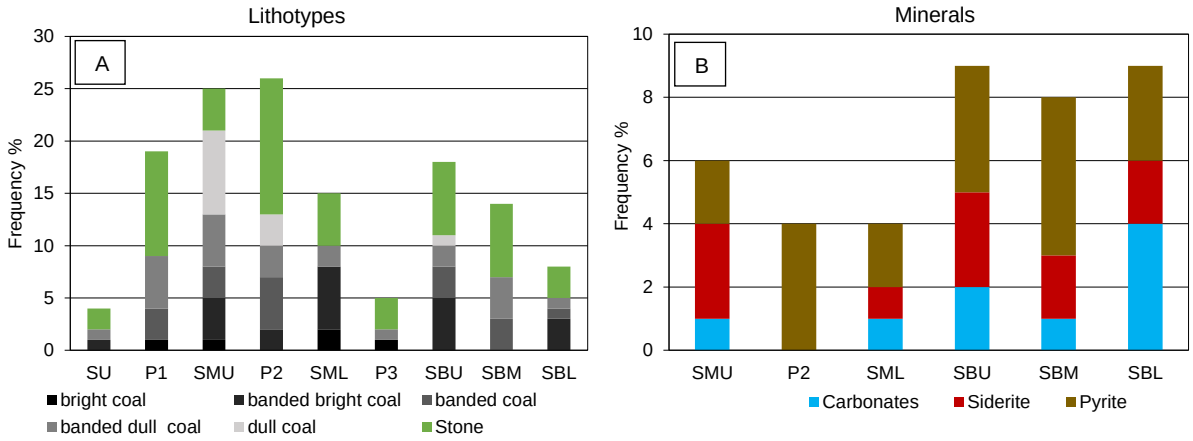

Figure 4.3. LD57 frequency distribution of (A) coal lithotypes and (B) major minerals. Note: No minerals were reported on the logs for SU and P1.

The scope of the research was covered in two parts. The laboratory test work was conducted on behalf of MC Mining by Bureau Veritas Inspectorate Laboratory in Middleburg and constitutes Part 1 of this research. Data processing and interpretation of Part 1 data were conducted by the author upon release of the results.

Part 2 of this research entailed characterising the geochemistry and petrography of selected beneficiated products from Part 1. Since the metallurgical coal properties are of interest in this research, the beneficiation products displaying the optimum particle size and cut point density for producing a 10% ash metallurgical product were selected. Figure 4.4 summarises all the analyses conducted on LD57 during Part 1 and Part 2 of this research.

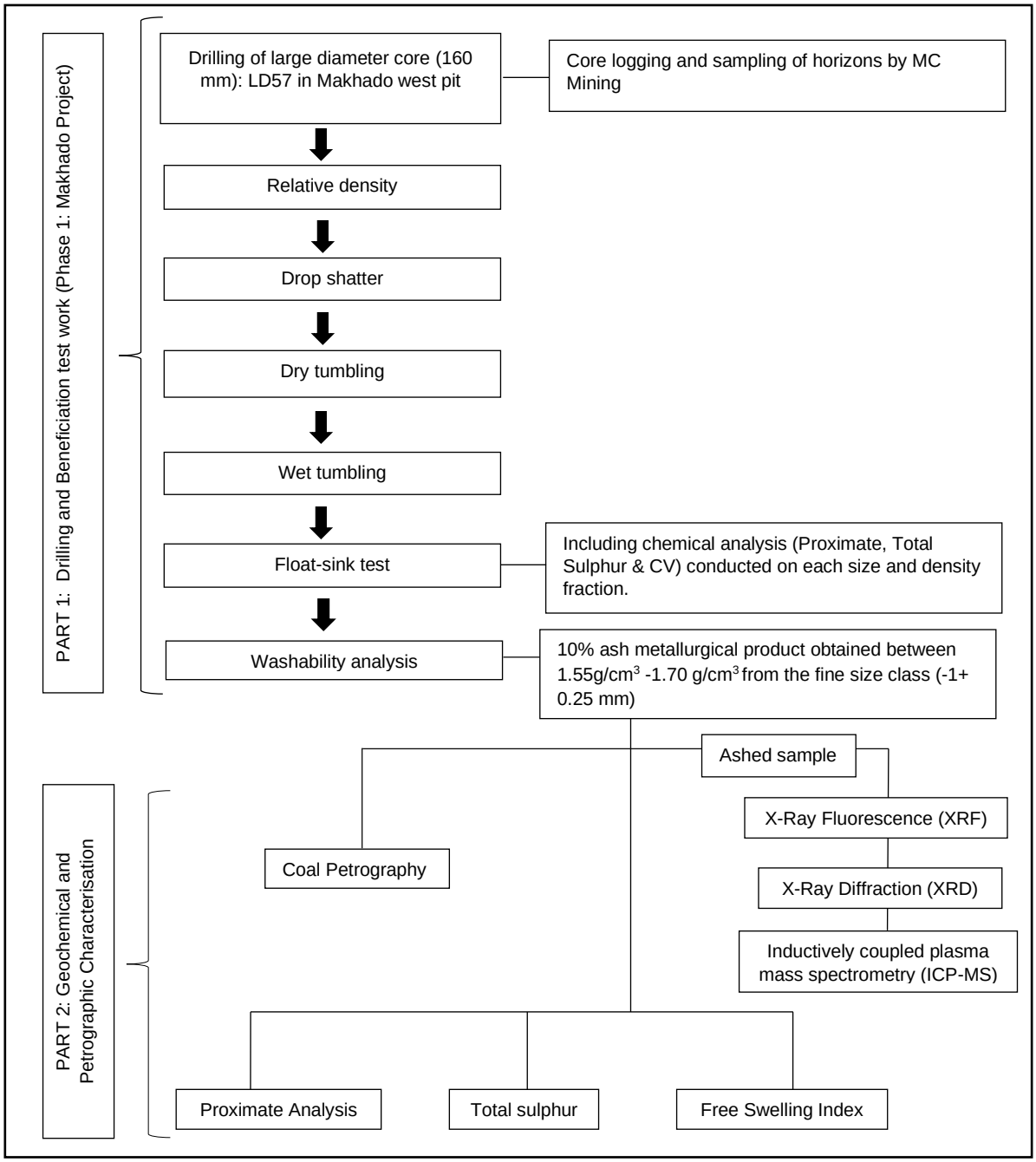

Figure 4.4. Flow diagram of methods and procedures followed during Part 1 and Part 2 of this research.

4.2.2. Relative density

Upon receipt of the large diameter cores at the Bureau Veritas Inspectorate Laboratory, the apparent relative density (Table 4.2) was determined for each seam and parting according to the Australian Standard, AS 1038.21.1.1. The data recorded in Table 4.2 was used to assist in the calculation of mass between original drill core and subsequent particles produced from processing.

Table 4.2. Relative density calculated from starting masses.

No. 6 Seam horizons	Starting mass (+2 mm) in air (g)	Mass (-2 mm) (g)	Mass (+2 mm) in water (g)	Apparent RD
SU	36260	140	15303	1.90
SMU	172070	830	70715	1.78
SML	106920	1310	46204	1.84
SBU	121860	3170	47338	1.64
SBM	123880	1820	57131	1.89
SBL	87430	600	39065	1.75
P1	108020	270	60860	2.29
P2	203400	580	91562	1.98
P3	238870	1000	103275	1.88

4.2.3. Drop shatter

The equipment used in the handling and processing of coal (e.g., conveyors, chutes, bins, end loaders, trucks etc.) result in coal breakage which affects the sizing of the coal and yields (Swanson *et al*., 1993). The drop shatter test is a means of approximating the degree to which coal will break during handling and transportation (including to the customer) after the coal is extracted from the mine (Hand, 2014). The force applied to the coal is considered to be low, resulting in gradual breakage (Shi *et al*., 2018). The drop shatter testing procedure as outlined in Esterle *et al*. (2002), Esterle (2008), and Lin *et al*. (2019), is carried out by releasing approximately 50kg of coal onto a steel plate from a predetermined height, usually 2 m. Each drop liberates particles of varying sizes based on the amount of energy exerted and the inherent properties of the coal. The resulting particle sizes reflect of the whole seam or individual ply properties in terms of rank, composition and strength. The friability of the coal is indicated by the percentage of material that has fractionated into the various size fractions investigated. The breakage data from the test is critical as it informs the design and operation of coal processing plants, which are uniquely tailored and assembled to treat coal over a specific range of particle sizes in order to maximise yields of sized coal products for end users with different specifications (Esterle *et al*.,2002; Lin *et al*., 2019).

Drop shatter testing was conducted according to the procedure outlined in AS 4156.8. 2007:

1. The entire seams and partings derived from the drill core were dropped onto a steel plate 20 times from a height of two metres. The samples ranged between 37-244kg in mass depending on seam thickness.

2. After 20 drops, the resultant daughter particles were dry screened into 13 different size fractions: +63 mm, -63+50 mm, -50+31.5 mm, -31.5+20 mm -20+16 mm, -16+12.5 mm, -12.5+8 mm, -8+6 mm, -6+4 mm, -4+2 mm, -2+1 mm, -1+0.5 mm and -0.5mm. This wide range of particle size distributions was selected to assess the breakage and partitioning behaviour of the coals as broadly as possible in order to characterise coal fine generation.

3. Each size fraction was then weighed, and the mass recorded to calculate the percentage of the original sample that partitioned into the above size fractions.

4. The drop shatter test results are presented and discussed in Chapter 5. The complete data for the drop shatter particle size distribution is tabulated in Appendix A.

It must be mentioned that a limitation of the drop shatter test as conducted in this study due to budget constraints and mine logistics; the particle size distribution was collectively determined after 20 drops and not over a number of set intervals as is common practice in the literature (Esterle *et al*., 2002, Esterle, 2008; Lin *et al*., 2019). However, this limitation is mitigated by comparing the particle distribution data after consecutive processing i.e., drop shatter followed by dry and wet tumbling, respectively.

4.2.4. Dry and wet tumbling

Dry and wet tumbling tests are conventionally used in conjunction with drop shatter and washability tests to predict the expected particle size distribution for the plant feed, as well as the amount of breakage that occurs during beneficiation, i.e., dry and wet sizing in the processing plant (Swanson, 2001; Esterle *et al*., 2002; Hand, 2014; Saurabh *et al*., 2017). The tests are important as underestimation of fine material can negatively impact plant performance in terms of loading/bottle necking (Saurabh *et al*., 2017).

Following the drop shatter test, the daughter particles of the individual seams and partings were recombined for dry tumbling. This ensures that the daughter particles are subjected to the progressive changes the parent sample undergoes at various stages of processing in the plant circuit, i.e., a single sample from transportation to dry beneficiation to wet beneficiation. The procedure is outlined as follows:

1. Dry tumbling was carried out for 5 minutes using steel cubes as per AS 4156.1 1994.
2. The samples were thereafter dry screened into eleven size fractions: +63 mm, -63+50 mm, -50+31.5 mm, -31.5+20 mm, -20+16 mm, -16+12.5 mm, -12.5+8 mm, -8+6 mm, -6+4 mm, -4+2 mm, -2+1 mm, -1+0.5 mm and -0.5 mm.
3. The weight was determined and recorded for the individual size fractions.
4. The samples of each individual seam and parting were gathered together for wet tumbling with steel cubes for 5 minutes (AS 4156.1 1994).
5. The final size distribution of the wet screen consisted of 11 size fractions as follows: -63+50 mm, -50+31.5 mm, -20+16 mm, -16+12.5 mm, -12.5+8 mm, -8+6 mm, -6+4 mm, -4+2 mm, -2+1 mm, -1+0.5 mm and -0.5+0.25 mm.
6. Particle sizes of +63mm were hand knapped, and the resultant fractions added to the respective screen sizes.
7. The weights were recorded for the different size fractions.
8. The results for the dry and wet tumble tests are presented and discussed in Chapter 5, the complete datasets are tabulated in Appendix B and C, respectively.

4.2.5. Float-sink test

The float-sink test is a gravity-based separation method that is carried out to determine the extent to which organic matter can be separated from mineral matter. To achieve this, raw coal that has been crushed and sized, is immersed in a liquid of a known density that allows the organic matter to float while the denser particles settle. The process is repeated on the sink material using liquids of different relative densities, typically in the range 1.30-2.0g/cm^3 (England *et al*., 2002; Thomas, 2012).

The objective of conducting float-sink test was to determine the optimal particle size and density to produce the desired nominal metallurgical product of 10% ash. The float-sink test was conducted according to ISO 7936 at the Bureau Veritas Inspectorate Laboratory, Middleburg, South Africa. Following the wet tumbling test as described in Section 4.2.4, the ‘wet screened’ fractions were gathered and screened into six conventional size fractions for float-sink testing: -63+50mm, -50 +31.5mm, -31.5+20mm, -20+6mm, -6+1mm and -1+ 0.25mm.

Typically, vitrinite-rich coals partition into the low-density fractions between 1.30-1.40 g/cm^3, whereas inertinite rich coals, tend to partition in the higher density fractions (1.40-1.70 g/cm^3) (Bergh *et al*., 2013). Hence, each size fraction in this study was floated at thirteen densities:

F1.30, F.1.32, F1.35, F1.38, F1.40, F.45, F1,50, F1.55, F1.60, F1.70, F1.80, F1.90, F2.00 and S2.00. Smaller density increments between 1.3 and 1.4 g/cm^3 were selected to test whether more of the vitrinite particles would concentrate within that range since vitrinite, the major constituent of coking coal, generally has a density between 1.22 and 1.40 g/cm^3 in bituminous coals.

Coal quality (proximate, total sulphur and calorific value) analyses were conducted on each float-sink fraction at the Bureau Veritas Inspectorate Laboratory. The proximate analysis entailed determination of moisture (SANS 5925), volatile matter (ISO 562), and ash (ISO 1171). In addition, total sulphur (ASTM: D4239) and the gross calorific value (ISO 1928) were also determined. The data is reported on air dried basis (adb) for both fractional and cumulative yields in Chapter 7.

4.1.5.1. Washability analysis

The results obtained from the float-sink test were used to prepare washability curves to assess the extent to which coal of varying size fractions can be efficiently separated from mineral matter (reported in Chapter 6), while maintaining suitable coal quality specifications in terms of calorific value, ash, total sulphur, fixed carbon, moisture and volatile matter at particular relative densities (reported in Chapter 7).

Standard washability entails plotting several washability curves to graphically illustrate the relationships between the yield of the float/sink material, density and ash (Figure 4.5). The fundamental washability curves are the elementary ash curve, cumulative float curve, cumulative sink curve, specific density curve and the near gravity material curve (Holuszko and Grieve, 1990; Thomas, 2012). These washability curves enable plant designers and operators to determine the yield that will be obtained at specific cut densities and the ash content of the discard material for different coal products that could be produced by the plant (Laskowski, 2001). However, since the analysis is performed under perfect or ideal separation conditions, all deduced values are considered as being theoretical and therefore may not truly be indicative of realistic yields and separation conditions (England *et al*., 2002).

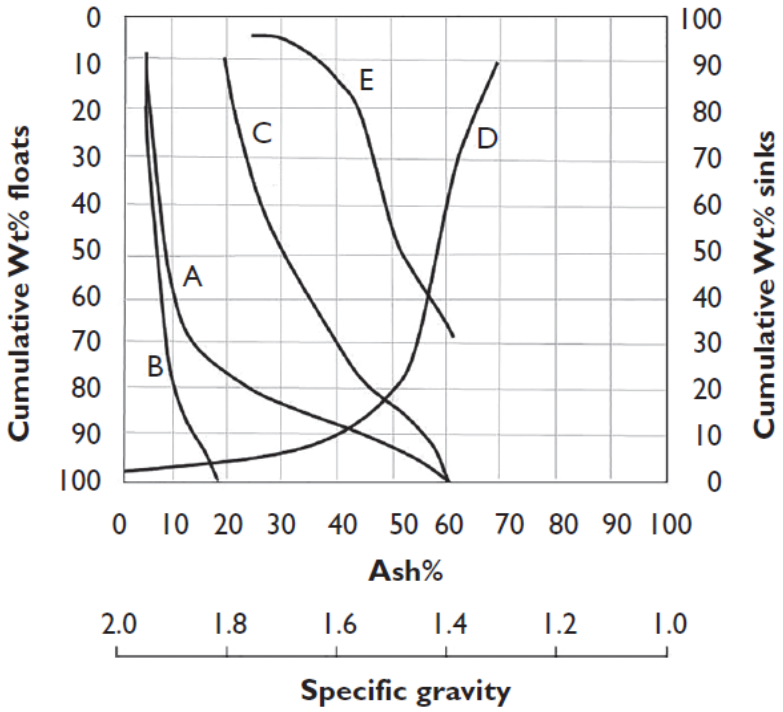

Figure 4.5. Fundamental washability curves: Elementary ash (A), cumulative float (B), cumulative sink (C), specific gravity (D), near gravity material (E) (Subba Rao and Gouricharan, 2016).

- **Elementary ash curve (A)**

  The elementary ash curve (Figure 4.5), also referred to as the characteristic curve, fractional yield curve or primary washability curve, is a direct approximation of the amount of ash present within the cumulative floats at set densities. It is obtained by plotting the cumulative yield percentage of floats versus the fractional ash yield percentage. (Thomas, 2012; Subba Rao and Gouricharan, 2016).

  Mathematically, the elementary curve is the derivative of the cumulative curve and shows the rate of change of the ash content at different yields (Coe,1938). In other words, the elementary curve is intended to show the ash percentage in the highest ash particle included in a floatation product of any given cumulative weight percentage. The elementary ash curve is said to indicate ease of separation which varies from easy to difficult based on the shape or slope of the elementary ash curve. L-shaped elementary ash curves positioned near the vertical axis approximate easier separation, while difficult separation conditions can be expected when elementary ash curves show a steep or near vertical slope that parallels the vertical axis (Bhattacharya *et al*., 2016; Subba Rao and Gouricharan, 2016).

- **Cumulative float curve (B)**

  The cumulative float or total floats curve (Figure 4.5) illustrates the relationship between the cumulative yield percentage of the floats at each relative density against the cumulative ash percentage of the total floats.

- **Cumulative sinks curve (C)**

  The cumulative sinks curve (Figure 4.5) is obtained by plotting the cumulative yield percentage of the sink material against the cumulative ash percentage of the sinks, at specific relative densities (Subba Rao and Gouricharan, 2016).

- **Densimetric curve (D)**

  The densimetric, density or specific gravity curve (Figure 4.5) illustrates the relationship between the relative density and the cumulative yield of clean coal that floats at that relative density. The curve is used to quantify the amount of coal that is expected to float at specified relative densities (England *et al*., 2002).

- **Near Gravity Material curve (E)**

  The near gravity material (NGM) or near density material (NDM) curve (Figure 4.5) shows the percentage (by weight) of coal that lies between ± 0.10 specific gravity unit at any given gravity of separation (Coe, 1938). The NGM is therefore a quantitative parameter to assess the ease or difficulty with which coal can be beneficiated. NGM are particles that have densities close (within ± 0.10 of the cut density) to that of the separation liquid, making separation difficult since additional time is required to allow the NGM to sink (Kumar and Kumar, 2018). The presence of NGM in coal coupled with prolonged settling time triggers the phenomenon of `misplaced material` during coal cleaning such that some of the float material may sink over time and incorrectly report to the sink fraction; conversely, some of the sink material may incorrectly report to the float fraction if insufficient time is given for settling (de Korte, 2008; Bhattacharya *et al*., 2016). Bird (1931) devised a classification scheme (Table 4.3) to interpret the ease or difficulty of separation based on the calculated percentage of ± 0.10 NGM (Equation 4.1).

Table 4.3. Bird`s Classification on the Ease of separations (Subba Rao and Gouricharan, 2016).

± 0.1 Specific gravity material %	Degree of separation	Suitable Process
0-7	Simple	Jigs, spirals, teetered bed separators
7-10	Moderate	
10-15	Difficult	Dense Medium Baths (DMB), Dense Media Cyclone (DMC)
15-20	Very difficult	
20-25	Exceedingly difficult	
>25	Formidable	Dense Medium Baths, DMC

The ± 0.10 near density values in this study were calculated as follows (Enslin and Bekker 2019):

$$\pm 0.10\ value\ at\ 1.40\ g/cm^3 = yield\ at\ 1.50\ g/cm^3 - yield\ 1.30\ g/cm^3 \qquad \text{[Equation 4.1]}$$

$$\pm 0.10\ value\ at\ 1.50\ g/cm^3 = yield\ at\ 1.60\ g/cm^3 - yield\ 1.40\ g/cm^3$$

$$\pm 0.10\ value\ at\ 1.60\ g/cm^3 = yield\ at\ 1.70\ g/cm^3 - yield\ 1.50\ g/cm^3$$

$$\pm 0.10\ value\ at\ 1.70\ g/cm^3 = yield\ at\ 1.80\ g/cm^3 - yield\ 1.60\ g/cm^3$$

$$\pm 0.10\ value\ at\ 1.80\ g/cm^3 = yield\ at\ 1.90\ g/cm^3 - yield\ 1.70\ g/cm^3$$

$$\pm 0.10\ value\ at\ 1.90\ g/cm^3 = yield\ at\ 1.80\ g/cm^3 - yield\ 2.00\ g/cm^3$$

Although the traditional ± 0.10 NGM criterion has been adopted almost universally across the coal industry, several issues have been encountered regarding the use thereof (de Korte, 2008; Bhattacharya *et al*., 2016). Bird's classification is based on coal washing in jigs and does not encompass variations in the efficiency of various coal cleaning methods available such as Dense Medium separation (DMS) (Bhattacharya *et al*., 2016). DMS is the common coal cleaning method employed on South African coals and is significantly more efficient than jigs. DMS allows for sharp separation and can accommodate coals with higher proportions of NGM i.e., greater than 25% (de Korte, 2008). The revised criterion summarized in Table 4.4 ensures that a narrower density range is applied to more efficient separation process where the effect of NGM is less, thereby reducing the tendency of coals being classified as formidable (Bhattacharya *et al*., 2016). Therefore, for comparison, the revised ± 0.05 NGM was determined for each seam and parting at densities of 1.35 g/cm^3, 1.40 g/cm^3, 1.45 g/cm^3, 1.50 g/cm^3 and 1.55 g/cm^3.

Table 4.4. Revision of Bird`s classification (Kumar and Kumar, 2018)

± 0.05 Specific gravity material %	Degree of separation
0-20	Easy
21-40	Moderately difficult
41-50	Difficult
>50	Extremely difficult

The ± 0.05 near density values in this study were calculated as follows:

$\pm 0.05\ value\ at\ 1.35\ g/cm^3 = yield\ at\ 1.30\ g/cm^3 - yield\ 1.40\ g/cm^3$ [Equation 4.2]

$\pm 0.05\ value\ at\ 1.40\ g/cm^3 = yield\ at\ 1.35 g/cm^3 - yield\ 1.45 g/cm^3$

$\pm 0.05\ value\ at\ 1.45\ g/cm^3 = yield\ at\ 1.40\ g/cm^3 - yield\ 1.50\ g/cm^3$

$\pm 0.05\ value\ at\ 1.50\ g/cm^3 = yield\ at\ 1.45\ g/cm^3 - yield\ 1.55\ g/cm^3$

$\pm 0.05\ value\ at\ 1.55\ g/cm^3 = yield\ at\ 1.50\ g/cm^3 - yield\ 1.60\ g/cm^3$

Due to the high volume of float-sink data obtained in this study, the results are discussed in two parts as follows:

- Chapter 6, Part 1 Washability

Washability curves for float and sink yields are reported at specific densities and particle sizes. The ease of separation for each seam is discussed based on ± 0.10 vs ± 0.05 NGM.

- Chapter 7, Part 2 Washability- coal quality

Washability curves in terms of coal quality (calorific value, ash, total sulphur, fixed carbon, moisture and volatile matter) are presented at specific densities and particle sizes.

4.3. Part 2: Geochemical and petrographic characterisation

The float fractions from the fine size class (-1+0.25mm) between the 1.30 -1.70g/cm^3 density interval, were selected for further analyses as this material yielded the desired 10% ash product in alignment with the main objective of this research, i.e., assessing the impact of beneficiation on metallurgical coal. Part 2 of this research focuses on characterising the geochemistry and petrography of this selected density and size fractions (fine-float samples).

4.3.1. Sample preparation for Part 2 analyses

Density fractions from the fine size class (-1+0.25mm) between 1.30 -1.70 g/cm^3, and ash ≤ 10% were combined to create a composite sample for further analysis for each of the nine horizons (Table 4.5). This procedure ensured enough sample material would be available for the various analyses for Part 2 of the research. The composite samples (fine-float) were cone and quartered such that the first quarter was reserved for coal petrography. The remaining three quarters were milled down to -212 µm and split further for the characterisation of the coal quality (Proximate analyses and Total sulphur), carbonization properties (FSI) and mineral composition (X-Ray Diffraction). Another quarter was ashed to determine the major oxide (XRF), trace element and REY+Sc composition using Inductively Coupled Plasma Mass Spectrometry (ICPMS).

Table 4.5. Selected density range for composite samples in -1+0.25mm size fraction.

No. 6 Seam horizons	Density range where ash ≤ 10%
SU	1.30 to 1.55 g/cm^3
P1	NO 10% ash BUT ash ≤ 9% between 1.30 to 1.50 g/cm^3
SMU	1.30 to 1.60 g/cm^3
P2	1.30 to 1.45 g/cm^3
SML	1.30 to 1.60 g/cm^3
P3	NO 10% ash BUT ash ≤ 9% between 1.30 to 1.70 g/cm^3
SBU	1.30 to 1.70 g/cm^3
SBM	1.30 to 1.70 g/cm^3
SBL	1.30 to 1.55 g/cm^3

4.3.2. Coal petrography

The application of coal petrography in this study was firstly used to assess the effect of gravity based separation on the microscopic coal composition. Lastly, to determine the suitability of this composition for metallurgical use, which is dependent on the type of organic and inorganic constituents occurring in the coal, their quantity, and mode of occurrence at a microscopic level.

Coal petrography was conducted using the Zeiss Axio Imager M2M petrographic microscope, equipped with a Hilgers Fossil system housed at the University of Johannesburg. The system enables routine coal analysis (vitrinite reflectance, maceral point count) and high-resolution imaging of samples using the monochromatic and colour cameras.

Petrography blocks for the fine-float samples were prepared according to SANS (ISO) 7404-2:2015, ensuring smooth, scratch free surface for analysis.

4.3.2.1. Maceral point count

The composition of the coal horizons was determined through the maceral point count, whereby various macerals and minerals were identified and quantified following SANS 7404-3:2016. The semi-automated point counting stage traversed across the polished block surfaces. A total magnification of x500 under oil immersion in reflected white light was used for the analysis to count a minimum of 500 points. This study considered twenty-eight macerals and minerals (Table 4.6), broadly following the classification system of the International Committee for Coal and Organic Petrology (ICCP). Furthermore, consideration for the presence of pseudovitrinite and the distinction of semifusinite into its reactive and inert forms was taken into account (Wagner *et al*., 2018).

Table 4.6. Maceral and mineral groups selected for identification.

Vitrinite (ICCP, 1998)	Inertinite (ICCP, 2001)	Liptinite (Pickel *et al*., 2017)	Mineral groups (ICCP, 1998)
Telinite (TEL)	Fusinite (FUS)	Sporinite (SP)	Carbonates (calcite (Cal), siderite (Si))
Collotelinite (COL)	Inert semifusinite (ISF)	Cutinite (CUT)	Silicates (quartz (Qu), clay minerals (Cl))
Gelinite (GEL)	Reactive semifusinite (RSF)	Resinite (RES)	Sulphides (pyrite (P))
Corpogelinte (COR)	Funginite (FG)	Alginite (ALG)	
Vitrodetrinite (VD)	Secretinite (SEC)	Liptodetrinite (LD)	
Collodetrinite (CD)	Macrinite (MAC)	Suberinite (EX)	
Pseudovitrinite (Ps)	Micrinite (MIC)	Exsudatinite (EX)	
	Inertodetrinite (IN)		

4.3.2.2. Vitrinite reflectance

Coal rank was determined using the mean random reflectance (%RoV), with values measured on collotelinite macerals. These macerals show consistent changes in carbon content and volatile matter with increasing rank, making them suitable for reliable measurements (ICCP, 1998). Maximum reflectance ($\%R_{max}$) readings are the preferred unit of measurement for metallurgical coals due to the increase in vitrinite anisotropy with rank (Davis, 1978; Lu *et al*., 2013). Both %RoV and $\%R_{max}$ measurements were taken on the samples.

The monochrome camera was used to measure the %RoV and $\%R_{max}$ on a minimum of 100 points of collotelinite present in each sample. Measurements were taken under green reflected light using a 50x oil objective as the semi-automated stage of the microscope moved in a predetermined raster pattern across the surface of the coal block.

For quality control purposes, the microscope was calibrated using a yttrium-aluminium-garnet (YAG) standard to ensure the intensity of reflected light at 0.90%, with standard deviation of 0.1% in accordance with SANS 7404-5:2016.

The reflectance measurements are presented as histograms in Appendix D, showing both $\%R_{max}$ and %RoV values.

In addition, the vitrinoid type (v-type) was determined for each fine-float sample. Each vitrinoid type represents 0.1% reflectance ranging from V-7 through V-18 or 19 (Davis, 1978; Raaness and Gray, 1995).

4.3.2.3. Microlithotype analysis

The microlithotype analysis is important for characterising the behaviour of coal based on the maceral interrelationships and maceral-mineral associations. Similar to the maceral point count, the microlithotypes were analysed under reflected white light with oil immersion. At least 500 points were characterised on a 25-micron radius of the cross hairs in the field reticule (SANS 7404-4:2020). Table 4.7 summarizes the microlithotype assemblage characterised in this study.

Table 4.7. Microlithotype assemblage (Hower, 2008: Suárez-Ruiz, and Crelling, 2008; Wagner *et al*., 2018).

Microlithotype		Composition (vol%)
Monomaceral	Vitrite	Vitrinite (V) > 95%
	Inertite	Inertinite (I) > 95%
	Liptite	Liptinite (L) > 95%
Bimaceral	Vitrinertite	V + I > 95%
	Clarite	V + L > 95%
	Durite	I + L > 95%
Trimaceral	Duroclarite	V > L, I; each > 5%
	Clarodurite	I > V, L; each > 5%
	Vitrinertoliptite	L > V, I; each > 5%
Carbominerite	Carbargilite	Coal + 20-60% clay minerals
	Carbosilicate	Coal + 20-60% quartz
	Carbopyrite	Coal + 5-20% sulphides
	Carbankerite	Coal + 20-60% carbonates
	Carbopolyminerite	Coal + *20-60% mineral matter
Rock	Minerite	> 60% mineral matter

*5% if high pyrite

4.3.3. Coal chemistry

The chemical composition of the fine-float samples was determined by proximate and total sulphur analyses. The analyses were conducted at the coal laboratory in the Council for Geosciences, Pretoria.

The proximate analysis entails determination of ash (ISO 1171), inherent moisture (SANS 5925), volatile matter (ISO 562:2010) and fixed carbon by difference. Total sulphur was determined using the Leco CHN 628 based on ASTM standard D4239-14-2014.

4.3.4. Free Swelling (FSI)

The FSI was used to assess the fine-float samples for metallurgical use in coke making (Wagner *et al*., 2018). The FSI was conducted according to ISO 501: 2012, at the Council for Geosciences Laboratory, Pretoria.

The FSI is carried out by weighing 1 g of sample into a silica crucible. Care must be taken to evenly distribute the sample material into the crucible to ensure that the extent of swelling in terms of shape or profile is accurate. The crucible is then sealed and heated for one minute and thirty seconds, during which the flame of the burner changes from orange to blue, signalling the release of volatiles. Once all the volatiles were driven off, the flame turns orange, and the burner is switched off. Samples are analysed in triplicate and a certified coal reference material with a known FSI value is used to verify the results. The average shape/profile is reported. After cooling, the resultant coke bottoms are classified using standard swell profiles (Figure 4.6).

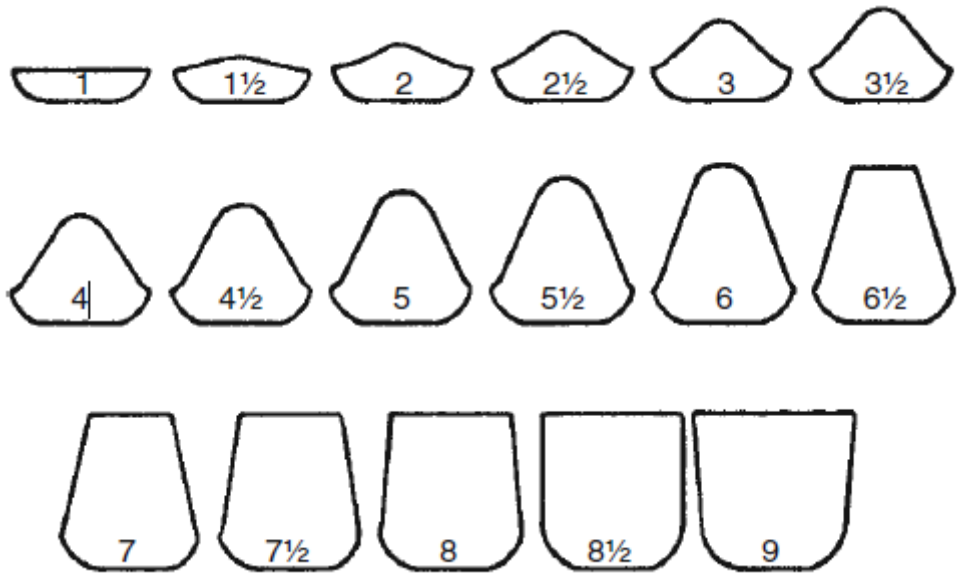

Figure 4.6. Characteristic coke buttons for FSI Test (Thomas, 2012).

4.3.5. X-Ray Diffraction (XRD)

X-Ray Diffraction is a non-destructive technique that was used to identify and quantify the mineral phases present in the fine-float samples described in Section 4.3.1. The samples were milled to -212 µm and at sent for analysis at XRD Analytical and Consulting cc, based in Pretoria. Diffractograms were obtained using a Malvern Panalytical Aeris diffractometer with PIXcel detector and fixed slits with Fe filtered Co-Kα radiation. The phases were identified

using X'Pert Highscore plus software. The relative phase amounts (weight %) were estimated using the Rietveld method.

4.3.6. X-Ray Fluorescence (XRF)

X-Ray fluorescence was utilised to determine the major oxide composition of the samples. The sample splits were ashed in preparation for the XRF and ICP-MS analysis. The ashing procedure involved gradually heating up the coal to a maximum temperature of 815°over a three-hour period as follows:

1. heat up sample from 25 ° to 500 ° C for 1 hour.
2. leave sample at 500° C for 30 minutes.
3. heat up sample from 500° C to 815° C for 30 minutes.
4. Leave sample at 815° C for 1 hour before cooling back to room temperature.

The above ashing procedure was carried out at, MAK Analytical Laboratory, Johannesburg.

The XRF analysis was carried out at the Earth Lab, University of the Witwatersrand. Major elements were determined using the Norrish Fusion 1 technique (Norrish and Hutton, 1969) using in-house correction procedures and using a Panalytical X-ray fluorescence spectrometer. Major elements were fused using Johnson Matthey Spectrolflux 105 at 1000°C into a glass bead and raw data corrected using in-house software. Standard calibrations were made up using synthetic oxide mixtures and international standard rocks as well as in-house controls. Sample weight used was 0.35g and flux weight 2.0g. Calibration standards were primary International Reference Materials USGS series (USA) and NIM series (South Africa). Precision is taken as 1% for elements in abundance of greater than 5% by weight, and 5% for elements in abundance less than 5%. The instrument used was the Panalytical Axios x-ray spectrometer and samples were analysed at 50kV and 50mA. Standard calibrations use BCR2, NIM-P, NIM-D, W-2, NIM-S, GSP-2, NIM-N, NIM-G, PCC1, BHVO2, AGV2, G2 DTS (Appendix E).

4.3.7. Inductively Coupled Plasma Mass Spectrometry (ICP-MS) analysis

For the purpose of this research, it was of interest to determine the level of trace elements and REEs, including yttrium (REY) and scandium (REY+Sc) occurring in the ash of the fine-float samples. Assessment of these elements in the samples is important to determine the level of potentially harmful elements, as well as to determine their economic potential as a secondary source of critical REE for the application in new technologies (Kumar and Kumar, 2018; Wagner and Matiane, 2018).

The ICP-MS method was utilised for the identification and quantification of trace elements and REEs present in the coal floats. Table 4.8 summarizes the suite of the trace elements and REEs analysed in this study.

Table 4.8. List of trace elements and REE studied in the research.

Symbol	Element	Symbol	Element
Li	Lithium	La	Lanthanum
P	Phosphorus	Ce	Cerium
Ti	Titanium	Pr	Praseodymium
V	Vanadium	Nd	Neodymium
Cr	Chromium	Sm	Samarium
Co	Cobalt	Eu	Europium
Ni	Nickel	Gd	Gadolinium
Cu	Copper	Tb	Terbium
Zn	Zinc	Dy	Dysprosium
Ga	Gallium	Ho	Holmium
Rb	Rubidium	Er	Erbium
Sr	Strontium	Tm	Thulium
Zr	Zircon	Yb	Ytterbium
Nb	Niobium	Lu	Lutetium
Sn	Tin	Y	Yttrium
Sb	Antimony	Sc	Scandium
Cs	Caesium		
Ba	Barium		
Hf	Hafnium		
Ta	Tantalum		
W	Tungsten		
Tl	Thallium		
Pb	Lead		
Th	Thorium		
U	Uranium		

The ICP-MS analysis was carried out using the Thermo Scientific iCAP RQ instrument at the Earth Lab, University of the Witwatersrand. The Thermo Scientific iCAP RQ is optimised for maximum counts on oxide levels set to less than 2% as well as doubly charged ions set to less than 2%. Three replicate measurements were taken for each sample and averaged. Replicates deviating by more than 2% were flagged.

The ashed samples were digested in a Microwave digester (MARS from CEM) as follows:

1. 50 mg was weighed into a teflon vessel containing a mixture of 6 ml of ultra-high purity 2:1 HF: HNO_3.

2. The mixture was microwaved for 40 minutes at 180°C and 400 PSI.
3. The sample was then transferred to a 15 ml savilex beaker and the teflon vessel was rinsed out thoroughly.
4. The savilex beaker was capped and placed on a hotplate for 24 hours at 70°C to allow the acid to evaporate.
5. 2 ml of HNO_3 was added to the sample and capped and placed on the hotplate for a further 24 hours.
6. The acid was dried at 70°C, and a further 2 ml of HNO_3 was added and allowed to evaporate off.
7. The samples were then removed from the hot plate and 300 µl HNO_3 was added, samples were stored in this state until ready to analyse.
8. The samples are diluted to 50 ml (Dilution Factor 1:1000) with 5% HNO_3 with 100 ppb Re and Rh as well as 50 ppb In and Bi, these elements are internal standards and are monitored throughout the analyses. Fluorides are minimised by allowing minimal contact between the sample and HF while still accomplishing total digestion. Samples are visually inspected for fluorides which occur as a precipitate once diluted.
9. Calibration standards are made at 5 different concentrations (10, 30, 50, 75 and 100 ppb) with all the elements to be analysed present (40 elements) from purchased International Certified Reference Materials (Appendix F).
10. The Certified Reference Materials (CRM) are digested and analysed with all unknowns, usually BCR-1, BHVO-2 and BIR-1. The CRM's must return less than 10% deviation from known concentrations for all elements to pass the quality controls, they are usually within 5%. A Total Procedural Blank (TPB) is analysed with all unknowns, this entails a beaker with no sample but taken through the whole sample digestion procedure. This gives an indication of Blank levels and how clean the preparation laboratory is. Ideally all data should be TPB subtracted.

For interpretation, the REY+Sc data was arranged into three classes according to Franus *et al*. (2015):

1. Light (LREE): Sc, La, Ce, Pr, Nd, Sm.
2. Medium (MREE/MREY): Y, Eu, Gd, Tb, Dy.
3. Heavy (HREE): Ho, Er, Tm, Yb, Lu.

Furthermore, the REY+Sc data of the fine-float samples was normalized using values calculated from the upper continental crust (UCC) for sediments derived from Taylor and McLennan (1985), as shown in Table 4.9. Moreover, REY+Sc values for hard coal and coal

ash determined by Ketris and Yudovich (2009) were used to compare with the results for the fine-float samples (Chapter 9).

Table 4.9. Concentration (ppm) of REY+Sc in the UCC and World hard coals.

Element	UCC values (Taylor and McLennan, 1985)	Coal Clarke values (Ketris and Yudovich. 2009)	
		Hard coal	Hard coal ash
La	30	11±1	76±3
Ce	64	23±1	140±10
Pr	7.1	3.4±2	26±3
Nd	26	12±1	75±4
Sm	4.5	2.2±0.1	14±1
Eu	0.88	0.43±0.02	2.6±0.1
Gd	3.8	2.7±0.2	16±1
Tb	0.64	0.31±0.02	2.1±0.1
Dy	3.5	2.1±0.1	15±1
Ho	0.8	0.57±0.04	4.8±0.2
Er	2.3	1±0.07	6.4±0.3
Tm	0.33	0.3±0.02	2.2±0.1
Yb	2.2	1.0±0.06	6.9±0.3
Lu	0.32	0.2±0.01	1.3±0.1
Y	22	8.2±0.5	57±12
Sc	11	3.7±0.2	24±11

Chapter 5: Drop Shatter and Tumbling tests

5.1. Introduction

The breakage properties of the LD57 coal samples were investigated with respect to coal strength, particularly friability, which describes the manner in which coal breaks during handling. The breakage characteristics were determined using standard techniques of drop shatter, dry tumbling and wet tumbling tests as described in Chapter 4. The change in the sample mass after drop shatter, dry tumble and wet tumble testing (Appendices A, B & C) were calculated as percentages presented and discussed in this chapter. The afore mentioned tests approximate relatively low energy events during production such as transportation and handling and do not necessarily account for high energy events such as blasting and crushing which occur in the mine pit during excavation and extraction. The tests are integral in estimating the distribution of particle sizes that will be beneficiated at the processing plant. This chapter addresses objectives for part one of this research.

For ease of discussion, the size fractions are grouped into the following size classes:

- **Coarse:** +63 mm, -63+50 mm, -50+31.5 mm and -31.5+20 mm
- **Intermediate:** -20+16 mm, -16+12.5 mm, -12.5+8 mm, -8+6 mm, -6+4 mm, -4+2 mm and -2+1 mm
- **Fine:** -1+0.50 mm
- **Ultrafine:** all particles -0.50 mm

5.2. Drop shatter results

After twenty drops, the daughter particles in the seams and partings predominantly partitioned into the coarse size class (59% to 88%), followed by intermediate (9% to 29%), ultrafine (2% to 9%) and fine (1% to 3%) size classes (Table 5.1). Furthermore, coarse particles were generally highest in the partings and uppermost seams: SU, SMU and SML. The lower most seams (SBU, SBM and SBL) contained slightly less proportions of coarse particles (Table 5.1). Intermediate particles were highest in the lowermost seams (26% to 29%) compared to the uppermost seams (21% to 25%). The partings have the lowest proportion of intermediate particles (10% to 20%). The proportion of fine particles is relatively uniform with depth, but the partings generally have fewer fine particles (1% to 2%) relative to the coal seams (3%). The proportion of ultrafine particles generally increases with depth such that the lower most seams have higher (4% to 9%) proportions of ultrafine particles compared to the uppermost seams (4% to 5%) and partings (2% to 3%).

Table 5.1 Drop shatter results (%) for LD57.

No. 6 Seam horizons	Strength Test	Coarse: +63mm to +20mm	Intermediate: -20mm to +1mm	Fine: -1mm to +0,5mm	Ultrafine: > -0,5mm	Total
	Drop shatter	69	25	3	4	100
	Dry tumbled	53	30	7	11	100
SU	Wet tumbled	50	28	5	7	90
	Drop shatter	71	21	3	5	100
	Dry tumbled	52	30	6	12	100
P1	Wet tumbled	51	27	5	8	94
	Drop shatter	68	25	3	4	100
	Dry tumbled	50	32	6	13	100
SMU	Wet tumbled	48	30	5	7	90
	Drop shatter	59	29	3	9	100
	Dry tumbled	48	33	6	13	100
P2	Wet tumbled	45	30	6	9	92
	Drop shatter	59	29	3	9	100
	Dry tumbled	49	34	6	11	100
SML	Wet tumbled	48	31	4	10	91
	Drop shatter	67	26	3	4	100
	Dry tumbled	51	32	7	11	100
P3	Wet tumbled	49	30	5	8	93
	Drop shatter	88	10	1	2	100
	Dry tumbled	68	21	3	8	100
SBU	Wet tumbled	66	22	2	4	90
	Drop shatter	81	15	2	2	100
	Dry tumbled	62	25	4	9	100
SBM	Wet tumbled	61	24	3	5	93
	Drop shatter	76	20	2	3	100
	Dry tumbled	64	26	3	7	100
SBL	Wet tumbled	61	26	3	4	91

5.3. Dry and wet tumbling results

Figure 5.1 graphically shows that the daughter particle size distributions after each tumble test follow a comparable partitioning pattern to that of the afore mentioned drop shatter trends, i.e., coarse > intermediate > ultrafine > fine. However, some stratigraphic variations are detected in the distribution of intermediate and fine particles after wet tumbling. Wet tumbled intermediates are higher in the uppermost seams (27% to 30%) compared to the lowermost seams (10% to 31%) hence, the proportion of intermediate particles decrease with depth after wet tumbling (Figure 5.1). The fine particle size distribution after wet tumbling shows that seams SMU, SML and SBU contain the highest proportion of fines, up to 6%, relative to seams SU, SBM and SBL which contain fines up to 5%.

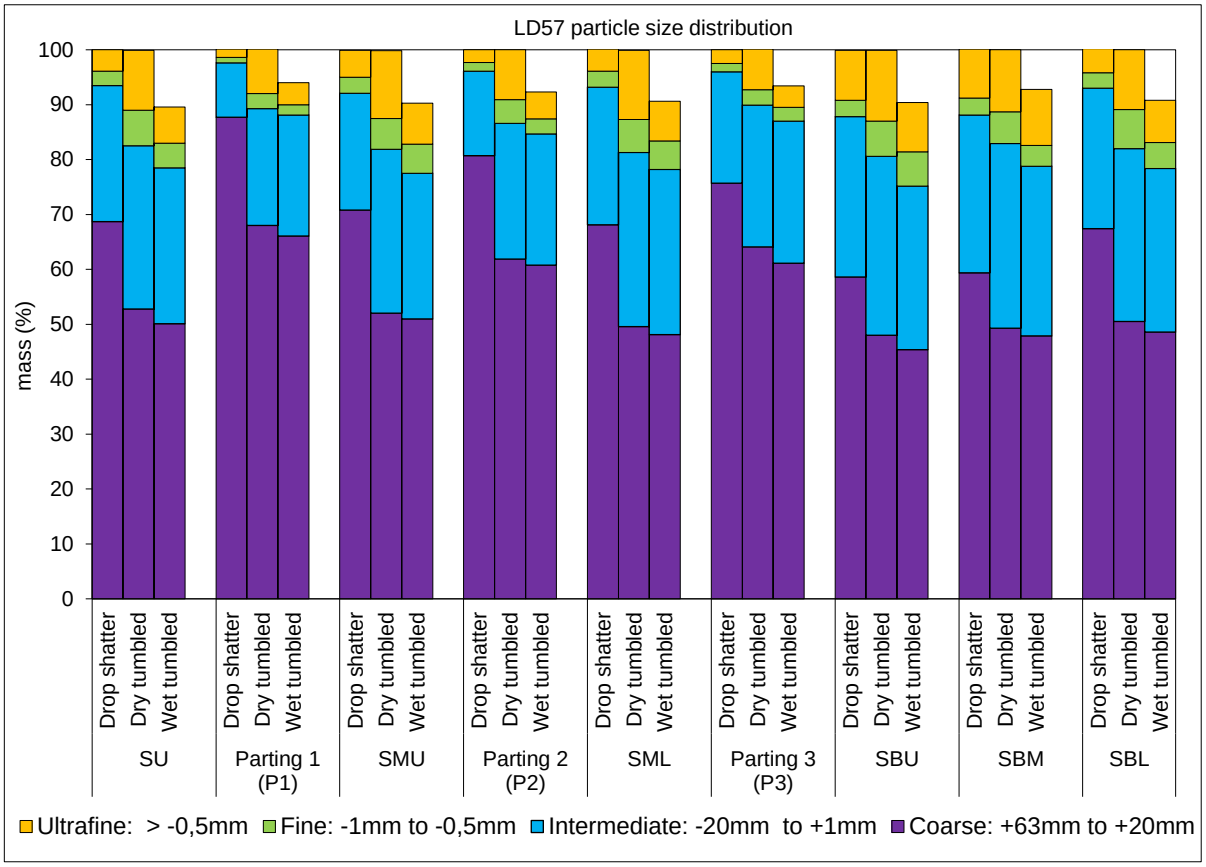

Figure 5.1. Particle size distribution for LD57.

Notably the total particles recovered after wet tumbling in LD57 do not amount to 100%, indicating a loss in the ultrafine material during testing (Figure 5.1). This is evident by the discrepancy in the mass recovered after drop shatter and dry tumbling, respectively (Table 5.1). To mitigate, the values of the actual material recovered in each seam and parting were used to calculate the amount of missing material, and the differences combined to predict the estimated quantity of ultrafine material that should have been retrieved after wet tumbling (Table 5.2). The calculations show that up to 10% of ultrafine material was lost during

successive breakage testing and that total ultrafines between 10%-12% can be expected in the partings, and as high as 17 to 19% for the seams.

Table 5.2. Calculation of ultrafine material after wet tumbling.

No. 6 Seam horizons	% Recovered Ultrafine	% Missing Ultrafine	% Estimated Ultrafine
SU	6.60	10.41	17.01
P1	4.00	6.04	10.04
SMU	7.50	9.74	17.24
P2	4.90	7.76	12.66
SML	7.20	9.29	16.49
P3	3.90	6.59	10.49
SBU	9.00	9.63	18.63
SBM	10.20	7.29	17.49
SBL	7.70	9.30	17.00

Given that the parent sample (i.e., the initially intact borehole, LD57) used for drop shatter produced 13 size fractions which were recombined for dry tumbling and wet tumbling, respectively, the percentage change in the particle size distributions was calculated after each test to quantify the % decrease or % increase after the initial particles were broken down further (Table 5.3).

With respect to the seams, daughter particles partitioning into the coarse size fraction decreased by an average of 23% from drop shatter to dry tumbling, and less so (4%) from dry tumbling to wet tumbling (Table 5.3). On average, intermediate particles increased by 23% from drop shatter to dry tumbling but decreased by 7% after wet tumbling. The fine-sized daughter particles generated after dry tumbling increased by an average of 118% but subsequently decreased by 20% after wet tumbling. Notably, the proportion of fine and ultrafine daughter particles produced from the seams and partings increased on average by more than 100% after dry tumbling, especially in the partings whereby an average increase of 311% was recorded (Table 5.3).

The estimated ultrafine values recorded in Table 5.2 were used to calculate the expected changes in the partitioning of ultrafine daughter particles for LD57 after wet tumbling. The results estimate an average increase of 47% and 35% in ultra-fine particles will be produced after wet tumbling for the seams and partings, respectively (Table 5.3). This contrasts with the average decrease of 32% in the seams and 48% in the partings, based on the actual recovered values (Table 5.1).

Table 5.3. Difference in daughter particles partitioning in each size fraction after consecutive strength testing for LD57.

No. 6 Seam horizons	% change	Coarse: +63 mm to +20 mm	Intermediate: -20 mm to +1 mm	Fine: -1 mm to +0.5 mm	Ultrafine: > -0.5 mm	Estimated Ultrafine: > -0.5 mm
SU	% change from drop shatter to dry tumble	-23	20	150	179	179
	% change from dry to wet tumble	-5	-4	-31	-39	54
	Total % change	-27	15	73	69	331
P1	% change from drop shatter to dry tumble	-22	115	170	440	440
	% change from dry to wet tumble	-3	3	-30	-51	24
	Total % change	-25	122	90	167	97
SMU	% change from drop shatter to dry tumble	-27	40	94	152	152
	% change from dry to wet tumble	-2	-11	-6	-39	40
	Total % change	-28	24	83	53	569
P2	% change from drop shatter to dry tumble	-23	60	169	296	296
	% change from dry to wet tumble	-2	-3	-37	-46	39
	Total % change	-25	55	69	113	286
SML	% change from drop shatter to dry tumble	-27	26	107	215	215
	% change from dry to wet tumble	-3	-5	-13	-43	31
	Total % change	-29	20	79	80	252
P3	% change from drop shatter to dry tumble	-15	27	87	196	196
	% change from dry to wet tumble	-5	0	-11	-47	42
	Total % change	-19	28	67	56	450
SBU	% change from drop shatter to dry tumble	-18	12	113	42	42
	% change from dry to wet tumble	-5	-9	-3	-30	44
	Total % change	-23	2	107	-1	312
SBM	% change from drop shatter to dry tumble	-17	17	87	27	27
	% change from dry to wet tumble	-3	-8	-34	-10	55
	Total % change	-19	8	23	15	319
SBL	% change from drop shatter to dry tumble	-25	23	154	148	148
	% change from dry to wet tumble	-4	-5	-34	-29	56
	Total % change	-28	16	68	75	105
COAL SEAMS	Average % change from drop shatter to dry tumble	-23	23	118	127	127
	Average % change from dry to wet tumble	-4	-7	-20	-32	47
	Total % change	-26	14	72	48	315
PARTINGS	Average % change from drop shatter to dry tumble	-20	68	142	311	311
	Average % change from dry to wet tumble	-3	0	-26	-48	35
	Total % change	-23	68	75	112	278

***Positive values denote an increase while negative values indicate a decrease.**

5.4. Discussion

The results from the drop shatter, dry tumbling and wet tumbling tests conducted on borehole LD57 show that more than 45% of the daughter particles are predominantly coarse (Table 5.1; Figure 5.1), indicating volume breakage as the major mechanism by which the coal and minerals have fragmented along existing planes of weakness such as cleats. Breakage of the seams and partings into coarse particles mostly occurred during drop shatter testing and subsequently decreased in excess of 23% after consecutive testing. Hence, the rate of volume breakage decreased with successive processing due to lower energy exerted during dry and wet tumbling. These observations are consistent with the literature (Teo *et al*., 1990; Sahoo and Roach, 2005). Overall, it can be summarized that the average particle distribution observed for the LD57 horizons is 60% coarse, 26% intermediate,7% ultrafine (10% when corrected) and 4% fine particles after handling.

As expected, the partings in borehole LD57 contained the highest proportion of coarse material (61% to 88%) after all three tests were conducted, which is a reflection of lower amounts of carbonaceous material and greater mineral matter occurring in the partings as indicated by the high proportion of stone in Figure 4.3. In contrast, the seams produced less coarse material, 45% to 67%. Intermediate, fine and ultra-fine particles are higher in the seams (3% to 34%) compared to the partings (1% to 26%), albeit in lower proportions compared to coarse particles. Drop tests conducted by Sahoo and Roach (2005) showed that less fines (< 20%) are generated when the impact energy is low as a result of a small drop height e.g., less than 3 m. Furthermore, particles partitioning into the fine size fractions in the tumbling tests were used as an indicator of surface breakage. Hence, in the present study the fine and ultrafine size classes can be jointly used to approximate surface breakage which accounts for only less than 19% of the breakage that occurred in borehole LD57 (Table 5.1).

Noticeably the number of ultrafine particles (1.50% to 12.90%) recorded after each test is higher than fine particles (1.00% to 7.10%) recorded across all seams and partings for the various size fractions analysed (Table 5.2). Makhado coals are known to possess large quantities of the vitrinite maceral, typically in quantities greater than 68.8% mmf (Mphaphuli, 2017). This led to the expectation that large quantities of fine to ultrafine particles would be produced consecutively after each test because vitrinite is generally known to be friable, breaking easily. This observation has been made in the literature (Mikhail and Patching, 1981; Esterle *et al*., 2002; Esterle *et al*., 2008; Lin *et al*., 2019) where bright coals, vitrinite-rich, produced more fines compared to dull coal after repetitive drops during drop shatter testing and/or tumbling.

To summarise, the large number of coarse particles compared to finer particles observed for the LD57 seams and partings after drop shatter testing show that the samples were exposed to low energy, resulting mainly in volumetric breakage (Table 5.3). Therefore, predominantly coarse particles can be expected during handling and transportation of the coal. These breakage characteristics do not account for the breakage behaviour of Makhado coal under high energy conditions such as initial blasting and extraction in the mine pit. This suggests that excessive fine material can be avoided by employing low charge energy during initial blasting and extraction in the mine pit. Therefore, contingency measures must be instituted to minimise creation and loss of fine and ultrafine particles at various points of handling along the mining value chain.

Chapter 6: Part 1 Washability

6.1. Introduction

The beneficiation characteristics of the coal seams and partings from drill core LD57 are presented herein in terms of standard washability curves derived from the float-sink tests. The float-sink data was used to assess the extent to which coal of varying size fractions can be efficiently separated from mineral matter taking into account the effect of particle size, density, and vertical seam variability on the overall washability characteristics. This chapter addresses objectives for part one of this research.

Due to the large data set acquired, the washability data is presented in two parts. This chapter constitutes Part 1 of the float-sink results and deals with the recovery of clean coal based on float yields, ash and near gravity material, while the complementary chemical analysis by size fraction data are discussed in Part 2 (Chapter 7).

6.2. Washability results

Where the term ‘size fraction’ is used, it refers to the individual screened fractions, i.e., specifically -63+50 mm, -50+31. mm, -31.5+20 mm, -20+6 mm, -6+1 mm, or -1+0.25 mm. For ease of discussion these size fractions are grouped into size classes as follows:

- Coarse: -63+5 mm, -50+31.5 mm and -31.5+20 mm
- Intermediate: -20+6 mm, -6+1 mm,
- Fine: -1+0.25 mm

The above size classes approximate as close as possible those typically employed in the South African coal industry (Bergh *et al.*, 2013).

It must be noted that the anomalies observed on some trends on the graphs are due to discrepancies in yield recovery during testing in the laboratory and do not arise due to the coal itself.

6.2.1 Seam Upper (SU)

The elementary ash curves of SU are predominantly near vertical in shape, suggesting the coal is difficult to clean. However, with decreasing particle size, the curves become more concave in shape, suggesting easier separation at finer particle sizes (and higher RD), specifically for the -1+0.25 mm size fraction (Figure 6.1). The shape of the -63+50 mm elementary curve is irregularly shaped as no coal was recovered at 1.60 g/cm^3.

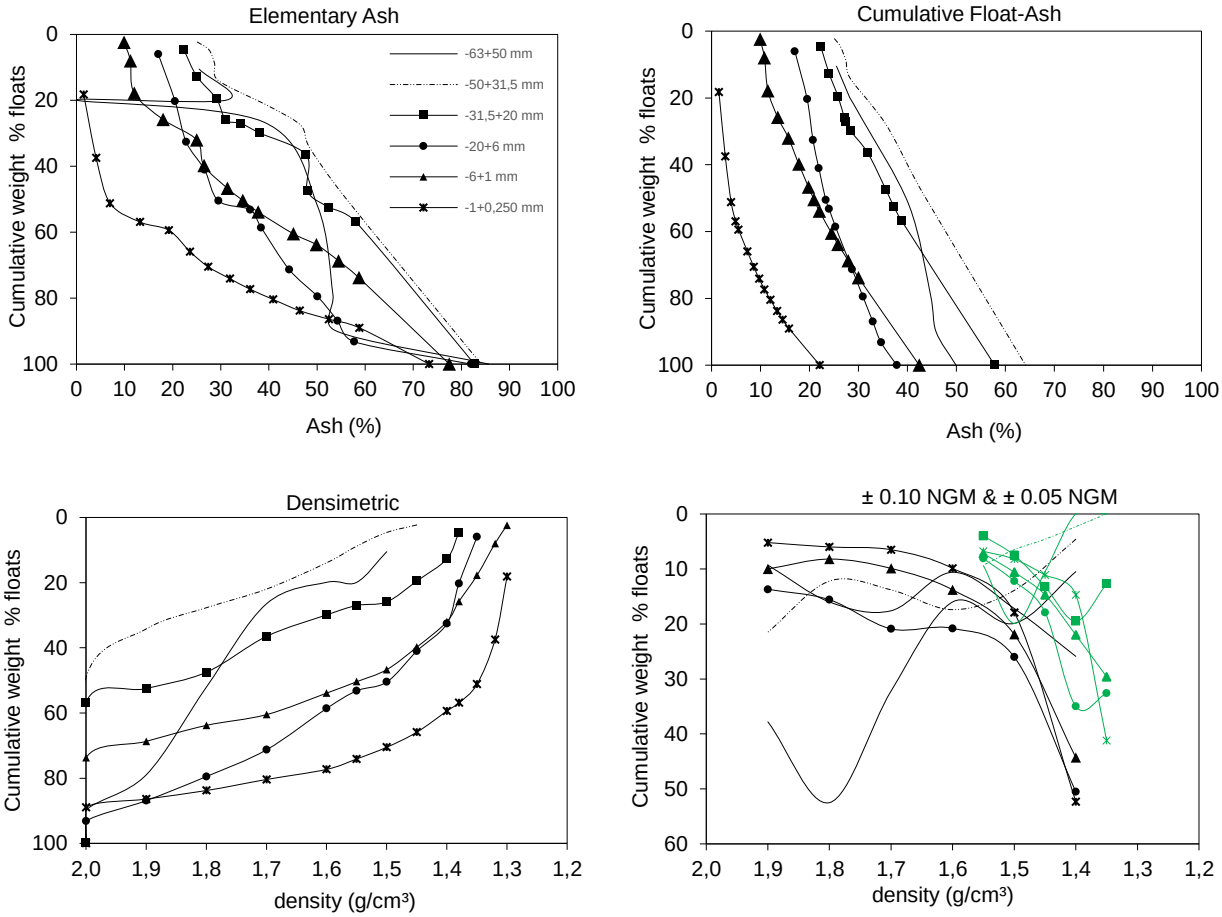

Figure 6.1. Standard washability curves for SU. -63+50 mm (–), -50 +31.5 mm (-••-), -31.5+20 mm (■), -20+6 mm(●), -6+1 mm (▲) and -1 + 0.25 mm (*); ± 0.05 NGM in green in bottom right graph.

The cumulative float ash curves in Figure 6.1 show that overall, relatively high float yields (2.3% to 93.2%) and high ash (2.4% to 43.4%) were recovered across all the size fractions. Table 6.1 shows that the float yields generally increase with decreasing particle size, and the lowest ash yields occur in the fine size class. However, the float yield recovery (10.5% to 89.9%) in the -63+50 mm size fraction is very similar to that recovered in the -1+0.25 mm size fraction (18% to 89%).

The trend of the densimetric curves show that higher float yields were recovered at high relative densities compared to lower densities at fixed particle sizes (Figure 6.1). Furthermore,

the highest proportion of floats were obtained at smaller particle sizes. No floats were recovered between 1.30 g/cm^3 and 1.50 g/cm^3 in the coarse size class, while float yields were mostly recovered over the full density range for the intermediate and fine size classes (Figure 6.1). Float yields of 50% ≥ were mainly recovered between 1.80 g/cm^3 and 2.00 g/cm^3 in the coarse size class, from 1.50 g/cm^3 and 1.55 g/cm^3 in the intermediate size class, and from 1.35 g/cm^3 to 2.00 g/cm^3 in the fine size class (Table 6.1).

The ± 0.10 NGM curves show an increase in the amount of NGM with increasing density in the -63+50 mm and -50 +31.5 mm size fraction. The amount of NGM decreased with increasing density in all other size fractions (Figure 6.1). Overall, ± 0.10 NGM in SU was in the range of 5% to 53% (Table 6.1), which is characterised with separation varying from simple to formidable. Simple to moderate separation conditions (i.e., ± 0.10 NGM less than 10%) are possible from 1.70 g/cm^3 to 1.90 g/cm^3 in the -1 +0.25 mm and -6+1 mm size fractions. As well as at 1.40 g/cm^3 and 1.90 g/cm^3 for the -50 +31.5 mm and -31.5+20 mm size fractions, respectively.

Likewise, the amount of ± 0.05 NGM decreased with increasing relative density for the intermediate and fine size classes (Figure 6.1). Overall, the calculated ± 0.05 NGM values for SU are in the range 1 to 41% (Table 6.1). According to the revised classification for ± 0.05 NGM, easy separation (± 0.05 NGM < 20%) is generally achievable from 1.45 g/cm^3 to 1.55 g/cm^3 in all size classes.

Table 6.1. Cumulative washability report for seam SU.

Separation density (g/cm³)	Yield %	Ash %	Elementary ash %	± 0.10 NGM density (g/cm³)	± 0.05 NGM density (g/cm³)	Yield %	Ash %	Elementary ash %	± 0.10 NGM density (g/cm³)	± 0.05 NGM density (g/cm³)	Yield %	Ash %	Elementary ash %	± 0.10 NGM density (g/cm³)	± 0.05 NGM density (g/cm³)
Fraction	**-63+50 mm**					**-50+31.5 mm**					**-31.5+20 mm**				
F1.30	0.00	0.00	0.00	-	-	0.00	0.00	0.00	-	-	0.00	0.00	0.00	-	-
F1.32	0.00	0.00	0.00	-	-	0.00	0.00	0.00	-	-	0.00	0.00	0.00	-	-
F1.35	0.00	0.00	0.00	-	0.00	0.00	0.00	0.00	-	0.00	0.00	0.00	0.00	-	12.70
F1.38	0.00	0.00	0.00	-	-	0.00	0.00	0.00	-	-	4.60	22.30	2.30	-	-
F1.40	0.00	0.00	0.00	10.50	0.00	0.00	0.00	0.00	4.60	2.30	12.70	24.00	8.65	25.90	19.50
F1.45	0.00	0.00	0.00	-	10.50	2.30	25.10	1.15	-	4.60	19.50	25.80	16.10	-	13.20
F1.50	10.50	25.50	5.25	19.90	19.90	4.60	26.30	3.50	13.90	6.50	25.90	27.10	22.70	17.20	7.50
F1.55	19.90	28.20	15.20	-	9.40	8.80	27.40	6.65	-	9.30	27.00	27.40	26.45	-	4.00
F1.60	19.90	28.20	19.90	16.00	-	13.90	28.20	11.40	17.40	-	29.90	28.40	28.45	10.60	-
F1.70	26.50	30.80	23.20	32.20	-	22.00	32.60	17.95	13.80	-	36.50	31.90	33.20	17.60	-
F1.80	52.10	40.30	39.25	52.50	-	27.70	35.50	24.85	12.20	-	47.50	35.60	42.00	16.00	-
F1.90	79.00	44.70	65.60	37.80	-	34.20	38.00	30.95	21.50	-	52.50	37.20	50.00	9.30	-
F2.00	89.90	45.80	84.45	-	-	49.20	43.40	41.70	-	-	56.80	38.80	54.65	-	-
S2.00	100.00	49.90	94.95	-	-	100.00	64.10	74.60	-	-	100.00	57.80	78.40	-	-
Fraction	**-20+6 mm**					**-6+1 mm**					**-1+0.25 mm**				
F1.30	0.00	0.00	0.00	-	-	2.40	9.90	1.20	-	-	18.20	1.50	9.10	-	-
F1.32	0.00	0.00	0.00	-	-	8.00	10.80	5.20	-	-	37.50	2.80	27.85	-	-
F1.35	6.00	17.00	3.00	-	32.60	17.80	11.50	12.90	-	-	51.20	4.00	44.40	-	41.20
F1.38	20.30	19.50	13.15	-	-	25.80	13.50	21.80	-	29.60	56.90	4.90	54.05	-	-
F1.40	32.60	20.70	26.45	50.50	35.00	32.00	15.70	28.90	44.30	22.00	59.40	5.50	58.15	52.30	14.70
F1.45	41.00	21.90	36.80	-	17.90	39.80	17.80	35.90	-	14.70	65.90	7.30	62.65	-	11.10
F1.50	50.50	23.30	45.75	26.00	12.20	46.70	19.80	43.25	21.90	10.60	70.50	8.60	68.20	17.90	8.20
F1.55	53.20	24.00	51.90	-	8.10	50.40	20.90	48.55	-	7.20	74.10	9.70	72.30	-	6.80
F1.60	58.60	25.30	55.90	20.80	-	53.90	22.00	52.20	13.80	-	77.30	10.80	75.70	9.90	-
F1.70	71.30	28.70	64.95	20.90	-	60.50	24.50	57.20	9.90	-	80.40	12.00	78.85	6.50	-
F1.80	79.50	30.90	75.40	15.60	-	63.80	25.80	62.15	8.20	-	83.80	13.40	82.10	6.00	-
F1.90	86.90	32.90	83.20	13.70	-	68.70	27.90	66.25	10.00	-	86.40	14.50	85.10	5.20	-
F2.00	93.20	34.60	90.00	-	-	73.80	30.00	71.30	-	-	89.00	15.80	87.70	-	-
S2.00	100.00	37.80	96.60	-	-	100.00	42.40	86.90	-	-	100.00	22.10	94.50	-	-

6.2.2. Parting 1 (P1)

The washability curves are grouped into two distinct clusters consisting of the coarse and intermediate size classes, while the curve for the fine size class lies separately (Figure 6.2).

The elementary ash curves are generally steeply inclined and become gentler in slope with decreasing particle size and therefore at higher relative density, suggesting easier washing conditions for fine particles compared to intermediates and coarse (Figure 6.2). The -1+0.25 mm curve is irregularly shaped due to no yield recovery at 1.38 g/cm^3.

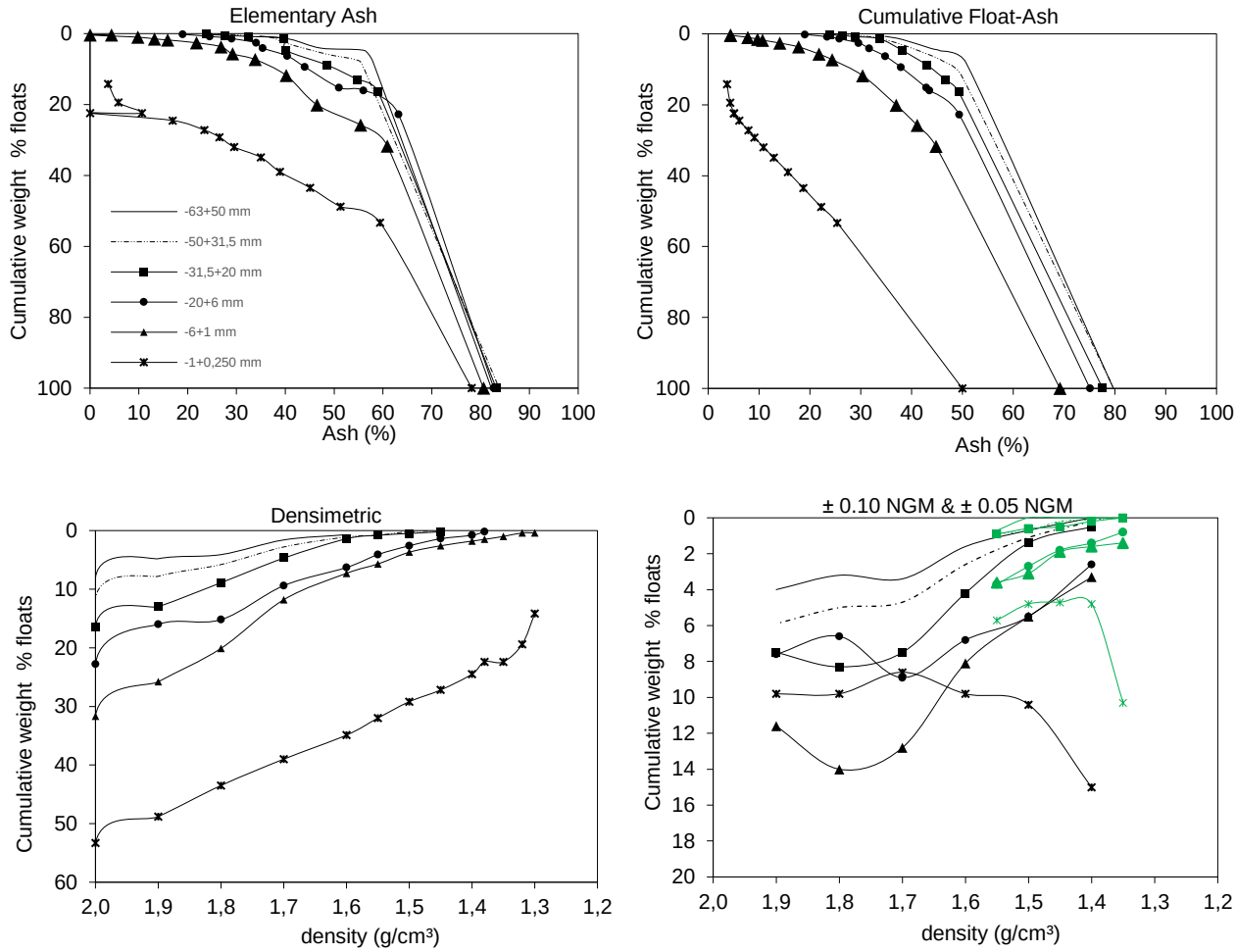

Figure 6.2. Standard washability curves for P1. -63+50 mm (–), -50 +31.5 mm (-••-), -31.5+20 mm (■), -20+6 mm(●), -6+1 mm (▲) and -1 + 0.25 mm (*); ± 0.05 NGM in green in bottom right graph.

The cumulative float-ash curves indicate a trend of increasing float yield and decreasing ash content with finer particle size (Figure 6.2). Float yield and ash yields in the coarse size class range from 0.1% to 16.4%, and 23.5% to 50.7%, respectively (Table 6.2). The intermediate size class consists of float yields in the range 0.2% to 31.7%, while ash varied from 4.4% to

49.4%. The fine size class is characterised by the highest proportion of float yields, 14.2% to 53.3%, and the lowest ash content, 3.7% to 25.4%.

The densimetric curves indicate that progressively higher float yields were obtained at high relative densities, particularly with decreasing particle size (Figure 6.2). Float yields above 50% were absent in all the size classes, except at 2.00 g/cm^3 in the -1+0.25 mm size class, where a yield of 53.3% was recovered (Table 6.2).

The trend of the ± 0.10 NGM curves show an increase in the amount of NGM with increasing density for the coarse and intermediate size classes (Figure 6.2). In contrast, the fine size class mostly shows a uniform distribution in the amount of NGM. The ± 0.10 NGM for P1 is in the range 1% to 15% (Table 6.2). The coarse and intermediate size classes are predominantly classified with simple to moderate separation conditions while, the fine size class is predominately difficult. In contrast, the amount of ± 0.05 NGM is mostly uniformly distributed across the density interval investigated. Moreover, ± 0.05 NGM in P1 is low (1% to 10%) and is therefore classified with easy separation.

Table 6.2. Cumulative washability report for parting P1.

Separation density (g/cm³)	Yield %	Ash %	Elementary ash %	± 0.10 NGM density (g/cm³)	± 0.05 NGM density (g/cm³)	Yield %	Ash %	Elementary ash %	± 0.10 NGM density (g/cm³)	± 0.05 NGM density (g/cm³)	Yield %	Ash %	Elementary ash %	± 0.10 NGM density (g/cm³)	± 0.05 NGM density (g/cm³)
Fraction	**-63+50 mm**					**-50+31.5 mm**					**-31.5+20 mm**				
F1.30	0.00	0.00	0.00	-	-	0.00	0.00	0.00	-	-	0.00	0.00	0.00	-	-
F1.32	0.00	0.00	0.00	-	-	0.00	0.00	0.00	-	-	0.00	0.00	0.00	-	-
F1.35	0.00	0.00	0.00	-	0.00	0.00	0.00	0.00	-	0.00	0.00	0.00	0.00	-	0.00
F1.38	0.00	0.00	0.00	-	-	0.00	0.00	0.00	-	-	0.00	0.00	0.00	-	-
F1.40	0.00	0.00	0.00	0.00	0.00	0.00	0.00	0.00	0.20	0.10	0.00	0.00	0.00	0.50	0.20
F1.45	0.00	0.00	0.00	-	0.00	0.10	23.50	0.05	-	0.20	0.20	23.90	0.10	-	0.50
F1.50	0.00	0.00	0.00	0.70	0.00	0.20	27.10	0.15	1.10	0.70	0.50	26.40	0.35	1.40	0.60
F1.55	0.00	0.00	0.00	-	0.70	0.80	31.70	0.50	-	0.90	0.80	29.00	0.65	-	0.90
F1.60	0.70	34.80	0.35	1.60	-	1.10	33.10	0.95	2.60	-	1.40	33.70	1.10	4.20	-
F1.70	1.60	38.20	1.15	3.40	-	2.80	37.60	2.00	4.70	-	4.70	38.20	3.05	7.50	-
F1.80	4.10	43.80	2.85	3.20	-	5.80	43.30	4.30	5.00	-	8.90	43.10	6.80	8.30	-
F1.90	4.80	45.70	4.45	4.00	-	7.80	46.30	6.80	5.90	-	13.00	46.70	10.90	7.50	-
F2.00	8.10	50.70	6.40	-	-	11.70	49.80	9.75	-	-	16.40	49.30	14.70	-	-
S2.00	100.00	79.70	54.05	-	-	100.00	79.80	55.85	-	-	100.00	77.60	58.20	-	-
Fraction	**-20+6 mm**					**-6+1 mm**					**-1+0.25 mm**				
F1.30	0.00	0.00	0.00	-	-	0.40	4.40	0.20	-	-	14.20	3.70	7.10	-	-
F1.32	0.00	0.00	0.00	-	-	0.40	4.40	0.40	-	-	19.40	4.30	16.80	-	-
F1.35	0.00	0.00	0.00	-	0.80	1.00	7.80	0.70	-	1.40	22.40	5.10	20.85	-	10.30
F1.38	0.20	19.00	0.10	-	-	1.50	9.70	1.30	-	-	22.40	5.10	22.40	-	-
F1.40	0.80	23.40	0.50	2.60	1.40	1.80	10.70	1.65	3.30	1.60	24.50	6.10	23.45	15.00	4.80
F1.45	1.40	25.80	1.10	-	1.80	2.60	14.10	2.20	-	1.90	27.20	7.90	25.85	-	4.70
F1.50	2.60	29.60	2.00	5.50	2.70	3.70	17.80	3.15	5.50	3.10	29.20	9.10	28.20	10.40	4.80
F1.55	4.10	31.70	3.35	-	3.70	5.70	21.80	4.70	-	3.60	32.00	10.90	30.55	-	5.70
F1.60	6.30	34.80	5.25	6.80	-	7.30	24.40	6.50	8.10	-	34.90	12.90	33.45	9.80	-
F1.70	9.40	37.90	7.85	8.90	-	11.80	30.40	9.55	12.80	-	39.00	15.70	36.95	8.60	-
F1.80	15.20	42.90	12.30	6.60	-	20.10	37.00	15.95	14.00	-	43.50	18.70	41.25	9.80	-
F1.90	16.00	43.50	15.55	7.60	-	25.80	41.10	22.95	11.60	-	48.80	22.20	46.10	9.80	-
F2.00	22.80	49.40	19.40	-	-	31.70	44.80	28.75	-	-	53.30	25.40	51.10	-	-
S2.00	100.00	75.10	61.40	-	-	100.00	69.20	65.85	-	-	100.00	50.00	76.65	-	-

6.2.3. Seam Middle Upper (SMU)

The elementary ash curves for SMU are inclined and near vertical, which suggests difficult separation for the range of coarse to fine particles (Figure 6.3). However, the slope of the -1+0.2 mm curve is gently sloping, suggesting easier separation. The -63+50 mm curve is noticeably irregular as no yields were recovered at 1.60 g/cm^3 and 1.70 g/cm^3.

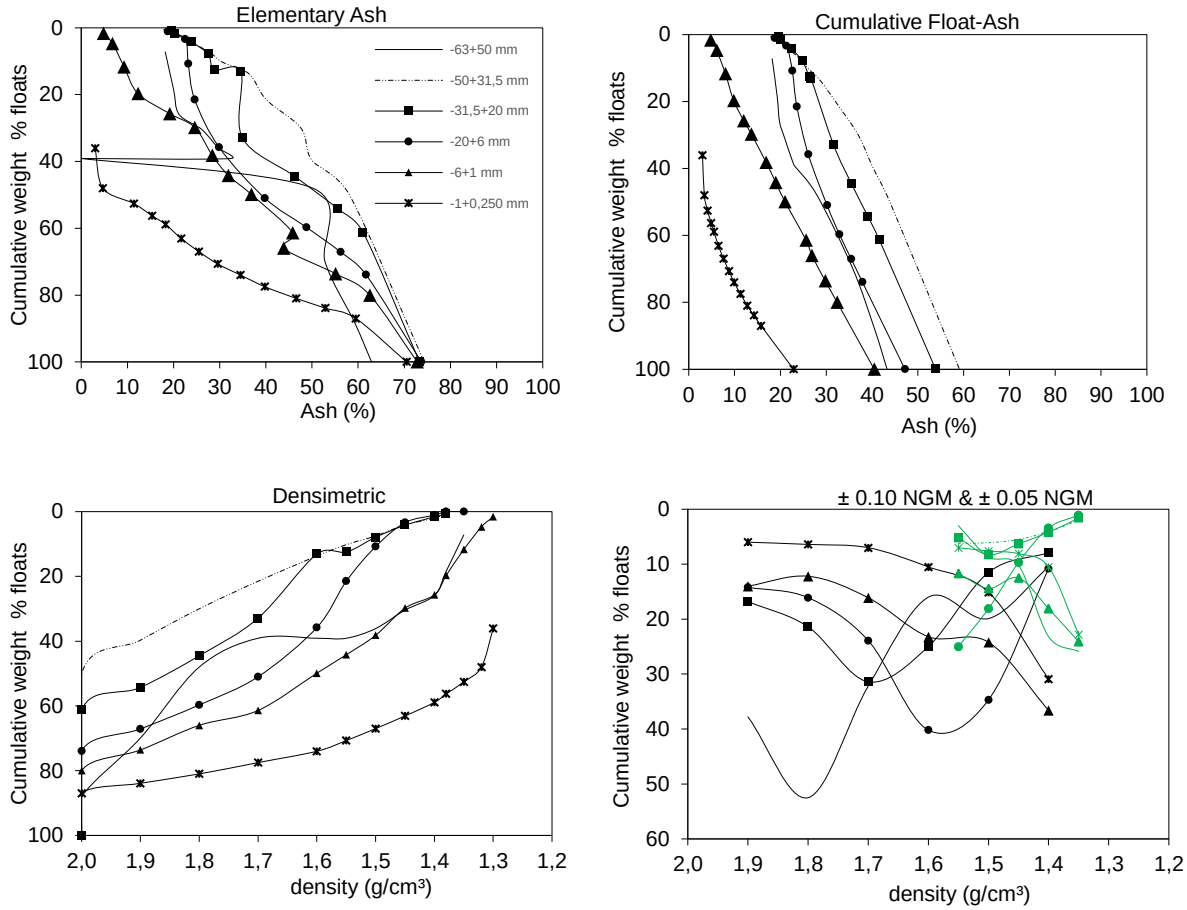

Figure 6.3. Standard washability curves for SMU. -63+50 mm (–), -50 +31.5 mm (-••-), -31.5+20 mm (■), -20+6 mm(●), -6+1 mm (▲) and -1 + 0.25 mm (*); ± 0.05 NGM in green in bottom right graph.

The cumulative float-ash curves show an increase in the proportion of floats and a decrease in ash content recovered at progressively finer particle sizes over the range of densities tested (Figure 6.3). The coarse size class comprises 0.5% to 88.1% float yields, with the corresponding ash being in the range 17.9% to 49.9% (Table 6.3). The intermediate and fine size classes comprise 1.1% to 80% and 36.1% to 87% float yields, respectively. The float yields correspond to ash in the range 4.8% to 37.9% in the intermediates, and 3% to 15.8% in the fines (Table 6.3).

Overall, the densimetric curves of SMU indicate higher float yields were obtained at high relative densities with decreasing particle size (Figure 6.3). Float yield recovery above 50%

commenced from 1.80 g/cm^3 and 1.90 g/cm^3 in the coarse size class, 1.70 g/cm^3 and 1.80 g/cm^3 in the intermediate size class and from 1.35 g/cm^3 to 2.00 g/cm^3 in the fine size class (Table 6.3).

The ± 0.10 NGM curves show 4 different trends across the size fractions: 1, that NGM increased with increasing density for -50 +31.5 mm. 2, the NGM decreased with increasing density for -6 +1 mm and -1+ 0.25 mm. 3, the amount of NGM was highest at the lowermost and uppermost densities while, the opposite trend occurred in -31.5 +2 mm and -20 +6 mm (Figure 6.3). Overall, ± 0.10 NGM is in the range 3% to 40% which is classified with simple to formidable separation (Table 6.3). Simple to moderate separation is achievable from 1.70 g/cm^3 to 1.90 g/cm^3 in -1+ 0.25 mm, at 1.40 g/cm^3 in 50 +31.5 mm and from 1.60 g/cm^3 and 1.70 g/cm^3 in -63+50 mm. The curves of the ± 0.05 NGM show NGM decreases with increasing density for the -63+50 mm, -50+31.5 mm and -1+0.25 mm size fractions (Figure 6.3). However, the curves 6displayed a decrease in NGM with increasing relative density in the -20 + 6 mm size fraction. The overall amount of ± 0.05 NGM in SMU ranges from 1% to 26% (Table 6.3). Hence easy separation is achievable in all the size fractions generally from 1.40 g/cm^3 and 1.55 g/cm^3.

Table 6.3. Cumulative washability report for seam SMU.

Separation density (g/cm³)	Yield %	Ash %	Elementary ash %	± 0.10 NGM density (g/cm³)	± 0.05 NGM density (g/cm³)	Yield %	Ash %	Elementary ash %	± 0.10 NGM density (g/cm³)	± 0.05 NGM density (g/cm³)	Yield %	Ash %	Elementary ash %	± 0.10 NGM density (g/cm³)	± 0.05 NGM density (g/cm³)
Fraction	**-63+50 mm**					**-50+31.5 mm**					**-31.5+20 mm**				
F1.30	0.00	0.00	0.00	-	-	0.00	0.00	0.00	-	-	0.00	0.00	0.00	-	-
F1.32	0.00	0.00	0.00	-	-	0.00	0.00	0.00	-	-	0.00	0.00	0.00	-	-
F1.35	7.20	18.20	3.60	-	25.90	0.00	0.00	0.00	-	2.00	0.00	0.00	0.00	-	1.60
F1.38	18.40	19.30	12.80	-	-	0.50	17.90	0.25	-	-	0.80	19.60	0.40	-	-
F1.40	25.90	19.80	22.15	36.10	23.20	2.00	19.60	1.25	7.50	4.10	1.60	20.00	1.20	7.90	4.20
F1.45	30.40	20.80	28.15	-	10.20	4.10	21.60	3.00	-	5.50	4.20	22.40	2.90	-	6.30
F1.50	36.10	22.20	33.25	13.20	8.70	7.50	24.50	5.85	11.70	6.10	7.90	24.80	6.05	11.50	8.30
F1.55	39.10	23.00	37.55	-	3.00	10.20	26.10	8.85	-	6.20	12.50	26.30	10.15	-	5.20
F1.60	39.10	23.00	39.10	3.00	-	13.70	28.70	11.95	14.00	-	13.10	26.70	12.85	25.00	-
F1.70	39.10	23.00	39.10	8.90	-	21.50	32.80	17.55	16.30	-	32.90	31.60	23.00	31.40	-
F1.80	48.00	28.00	43.55	30.80	-	30.00	37.00	25.75	18.20	-	44.50	35.50	38.70	21.40	-
F1.90	69.90	35.80	58.95	40.10	-	39.70	40.20	34.85	20.00	-	54.30	39.10	49.40	16.80	-
F2.00	88.10	40.60	79.00	-	-	50.00	43.90	44.85	-	-	61.30	41.60	57.80	-	-
S2.00	100.00	43.30	94.05	-	-	100.00	59.10	75.00	-	-	100.00	53.90	80.65	-	-
Fraction	**-20+6 mm**					**-6+1 mm**					**-1+0.25 mm**				
F1.30	0.00	0.00	0.00	-	-	1.60	4.80	0.80	-	-	36.10	3.00	18.05	-	-
F1.32	0.00	0.00	0.00	-	-	4.70	6.10	3.20	-	-	48.00	3.40	42.05	-	-
F1.35	0.00	0.00	0.00	-	1.10	11.70	8.00	8.20	-	24.10	52.60	4.10	50.30	-	22.8
F1.38	0.00	0.00	0.00	-	-	19.70	9.80	15.70	-	-	56.30	4.90	54.40	-	-
F1.40	1.10	18.80	0.55	10.80	3.40	25.70	12.00	22.70	36.60	18.10	58.90	5.50	57.60	30.90	10.50
F1.45	3.40	21.30	2.25	-	9.70	29.80	13.70	27.75	-	12.50	63.10	6.50	61.00	-	8.10
F1.50	10.80	22.60	7.10	34.70	18.10	38.20	16.90	34.00	24.20	14.40	67.00	7.60	65.05	15.10	7.60
F1.55	21.50	23.60	16.15	-	25.00	44.20	19.00	41.20	-	11.70	70.70	8.80	68.85	-	7.00
F1.60	35.80	26.10	28.65	40.20	-	49.90	21.00	47.05	23.20	-	74.00	9.90	72.35	10.50	-
F1.70	51.00	30.20	43.45	23.90	-	61.40	25.60	55.65	16.10	-	77.50	11.30	75.75	7.00	-
F1.80	59.70	32.90	55.35	16.10	-	66.00	26.90	63.70	12.20	-	81.00	12.80	79.25	6.40	-
F1.90	67.10	35.50	63.35	14.20	-	73.60	29.80	69.80	14.00	-	83.90	14.20	82.45	6.00	-
F2.00	73.90	37.90	70.50	-	-	80.00	32.40	76.80	-	-	87.00	15.80	85.45	-	-
S2.00	100.00	47.20	86.95	-	-	100.00	40.50	90.00	-	-	100.00	22.90	93.50	-	-

6.2.4. Parting 2 (P2)

The various parameters of the washability curves for P2 occur in two clusters: coarse and intermediate size classes, and the fine size class (Figure 6.4).

The elementary ash curves are generally steeply inclined for the coarse and intermediate size classes, indicating that the coal will be difficult to clean (Figure 5.4). However, with decreasing particle size and higher relative density, the slope of the elementary ash curves becomes gentler, suggesting easier separation, particularly for the fine size class, -1+0.25 mm.

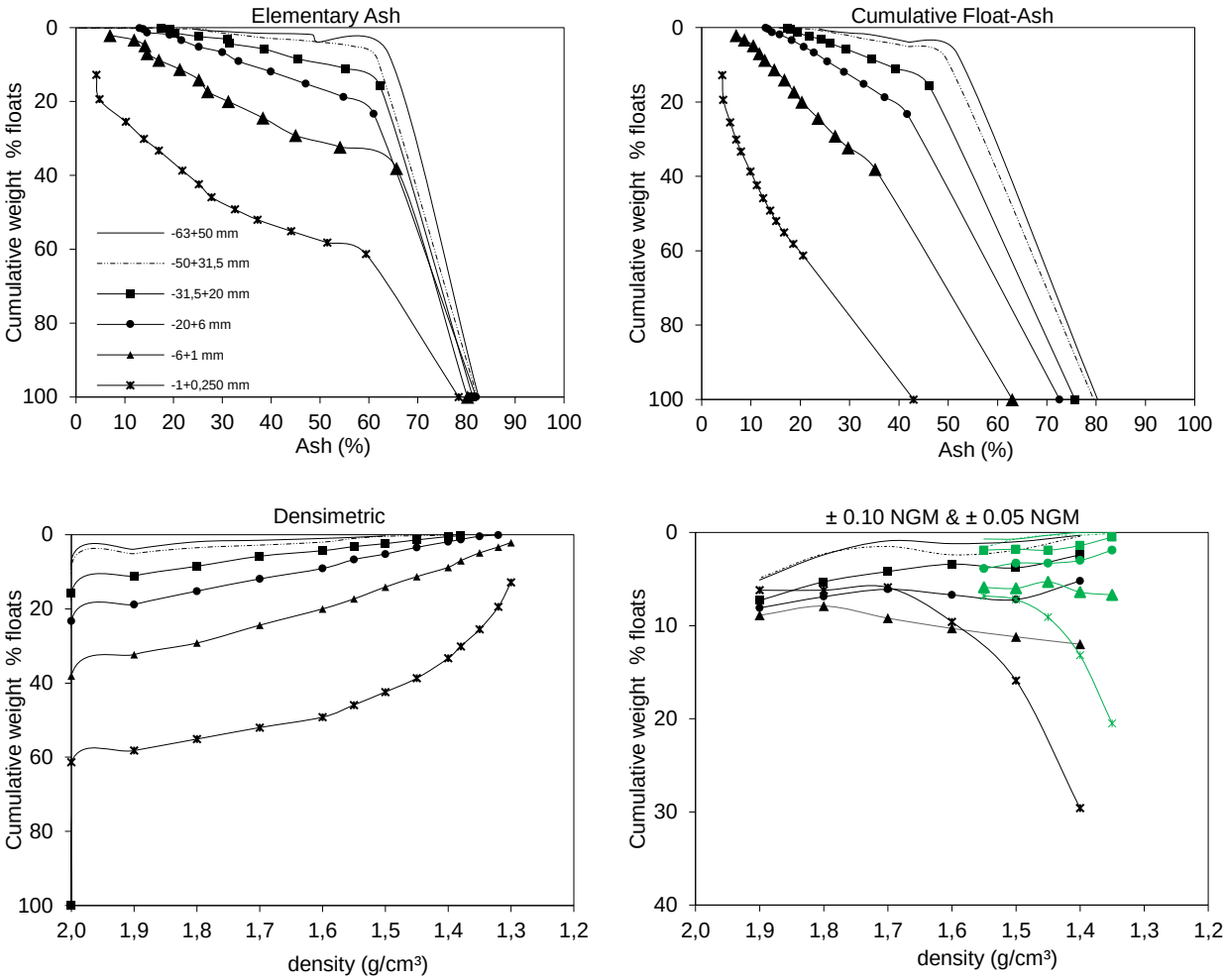

Figure 6.4. Standard washability curves for P2. -63+50 mm (–), -50 +31.5 mm (–••–), -31.5+20 mm (■), -20+6 mm(●), -6+1 mm (▲) and -1 + 0.25 mm (*); ± 0.05 NGM in green in bottom right graph.

The cumulative float-ash curves display a trend of increasing float yield with decreasing particle size, while the proportion of ash decreased with decreasing particle size (Figure 6.4). As such, the float and ash in the coarse size class in in the range 0.1% to 15.8% and 15.7% to 51.8%, respectively (Table 6.4). The intermediate size class consists of float and ash in the range 0.1% to 38.1% and 7% to 41.7%, respectively, while the fine size class consists of floats from 12.8% to 61.3%, and ash in the range 4.2% to 20%.

The trend of the densimetric curves show that higher float yields were recovered at relatively high relative densities and fine particle sizes (Figure 6.4). For example, the yield at 1.50 g/cm^3 and 2.00 g/cm^3 is 0.4% and 8.4%, respectively in the -50+31.5 mm size fraction (Table 6.4). For the same separation step the float yield is 5.2% and 23.3%, and 42.4% and 61.3%, in the -20+ 6 mm and -1+0.25 mm size fractions, respectively.

The ± 0.10 NGM curves indicate that NGM increases with decreasing particle size, therefore separation is most difficult in the fine size class (Figure 6.4). However, the amount of NGM in P2 is generally low overall, ranging between 1-30% (Table 6.4). All size fractions are characterised with simple separation across the entire density interval, excluding -6+1 mm and -1+0.25 mm whereby simple to moderate separation is only achievable from 1.70 g/cm^3 to 1.90 g/cm^3.

Comparatively, only the fine size class displays a decrease in the ± 0.05 NGM with increasing relative density (Figure 6.4). Due to the low float yields obtained, the ± 0.05 NGM for P2 is in the range 1% to 26% and therefore predominantly classified with easy separation (Table 6.4).

Table 6.4. Cumulative washability report for parting P2.

Separation density (g/cm³)	Yield %	Ash %	Elementary ash %	± 0.10 NGM density (g/cm³)	± 0.05 NGM density (g/cm³)	Yield %	Ash %	Elementary ash %	± 0.10 NGM density (g/cm³)	± 0.05 NGM density (g/cm³)	Yield %	Ash %	Elementary ash %	± 0.10 NGM density (g/cm³)	± 0.05 NGM density (g/cm³)
Fraction	**-63+50 mm**					**-50+31.5 mm**					**-31.5+20 mm**				
F1.30	0.00	0.00	0.00	-	-	0.00	0.00	0.00	-	-	0.00	0.00	0.00	-	-
F1.32	0.00	0.00	0.00	-	-	0.00	0.00	0.00	-	-	0.00	0.00	0.00	-	-
F1.35	0.00	0.00	0.00	-	0.00	0.00	0.00	0.00	-	0.10	0.00	0.00	0.00	-	0.50
F1.38	0.00	0.00	0.00	-	-	0.10	15.70	0.05	-	-	0.30	17.50	0.15	-	-
F1.40	0.00	0.00	0.00	0.30	0.00	0.10	15.70	0.10	0.40	0.30	0.50	18.10	0.40	2.40	1.40
F1.45	0.00	0.00	0.00	-	0.30	0.30	18.20	0.15		0.30	1.40	19.40	0.95	-	1.90
F1.50	0.30	23.80	0.15	1.00	0.70	0.40	21.90	0.40	1.90	0.70	2.40	21.90	1.90	3.80	1.80
F1.55	0.70	24.90	0.50	-	0.70	1.00	24.90	0.70		1.60	3.20	24.20	2.80	-	1.90
F1.60	1.00	26.40	0.85	1.20	-	2.00	29.30	1.50	2.40	-	4.30	26.00	3.70	3.40	-
F1.70	1.50	30.20	1.25	0.90	-	2.80	32.00	2.40	1.50	-	5.80	29.30	5.05	4.20	-
F1.80	1.90	34.20	1.70	2.40	-	3.50	35.10	3.15	2.30	-	8.50	34.50	7.15	5.30	-
F1.90	3.90	41.90	2.90	5.10	-	5.10	41.70	4.25	4.90	-	11.10	39.30	9.80	7.30	-
F2.00	7.00	51.80	5.45	-	-	8.40	49.60	6.75	-	-	15.80	46.20	13.50	-	-
S2.00	100.00	80.30	53.50	-	-	100.00	79.50	54.20	-	-	100.00	75.70	57.90	-	-
Fraction	**-20+6 mm**					**-6+1 mm**					**-1+0.25 mm**				
F1.30	0.00	0.00	0.00	-	-	2.10	7.00	1.05	-	-	12.80	4.20	6.40	-	-
F1.32	0.10	13.00	0.05	-	-	3.30	8.70	2.65	-	-	19.40	4.40	16.15	-	-
F1.35	0.40	13.50	0.20	-	1.90	4.90	10.50	4.10	-	6.70	25.50	5.80	22.45	-	20.50
F1.38	1.30	14.30	0.85	-	-	7.00	11.70	5.95	-	-	30.10	7.00	27.80	-	-
F1.40	1.90	15.80	1.60	5.20	3.00	8.80	12.80	7.85	12.00	6.40	33.30	8.00	31.70	29.60	13.20
F1.45	3.40	18.30	2.65	-	3.30	11.30	14.70	10.05		5.30	38.70	9.90	36.00	-	9.10
F1.50	5.20	20.70	4.30	7.20	3.30	14.10	16.80	12.70	11.20	6.00	42.40	11.20	40.55	15.90	7.20
F1.55	6.70	22.80	5.95	-	3.90	17.30	18.70	15.70		5.90	45.90	12.50	44.20	-	6.80
F1.60	9.10	25.50	7.90	6.70	-	20.00	20.30	18.60	10.30	-	49.20	13.90	47.55	9.60	-
F1.70	11.90	28.90	10.50	6.10	-	24.40	23.60	22.20	9.20	-	52.00	15.10	50.55	5.90	-
F1.80	15.20	32.90	13.55	6.90	-	29.20	27.10	26.80	7.90	-	55.10	16.70	53.55	6.20	-
F1.90	18.80	37.10	17.00	8.10	-	32.30	29.70	30.70	8.90	-	58.20	18.60	56.70	6.20	-
F2.00	23.30	41.70	21.05	-	-	38.10	35.20	35.20	-	-	61.30	20.60	59.70	-	-
S2.00	100.00	72.60	61.65	-	-	100.00	63.00	69.05	-	-	100.00	43.00	80.65	-	-

6.2.5. Seam Middle Lower (SML)

The elementary ash curves for SML are steep and concave down in shape for the -50+31.5 mm and -31.5+20 mm size fractions, while the rest are concave up and become gentler, suggesting the coal becomes easier to wash with decreasing particle size and at higher relative densities (Figure 6.5). The -63+50 mm elementary ash curve is irregularly shaped as no yields are recovered between 1.60 g/cm^3 to 1.80 g/cm^{3}and 2.00 g/cm^3.

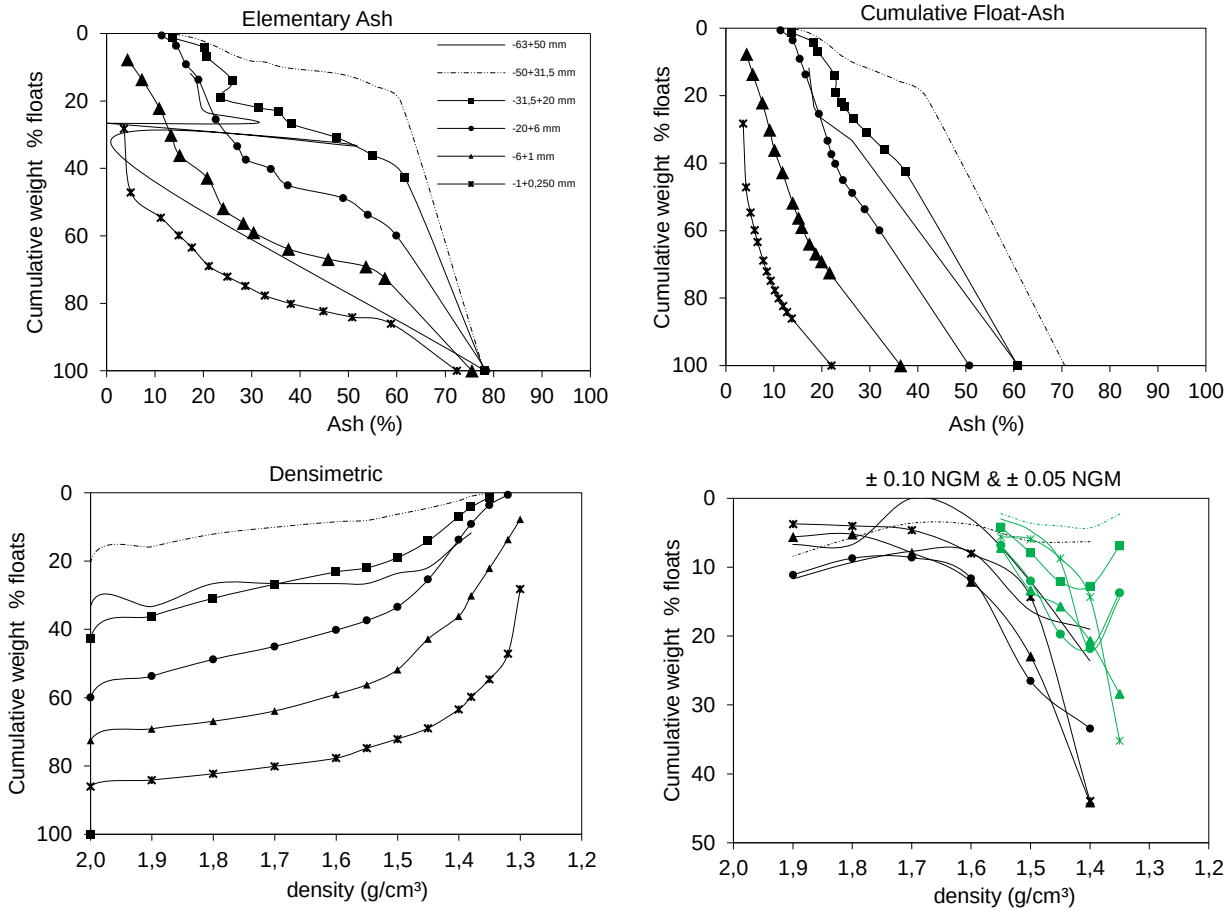

Figure 6.5. Standard washability curves for SML. -63+50 mm (–), -50 +31.5 mm (-••-), -31.5+20 mm (■), -20+6 mm(●), -6+1 mm (▲) and -1 + 0.25 mm (*); ± 0.05 NGM in green in bottom right graph.

The trend of the cumulative float-ash curves indicates the ash content decreases with decreasing particle size, while the proportion of floats obtained increases over the range of densities tested (Figure 6.5). The quantities of the float-ash yields can be summarised according to size classes as follows: 0.2% to 42.6% float yields and ash from 13.7% to 41.8% for the coarse size class (Table 6.5). The intermediate size class consists of float yields in the range 0.6% to 72.5% and ash ranging from 4% to 32%. The fine size class consists of float yields from 28.2% to 86.00% and ash in the range 3.6% to 13.7%.

The densimetric curves indicate higher float yields were obtained at higher relative densities with decreasing particle size (Figure 6.5). Float yields above 50% were not recovered in the coarse size class but were recovered from 1.50 g/cm^3 to 2.00 g/cm^3 in the intermediate size class, and from 1.35 g/cm^3 to 2.00 g/cm^3 in the fine size class (Table 6.5).

The ±0.10 NGM curves for SML display a trend of decreasing NGM with increasing relative density hence, separation is easier at higher densities for all size fractions excluding -50+31.5 mm whereby the NGM remained relatively uniform across the entire density range tested. (Figure 6.5). The ±0.10 NGM for SML ranges from 3% to 44% with simple to moderate separation generally occurring from 1.60 g/cm^3 to 1.70 g/cm^3 in all the size fractions (Table 6.5). Simple to moderate separation is however achievable throughout the entire density range in -50+31.5 mm.

In comparison, the amount of ± 0.05 NGM decreased with increasing relative density for the -63+50 mm, -6+ 1 mm and -1+0.25 mm size classes (Figure 6.5). Overall, the calculated ± 0.05 NGM values for SU are in the range 2% to 35% and therefore predominantly classified with easy separation (Table 6.5).

Table 6.5. Cumulative washability report for seam SML.

Separation density (g/cm³)	Yield %	Ash %	Elementary ash %	± 0.10 NGM density (g/cm³)	± 0.05 NGM density (g/cm³)	Yield %	Ash %	Elementary ash %	± 0.10 NGM density (g/cm³)	± 0.05 NGM density (g/cm³)	Yield %	Ash %	Elementary ash %	± 0.10 NGM density (g/cm³)	± 0.05 NGM density (g/cm³)
Fraction	**-63+50 mm**					**-50+31.5 mm**					**-31.5+20 mm**				
F1.30	0.00	0.00	0.00	-	-	0.00	0.00	0.00	-	-	0.00	0.00	0.00	-	-
F1.32	0.00	0.00	0.00	-	-	0.00	0.00	0.00	-	-	0.00	0.00	0.00	-	-
F1.35	0.00	0.00	0.00	-	14.50	0.20	14.20	0.10	-	2.30	1.30	13.70	0.65	-	6.90
F1.38	11.80	17.30	5.90	-	-	1.00	16.60	0.60	-	-	4.20	18.30	2.75	-	-
F1.40	14.50	17.50	13.15	23.60	21.90	2.30	18.60	1.65	6.30	4.30	6.90	19.20	5.55	19.00	12.80
F1.45	21.90	18.20	18.25	-	9.10	4.50	21.00	3.40	-	4.00	14.10	22.70	10.55	-	12.10
F1.50	23.60	18.40	22.70	12.10	4.70	6.30	22.50	5.40	6.20	3.60	19.00	22.90	16.55	16.30	7.90
F1.55	26.60	19.80	25.10	-	3.00	8.10	24.00	7.20	-	2.20	22.00	24.10	20.50	-	4.20
F1.60	26.60	19.80	26.60	3.00	-	8.50	24.50	8.35	3.80	-	23.20	24.70	22.60	7.80	-
F1.70	26.60	19.80	26.60	0.00	-	10.10	26.40	9.30	3.60	-	26.80	26.50	24.95	7.70	-
F1.80	26.60	19.80	26.60	6.70	-	12.10	30.00	11.10	5.70	-	30.90	29.30	28.85	9.30	-
F1.90	33.30	26.30	29.95	6.70	-	15.80	36.20	14.00	8.40	-	36.10	33.00	33.50	11.70	-
F2.00	33.30	26.30	33.30	-	-	20.50	41.80	18.15	-	-	42.60	37.40	39.35	-	-
S2.00	100.00	60.90	66.65	-	-	100.00	70.60	60.25	-	-	100.00	60.80	71.30	-	-
Fraction	**-20+6 mm**					**-6+1 mm**					**-1+0.25 mm**				
F1.30	0.00	0.00	0.00	-	-	7.70	4.30	3.85	-	-	28.20	3.60	14.10	-	-
F1.32	0.60	11.40	0.30	-	-	13.60	5.60	10.65	-	-	47.10	4.20	37.60	-	-
F1.35	3.60	13.90	2.10	-	13.70	22.10	7.60	17.85	-	28.40	54.60	5.10	50.85	-	35.20
F1.38	9.10	15.40	6.35	-	-	30.10	9.10	26.05	-	-	59.80	6.00	57.20	-	-
F1.40	13.70	16.60	11.40	33.40	21.80	36.10	10.10	33.10	44.10	20.70	63.40	6.60	61.60	43.90	14.30
F1.45	25.40	19.40	19.60	-	19.70	42.80	11.80	39.45	-	15.70	68.90	7.80	66.15	-	8.70
F1.50	33.40	21.20	29.35	26.50	12.00	51.80	13.90	47.30	22.90	13.40	72.10	8.50	70.50	14.30	5.90
F1.55	37.40	22.00	35.40	-	6.80	56.20	15.10	54.00	-	7.20	74.80	9.30	73.50	-	5.60
F1.60	40.20	22.80	38.80	11.60	-	59.00	15.80	57.55	12.10	-	77.70	10.20	76.25	8.00	-
F1.70	45.00	24.40	42.60	8.60	-	63.90	17.40	61.45	7.90	-	80.10	11.00	78.90	4.60	-
F1.80	48.80	26.30	46.90	8.70	-	66.90	18.70	65.45	5.20	-	82.30	11.90	81.15	4.00	-
F1.90	53.70	28.90	51.25	11.10	-	69.10	19.90	68.00	5.60	-	84.10	12.70	83.25	3.70	-
F2.00	59.90	32.00	56.75	-	-	72.50	21.60	70.80	-	-	86.00	13.70	85.05	-	-
S2.00	100.00	50.70	79.95	-	-	100.00	36.40	86.25	-	-	100.00	22.00	93.00	-	-

6.2.6. Parting 3 (P3)

The washability curves are grouped into two distinct clusters, coarse and intermediate size classes, and the fine size classes (Figure 6.6).

The slope of the elementary ash curves is near horizontal and tappers off sharply, suggesting easy separation conditions for the coarse and intermediate size classes, while the slope of the fine size class curve is slightly steeper, indicating more difficult separation (Figure 6.6).

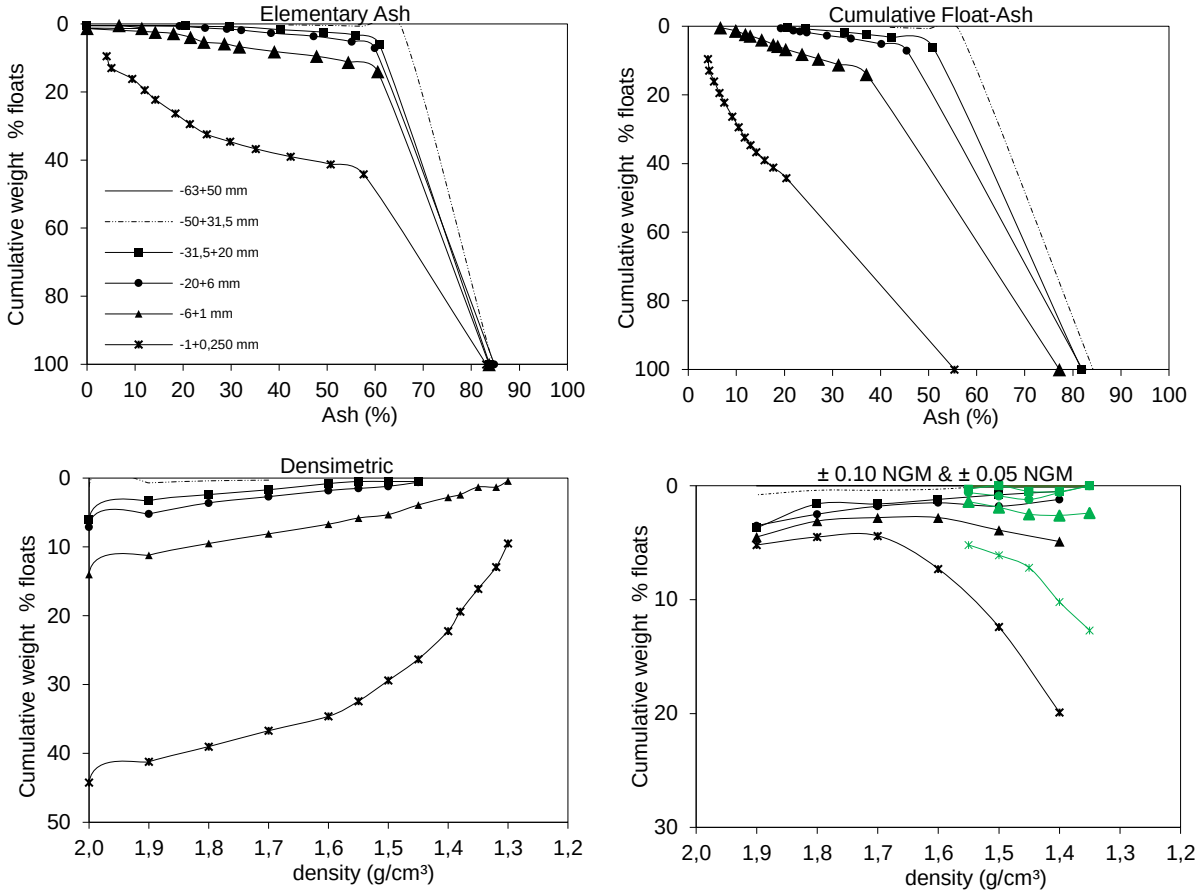

Figure 6.6. Standard washability curves for P3. -63+50 mm (–), -50 +31.5 mm (-••-), -31.5+20 mm (■), -20+6 mm (●), -6+1 mm (▲) and -1 + 0.25 mm (*); ± 0.05 NGM in green in bottom right graph.

The cumulative float-ash curves (Figure 6.6) show that float yields increase with decreasing particle size and with increasing relative density, albeit relatively a low amount of float yields (0.3% to 44.2%) and associated ash (4.1% to 56.4%) were recovered over the full range of relative densities tested. The distribution of float yields, and complementary ash content can therefore be summarized as follows: Floats are in the range 0.3% to 6.1% and ash content from 20.6% to 56.4%, in the coarse size class (Table 6.6). Float yield varies from 0.6% to

14% and ash content varies from 6.7% to 45.5%, in the intermediate size class. The fine size class consists of float yields in the range 9.5% to 44.2% and ash from 4.1% to 20.4%.
The densimetric curves show that the highest proportion of float yields coincide with high relative densities (Figure 6.6). Furthermore, this trend becomes more pronounced with decreasing particle size. No floats were recovered in the -63+ 50 mm size fraction. Float recovery commenced at 1.70 g/cm^3 in the -50+ 31.5 mm size fraction, albeit producing a very low float yield (0.3%), characterised by high ash, 42% (Table 6.6).

Figure 6.6 shows the ± 0.10 NGM curves for P3 have a uniform distribution in the amount of NGM in the -31+ 20 mm, +20, -6 mm and -6 +1 mm size fractions. Simple separation is expected in these size fractions (Table 6.6). The -1+0.025 mm size fraction curve shows a decrease in the amount of NGM with increasing density. Furthermore, simple separation is expected in the afore mentioned size fraction. NGM is not reported for -63 +50 mm, nor -50 + 31.5 mm because no float yields were recovered. Comparably, the ± 0.05 NGM curves show an increase in the amount of NGM with increasing relative density for the fine size class while the other curves indicate a uniform distribution (Figure 6.6). Easy separation conditions are expected in P3 due to the overall low amount (1% to 13%) of ± 0.05 NGM (Table 6.6).

Table 6.6. Cumulative washability report for parting P3.

Separation density (g/cm³)	Yield %	Ash %	Elementary ash %	± 0.10 NGM density (g/cm³)	± 0.05 NGM density (g/cm³)	Yield %	Ash %	Elementary ash %	± 0.10 NGM density (g/cm³)	± 0.05 NGM density (g/cm³)	Yield %	Ash %	Elementary ash %	± 0.10 NGM density (g/cm³)	± 0.05 NGM density (g/cm³)
Fraction	**-63+50 mm**					**-50+31.5 mm**					**-31.5+20 mm**				
F1.30	0.00	0.00	0.00	-	-	0.00	0.00	0.00	-	-	0.00	0.00	0.00	-	-
F1.32	0.00	0.00	0.00	-	-	0.00	0.00	0.00	-	-	0.00	0.00	0.00	-	-
F1.35	0.00	0.00	0.00	-	0.00	0.00	0.00	0.00	-	0.00	0.00	0.00	0.00	-	0.00
F1.38	0.00	0.00	0.00	-	-	0.00	0.00	0.00	-	-	0.00	0.00	0.00	-	-
F1.40	0.00	0.00	0.00	0.00	0.00	0.00	0.00	0.00	0.00	0.00	0.00	0.00	0.00	0.50	0.50
F1.45	0.00	0.00	0.00	-	0.00	0.00	0.00	0.00	-	0.00	0.50	20.60	0.25	-	0.50
F1.50	0.00	0.00	0.00	0.00	0.00	0.00	0.00	0.00	0.00	0.00	0.50	20.60	0.50	0.80	0.00
F1.55	0.00	0.00	0.00	-	0.00	0.00	0.00	0.00	-	0.00	0.50	20.60	0.50	-	0.30
F1.60	0.00	0.00	0.00	0.00	-	0.00	0.00	0.00	0.30	-	0.80	24.50	0.70	1.20	-
F1.70	0.00	0.00	0.00	0.00	-	0.30	42.00	0.15	0.40	-	1.70	32.50	1.25	1.60	-
F1.80	0.00	0.00	0.00	0.00	-	0.40	43.40	0.35	0.40	-	2.40	37.20	2.05	1.60	-
F1.90	0.00	0.00	0.00	0.00	-	0.70	50.10	0.55	0.80	-	3.30	42.30	2.85	3.70	-
F2.00	0.00	0.00	0.00	-	-	1.20	56.40	0.95	-	-	6.10	50.90	4.70	-	-
S2.00	100.00	83.70	50.00	-	-	100.00	84.20	50.60	-	-	100.00	81.80	53.05	-	-
Fraction	**-20+6 mm**					**-6+1 mm**					**-1+0.25 mm**				
F1.30	0.00	0.00	0.00	-	-	0.40	6.70	0.20	-	-	9.50	4.10	4.75	-	-
F1.32	0.00	0.00	0.00	-	-	1.30	9.90	0.85	-	-	12.90	4.40	11.20	-	-
F1.35	0.00	0.00	0.00	-	0.00	1.30	9.90	1.30	-	2.40	16.10	5.40	14.50	-	12.70
F1.38	0.00	0.00	0.00	-	-	2.40	11.90	1.85	-	-	19.40	6.50	17.75	-	-
F1.40	0.00	0.00	0.00	1.20	0.60	2.80	12.90	2.65	4.90	2.60	22.20	7.50	20.80	19.90	10.20
F1.45	0.60	19.30	0.30	-	1.20	3.90	15.30	3.35	-	2.50	26.30	9.20	24.25	-	7.20
F1.50	1.20	21.90	0.90	1.80	0.90	5.30	17.70	4.60	3.90	1.90	29.40	10.50	27.85	12.40	6.10
F1.55	1.50	23.30	1.35	-	0.60	5.80	18.60	5.55	-	1.40	32.40	11.80	30.85	-	5.20
F1.60	1.80	24.70	1.65	1.50	-	6.70	20.30	6.25	2.80	-	34.60	13.00	33.55	7.30	-
F1.70	2.70	28.90	2.20	1.80	-	8.10	23.70	7.45	2.80	-	36.70	14.20	35.65	4.40	-
F1.80	3.60	33.90	3.20	2.50	-	9.50	27.10	8.75	3.10	-	39.00	15.90	37.85	4.50	-
F1.90	5.20	40.20	4.35	3.50	-	11.20	31.30	10.35	4.50	-	41.20	17.70	40.10	5.20	-
F2.00	7.10	45.50	6.15	-	-	14.00	37.10	12.60		-	44.20	20.40	42.70	-	-
S2.00	100.00	82.00	53.55	-	-	100.00	77.20	57.00		-	100.00	55.40	72.10	-	-

6.2.7. Seam Bottom Upper (SBU)

The shape of the elementary ash curves for SBU approximate easy cleaning for the -1+0.25 mm and -6+1 mm curves, while the -50 +31.5 mm, -31.5+20 mm and -20+6 mm curves are more steeply inclined hence, approximating more difficult cleaning conditions for this particle size interval (Figure 6.7). The -6+1 mm curve is irregular due to variation/fluctuation in the fractional ash content with increasing float yield. Although the -63+50 mm curve approximates the L-shape, it lies a distance away from the vertical axis and may therefore allude to difficult cleaning conditions.

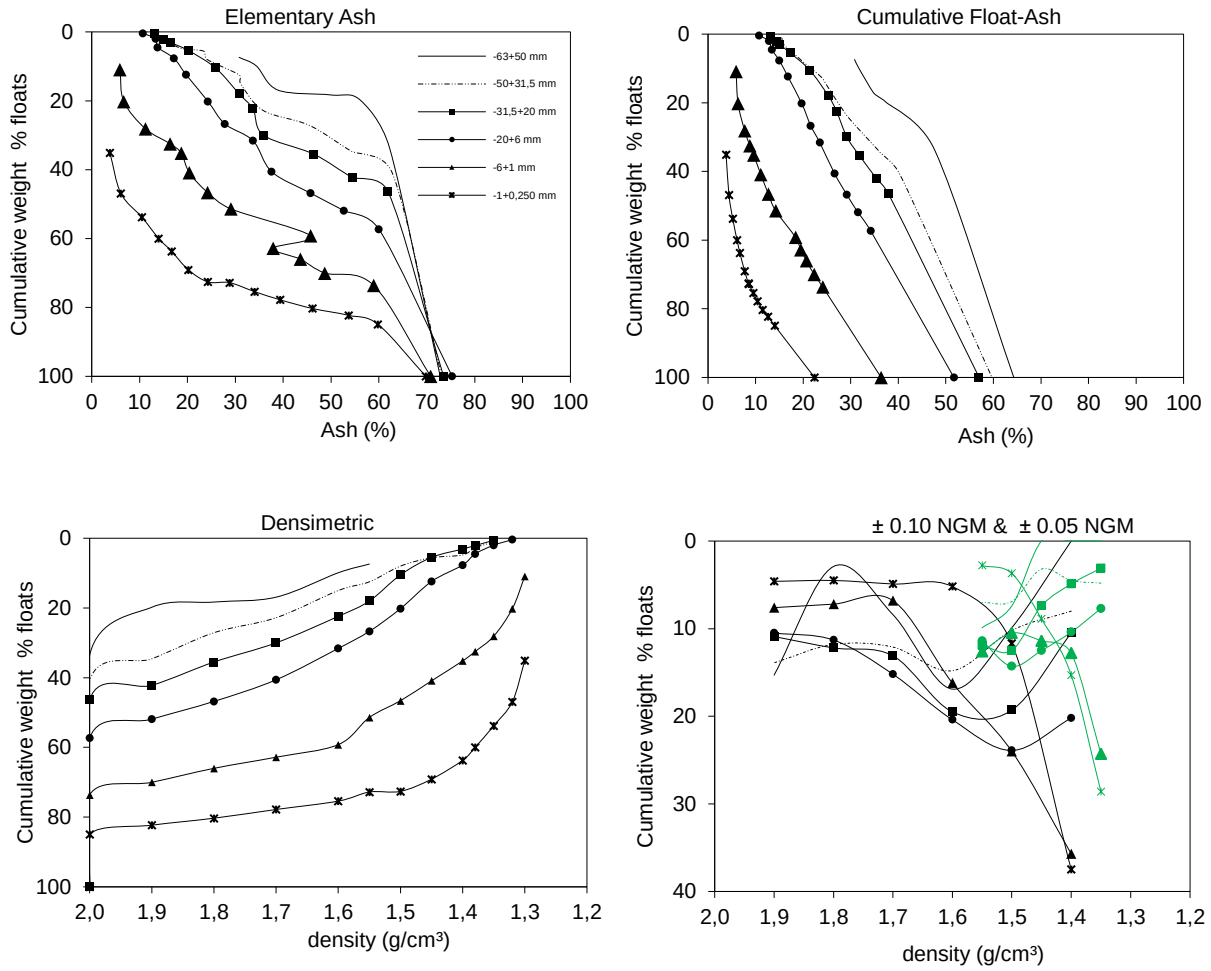

Figure 6.7. Standard washability curves for SBU. -63+50 mm (—), -50 +31.5 mm (-••-), -31.5+20 mm (■), -20+6 mm(●), -6+1 mm (▲) and -1 + 0.25 mm (*); ± 0.05 NGM in green in bottom right graph.

The trend of the cumulative float-ash curves (Figure 6.7) indicates a decrease in the ash content with decreasing particle size. In other words, the -1+0.25 mm particles have the lowest ash content over the full range of densities tested (3.8% to 14%), compared to the intermediate (5.9% to 34.2%) and coarse size classes (15.5% to 47.6%). An inverse relationship exits for the recovered clean coal, as the float yield increased with decreasing particle size over the full range of densities tested as follows: coarse size class (0.6% to 57.3%), intermediate size class (0.4% to 73.6%) and fine size class (35.1% to 84.9%).

The trend of the densimetric curves show increasing float yield at higher densities, more so with decreasing particle size (Figure 6.7). Float yields are below 50% over the full range of densities in the coarse size class whereas float yields greater than 50% were attainable from 1.55 g/cm^3 to 2.00 g/cm^3 in the intermediate size class, and from 1.35 g/cm^3 to 2.00 g/cm^3 in the fine size class (Table 6.7).

The trend of the NGM curves show decreasing NGM with increasing relative density for all size fractions excluding -63+50 mm nor -50-31.5mm of which no distinct trend was observed (Figure 6.7). The overall proportion of ± 0.10 NGM present in SBU ranged from 1% to 38% whereby the fine size class is characterised with simple separation from 1.60 g/cm^3 to 1.90 g/cm^3 (Table 6.7). Moderate to simple separation are generally expected from 1.70 g/cm^3 to 1.90 g/cm^3 for -63 +50mm and -6+1 mm. Moderate separation is only possible at 1.40 g/cm^3 for -50-31.5 mm. Comparably, the ± 0.05 NGM curves show an increase in the amount of NGM with increasing relative density for the -31.5 + 20 mm size fraction while the -1 + 0.25 mm size fractions display the reverse (Table 6.7). Overall, easy separation conditions are expected in SBU due to the overall low amount (3% to 29%) of ± 0.05 NGM.

Table 6.7. Cumulative washability report for seam SBU.

Separation density (g/cm³)	Yield %	Ash %	Elementary ash %	± 0.10 NGM density (g/cm³)	± 0.05 NGM density (g/cm³)	Yield %	Ash %	Elementary ash %	± 0.10 NGM density (g/cm³)	± 0.05 NGM density (g/cm³)	Yield %	Ash %	Elementary ash %	± 0.10 NGM density (g/cm³)	± 0.05 NGM density (g/cm³)
Fraction	**-63+50 mm**					**-50+31.5 mm**					**-31.5+20 mm**				
F1.30	0.00	0.00	0.00	-	-	0.00	0.00	0.00	-	-	0.00	0.00	-	-	-
F1.32	0.00	0.00	0.00	-	-	0.00	0.00	0.00	-	-	0.00	0.00	-	-	-
F1.35	0.00	0.00	0.00	-	0.00	1.10	15.50	0.55	-	4.80	0.60	13.10	0.30	-	3.10
F1.38	0.00	0.00	0.00	-	-	2.70	15.80	1.90	-	-	2.10	14.40	1.35	-	-
F1.40	0.00	0.00	0.00	0.00	0.00	4.80	17.10	3.70	8.00	4.50	3.10	15.10	2.60	10.50	4.90
F1.45	0.00	0.00	0.00	-	0.00	5.60	18.00	5.20	-	3.20	5.50	17.30	4.25	-	7.40
F1.50	0.00	0.00	0.00	9.90	7.40	8.00	19.90	6.80	10.20	6.90	10.50	21.40	8.00	19.30	12.50
F1.55	7.40	30.80	3.70	-	9.90	12.50	23.80	10.20	-	7.00	18.00	25.30	14.25	-	11.90
F1.60	9.90	31.70	8.65	16.90	-	15.00	25.00	13.75	14.80	-	22.40	27.00	20.20	19.50	-
F1.70	16.90	34.70	13.40	8.40	-	22.80	28.70	18.90	12.10	-	30.00	29.20	26.20	13.10	-
F1.80	18.30	35.90	17.60	2.90	-	27.10	31.30	24.95	11.80	-	35.50	31.90	32.75	12.20	-
F1.90	19.80	37.40	19.05	15.30	-	34.60	36.30	30.85	13.90	-	42.20	35.50	38.90	10.90	-
F2.00	33.60	47.60	26.70	-	-	41.00	40.40	37.80	-	-	46.40	37.90	44.30	-	-
S2.00	100.00	64.30	66.80	-	-	100.00	59.70	70.50	-	-	100.00	57.00	73.20	-	-
Fraction	**-20+6 mm**					**-6+1 mm**					**-1+0.25 mm**				
F1.30	0.00	0.00	0.00	-	-	10.90	5.90	5.45	-	-	35.10	3.80	17.55	-	-
F1.32	0.40	10.70	0.20	-	-	20.20	6.30	15.50	-	-	46.90	4.40	40.95	-	-
F1.35	2.00	12.80	1.20	-	7.70	28.10	7.70	24.15	-	24.30	53.80	5.20	50.35	-	28.60
F1.38	4.50	13.40	3.20	-	-	32.50	8.80	30.30	-	-	60.00	6.10	56.90	-	-
F1.40	7.70	15.00	6.15	20.20	10.40	35.20	9.60	33.85	35.70	12.80	63.70	6.70	61.85	37.50	15.30
F1.45	12.40	16.80	10.05	-	12.50	40.90	11.10	38.10	-	11.40	69.10	7.70	66.40	-	8.90
F1.50	20.20	19.70	16.30	23.90	14.30	46.60	12.70	43.70	24.00	10.50	72.60	8.50	70.85	11.70	3.70
F1.55	26.70	21.60	23.40	-	11.40	51.40	14.20	49.00	-	12.60	72.80	8.60	72.70	-	2.80
F1.60	31.60	23.50	29.15	20.40	-	59.20	18.40	55.30	16.20	-	75.40	9.50	74.15	5.20	-
F1.70	40.60	26.60	36.10	15.20	-	62.80	19.50	61.00	6.80	-	77.80	10.40	76.60	4.90	-
F1.80	46.80	29.20	43.70	11.30	-	66.00	20.70	64.45	7.20	-	80.30	11.50	79.05	4.50	-
F1.90	51.90	31.50	49.30	10.50	-	70.00	22.30	68.00	7.60	-	82.30	12.60	81.35	4.60	-
F2.00	57.30	34.20	54.65	-	-	73.60	24.10	71.80	-	-	84.90	14.00	83.60	-	-
S2.00	100.00	51.70	78.65	-	-	100.00	36.40	86.80	-	-	100.00	22.40	92.45	-	-

6.2.8. Seam Bottom Middle (SBM)

The elementary ash curves (Figure 6.8) for SBM are distinctly clustered in two groups in which the shape of the -1 + 0.25 mm curve approximates easy cleaning, while curves for the -63+50 mm, -50 +31.5 mm, -31.5+20 mm, -20+6 mm and -6+1 mm particle sizes are more inclined, indicating difficult cleaning conditions. The -63+50 mm curve is irregular due to fluctuation in the fractional ash content with increasing float yield.

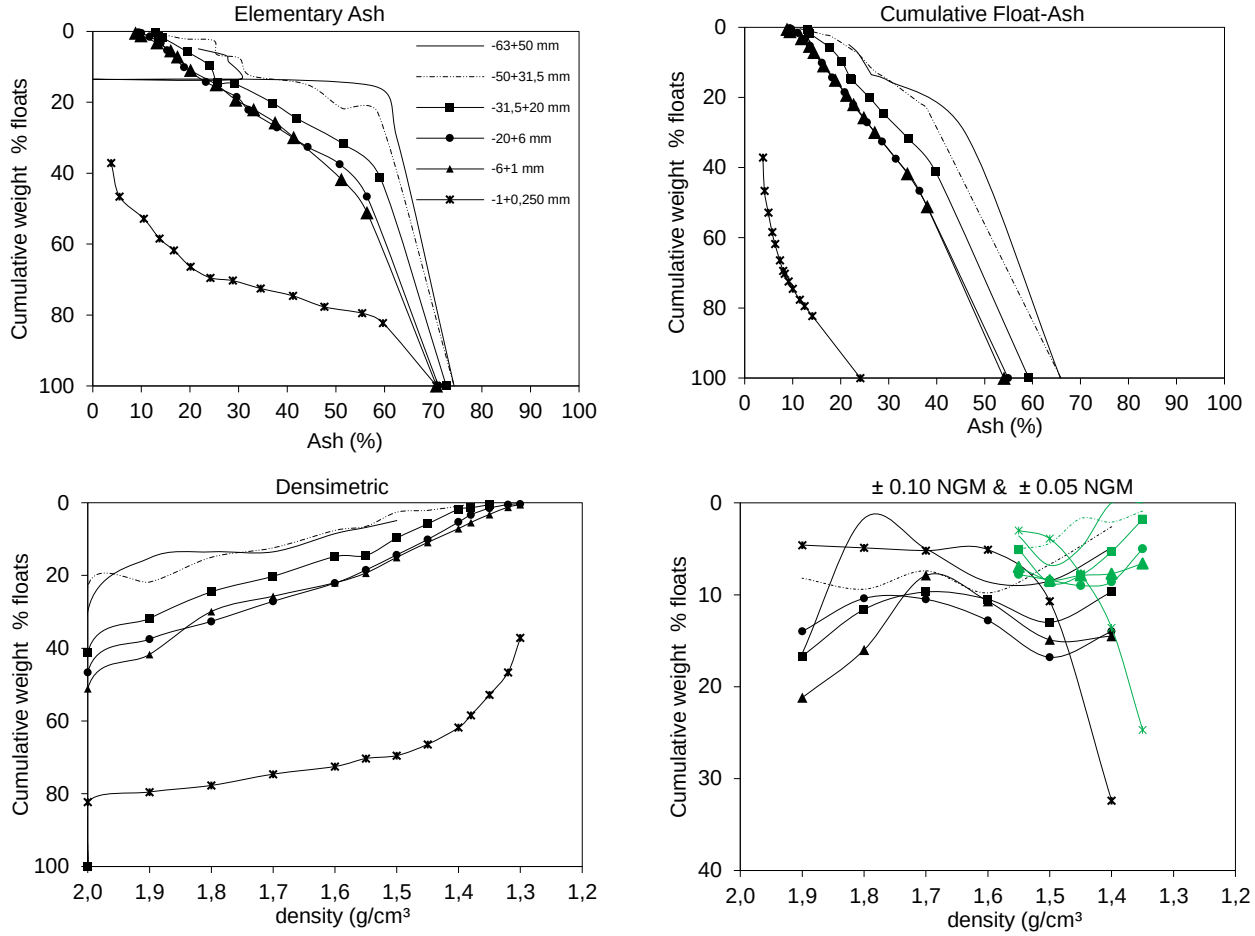

Figure 6.8. Standard washability curves for SBM. -63+50 mm (—), -50 +31.5 mm (-••-), -31.5+20 mm (■), -20+6 mm(●), -6+1 mm (▲) and -1 + 0.25 mm (*); ± 0.05 NGM in green in bottom right graph.

Similarly, the cumulative float ash curves occur in two clusters characterised by high ash and relatively low float yields (coarse and intermediate size classes), and low ash with relatively higher float yields (fine size class) as shown in Figure 6.8. In other words, the -1+ 0.25 mm particles have the highest float yields (37.1% to 82.3%) and lowest ash content (3.8% to 14%) over the full range of densities tested, compared to the coarse (float yield: 0.4% to 41.2%, ash: 9.4% to 45.9%), and intermediate size classes (float yield: 0.3% to 51.1%, ash: 8.8% to 38%) as shown in Table 6.8.

The densimetric curves for the coarse and intermediate size classes are also clustered together and characterised by relatively low float yields compared to the fine size class curve which is characterised by a higher recovery of float yields (Figure 6.8). Overall, the densimetric curves show that the float yield increases with increasing relative density. and with decreasing particle size (Table 6.8). Float yields above 50% were not recovered over the full range of densities tested in the coarse and intermediate size classes. Only a yield of 51.10% was obtained at 2.00 g/cm^3 in the -20+6 mm size fraction. In contrast, float yields above 50% were recoverable from 1.35 g/cm^3 to 2.00 g/cm^3 in the fine size class (Table 6.8).

Three distinct trends are observed in the ± 0.10 NGM curves for SBM in Figure 5.8. Firstly, the amount of NGM decreases with increasing density in -1 + 0.025 mm. Secondly, NGM is generally low at the lowermost and uppermost densities in -50 +31.5 mm. Lastly, NGM is generally highest at the lowermost and uppermost densities in -6+ 1 mm. Simple to moderate separation is possible from 1.40 g/cm^3 to 1.80 g/cm^3 in the -63+50 mm size fraction, and at all densities excluding 1.60 g/cm^3 in -50 +31.5 mm, and at 1.70 g/cm^3 in -6 +1 mm (Table 6.8). Only simple separation is achievable from 1.60 g/cm^3 to 1.90 g/cm^3 in -1 +0.25 mm.

In comparison, the ± 0.05 NGM curves show a uniform for the coarse and intermediate size classes, while the fine classes show a decrease in NGM with increasing relative density (Figure 6.8). Overall, the ± 0.05 NGM in SBM is in the range 1% to 25% and therefore predominately classified with easy separation conditions (Table 6.8).

Table 6.8. Cumulative washability report for seam SBM.

Separation density (g/cm³)	Yield %	Ash %	Elementary ash %	± 0.10 NGM density (g/cm³)	± 0.05 NGM density (g/cm³)	Yield %	Ash %	Elementary ash %	± 0.10 NGM density (g/cm³)	± 0.05 NGM density (g/cm³)	Yield %	Ash %	Elementary ash %	± 0.10 NGM density (g/cm³)	± 0.05 NGM density (g/cm³)
Fraction	**-63+50 mm**					**-50+31.5 mm**					**-31.5+20 mm**				
F1.30	0.00	0.00	0.00	-	-	0.00	0.00	0.00	-	-	0.00	0.00	0.00	-	-
F1.32	0.00	0.00	0.00	-	-	0.00	0.00	0.00	-	-	0.00	0.00	0.00	-	-
F1.35	0.00	0.00	0.00	-	0.00	0.00	0.00	0.00	-	0.90	0.50	13.00	0.25	-	1.80
F1.38	0.00	0.00	0.00	-	-	0.40	11.50	0.20	-		1.40	13.30	0.95	-	-
F1.40	0.00	0.00	0.00	4.90	0.00	0.90	13.20	0.65	2.60	2.10	1.80	13.60	1.60	9.70	5.30
F1.45	0.00	0.00	0.00	-	4.90	2.10	16.60	1.50	-	1.70	5.80	17.70	3.80	-	7.90
F1.50	4.90	21.70	2.45	8.50	6.80	2.60	18.10	2.35	6.70	4.40	9.70	20.20	7.75	13.00	8.70
F1.55	6.80	23.30	5.90	-	3.60	6.50	22.50	4.55	-	5.00	14.50	22.00	12.15	-	5.10
F1.60	8.50	24.20	7.65	8.60	-	7.60	23.70	7.05	9.80	-	14.80	22.20	14.65	10.50	-
F1.70	13.50	26.40	11.00	5.00	-	12.40	27.00	10.00	7.40	-	20.20	26.10	17.50	9.70	-
F1.80	13.50	26.40	13.50	1.70	-	15.00	30.00	13.75	9.40	-	24.50	28.90	22.35	11.60	-
F1.90	15.20	29.90	14.35	16.40	-	21.80	36.70	18.35	8.20	-	31.80	34.10	28.15	16.70	-
F2.00	29.90	45.90	22.55	-	-	23.20	38.00	22.50	-	-	41.20	39.80	36.50	-	-
S2.00	100.00	65.80	64.95	-	-	100.00	65.90	61.60	-	-	100.00	59.20	70.60	-	-
Fraction	**-20+6 mm**					**-6+1 mm**					**-1+0.25 mm**				
F1.30	0.30	9.40	0.15	-	-	0.50	8.80	0.25	-	-	37.10	3.80	18.55	-	-
F1.32	0.50	9.70	0.40	-	-	1.20	9.40	0.85	-	-	46.60	4.10	41.85	-	-
F1.35	1.50	11.00	1.00	-	5.00	3.20	11.80	2.20	-	6.60	52.80	4.90	49.65	-	24.70
F1.38	3.30	12.60	2.40	-	-	5.40	13.50	4.25	-	-	58.40	5.70	55.60	-	-
F1.40	5.30	13.60	4.25	14.00	8.60	7.10	14.40	6.25	14.50	7.70	61.80	6.30	60.10	32.40	13.60
F1.45	10.10	16.10	7.70	-	9.00	10.90	16.40	9.05	-	7.90	66.40	7.30	64.10	-	7.70
F1.50	14.30	18.20	12.25	16.80	8.40	15.00	18.90	12.95	14.90	8.40	69.50	8.00	67.95	10.70	3.90
F1.55	18.50	20.80	16.40	-	7.80	19.30	21.20	17.15	-	7.00	70.30	8.30	69.90	-	3.00
F1.60	22.10	22.60	20.30	12.80	-	22.00	22.70	20.70	10.70	-	72.50	9.10	71.45	5.10	-
F1.70	27.10	25.50	24.60	10.50	-	25.70	24.80	23.85	7.90	-	74.60	10.00	73.55	5.20	-
F1.80	32.60	28.60	29.85	10.40	-	29.90	27.10	27.80	16.00	-	77.70	11.50	76.15	4.90	-
F1.90	37.50	31.50	35.00	14.00	-	41.70	33.90	35.75	21.20	-	79.50	12.50	78.60	4.60	-
F2.00	46.60	36.40	42.05	-	-	51.10	38.00	46.45	-	-	82.30	14.10	80.90	-	-
S2.00	100.00	54.90	73.30	-	-	100.00	54.00	75.55	-	-	100.00	24.10	91.15	-	-

6.2.9. Seam Bottom Lower (SBL)

The washability curves for SBL occur in three distinct clusters for each of the parameters considered on the basis of particle size viz, coarse size class, intermediate size class and fine size class (Figure 6.9). The elementary ash curves are generally steeply inclined, more so with increasing particle size, suggesting difficult separation for the intermediate and coarse size classes (Figure 6.9). However, the slope of the -1+0.25 mm curve is gentler and concave upward in shape approximating easier separation conditions. The -63+50 mm curve is irregularly shaped due to a lack of yield recovery at 1.55 g/cm^3 and 2.00 g/cm^3.

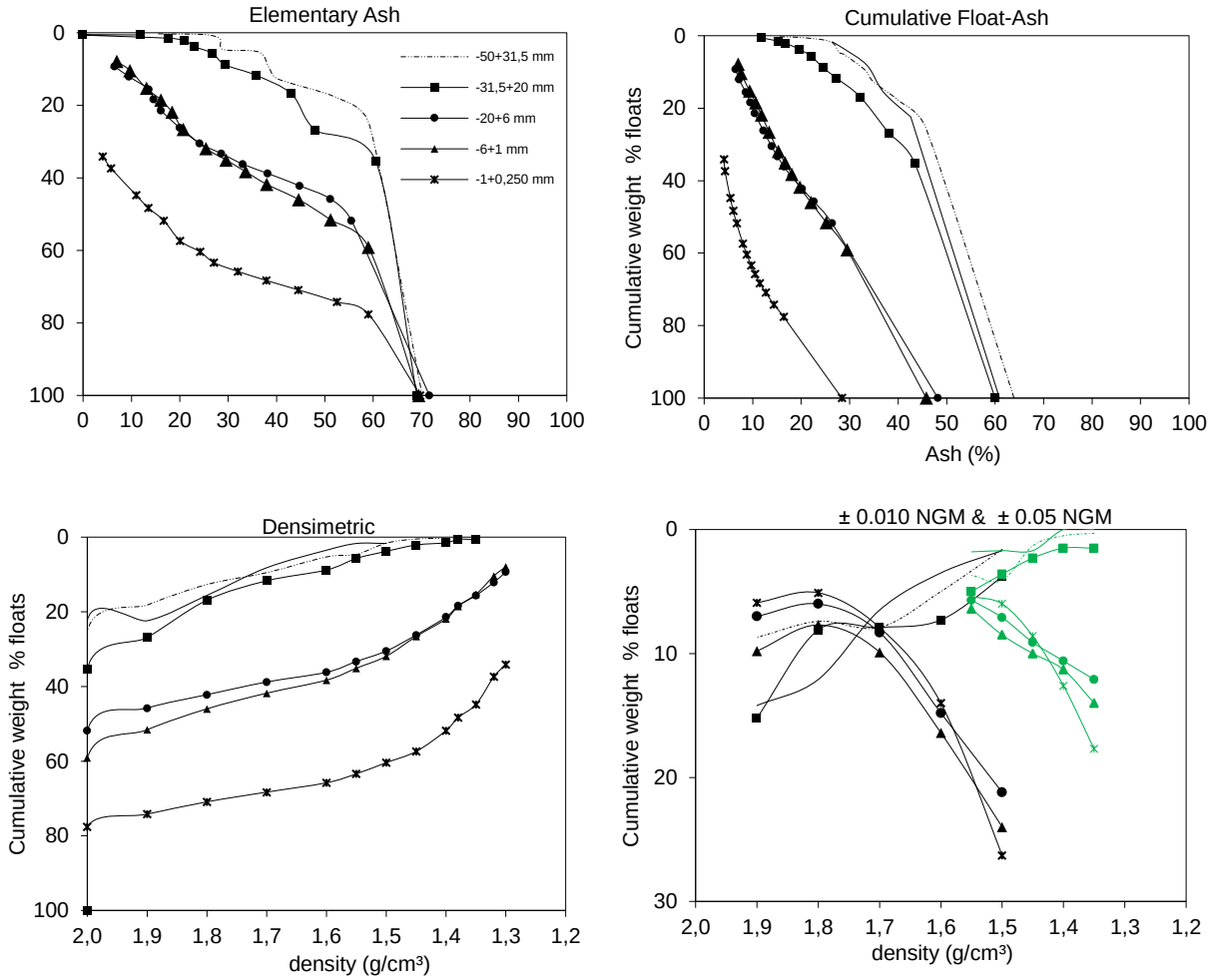

Figure 6.9. Standard washability curves for SBL. -63+50 mm (–), -50 +31.5 mm (-••-), -31.5+20 mm (■), -20+6 mm(●), -6+1 mm (▲) and -1 + 0.25 mm (*); ± 0.05 NGM in green in bottom right graph.

The proportion of cumulative float yields recovered increased with decreasing particle size, while the inverse applies to the ash content (Figure 6.9). As highlighted in Table 6.9, the coarse size class consists of float yields in the range 0.6% to 35.4% and ash, 11.8% to 45.7%. The intermediate size class consists of float yields in the range 7.9% to 59.1% and ash, 6.5% to

29.5%. The fine size class consists of float yields in the range 34.1% to 77.6% and ash, 4.1% to 16.4%.

The amount of ± 0.10 NGM increased with increasing relative density in the coarse size class while, the NGM decreased with increasing relative density in the intermediate and fine size classes (Figure 6.9). Hence, easier separation is expected at smaller particle sizes. The NGM in SBL ranges from 2% to 26%, yet simple to moderate separation is generally possible from 1.40 g/cm^3 to 1.90 g/cm^3 in the coarse size class. While, simple to moderate separation can generally be achieved from 1.60 g/cm^3 to 1.90 g/cm^3 in the intermediate and fine size classes.

Formidable separation is predicted for the fine size class as NGM is in the range 33.50%-70.12%. Similarly, the intermediate size class is characterised by formidable separation conditions from 1.60 g/cm^3 to 1.90 g/cm^3. However, moderate and extremely difficult conditions are predicted at 1.40 g/cm^3 and 1.50 g/cm^3. The coarse size class is characterised by simple separation from1.40 g/cm^3 to 1.60 g/cm^3, while moderate to very difficult separation is expected from 1.70 g/cm^3 to 1.90 g/cm^3.

In comparison, the ± 0.05 NGM curves for SBL display a decrease of NGM with increasing relative density for the intermediate and fine size classes, while a uniform distribution is observed for the coarse size class (Figure 6.9). Easy separation conditions are expected for SBL as the overall amount of ± 0.05 NGM is in the range 1% to 18% (Table 6.9).

Table 6.9. Cumulative washability report for seam SBL.

Separation density (g/cm³)	Yield %	Ash %	Elementary ash %	± 0.10 NGM density (g/cm³)	± 0.05 NGM density (g/cm³)	Yield %	Ash %	Elementary ash %	± 0.10 NGM density (g/cm³)	± 0.05 NGM density (g/cm³)	Yield %	Ash %	Elementary ash %	± 0.10 NGM density (g/cm³)	± 0.05 NGM density (g/cm³)
Fraction	-63+50 mm					**-50+31.5 mm**					**-31.5+20 mm**				
F1.30	0.00	0.00	0.00	-	-	0.00	0.00	100.00	-	-	0.00	0.00	100.00	-	-
F1.32	0.00	0.00	0.00	-	-	0.00	0.00	0.00	-	-	0.00	0.00	0.00	-	-
F1.35	0.00	0.00	0.00	-	0.00	0.00	0.00	0.00	-	0.30	0.60	11.80	0.30	-	1.50
F1.38	0.00	0.00	0.00	-	-	0.00	0.00	0.00	-	-	0.60	11.80	0.60	-	-
F1.40	0.00	0.00	0.00	1.70	0.00	0.30	15.60	0.15	1.60	0.50	1.50	15.30	1.05	3.80	1.50
F1.45	0.00	0.00	0.00	-	1.70	0.50	19.90	0.40	-	1.30	2.10	16.80	1.80	-	2.30
F1.50	1.70	26.40	0.85	3.50	1.70	1.60	26.00	1.10	5.00	4.10	3.80	19.70	3.00	7.30	3.60
F1.55	1.70	26.40	1.70	-	1.80	4.60	27.80	3.05	-	3.70	5.70	22.10	4.75	-	5.00
F1.60	3.50	28.70	2.60	6.50	-	5.30	29.00	4.95	7.90	-	8.80	24.50	7.20	7.90	-
F1.70	8.20	33.60	5.85	12.10	-	9.50	33.20	7.40	7.40	-	11.70	27.30	10.25	8.10	-
F1.80	15.60	37.00	11.95	14.20	-	12.70	34.90	11.10	8.70	-	16.90	32.20	14.35	15.20	-
F1.90	22.40	42.60	18.95	6.80	-	18.20	40.40	15.45	12.70	-	26.90	38.10	21.85	18.50	-
F2.00	22.40	42.60	22.40	-	-	25.40	45.70	21.80	-	-	35.40	43.50	31.15	-	-
S2.00	100.00	60.90	61.20	-	-	100.00	63.90	62.70	-	-	100.00	60.00	67.70	-	-
Fraction	**-20+6 mm**					**-6+1 mm**					**-1+0.25 mm**				
F1.30	9.30	6.50	4.65	-	-	7.90	7.00	3.95	-	-	34.10	4.10	17.05	-	-
F1.32	12.10	7.20	10.70	-	-	10.40	7.60	9.15	-	-	37.40	4.30	35.75	-	-
F1.35	15.60	8.60	13.80	-	12.10	15.30	9.40	12.85	-	14.00	44.80	5.40	41.15	-	17.70
F1.38	18.40	9.50	17.00	-	-	18.50	10.60	16.90	-	-	48.30	6.00	46.55	-	-
F1.40	21.40	10.40	19.90	21.20	10.60	21.90	11.80	20.20	24.00	11.30	51.80	6.70	50.00	26.30	12.60
F1.45	26.20	12.20	23.80	-	9.10	26.60	13.40	24.25	-	10.00	57.40	8.00	54.65	-	8.60
F1.50	30.50	13.90	28.35	14.80	7.10	31.90	15.30	29.20	16.40	8.50	60.40	8.80	58.85	14.00	6.00
F1.55	33.30	15.10	31.95	-	5.70	35.10	16.70	33.55	-	6.40	63.40	9.70	61.90	-	5.40
F1.60	36.20	16.50	34.75	8.30	-	38.30	18.10	36.70	9.90	-	65.80	10.50	64.65	7.90	-
F1.70	38.80	18.00	37.50	6.00	-	41.80	19.70	40.05	7.70	-	68.30	11.50	67.05	5.10	-
F1.80	42.20	20.20	40.50	7.00	-	46.00	22.00	43.90	9.80	-	70.90	12.70	69.60	5.90	-
F1.90	45.80	22.60	44.00	9.60	-	51.60	25.20	48.80	13.10	-	74.20	14.40	72.55	6.70	-
F2.00	51.80	26.40	48.80	-	-	59.10	29.50	55.35	-	-	77.60	16.40	75.90	-	-
S2.00	100.00	48.20	75.90	-	-	100.00	45.80	79.55	-	-	100.00	28.40	88.80	-	-

6.3. Discussion

The general observations regarding the cumulative float ash curves for the seams and partings indicate that the highest proportion of float yields is recovered in the fine size class over the full range of relative densities considered. Hence, the proportion of clean coal recovered increased with decreasing particle size. This observation agrees with literature (Magwai and Claassen, 2013) and the test work conducted on the bulk Makhado sample (Mostert, 2016). However, seams SU and SMU deviated from the preceding general observation since the proportion of clean coal recovered in the -63+50mm size fraction were very similar to those recovered in the -1+0.25 mm size fraction, which may be as a result of the friable nature of the coal in these seams. Overall, there appears to be an average 30% decrease in float yield obtained with depth, with seams SU and SMU having the highest float yield recovery. Of the partings, P2 had the highest proportion of recovered floats across all size fractions, followed by P1, while P3 had the poorest recovery of floats. The highest float yields recovered from the partings, albeit low compared to the seams, were obtained in the -1+0.25 mm size fraction for all partings.

The inverse behaviour was observed for the ash content, in other words, ash decreased with decreasing particle size and relative density. Similar results have been reported in literature (de Souza *et al*., 2012; Nasir *et al*., 2012; Mir, 2014; Sana *et al*., 2017). As expected, the highest amount of ash occurred in the partings. Seams SML and SBM had the highest ash while SU and SMU had the lowest ash overall. Stratigraphically, the ash content associated with the floats increased with depth.

A qualitative assessment of the ease or difficulty of washing was conducted by observing the shape of the elementary ash curves for each seam and parting. Overall, the slope of the elementary ash curves is steeply inclined for the uppermost seams, SU, SMU and SML therefore, difficult separation conditions are expected in these horizons. In contrast, the slope of the elementary ash slopes are gentler in the lowermost seams SBU, SBM and SBL, including the partings. Hence, separation may be easier for the three lowermost seams and partings compared to the uppermost seams. Furthermore, the slope of the elementary ash curves for all seams and partings becomes more L-shaped with decreasing particle size (and at high relative density in some instances), indicating that the difficulty of separation decreased with decreasing particle size (and at high relative density in some instances).

Further assessment of the ease or difficulty of washing was conducted by calculating the ± 0.10 NGM for each seam and parting. The coals from LD57 have up to 53% ± 0.10 NGM, which is similar to those reported in the literature for South African coals, typically 25% to 51%

± 0.10 NGM (Bunt, 1997; Bhattacharya *et al*., 2016). Despite the considerably high amounts of NGM observed at some density intervals, easy to moderate separation conditions were prevalent from 1.60 g/cm^3 to 1.90 g/cm^3 in the fine size class for all seams and partings. Overall, the proportion of ± 0.10 NGM decreased with depth. The uppermost seams SU, SMU and SML have the highest proportion of NGM (1% to 53%) while the lowermost seams (SBU, SBM and SBL) and partings have less NGM in the range 1% to 38%. This observation is in agreement with the general trend in which the NGM tends to be lowest at the lowermost and higher most ends of the relative density range (Bhattacharya *et al*., 2016; Subba Rao and Gouricharan, 2016).

Comparatively, the amount of ± 0.05 NGM in the coals from LD57 is less than the ± 0.10 NGM at comparable relative densities and size classes; up to 41% for the seams and up to 21% for the partings. Similarly, Magwai and Claassen (2013) found that the ± 0.05 NGM (up to 60%) was less than the ± 0.10 NGM (up to 80%) at Leeuwpan coal mine. Like the elementary ash curves and ± 0.10 NGM, the amount of ± 0.05 NGM decreased with depth as there was less ± 0.05 NGM in the lower most coal seams compared to the upper coal seams. Furthermore, given the overall low amount of ± 0.05 NGM, easy separation conditions were achievable over much of the density range irrespective of size class, particularly in the lowermost seams SBU, SBM and SBL, and more so in the partings due to poor float yields.

Taking into account the clean coal yields and ash content, the 10% nominal ash requirement by MC Mining for a metallurgical coal product is theoretically achievable in the fine class fraction at a density range from 1.55 -1.70 g/cm^3, with a recoverable yield ranging from 63%-78% for all the seams. Only P2 yielded a float recovery of 39% with 10% ash at 1.45 g/cm^3. In contrast, float yields of 29% (1.50 g/cm^3) and 26% (1.45 g/cm^3) could be achieved at 9% ash for P1 and P3, respectively. The ash in P1 and P3 exceeded the 10% ash limit at specified densities for these samples. In the -6 + 1 mm size fraction, 10% ash is achievable in SU, P1, SMU, SML, P3 and SBU from 1.30-1.40 g/cm^3, with yields from 1-35%. Ash yields of 10% are not recoverable above a particle size of 6 mm. Given the 1.55 -1.70 g/cm^3 density range for the fine size fraction, simple to moderate separation is predicted for the coal plies mentioned above the basis of ± 0.10 NGM, and similarly easy separation is predicted based on ± 0.05 NGM. The ease of separation in the - 6 + 1 mm size fraction is predicted to be simple (± 0.10 NGM) or easy (± 0.05 NGM) for P1 and P3. In contrast, separation conditions for the previously mentioned seams in the - 6 + 1 mm size fraction are predicted to be very difficult to formidable for the seams on the basis of ± 0.10 NGM compared to moderately difficult on the basis of ± 0.05 NGM.

Taking into account all the washability parameters discussed herein, it can be concluded that the optimal cut point density required to achieve a primary metallurgical product of 10% ash content, lies between 1.55 and 1.70 g/cm^3 at a particle size of -1+0.25 mm for all seams. Only P2 should be considered at 1.45 g/cm^3 for this purpose. Simple to moderate separation is predicted based on ± 0.10 NGM. It can also be inferred that easy separation conditions will occur based on the observed ± 0.05 NGM trends.

Chapter 7: Part 2 Washability-Coal quality

7.1. Introduction

The complementary coal quality data (proximate, CV, and total sulphur) for the float -sink products are presented herein to assess the efficiency of beneficiation in yielding suitable coal quality for utilisation purposes. This chapter addresses objectives for part one of this research.

As previously stated, the anomalies observed on some trends on the graphs are due discrepancies in yield recovery during testing in the laboratory and do not arise due to the coal itself.

7.2. Coal quality washability of float-sink fractions

7.2.1. Seam Upper (SU)

The coal quality washability data for SU is illustrated in Figure 7.1 and summarized in Table 7.1.

The reported moisture content in SU varied from 1.2% to 1.7% in the coarse and intermediate size classes (Table 7.1). But remained generally constant at 1.2% over the full density range in the fine size class. Overall, volatile matter, total sulphur and the CV increased with decreasing particle size, with the volatile matter and CV being highest at low densities. Total sulphur varied across the density range in the coarse size fraction. In contrast the total sulphur was uniformly distributed across the entire the density range in the fine and intermediate size fractions but varied for the coarser fractions. The sink fractions of SU are characterised by very high ash (up to 64%), and volatile matter (up to 29%) while the CV and total sulphur contents are lower relative to the float fractions. The sink fraction in the fine size class contains high CV (27 MJ/kg) and volatile matter (28.8%) which is comparable to that of the float fractions (Table 7.1).

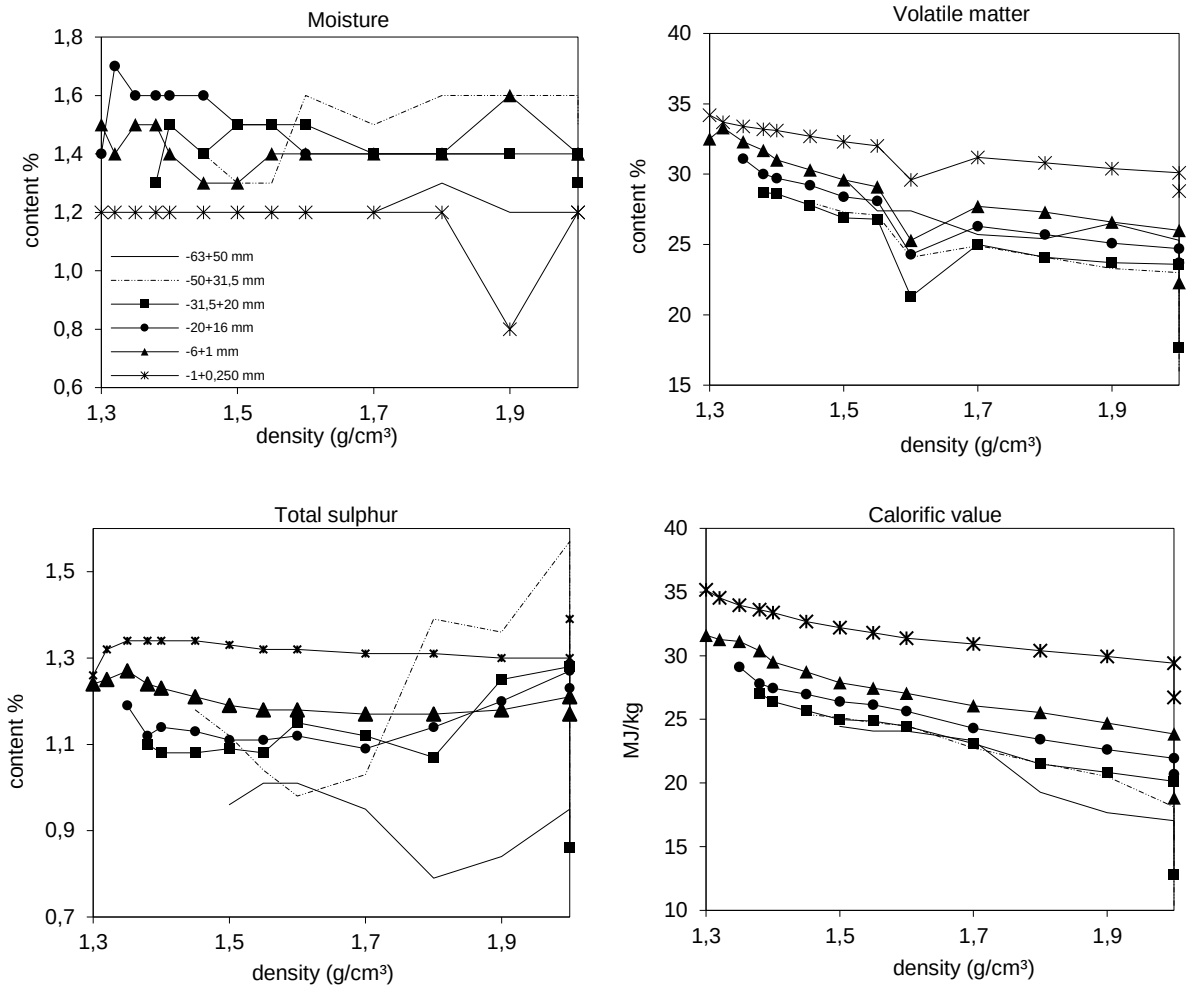

Figure 7.1. Chemical analyses (adb) by size fraction for SU. -63+50 mm (—), -50 +31.5 mm (- - -), -31.5+20 mm (■), -20+6 mm (●), -6+1 mm (▲) and -1 + 0.25 mm (*).

Table 7.1. Cumulative coal quality for SU (adb).

Separation density (g/cm³)	Moisture (%)	Ash (%)	Volatile matter (%)	Calorific value (MJ/kg)	Total sulphur (%)	Moisture (%)	Ash (%)	Volatile matter (%)	Calorific value (MJ/kg)	Total sulphur (%)	Moisture (%)	Ash (%)	Volatile matter (%)	Calorific value (MJ/kg)	Total sulphur (%)
Fraction	**-63+50 mm**					**-50+31.5 mm**					**-31.5+20 mm**				
F1.30	-	-	-	-	-	-	-	-	-	-	-	-	-	-	-
F1.32	-	-	-	-	-	-	-	-	-	-	-	-	-	-	-
F1.35	-	-	-	-	-	-	-	-	-	-	-	-	-	-	-
F1.38	-	-	-	-	-	-	-	-	-	-	1.30	22.30	28.70	27.06	1.10
F1.40	-	-	-	-	-	-	-	-	-	-	1.50	24.00	28.60	26.39	1.08
F1.45	-	-	-	-	-	1.40	25.10	28.00	25.39	1.18	1.40	25.80	27.80	25.69	1.08
F1.50	1.20	25.50	29.70	24.45	0.96	1.30	26.30	27.30	25.13	1.12	1.50	27.10	26.90	24.98	1.09
F1.55	1.20	28.20	27.40	24.09	1.01	1.30	27.40	27.10	24.74	1.04	1.50	27.40	26.80	24.87	1.08
F1.60	1.20	28.20	27.40	24.09	1.01	1.60	28.20	24.10	24.50	0.98	1.50	28.40	21.30	24.45	1.15
F1.70	1.20	30.80	25.70	23.32	0.95	1.50	32.60	24.90	22.75	1.03	1.40	31.90	25.00	23.10	1.12
F1.80	1.30	40.30	25.40	19.28	0.79	1.60	35.50	24.10	21.56	1.39	1.40	35.60	24.10	21.50	1.07
F1.90	1.20	44.70	26.50	17.67	0.84	1.60	38.00	23.30	20.52	1.36	1.40	37.20	23.70	20.84	1.25
F2.00	1.20	45.80	25.30	17.05	0.95	1.60	43.40	23.00	18.12	1.57	1.40	38.80	23.60	20.14	1.28
S2.00	1.20	49.90	23.60	15.50	0.87	1.50	64.10	16.00	10.22	0.93	1.30	57.80	17.70	12.78	0.86
Fraction	**-20+6 mm**					**-6+1 mm**					**-1+0.25 mm**				
F1.30	-	-	-	-	-	1.50	9.90	32.50	31.61	1.24	1.20	1.50	34.20	35.16	1.26
F1.32	-	-	-	-	-	1.40	10.80	33.30	31.26	1.25	1.20	2.80	33.70	34.54	1.32
F1.35	1.40	17.00	31.10	29.11	1.19	1.50	11.50	32.30	31.12	1.27	1.20	4.00	33.40	33.96	1.34
F1.38	1.70	19.50	30.00	27.81	1.12	1.50	13.50	31.70	30.38	1.24	1.20	4.90	33.20	33.60	1.34
F1.40	1.60	20.70	29.70	27.45	1.14	1.40	15.70	31.00	29.50	1.23	1.20	5.50	33.10	33.39	1.34
F1.45	1.60	21.90	29.20	26.98	1.13	1.30	17.80	30.30	28.72	1.21	1.20	7.30	32.70	32.68	1.34
F1.50	1.60	23.30	28.40	26.40	1.11	1.30	19.80	29.60	27.87	1.19	1.20	8.60	32.30	32.21	1.33
F1.55	1.60	24.00	28.10	26.14	1.11	1.40	20.90	29.10	27.46	1.18	1.20	9.70	32.00	31.79	1.32
F1.60	1.50	25.30	24.30	25.63	1.12	1.40	22.00	25.30	27.04	1.18	1.20	10.80	29.60	31.37	1.32
F1.70	1.50	28.70	26.30	24.30	1.09	1.40	24.50	27.70	26.06	1.17	1.20	12.00	31.20	30.93	1.31
F1.80	1.40	30.90	25.70	23.43	1.14	1.40	25.80	27.30	25.54	1.17	1.20	13.40	30.80	30.39	1.31
F1.90	1.40	32.90	25.10	22.63	1.20	1.60	27.90	26.60	24.72	1.18	0.80	14.50	30.40	29.93	1.30
F2.00	1.40	34.60	24.70	21.95	1.27	1.40	30.00	26.00	23.85	1.21	1.20	15.80	30.10	29.42	1.30
S2.00	1.40	37.80	23.70	20.68	1.23	1.40	42.40	22.30	18.83	1.17	1.20	22.10	28.80	26.73	1.39

7.2.2. Parting 1 (P1)

The coal quality washability data for P1 is illustrated in Figure 7.2 and summarized in Table 7.2.

The results show the moisture content in P1 varied from 0.4% to 1.8%, and generally decreased with particle size but was found to be highest at high relative density in each size fraction. The volatile matter and CV are characterised by an increase with decreasing particle size and decreasing relative density (Figure 7.2). Total sulphur in P1 varied from 0.93% to 1.48%. The coarse and intermediate size classes displayed an increase in the sulphur content with increasing relative density but is uniformly distributed in the fine size class. The sink fractions of P1 retained significantly higher amounts of ash of up to 79.8% while, the volatile matter, CV and total sulphur contents are much lower relative to the float fractions (Figure 7.2). Despite reporting high ash of 50%, the sink fraction from the fine size class contains good amounts of volatile matter (20.4 MJ/kg) and total sulphur (1.2%).

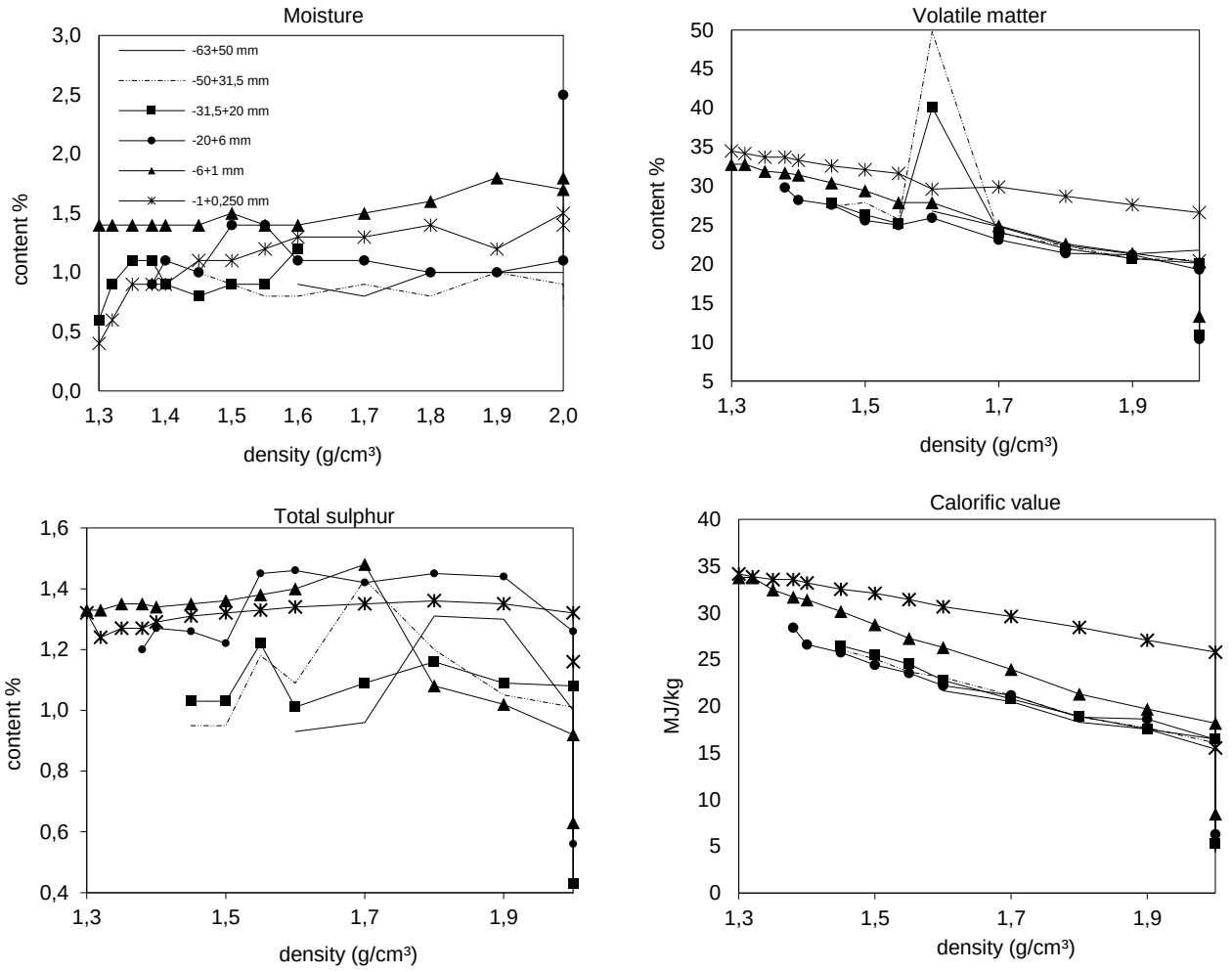

Figure 7.2. Chemical analyses (adb) by size fraction for P1. -63+50 mm (–), -50 +31.5 mm (- - -), -31.5+20 mm (■), -20+6 mm (●), -6+1 mm (▲) and -1 + 0.25 mm (*).

Table 7.2. Cumulative coal quality for P1 (adb).

Separation density (g/cm³)	Moisture (%)	Ash (%)	Volatile matter (%)	Calorific value (MJ/kg)	Total sulphur (%)	Moisture (%)	Ash (%)	Volatile matter (%)	Calorific value (MJ/kg)	Total sulphur (%)	Moisture (%)	Ash (%)	Volatile matter (%)	Calorific value (MJ/kg)	Total sulphur (%)
Fraction	**-63+50 mm**					**-50+31.5 mm**					**-31.5+20 mm**				
F1.30	-	-	-	-	-	-	-	-	-	-	-	-	-	-	-
F1.32	-	-	-	-	-	-	-	-	-	-	-	-	-	-	-
F1.35	-	-	-	-	-	-	-	-	-	-	-	-	-	-	-
F1.38	-	-	-	-	-	-	-	-	-	-	-	-	-	-	-
F1.40	-	-	-	-	-	-	-	-	-	-	-	-	-	-	-
F1.45	-	-	-	-	-	1.00	23.50	27.40	26.05	0.95	0.60	23.90	27.80	26.47	1.03
F1.50	-	-	-	-	-	0.90	27.10	27.90	25.04	0.95	0.90	26.40	26.30	25.52	1.03
F1.55	-	-	-	-	-	0.80	31.70	25.70	23.67	1.18	1.10	29.00	25.20	24.52	1.22
F1.60	0.90	34.80	26.80	21.65	0.93	0.80	33.10	49.80	23.06	1.09	1.10	33.70	40.10	22.78	1.01
F1.70	0.80	38.20	24.80	20.50	0.96	0.90	37.60	24.00	21.15	1.43	0.90	38.20	24.10	20.75	1.09
F1.80	1.00	43.80	22.40	18.29	1.31	0.80	43.30	22.30	18.86	1.20	0.80	43.10	22.00	18.92	1.16
F1.90	1.00	45.70	21.30	17.56	1.30	1.00	46.30	20.70	17.68	1.05	0.90	46.70	20.70	17.56	1.09
F2.00	1.00	50.70	21.80	15.40	1.00	0.90	49.80	20.50	16.07	1.01	0.90	49.30	20.10	16.49	1.08
S2.00	1.00	79.70	11.10	4.38	0.44	0.70	79.80	11.10	4.34	0.39	1.20	77.60	10.90	5.32	0.43
Fraction	**-20+6 mm**					**-6+1 mm**					**-1+0.25 mm**				
F1.30	-	-	-	-	-	1.40	4.40	32.80	33.78	1.33	0.40	3.70	34.50	34.15	1.32
F1.32	-	-	-	-	-	1.40	4.40	32.80	33.78	1.33	0.60	4.30	34.20	33.87	1.24
F1.35	-	-	-	-	-	1.40	7.80	31.90	32.47	1.35	0.90	5.10	33.70	33.57	1.27
F1.38	0.90	19.00	29.80	28.41	1.20	1.40	9.70	31.70	31.70	1.35	0.90	5.10	33.70	33.57	1.27
F1.40	1.10	23.40	28.20	26.58	1.27	1.40	10.70	31.40	31.38	1.34	0.90	6.10	33.30	33.20	1.29
F1.45	1.00	25.80	27.60	25.77	1.26	1.40	14.10	30.40	30.15	1.35	1.10	7.90	32.60	32.54	1.31
F1.50	1.40	29.60	25.60	24.41	1.22	1.50	17.80	29.40	28.74	1.36	1.10	9.10	32.10	32.08	1.32
F1.55	1.40	31.70	25.00	23.54	1.45	1.40	21.80	27.90	27.26	1.38	1.20	10.90	31.60	31.43	1.33
F1.60	1.10	34.80	25.90	22.21	1.46	1.40	24.40	27.90	26.28	1.40	1.30	12.90	29.60	30.65	1.34
F1.70	1.10	37.90	23.10	21.16	1.42	1.50	30.40	24.90	23.93	1.48	1.30	15.70	29.90	29.61	1.35
F1.80	1.00	42.90	21.40	18.82	1.45	1.60	37.00	22.60	21.30	1.08	1.40	18.70	28.70	28.44	1.36
F1.90	1.00	43.50	21.20	18.61	1.44	1.80	41.10	21.40	19.70	1.02	1.20	22.20	27.60	27.06	1.35
F2.00	1.10	49.40	19.30	16.44	1.26	1.70	44.80	20.20	18.18	0.92	1.50	25.40	26.60	25.79	1.32
S2.00	2.50	75.10	10.40	6.30	0.56	1.80	69.20	13.30	8.45	0.63	1.40	50.00	20.40	15.54	1.16

7.2.3. Seam Middle Upper (SMU)

The coal quality washability data for SMU is illustrated in Figure 7.3 and summarized in Table 7.3.

The overall moisture content displayed variability. It can be seen that the volatile matter, total sulphur and CV for SMU increased with decreasing particle size (Figure 7.3). In comparison, the sink fractions of SMU are characterised by very high ash (up to 59%), and volatile matter (up to 28%) while the CV and total sulphur contents are lower relative to the float fractions (Table 7.3). However, the sink fraction in the fine size class contains high CV (26.68 MJ/kg) and volatile matter (28.8%).

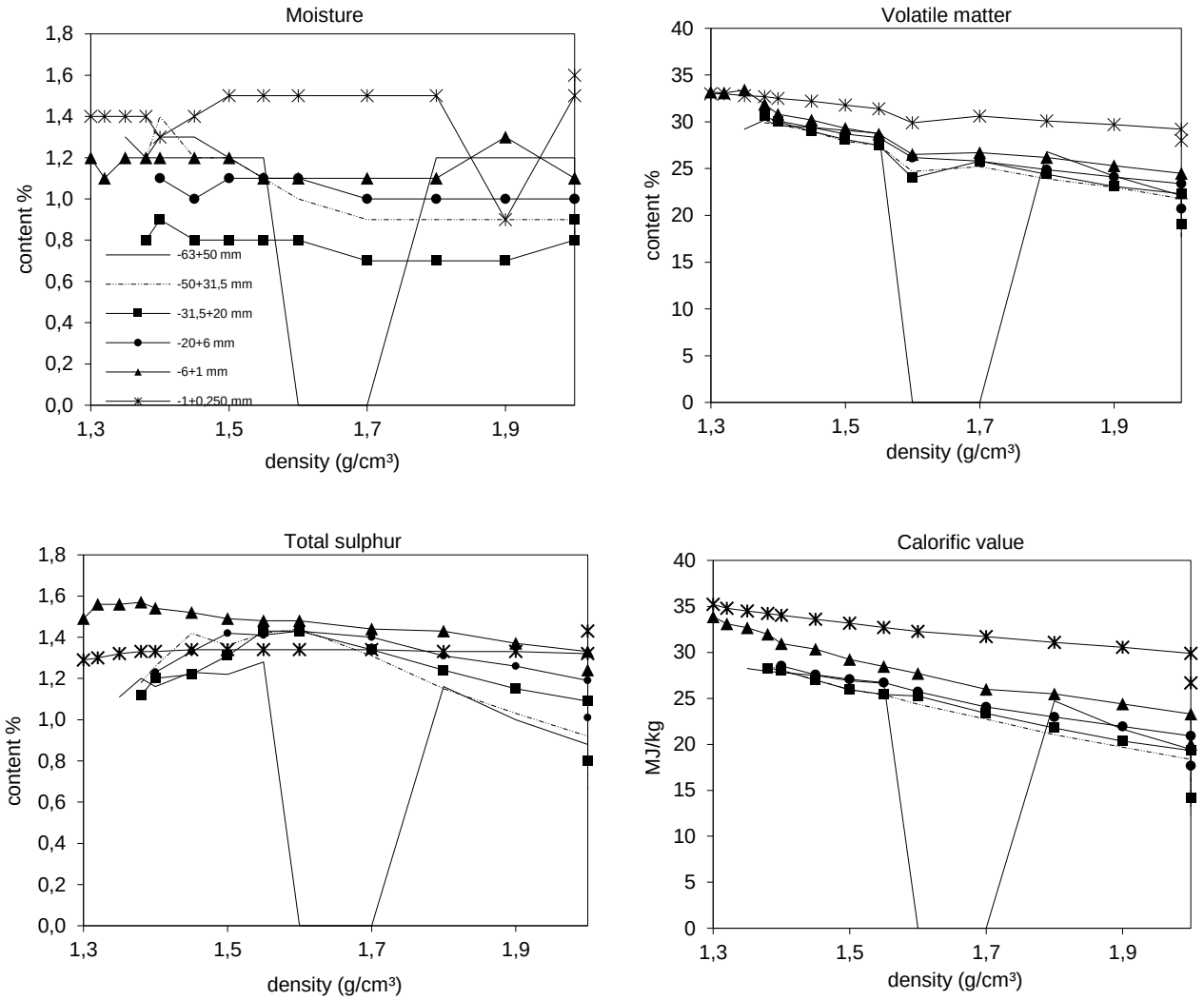

Figure 7.3. Chemical analyses (adb) by size fraction for SMU. -63+50 mm (—), -50 +31.5 mm (- - -), -31.5+20 mm (■), -20+6 mm (●), -6+1 mm (▲) and -1 + 0.25 mm (*).

Table 7.3. Cumulative coal quality for SMU (adb).

Separation density (g/cm³)	Moisture (%)	Ash (%)	Volatile matter (%)	Calorific value (MJ/kg)	Total sulphur (%)	Moisture (%)	Ash (%)	Volatile matter (%)	Calorific value (MJ/kg)	Total sulphur (%)	Moisture (%)	Ash (%)	Volatile matter (%)	Calorific value (MJ/kg)	Total sulphur (%)
Fraction	**-63+50 mm**					**-50+31.5 mm**					**-31.5+20 mm**				
F1.30	-	-	-	-	-	-	-	-	-	-	-	-	-	-	-
F1.32	-	-	-	-	-	-	-	-	-	-	-	-	-	-	-
F1.35	1.30	18.20	29.20	28.24	1.11	-	-	-	-	-	-	-	-	-	-
F1.38	1.20	19.30	30.20	27.94	1.20	1.20	17.90	29.90	28.70	1.18	0.80	19.60	30.60	28.28	1.12
F1.40	1.30	19.80	29.60	27.80	1.16	1.40	19.60	29.70	28.00	1.26	0.90	20.00	30.00	28.07	1.20
F1.45	1.30	20.80	29.40	27.49	1.23	1.20	21.60	29.00	27.04	1.42	0.80	22.40	29.00	26.98	1.22
F1.50	1.20	22.20	29.10	26.91	1.22	1.20	24.50	27.90	25.91	1.36	0.80	24.80	28.10	25.95	1.31
F1.55	1.20	23.00	28.80	26.63	1.28	1.10	26.10	27.50	25.38	1.42	0.80	26.30	27.50	25.41	1.43
F1.60	0.00	0.00	0.00	0.00	0.00	1.00	28.70	24.70	24.37	1.44	0.80	26.70	24.00	25.25	1.43
F1.70	0.00	0.00	0.00	0.00	0.00	0.90	32.80	25.20	22.75	1.31	0.70	31.60	25.80	23.35	1.34
F1.80	1.20	28.00	26.80	24.73	1.16	0.90	37.00	23.90	21.05	1.15	0.70	35.50	24.40	21.79	1.24
F1.90	1.20	35.80	24.20	21.64	1.00	0.90	40.20	23.00	19.70	1.03	0.70	39.10	23.10	20.34	1.15
F2.00	1.20	40.60	22.10	19.46	0.88	0.90	43.90	21.80	18.37	0.92	0.80	41.60	22.30	19.33	1.09
S2.00	1.20	49.90	23.60	15.50	0.87	1.50	64.10	16.00	10.22	0.93	0.90	53.90	19.10	14.19	0.80
Fraction	**-20+6 mm**					**-6+1 mm**					**-1+0.25 mm**				
F1.30	-	-	-	-	-	1.20	4.80	33.20	33.87	1.49	1.40	3.00	33.00	35.21	1.29
F1.32	-	-	-	-	-	1.10	6.10	33.10	33.09	1.56	1.40	3.40	33.00	34.79	1.30
F1.35	-	-	-	-	-	1.20	8.00	33.40	32.67	1.56	1.40	4.10	32.80	34.48	1.32
F1.38	-	-	-	-	-	1.20	9.80	31.90	31.99	1.57	1.40	4.90	32.70	34.23	1.33
F1.40	1.10	18.80	30.10	28.52	1.23	1.20	12.00	30.80	30.96	1.54	1.30	5.50	32.50	34.02	1.33
F1.45	1.00	21.30	29.40	27.57	1.33	1.20	13.70	30.20	30.35	1.52	1.40	6.50	32.20	33.59	1.34
F1.50	1.10	22.60	28.70	27.06	1.42	1.20	16.90	29.30	29.22	1.49	1.50	7.60	31.80	33.16	1.34
F1.55	1.10	23.60	28.30	26.72	1.41	1.10	19.00	28.70	28.46	1.48	1.50	8.80	31.40	32.71	1.34
F1.60	1.10	26.10	26.20	25.70	1.43	1.10	21.00	26.50	27.71	1.48	1.50	9.90	29.90	32.27	1.34
F1.70	1.00	30.20	25.80	24.06	1.40	1.10	25.60	26.70	25.99	1.44	1.50	11.30	30.60	31.70	1.34
F1.80	1.00	32.90	24.90	22.97	1.31	1.10	26.90	26.20	25.49	1.43	1.50	12.80	30.10	31.09	1.33
F1.90	1.00	35.50	24.10	21.95	1.26	1.30	29.80	25.30	24.38	1.37	0.90	14.20	29.70	30.54	1.33
F2.00	1.00	37.90	23.40	20.91	1.19	1.10	32.40	24.50	23.29	1.33	1.50	15.80	29.20	29.88	1.32
S2.00	1.00	47.20	20.70	17.68	1.01	1.10	40.50	22.40	20.01	1.24	1.60	22.90	28.00	26.68	1.43

7.2.4. Parting 2 (P2)

The coal quality washability data for P2 is illustrated in Figure 7.4 and summarized in Table 7.4.

Moisture content varied from 0.9% to 1.9% across the size fractions and density ranges. While the volatile matter, total sulphur and CV increased with decreasing particle size and reaching the maximum values at high relative densities (Figure 7.4). In comparison, the sink fractions of P2 are characterised by extremely high ash (up to 80%). However, the sink fraction in the fine size class contains high volatile matter (21.6%) and low sulphur (0.93%).

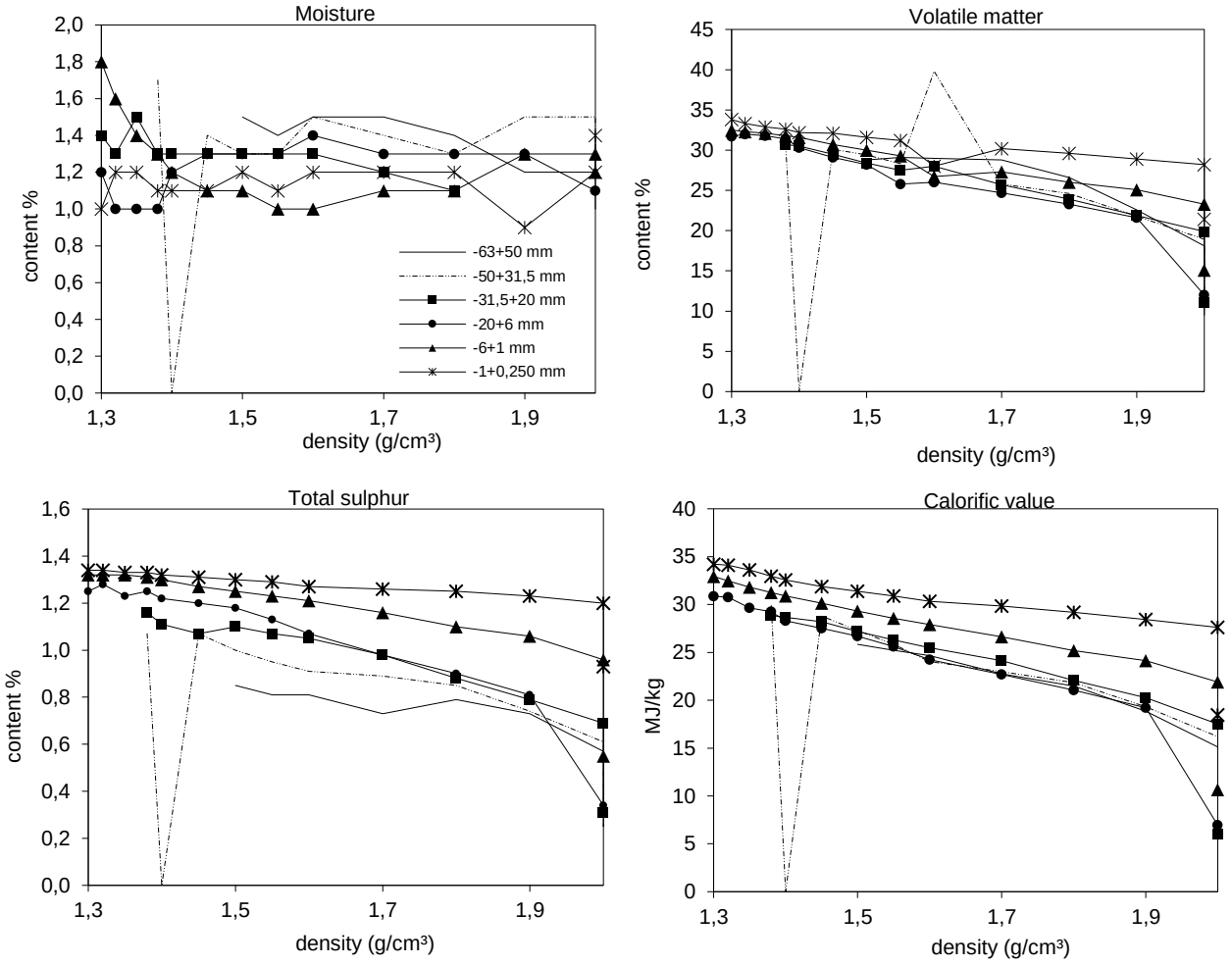

Figure 7.4. Chemical analyses by size fraction for P2. -63+50 mm (—), -50 +31.5 mm (- - -), -31.5+20 mm (■), -20+6 mm (●), -6+1 mm (▲) and -1 + 0.25 mm (*).

Table 7.4. Cumulative coal quality for P2.

Separation density (g/cm³)	Moisture (%)	Ash (%)	Volatile matter (%)	Calorific value (MJ/kg)	Total sulphur (%)	Moisture (%)	Ash (%)	Volatile matter (%)	Calorific value (MJ/kg)	Total sulphur (%)	Moisture (%)	Ash (%)	Volatile matter (%)	Calorific value (MJ/kg)	Total sulphur (%)
Fraction	**-63+50 mm**					**-50+31.5 mm**					**-31.5+20 mm**				
F1.30	-	-	-	-	-	-	-	-	-	-	-	-	-	-	-
F1.32	-	-	-	-	-	-	-	-	-	-	-	-	-	-	-
F1.35	-	-	-	-	-	-	-	-	-	-	-	-	-	-	-
F1.38	-	-	-	-	-	1.70	15.70	30.70	29.88	1.07	1.40	17.50	30.70	28.86	1.16
F1.40	-	-	-	-	-	0.00	0.00	0.00	0.00	0.00	1.30	18.10	30.50	28.67	1.11
F1.45	-	-	-	-	-	1.40	18.20	30.10	28.80	1.07	1.50	19.40	29.50	28.20	1.07
F1.50	1.50	23.80	28.80	25.84	0.85	1.30	21.90	29.40	27.27	1.00	1.30	21.90	28.40	27.17	1.10
F1.55	1.40	24.90	29.10	25.22	0.81	1.30	24.90	28.30	25.83	0.95	1.30	24.20	27.50	26.30	1.07
F1.60	1.50	26.40	29.00	24.66	0.81	1.50	29.30	39.80	24.05	0.91	1.30	26.00	28.00	25.48	1.05
F1.70	1.50	30.20	28.80	22.75	0.73	1.40	32.00	25.80	23.00	0.89	1.30	29.30	25.70	24.15	0.98
F1.80	1.40	34.20	26.60	21.48	0.79	1.30	35.10	24.60	21.83	0.85	1.30	34.50	23.90	22.08	0.88
F1.90	1.20	41.90	22.60	18.86	0.73	1.50	41.70	21.80	19.30	0.74	1.30	39.30	21.90	20.28	0.79
F2.00	1.20	51.80	18.10	15.12	0.57	1.50	49.60	18.90	16.19	0.61	1.20	46.20	19.90	17.50	0.69
S2.00	1.00	80.30	9.50	4.18	0.25	1.30	79.50	10.10	4.32	0.25	1.10	75.70	11.10	6.02	0.31
Fraction	**-20+6 mm**					**-6+1 mm**					**-1+0.25 mm**				
F1.30	-	-	-	-	-	1.80	7.00	32.50	32.94	1.32	1.00	4.20	33.80	34.22	1.34
F1.32	1.20	13.00	31.70	30.87	1.25	1.60	8.70	32.30	32.46	1.32	1.20	4.40	33.30	34.12	1.34
F1.35	1.00	13.50	32.00	30.75	1.28	1.40	10.50	32.10	31.81	1.32	1.20	5.80	32.90	33.63	1.33
F1.38	1.00	14.30	31.80	29.64	1.23	1.30	11.70	31.80	31.25	1.31	1.10	7.00	32.60	32.96	1.33
F1.40	1.00	15.80	31.40	29.25	1.25	1.20	12.80	31.60	30.88	1.30	1.10	8.00	32.20	32.58	1.32
F1.45	1.20	18.30	30.30	28.31	1.22	1.10	14.70	30.70	30.15	1.27	1.10	9.90	32.10	31.88	1.31
F1.50	1.30	20.70	29.10	27.50	1.20	1.10	16.80	30.00	29.33	1.25	1.20	11.20	31.60	31.38	1.30
F1.55	1.30	22.80	28.20	26.68	1.18	1.00	18.70	29.30	28.56	1.23	1.10	12.50	31.20	30.90	1.29
F1.60	1.30	25.50	25.80	25.61	1.13	1.00	20.30	26.70	27.91	1.21	1.20	13.90	28.00	30.34	1.27
F1.70	1.40	28.90	26.00	24.24	1.07	1.10	23.60	27.30	26.62	1.16	1.20	15.10	30.20	29.84	1.26
F1.80	1.30	32.90	24.70	22.69	0.98	1.10	27.10	26.00	25.17	1.10	1.20	16.70	29.60	29.20	1.25
F1.90	1.30	37.10	23.30	21.04	0.90	1.30	29.70	25.10	24.15	1.06	0.90	18.60	28.90	28.44	1.23
F2.00	1.30	41.70	21.60	19.22	0.81	1.30	35.20	23.30	21.92	0.96	1.20	20.60	28.20	27.62	1.20
S2.00	1.10	72.60	12.00	6.94	0.34	1.20	63.00	15.10	10.67	0.55	1.40	43.00	21.40	18.46	0.93

7.2.5. Seam Middle Lower (SML)

The coal quality washability data for SML is illustrated in Figure 7.5 and summarized in Table 7.5.

The results show the all the coal quality parameters increased with decreasing particle size, and reached their maximum at high relative densities (Figure 7.5). The volatile matter and CV are more concentrated in the fine size class (Table 7.5). The ash content in the sink fractions of SML reaches a high of 70.6%, however the sulphur content associated with this ash is quite low (0.3% to 1%). In contrast, the CV, volatile matter and total sulphur in the sinks of the -6 + 1 mm and -1+0.25 mm are comparable to the floats.

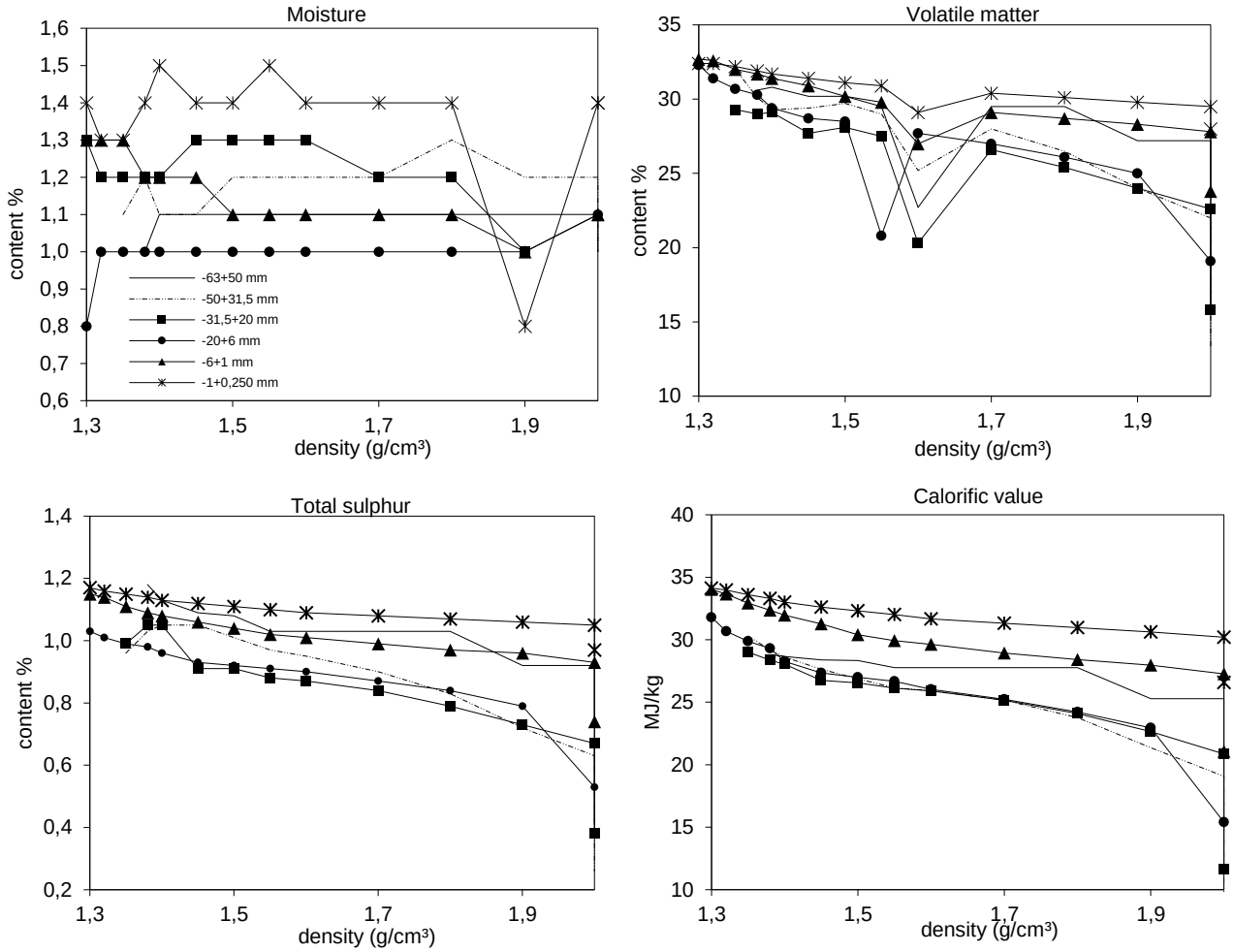

Figure 7.5. Chemical analyses (adb) by size fraction for SML. -63+50 mm (—), -50 +31.5 mm (- - -), -31.5+20 mm (■), -20+6 mm (●), -6+1 mm (▲) and -1 + 0.25 mm (*).

Table 7.5. Cumulative coal quality for SML (adb).

Separation density (g/cm³)	Moisture (%)	Ash (%)	Volatile matter (%)	Calorific value (MJ/kg)	Total sulphur (%)	Moisture (%)	Ash (%)	Volatile matter (%)	Calorific value (MJ/kg)	Total sulphur (%)	Moisture (%)	Ash (%)	Volatile matter (%)	Calorific value (MJ/kg)	Total sulphur (%)
Fraction	**-63+50 mm**					**-50+31.5 mm**					**-31.5+20 mm**				
F1.30	-	-	-	-	-	-	-	-	-	-	-	-	-	-	-
F1.32	-	-	-	-	-	-	-	-	-	-	-	-	-	-	-
F1.35	-	-	-	-	-	1.10	14.20	32.00	30.30	0.96	1.30	13.70	29.30	29.01	0.99
F1.38	1.00	17.30	30.60	28.80	1.18	1.20	16.60	30.10	29.18	1.03	1.20	18.30	29.00	28.37	1.05
F1.40	1.10	17.50	30.80	28.67	1.13	1.10	18.60	29.30	28.60	1.05	1.20	19.20	29.10	28.04	1.05
F1.45	1.10	18.20	30.20	28.38	1.09	1.10	21.00	29.40	27.63	1.05	1.20	22.70	27.70	26.76	0.91
F1.50	1.10	18.40	30.20	28.33	1.08	1.20	22.50	29.70	26.88	1.01	1.20	22.90	28.10	26.55	0.91
F1.55	1.10	19.80	29.50	27.77	1.03	1.20	24.00	29.00	26.15	0.97	1.30	24.10	27.50	26.13	0.88
F1.60	1.10	19.80	22.70	27.77	1.03	1.20	24.50	25.20	25.92	0.95	1.30	24.70	20.30	25.90	0.87
F1.70	1.10	19.80	29.50	27.77	1.03	1.20	26.40	28.00	25.17	0.90	1.30	26.50	26.60	25.16	0.84
F1.80	1.10	19.80	29.50	27.77	1.03	1.30	30.00	26.50	23.77	0.83	1.30	29.30	25.40	24.09	0.79
F1.90	1.10	26.30	27.20	25.28	0.92	1.20	36.20	24.00	21.35	0.72	1.20	33.00	24.00	22.65	0.73
F2.00	1.10	26.30	27.20	25.28	0.92	1.20	41.80	22.00	19.07	0.63	1.20	37.40	22.60	20.87	0.67
S2.00	1.00	60.90	16.10	11.35	0.41	1.00	70.60	13.30	7.46	0.26	1.00	60.80	15.80	11.60	0.38
Fraction	**-20+6 mm**					**-6+1 mm**					**-1+0.25 mm**				
F1.30	-	-	-	-	-	1.30	4.30	32.70	34.03	1.15	1.40	3.60	32.40	34.13	1.17
F1.32	0.80	11.40	32.30	31.80	1.03	1.30	5.60	32.60	33.65	1.14	1.30	4.20	32.40	33.98	1.16
F1.35	1.00	13.90	31.40	30.68	1.01	1.30	7.60	32.00	32.93	1.11	1.30	5.10	32.20	33.61	1.15
F1.38	1.00	15.40	30.70	29.88	0.99	1.20	9.10	31.70	32.36	1.09	1.40	6.00	31.90	33.30	1.14
F1.40	1.00	16.60	30.30	29.31	0.98	1.20	10.10	31.40	31.96	1.08	1.50	6.60	31.70	33.01	1.13
F1.45	1.00	19.40	29.40	28.26	0.96	1.20	11.80	30.90	31.28	1.06	1.40	7.80	31.40	32.62	1.12
F1.50	1.00	21.20	28.70	27.34	0.93	1.10	13.90	30.20	30.39	1.04	1.40	8.50	31.10	32.31	1.11
F1.55	1.00	22.00	28.50	27.00	0.92	1.10	15.10	29.80	29.92	1.02	1.50	9.30	30.90	32.01	1.10
F1.60	1.00	22.80	20.80	26.67	0.91	1.10	15.80	27.00	29.62	1.01	1.40	10.20	29.10	31.66	1.09
F1.70	1.00	24.40	27.70	26.02	0.90	1.10	17.40	29.10	28.94	0.99	1.40	11.00	30.40	31.32	1.08
F1.80	1.00	26.30	27.00	25.24	0.87	1.10	18.70	28.70	28.42	0.97	1.40	11.90	30.10	30.97	1.07
F1.90	1.00	28.90	26.10	24.21	0.84	1.00	19.90	28.30	27.97	0.96	0.80	12.70	29.80	30.61	1.06
F2.00	1.00	32.00	25.00	22.95	0.79	1.10	21.60	27.80	27.26	0.93	1.40	13.70	29.50	30.21	1.05
S2.00	1.10	50.70	19.10	15.40	0.53	1.10	36.40	23.80	21.05	0.74	1.40	22.00	28.00	26.58	0.97

7.2.6. Parting 3 (P3)

The coal quality washability data for P3 is illustrated in Figure 7.6 and summarized in Table 7.6.

The overall moisture content in P3 varied from 1.0% to 2.0% and is therefore higher than the initial value of 1.1%. The overall volatile matter, total sulphur and CV increased with decreasing particle size, and are lowest at high relative densities (Figure 7.6). However, total sulphur is enriched at high relative densities, especially in the finer particles (Table 7.6). Significantly high amounts of ash of up to 84,2% occur in the sink fractions of P3, along with extremely low amounts of volatile matter, CV and total sulphur contents owing to the low float recoveries as discussed in Chapter 6.

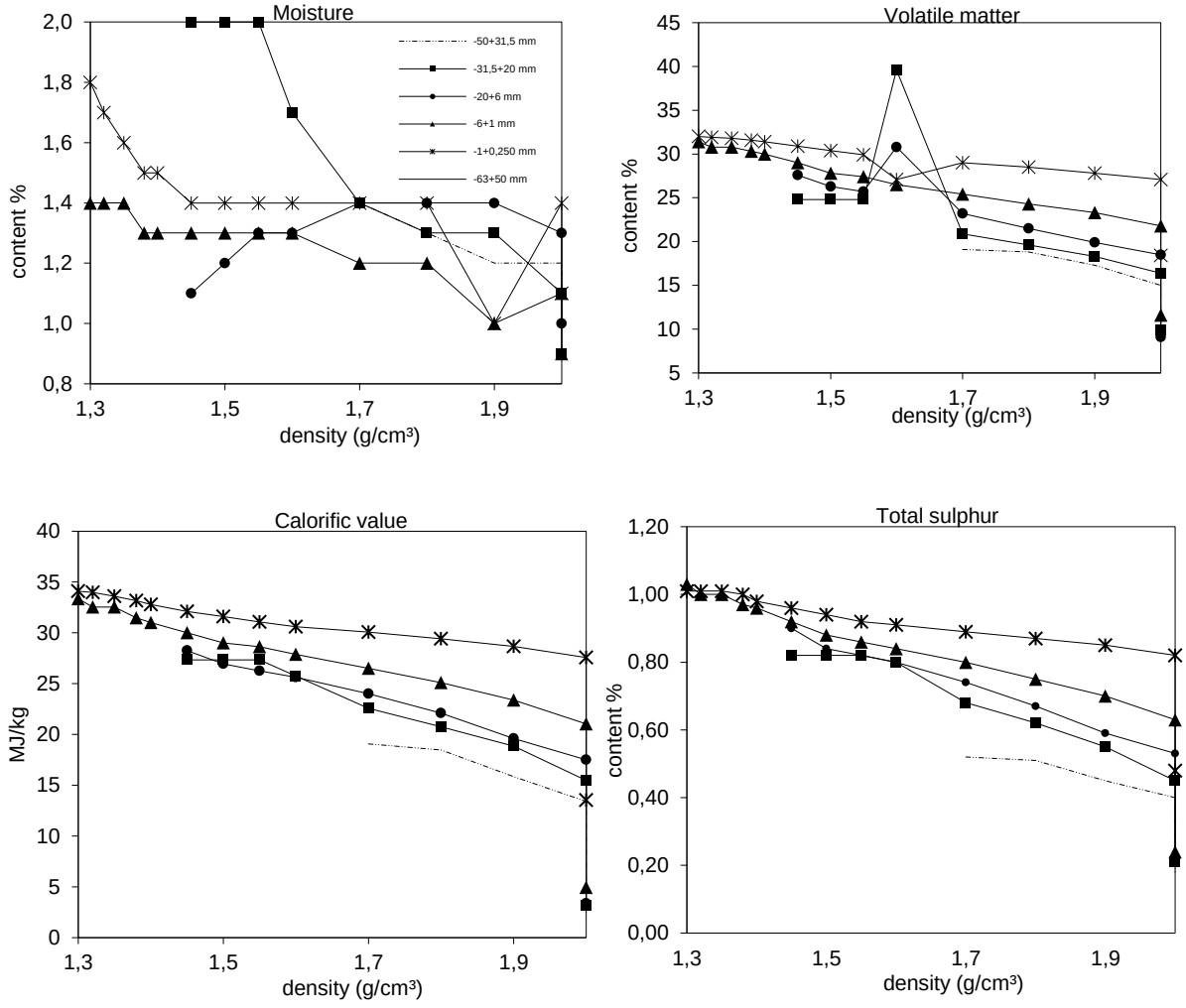

Figure 7.6. Chemical analyses by size fraction for P3. -63+50 mm (—), -50 +31.5 mm (- - -), -31.5+20 mm (■), -20+6 mm (●), -6+1 mm (▲) and -1 + 0.25 mm (*).

Table 7.6. Cumulative coal quality for P3 (adb).

Separation density (g/cm³)	Moisture (%)	Ash (%)	Volatile matter (%)	Calorific value (MJ/kg)	Total sulphur (%)	Moisture (%)	Ash (%)	Volatile matter (%)	Calorific value (MJ/kg)	Total sulphur (%)	Moisture (%)	Ash (%)	Volatile matter (%)	Calorific value (MJ/kg)	Total sulphur (%)
Fraction	**-63+50 mm**					**-50+31.5 mm**					**-31.5+20 mm**				
F1.30	-	-	-	-	-	-	-	-	-	-	-	-	-	-	-
F1.32	-	-	-	-	-	-	-	-	-	-	-	-	-	-	-
F1.35	-	-	-	-	-	-	-	-	-	-	-	-	-	-	-
F1.38	-	-	-	-	-	-	-	-	-	-	-	-	-	-	-
F1.40	-	-	-	-	-	-	-	-	-	-	-	-	-	-	-
F1.45	-	-	-	-	-	-	-	-	-	-	2.00	20.60	24.80	27.34	0.82
F1.50	-	-	-	-	-	-	-	-	-	-	2.00	20.60	24.80	27.34	0.82
F1.55	-	-	-	-	-	-	-	-	-	-	2.00	20.60	24.80	27.34	0.82
F1.60	-	-	-	-	-	-	-	-	-	-	1.70	24.50	39.60	25.76	0.80
F1.70	-	-	-	-	-	1.40	42.00	19.10	19.07	0.52	1.40	32.50	20.90	22.58	0.68
F1.80	-	-	-	-	-	1.30	43.40	18.80	18.48	0.51	1.30	37.20	19.60	20.77	0.62
F1.90	-	-	-	-	-	1.20	50.10	17.30	15.84	0.45	1.30	42.30	18.30	18.86	0.55
F2.00	-	-	-	-	-	1.20	56.40	15.00	13.42	0.40	1.10	50.90	16.40	15.48	0.45
S2.00	1.10	83.70	8.60	2.49	0.18	1.00	84.20	8.90	2.22	0.18	0.90	81.80	9.90	3.18	0.21
Fraction	**-20+6 mm**					**-6+1 mm**					**-1+0.25 mm**				
F1.30	-	-	-	-	-	1.40	6.70	31.40	33.36	1.03	1.80	4.10	32.00	34.10	1.01
F1.32	-	-	-	-	-	1.40	9.90	30.80	32.55	1.00	1.70	4.40	31.90	33.98	1.01
F1.35	-	-	-	-	-	1.40	9.90	30.80	32.55	1.00	1.60	5.40	31.80	33.59	1.01
F1.38	-	-	-	-	-	1.30	11.90	30.30	31.48	0.97	1.50	6.50	31.60	33.16	1.00
F1.40	-	-	-	-	-	1.30	12.90	30.00	31.01	0.96	1.50	7.50	31.40	32.78	0.98
F1.45	1.10	19.30	27.60	28.25	0.90	1.30	15.30	29.00	30.00	0.92	1.40	9.20	30.90	32.11	0.96
F1.50	1.20	21.90	26.30	26.94	0.84	1.30	17.70	27.80	29.00	0.88	1.40	10.50	30.40	31.59	0.94
F1.55	1.30	23.30	25.70	26.26	0.82	1.30	18.60	27.40	28.62	0.86	1.40	11.80	29.90	31.07	0.92
F1.60	1.30	24.70	30.80	25.64	0.80	1.30	20.30	26.50	27.89	0.84	1.40	13.00	27.10	30.59	0.91
F1.70	1.40	28.90	23.20	24.00	0.74	1.20	23.70	25.40	26.50	0.80	1.40	14.20	29.00	30.07	0.89
F1.80	1.40	33.90	21.50	22.09	0.67	1.20	27.10	24.30	25.10	0.75	1.40	15.90	28.50	29.40	0.87
F1.90	1.40	40.20	19.90	19.61	0.59	1.00	31.30	23.30	23.38	0.70	1.00	17.70	27.80	28.67	0.85
F2.00	1.30	45.50	18.50	17.51	0.53	1.10	37.10	21.80	21.04	0.63	1.40	20.40	27.10	27.56	0.82
S2.00	1.00	82.00	9.10	3.39	0.21	0.90	77.20	11.60	4.95	0.24	1.10	55.40	18.40	13.52	0.48

7.2.7. Seam Bottom Upper (SBU)

The coal quality washability data for SBU is illustrated in Figure 7.7 and summarized in Table 7.7.

The overall moisture content in SBU is in the range, 0.70% to 1.70%, and was uniformly distributed across the density ranges. While the overall volatile matter, total sulphur and CV increased with decreasing particle size and reached their maximum at low relative densities (Figure 7.7). With respect to the sink fractions of SBU, the ash content ranges between 22.4% and 64.3%. However, the ash content is considerably lower (< 36.4%) in the -6 + 1 mm and -1+0.25 mm size fractions, and the coal quality in are comparable to those of the floats (Table 7.7).

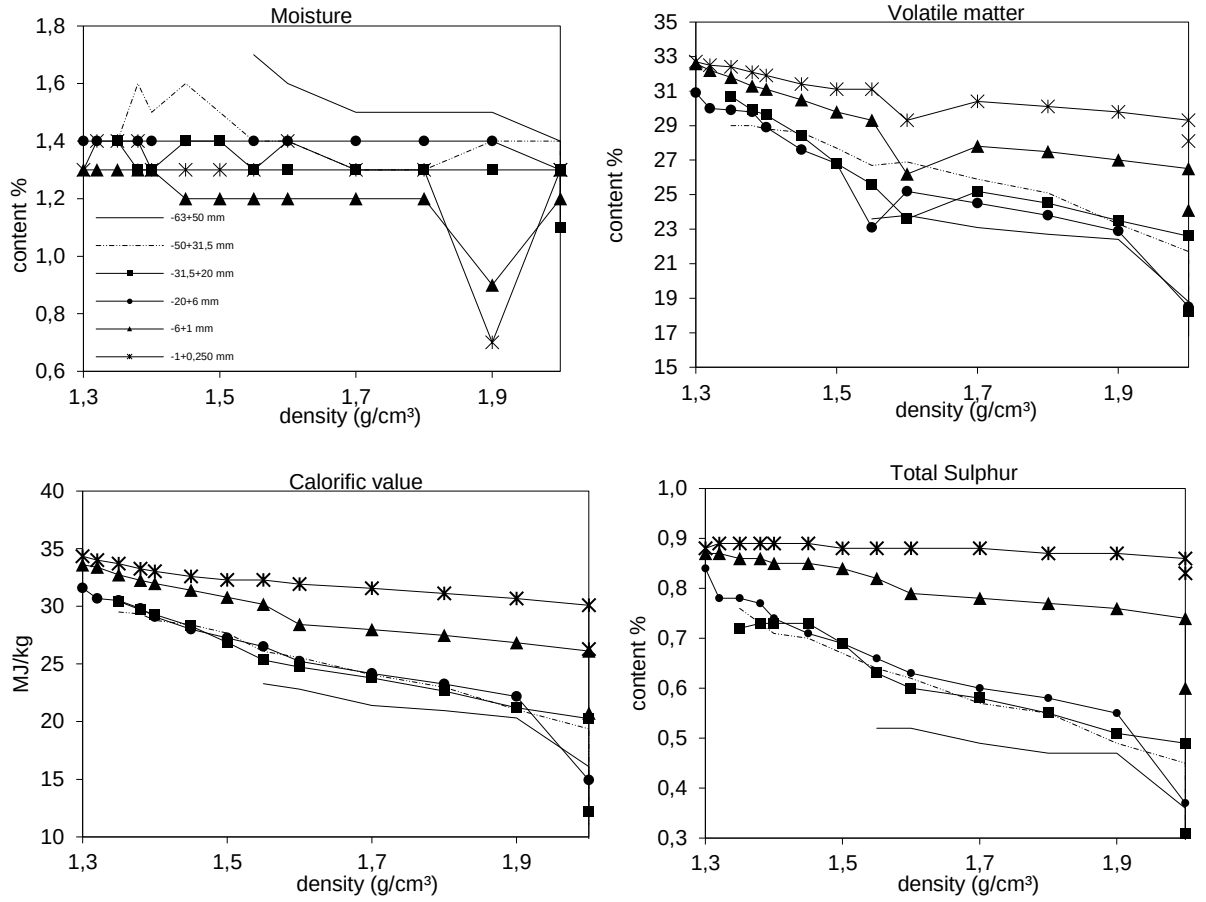

Figure 7.7. Chemical analyses (adb) by size fraction for SBU. -63+50 mm (—), -50 +31.5 mm (- - -), -31.5+20 mm (■), -20+6 mm (●), -6+1 mm (▲) and -1 + 0.25 mm (*).

Table 7.7. Cumulative coal quality for SBU (adb).

Separation density (g/cm³)	Moisture (%)	Ash (%)	Volatile matter (%)	Calorific value (MJ/kg)	Total sulphur (%)	Moisture (%)	Ash (%)	Volatile matter (%)	Calorific value (MJ/kg)	Total sulphur (%)	Moisture (%)	Ash (%)	Volatile matter (%)	Calorific value (MJ/kg)	Total sulphur (%)
Fraction	**-63+50 mm**					**-50+31.5 mm**					**-31.5+20 mm**				
F1.30	-	-	-	-	-	-	-	-	-	-	-	-	-	-	-
F1.32	-	-	-	-	-	-	-	-	-	-	-	-	-	-	-
F1.35	-	-	-	-	-	1.40	15.50	29.00	29.51	0.76	1.40	13.10	30.70	30.43	0.72
F1.38	-	-	-	-	-	1.60	15.80	29.00	29.34	0.73	1.30	14.40	29.90	29.70	0.73
F1.40	-	-	-	-	-	1.50	17.10	28.80	28.78	0.71	1.30	15.10	29.60	29.28	0.73
F1.45	-	-	-	-	-	1.60	18.00	28.60	28.41	0.70	1.40	17.30	28.40	28.29	0.73
F1.50	-	-	-	-	-	1.50	19.90	27.70	27.67	0.67	1.40	21.40	26.80	26.86	0.69
F1.55	1.70	30.80	23.60	23.29	0.52	1.40	23.80	26.70	26.10	0.64	1.30	25.30	25.60	25.35	0.63
F1.60	1.60	31.70	23.80	22.81	0.52	1.40	25.00	26.90	25.57	0.62	1.30	27.00	23.60	24.73	0.60
F1.70	1.50	34.70	23.10	21.40	0.49	1.30	28.70	25.90	24.06	0.57	1.30	29.20	25.20	23.79	0.58
F1.80	1.50	35.90	22.70	20.96	0.47	1.30	31.30	25.10	22.97	0.55	1.30	31.90	24.50	22.66	0.55
F1.90	1.50	37.40	22.40	20.31	0.47	1.40	36.30	23.30	21.03	0.49	1.30	35.50	23.50	21.21	0.51
F2.00	1.40	47.60	18.80	16.11	0.36	1.40	40.40	21.70	19.36	0.45	1.30	37.90	22.60	20.27	0.49
S2.00	1.10	64.30	16.80	8.84	0.21	1.20	59.70	18.70	11.10	0.26	1.10	57.00	18.20	12.16	0.31
Fraction	**-20+6 mm**					**-6+1 mm**					**-1+0.25 mm**				
F1.30	-	-	-	-	-	1.30	5.90	32.60	33.60	0.87	1.30	3.80	32.70	34.34	0.88
F1.32	1.40	10.70	30.90	31.59	0.84	1.30	6.30	32.20	33.39	0.87	1.40	4.40	32.50	34.00	0.89
F1.35	1.40	12.80	30.00	30.68	0.78	1.30	7.70	31.80	32.74	0.86	1.40	5.20	32.40	33.71	0.89
F1.38	1.40	13.40	29.90	30.52	0.78	1.30	8.80	31.30	32.26	0.86	1.40	6.10	32.10	33.26	0.89
F1.40	1.40	15.00	29.80	29.81	0.77	1.30	9.60	31.10	31.98	0.85	1.30	6.70	31.90	33.03	0.89
F1.45	1.40	16.80	28.90	29.10	0.74	1.20	11.10	30.50	31.41	0.85	1.30	7.70	31.40	32.60	0.89
F1.50	1.40	19.70	27.60	28.02	0.71	1.20	12.70	29.80	30.78	0.84	1.30	8.50	31.10	32.30	0.88
F1.55	1.40	21.60	26.80	27.25	0.69	1.20	14.20	29.30	30.17	0.82	1.30	8.60	31.10	32.28	0.88
F1.60	1.40	23.50	23.10	26.52	0.66	1.20	18.40	26.20	28.44	0.79	1.40	9.50	29.30	31.93	0.88
F1.70	1.40	26.60	25.20	25.22	0.63	1.20	19.50	27.80	27.98	0.78	1.30	10.40	30.40	31.56	0.88
F1.80	1.40	29.20	24.50	24.18	0.60	1.20	20.70	27.50	27.48	0.77	1.30	11.50	30.10	31.13	0.87
F1.90	1.40	31.50	23.80	23.25	0.58	0.90	22.30	27.00	26.84	0.76	0.70	12.60	29.80	30.68	0.87
F2.00	1.40	34.20	22.90	22.19	0.55	1.20	24.10	26.50	26.11	0.74	1.30	14.00	29.30	30.10	0.86
S2.00	1.30	51.70	18.50	14.93	0.37	1.30	36.40	24.10	20.74	0.60	1.30	22.40	28.10	26.30	0.83

7.2.8. Seam Bottom Middle (SBM)

The coal quality washability data for SBM is illustrated in Figure 7.8 and summarized in Table 7.8.

Moisture content in SBM is in the range 0.7% to 1.7%, with minor variations observed between the coarse (0.9% to 1.5%), intermediate (0.7% to 1.7%) and fine (0.8%) size classes. In general, high moisture values occurred at low relative density and tended to decrease with decreasing relative density (Figure 7.8). The volatile matter, total sulphur and CV show an increasing trend with decreasing particle size but decreased with increasing relative density, respectively. Total sulphur shows a decreasing tend with decreasing particle size, and with increasing relative density. High ash values of up to 65.9% are reported for the sink fractions of SBM and correspond to very low volatile matter, CV and total sulphur (Table 7.8). However, the sink fraction in the fine size class has comparable quality to the floats.

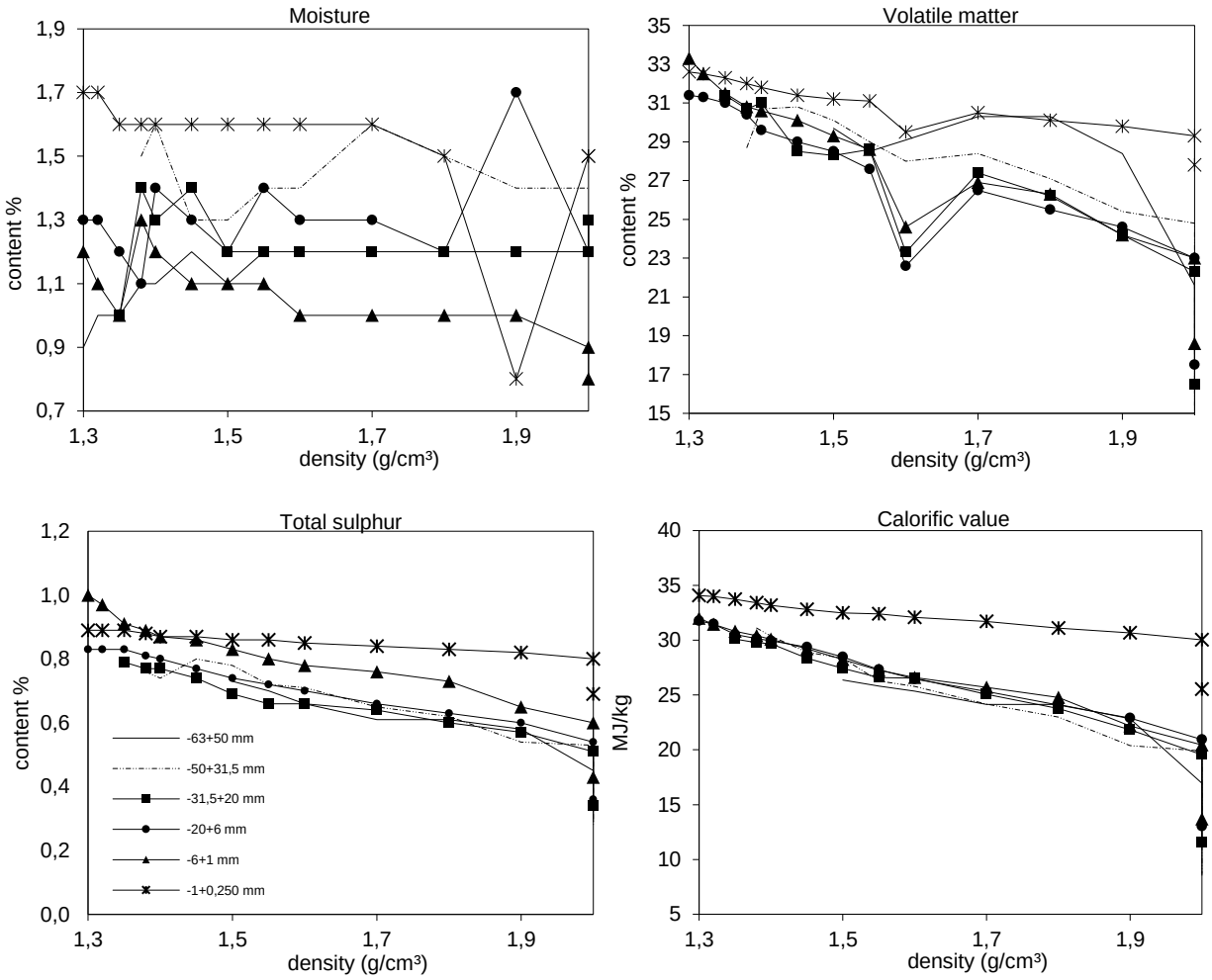

Figure 7.8. Chemical analyses (adb) by size fraction for SBM. -63+50 mm (—), -50 +31.5 mm (- - -), -31.5+20 mm (■), -20+6 mm (●), -6+1 mm (▲) and -1 + 0.25 mm (*).

Table 7.8. Cumulative coal quality for SBM.

Separation density (g/cm³)	Moisture (%)	Ash (%)	Volatile matter (%)	Calorific value (MJ/kg)	Total sulphur (%)	Moisture (%)	Ash (%)	Volatile matter (%)	Calorific value (MJ/kg)	Total sulphur (%)	Moisture (%)	Ash (%)	Volatile matter (%)	Calorific value (MJ/kg)	Total sulphur (%)
Fraction	**-63+50 mm**					**-50+31.5 mm**					**-31.5+20 mm**				
F1.30	-	-	-	-	-	-	-	-	-	-	-	-	-	-	-
F1.32	-	-	-	-	-	-	-	-	-	-	-	-	-	-	-
F1.35	-	-	-	-	-	-	-	-	-	-	1.00	13.00	31.40	30.11	0.79
F1.38	-	-	-	-	-	1.50	11.50	28.70	31.11	0.76	1.40	13.30	30.70	29.78	0.77
F1.40	-	-	-	-	-	1.60	13.20	30.70	30.38	0.74	1.30	13.60	31.00	29.70	0.77
F1.45	-	-	-	-	-	1.30	16.60	30.80	28.91	0.80	1.40	17.70	28.50	28.36	0.74
F1.50	0.90	21.70	29.70	26.37	0.73	1.30	18.10	30.10	28.35	0.78	1.20	20.20	28.30	27.44	0.69
F1.55	1.00	23.30	28.50	25.81	0.70	1.40	22.50	29.00	26.28	0.72	1.20	22.00	28.60	26.59	0.66
F1.60	1.00	24.20	29.10	25.36	0.66	1.40	23.70	28.00	25.78	0.71	1.20	22.20	23.30	26.54	0.66
F1.70	1.10	26.40	30.30	24.13	0.61	1.60	27.00	28.40	24.18	0.65	1.20	26.10	27.40	25.07	0.64
F1.80	1.10	26.40	30.30	24.13	0.61	1.50	30.00	27.10	23.00	0.62	1.20	28.90	26.20	23.78	0.60
F1.90	1.20	29.90	28.40	22.85	0.58	1.40	36.70	25.40	20.39	0.54	1.20	34.10	24.20	21.84	0.57
F2.00	1.10	45.90	21.60	16.96	0.45	1.40	38.00	24.80	19.89	0.53	1.20	39.80	22.30	19.54	0.51
S2.00	1.20	65.80	14.70	8.73	0.29	1.40	65.90	15.40	8.56	0.28	1.30	59.20	16.50	11.57	0.34
Fraction	**-20+6 mm**					**-6+1 mm**					**-1+0.25 mm**				
F1.30	1.30	9.40	31.40	31.76	0.83	1.20	8.80	33.30	31.99	1.00	1.70	3.80	32.60	34.07	0.89
F1.32	1.30	9.70	31.30	31.49	0.83	1.10	9.40	32.50	31.44	0.97	1.70	4.10	32.50	33.99	0.89
F1.35	1.20	11.00	31.00	30.51	0.83	1.00	11.80	31.50	30.82	0.91	1.60	4.90	32.30	33.73	0.89
F1.38	1.10	12.60	30.40	30.14	0.81	1.30	13.50	30.80	30.41	0.89	1.60	5.70	32.00	33.41	0.88
F1.40	1.40	13.60	29.60	29.94	0.80	1.20	14.40	30.60	30.08	0.87	1.60	6.30	31.80	33.18	0.87
F1.45	1.30	16.10	29.00	29.38	0.77	1.10	16.40	30.10	29.21	0.86	1.60	7.30	31.40	32.80	0.87
F1.50	1.20	18.20	28.50	28.46	0.74	1.10	18.90	29.30	28.23	0.83	1.60	8.00	31.20	32.50	0.86
F1.55	1.40	20.80	27.60	27.31	0.72	1.10	21.20	28.60	27.25	0.80	1.60	8.30	31.10	32.41	0.86
F1.60	1.30	22.60	22.60	26.45	0.70	1.00	22.70	24.60	26.59	0.78	1.60	9.10	29.50	32.08	0.85
F1.70	1.30	25.50	26.50	25.33	0.66	1.00	24.80	26.90	25.71	0.76	1.60	10.00	30.50	31.72	0.84
F1.80	1.20	28.60	25.50	24.08	0.63	1.00	27.10	26.30	24.77	0.73	1.50	11.50	30.10	31.11	0.83
F1.90	1.70	31.50	24.60	22.91	0.60	1.00	33.90	24.20	22.19	0.65	0.80	12.50	29.80	30.68	0.82
F2.00	1.20	36.40	23.00	20.95	0.54	0.90	38.00	23.00	20.45	0.60	1.50	14.10	29.30	30.02	0.80
S2.00	1.30	54.90	17.50	13.03	0.36	0.80	54.00	18.60	13.68	0.43	1.50	24.10	27.80	25.52	0.69

7.2.9. Seam Bottom Lower (SBL)

The coal quality washability data for SBL is illustrated in Figure 7.9 and summarized in Table 7.9.

The moisture content varied with particle size and relative density, but overall, increased with decreasing particle size. Volatile matter increased with decreasing particle size in the coarse size class, while the volatile matter was highest at high relative densities fine size class. Similarly, the total sulphur and the CV increased with decreasing particle size while also decreasing with increasing relative density (Figure 7.9). The sulphur content is concentrated, particularly in the high densities of the fine size class. Coal quality in the sink fractions is characterised by very high ash of up to 63,9%, while the other quality parameters are poor. However, coal quality in the sink fraction of the fine size class is comparable to that of the float fractions (Table 7.9).

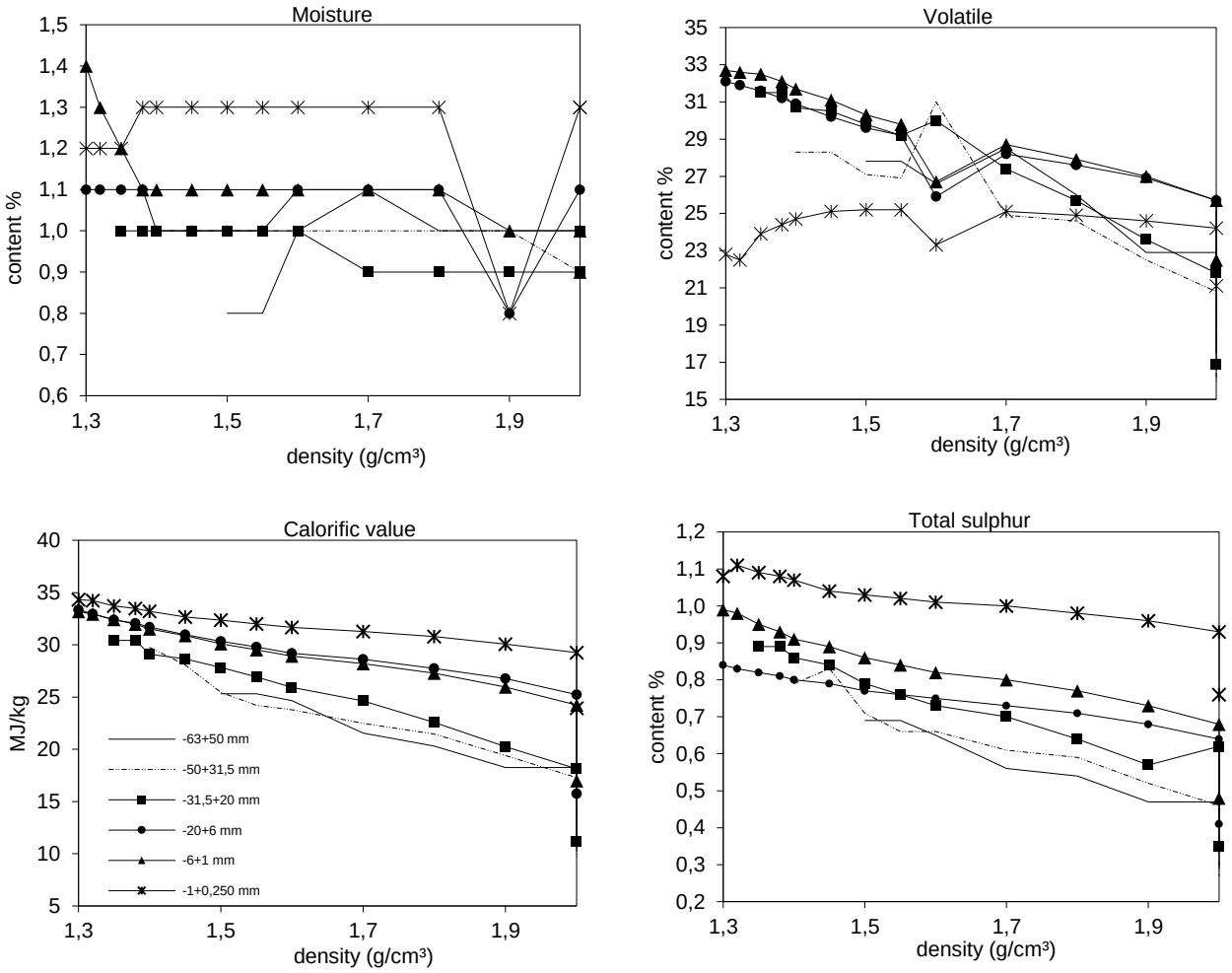

Figure 7.9. Chemical analyses by size fraction for SBL. -63+50 mm (–), -50 +31.5 mm (- - -), -31.5+20 mm (■), -20+6 mm (●), -6+1 mm (▲) and -1 + 0.25 mm (*).

Table 7.9. Cumulative coal quality for SBL.

Separation density (g/cm³)	Moisture (%)	Ash (%)	Volatile matter (%)	Calorific value (MJ/kg)	Total sulphur (%)	Moisture (%)	Ash (%)	Volatile matter (%)	Calorific value (MJ/kg)	Total sulphur (%)	Moisture (%)	Ash (%)	Volatile matter (%)	Calorific value (MJ/kg)	Total sulphur (%)
Fraction	**-63+50 mm**					**-50+31.5 mm**					**-31.5+20 mm**				
F1.30	-	-	-	-	-	-	-	-	-	-	-	-	-	-	-
F1.32	-	-	-	-	-	-	-	-	-	-	-	-	-	-	-
F1.35	-	-	-	-	-	-	-	-	-	-	1.00	11.80	31.50	30.42	0.89
F1.38	-	-	-	-	-	-	-	-	-	-	1.00	11.80	31.50	30.42	0.89
F1.40	-	-	-	-	-	1.00	15.60	28.30	29.75	0.79	1.00	15.30	30.70	29.09	0.86
F1.45	-	-	-	-	-	1.00	19.90	28.30	28.07	0.83	1.00	16.80	30.50	28.64	0.84
F1.50	0.80	26.40	27.80	2 5.31	0.69	1.00	26.00	27.10	25.44	0.71	1.00	19.70	29.80	27.82	0.79
F1.55	0.80	26.40	27.80	25.31	0.69	1.00	27.80	26.90	24.20	0.66	1.00	22.10	29.20	26.91	0.76
F1.60	1.00	28.70	26.60	24.67	0.65	1.00	29.00	31.00	23.78	0.66	1.00	24.50	30.00	25.92	0.73
F1.70	1.10	33.60	28.50	21.54	0.56	1.00	33.20	24.90	22.47	0.61	0.90	27.30	27.40	24.64	0.70
F1.80	1.00	37.00	26.00	20.32	0.54	1.00	34.90	24.60	21.45	0.59	0.90	32.20	25.70	22.57	0.64
F1.90	1.00	42.60	22.90	18.25	0.47	1.00	40.40	22.50	19.40	0.52	0.90	38.10	23.60	20.25	0.57
F2.00	1.00	42.60	22.90	18.25	0.47	0.90	45.70	20.80	17.28	0.46	0.90	43.50	21.80	18.14	0.62
S2.00	0.90	60.90	17.50	11.06	0.29	1.00	63.90	16.00	9.70	0.27	1.00	60.00	16.90	11.21	0.35
Fraction	**-20+6 mm**					**-6+1 mm**					**-1+0.25 mm**				
F1.30	1.10	6.50	32.10	33.36	0.84	1.40	7.00	32.70	33.18	0.99	1.20	4.10	22.80	34.31	1.08
F1.32	1.10	7.20	31.90	32.96	0.83	1.30	7.60	32.60	32.94	0.98	1.20	4.30	22.50	34.24	1.11
F1.35	1.10	8.60	31.60	32.39	0.82	1.20	9.40	32.50	32.43	0.95	1.20	5.40	23.90	33.72	1.09
F1.38	1.10	9.50	31.20	32.05	0.81	1.10	10.60	32.10	31.98	0.93	1.30	6.00	24.40	33.47	1.08
F1.40	1.00	10.40	30.90	31.68	0.80	1.10	11.80	31.70	31.52	0.91	1.30	6.70	24.70	33.20	1.07
F1.45	1.00	12.20	30.20	30.98	0.79	1.10	13.40	31.10	30.88	0.89	1.30	8.00	25.10	32.67	1.04
F1.50	1.00	13.90	29.60	30.32	0.77	1.10	15.30	30.30	30.08	0.86	1.30	8.80	25.20	32.36	1.03
F1.55	1.00	15.10	29.20	29.80	0.76	1.10	16.70	29.80	29.53	0.84	1.30	9.70	25.20	32.01	1.02
F1.60	1.10	16.50	25.90	29.20	0.75	1.10	18.10	26.70	28.91	0.82	1.30	10.50	23.30	31.67	1.01
F1.70	1.10	18.00	28.20	28.62	0.73	1.10	19.70	28.70	28.20	0.80	1.30	11.50	25.10	31.27	1.00
F1.80	1.10	20.20	27.60	27.73	0.71	1.10	22.00	27.90	27.27	0.77	1.30	12.70	24.90	30.78	0.98
F1.90	0.80	22.60	26.90	26.78	0.68	1.00	25.20	27.00	25.96	0.73	0.80	14.40	24.60	30.06	0.96
F2.00	1.10	26.40	25.70	25.22	0.64	1.00	29.50	25.70	24.22	0.68	1.30	16.40	24.20	29.25	0.93
S2.00	1.00	48.20	22.10	15.76	0.41	0.90	45.80	22.50	16.99	0.48	1.30	28.40	21.10	23.92	0.76

7.3. Discussion

It can be summarized that the volatile matter, total sulphur and CV of the floats increased with decreasing particle size in all seams and partings, generally reaching their maximum at low relative densities. Although the moisture content showed the greatest variability in relation to changes with particle size and density, it is low. As expected, the sink fractions (S 2.00 g/cm^3) are characterised by very high ash, but the coal quality reported for the sink fractions of all seams and partings (excluding P3) at -1 + 0.25 mm show potential for further beneficiation as the quality is comparable to that of the floats.

The float-sink data shows that higher total sulphur values concentrated in the smaller particles, and also at low relative densities. The higher total sulphur in the fine fractions could be related to finely dispersed sulphur forms, including pyrite. The strong negative correlation coefficients determined for the total sulphur content versus ash (Figure 7.10) for all horizons excluding the upper seams, SU, P1 and SMU suggests the sulphur in the LD57 samples may have a predominantly organic association, more so in the finer fractions. The correlation coefficients for the total sulphur vs ash are tabulated in Appendix G.

As discussed in Chapter 6, a cut point density between 1.55-1.70 g/cm^3 and particle size of -1+0.25 mm was selected as optimal to meet the mines objective of producing a metallurgical product of 10% ash for all seams and P2. Only SBU and SBL meet the requirement of ≤ 1% total sulphur at the selected cut point density and particle size. Therefore, all other seams require further reduction of the total sulphur, which is slightly elevated, up to 1.34% in the -1+0.25 mm size fraction. A further beneficiation step is therefore necessary to ensure the total sulphur is at a maximum level of 1%, as is required for metallurgical coals (Falcon, 2013). Advanced fine coal washing processes such as froth floatation maybe required to reduce the remaining sulphur and other inherent mineral matter occurring in metallurgical coal (Mackinnon and Swanson, 2010: Bergh *et al*., 2013). It must be noted that froth floatation was proposed as a further beneficiation step to process the Makhado fine-size fractions as part of the test work carried during the Makhado Phase 1 development (Section 4.1 and 4.2). However, froth floatation on the fine size fraction could not be conducted due to financial constraints and was therefore beyond the scope of the present research.

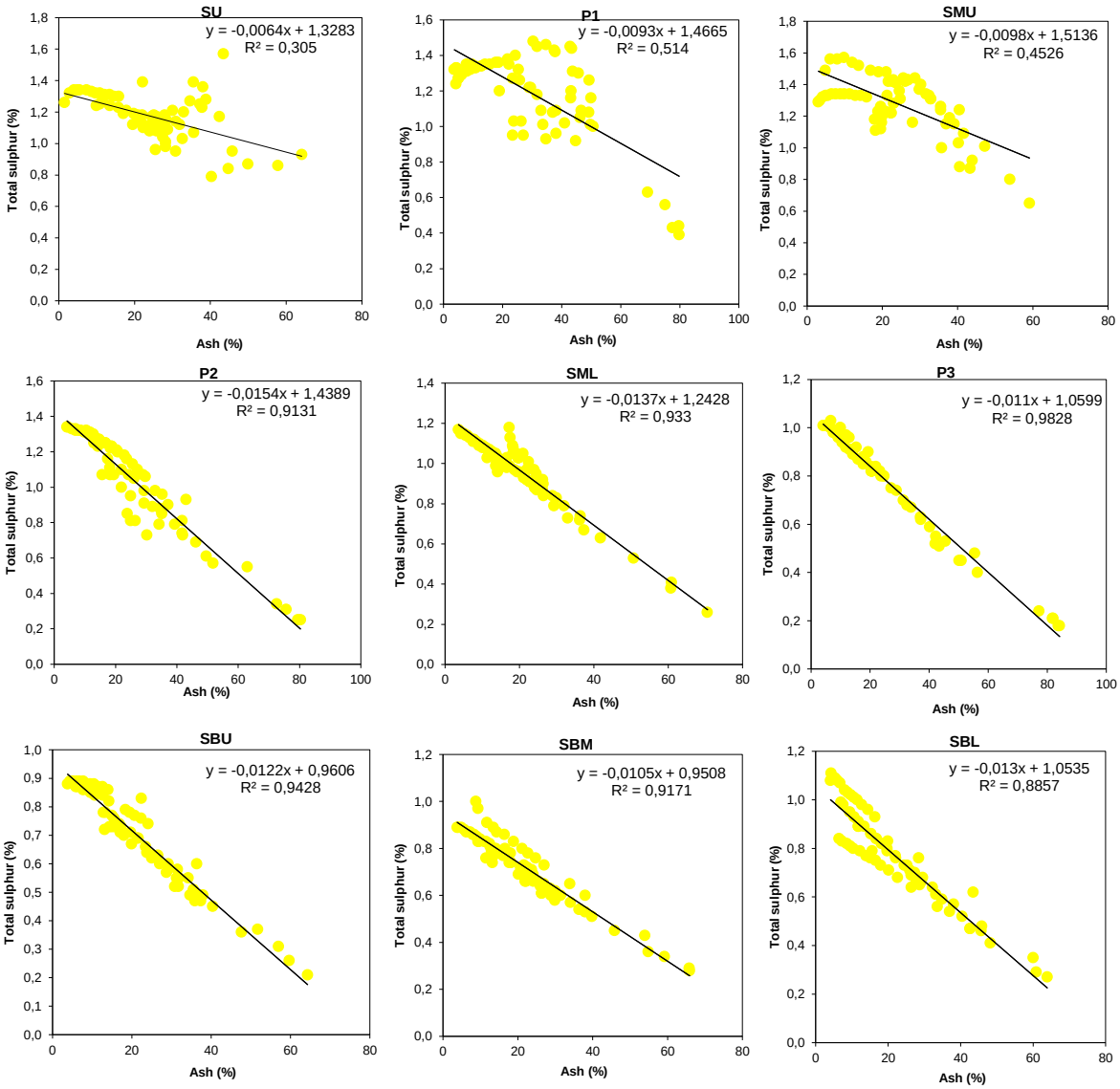

Figure 7.10. Relationship between total sulphur vs ash for the LD57 float samples among different size fractions (-63+0.25 0mm) and densities (F1.30 to F2.00).

Chapter 8: Petrography

8.1. Introduction

The petrographic composition of the fine-float samples (-1+0.25 mm) are characterised in this chapter, with emphasis on the liberation of inorganic constituents for the production of metallurgical coal. The associations of the organic and inorganic components and their implications on metallurgical/technological applications are discussed. This chapter addresses objectives for part two of the study.

8.2. Coal rank

The data in Table 8.1 shows the fine fraction samples are classified as Medium Rank Bituminous C coal (ECE-UN, 1998), showing average %RoV values of 0.88%. The $\%R_{max}$ readings show average values of 0.92% (Table 8.1). The %RoV and $\%R_{max}$ reflectance values are illustrated in Figure 8.1. The reflectance histograms for all samples display normal distributions and are presented in Appendix D.

Table 8.1. Reflectance measurements for the fine-float samples.

	Random Reflectance %RoV					Maximum Reflectance $\%R_{max}$				
Fine-float sample	%RoV	Min	Max	Rank	St.dev.	$\%R_{max}$	Min	Max	St.dev.	Vitrinoid type (v-type)
SU	0.87	0.60	1.10	Medium rank C	0.077	0.90	0.60	1.15	0.079	V9
P1	0.89	0.65	1.10	Medium rank C	0.068	0.92	0.70	1.10	0.068	V9
SMU	0.87	0.65	1.05	Medium rank C	0.065	0.90	0.70	1.05	0.064	V9
P2	0.88	0.65	1.05	Medium rank C	0.065	0.92	0.75	1.10	0.066	V9
SML	0.91	0.70	1.05	Medium rank C	0.061	0.94	0.75	1.10	0.063	V9
P3	0.87	0.60	1.10	Medium rank C	0.079	0.90	0.65	1.10	0.081	V9
SBU	0.89	0.70	1.05	Medium rank C	0.067	0.93	0.75	1.10	0.069	V9
SBM	0.89	0.75	1.10	Medium rank C	0.064	0.92	0.75	1.10	0.066	V9
SBL	0.87	0.60	1.10	Medium rank C	0.078	0.91	0.65	1.15	0.080	V9

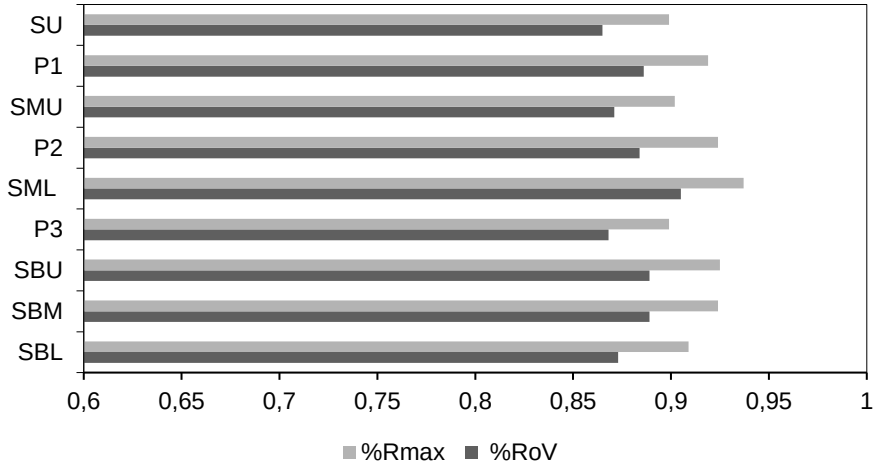

Figure 8.1. Mean random (%RoV) and maximum ($\%R_{max}$) vitrinite reflectance of fine-float samples.

8.3. Maceral analysis

Compositionally, vitrinite is the dominant maceral group in the fine fraction of the LD57 coals. It accounts for more than 94 vol% (mmf) of the coal composition in all the samples (Figure 8.2). In contrast, inertinite only constitutes up to 6 vol% (mmf). Minor occurrences of liptinite were observed in the samples. However, liptinite was not quantified during the maceral point count because it did not fall within the designated area of the cross hairs during the maceral count. Mineral matter was observed in low quantities, up to 7 vol%. Figure 8.2 illustrates the overall decrease in vitrinite content with depth, while inertinite increases with depth. Mineral matter is variable with depth, with no minerals petrographically observable for P3. The petrographic composition data for the fine-floats is reported in Table 8.2.

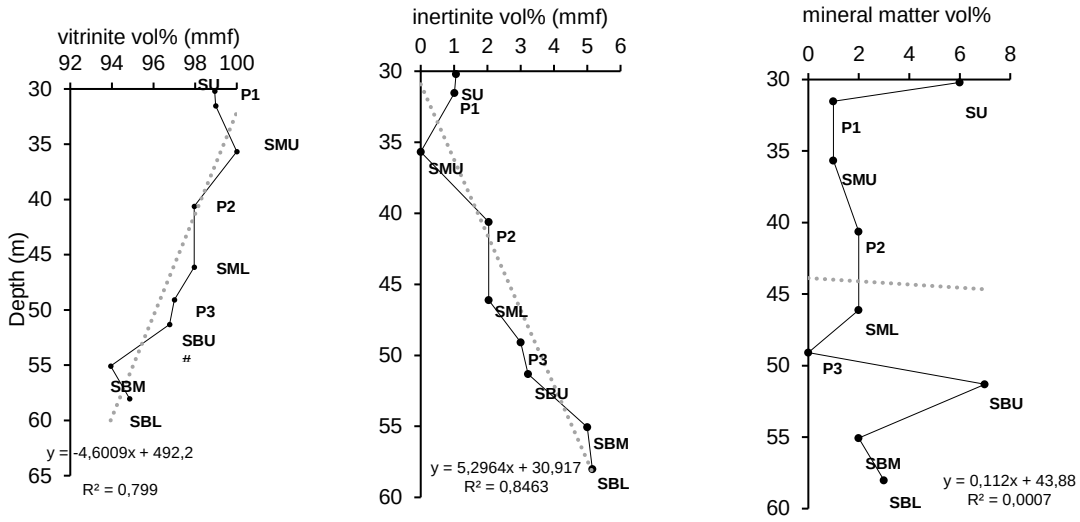

Figure 8.2. Petrographic depth profile composition for the fine-float samples.

Table 8.2. Maceral data for fine-float samples (vol%).

Maceral	SU		P1		SMU		P2		SML		P3		SBU		SBM		SBL	
(vol%)	inc. mm	mmf	inc. mm	mmf	inc. mm	mmf	inc. mm	mmf	inc. mm	mmf	inc. mm	mmf	inc. mm	mmf	inc. mm	mmf	inc. mm	mmf
Telinite	2.0	2.1	2.0	2.0	1.0	1.0	1.0	1.0	1.0	1.0	0.0	0.0	1.0	1.1	2.0	2.0	2.0	2.1
Collotelinite	81.0	86.2	86.0	86.9	88.0	88.9	78.0	79.6	71.0	72.4	79.0	79.0	80.0	86.0	81.0	82.7	79.0	81.4
Vitrodetrinite	1.0	1.1	0.0	0.0	0.0	0.0	0.0	0.0	1.0	1.0	1.0	1.0	0.0	0.0	0.0	0.0	0.0	0.0
Collodetrinite	2.0	2.1	5.0	5.1	1.0	1.0	5.0	5.1	3.0	3.1	8.0	8.0	1.0	1.1	5.0	5.1	2.0	2.1
Corpogelinite	1.0	1.1	3.0	3.0	1.0	1.0	1.0	1.0	0.0	0.0	2.0	2.0	1.0	1.1	0.0	0.0	3.0	3.1
Gelinite	0.0	0.0	0.0	0.0	0.0	0.0	0.0	0.0	0.0	0.0	0.0	0.0	0.0	0.0	0.0	0.0	0.0	0.0
Pseudovitrinite	6.0	6.4	2.0	2.0	8.0	8.1	11.0	11.2	20.0	20.4	7.0	7.0	7.0	7.5	5.0	5.1	6.0	6.2
Total vitrinite	**93.0**	**98.9**	**98.0**	**99.0**	**99.0**	**100.0**	**96.0**	**98.0**	**96.0**	**98.0**	**97.0**	**97.0**	**90.0**	**96.8**	**93.0**	**94.9**	**92.0**	**94.8**
Fusinite	1.0	1.1	1.0	1.0	0.0	0.0	1.0	1.0	1.0	1.0	1.0	1.0	1.0	1.1	2.0	2.0	3.0	3.1
Reactive semifusinite	0.0	0.0	0.0	0.0	0.0	0.0	0.0	0.0	0.0	0.0	1.0	1.0	0.0	0.0	0.0	0.0	0.0	0.0
Inert semifusinite	0.0	0.0	0.0	0.0	0.0	0.0	1.0	1.0	1.0	1.0	1.0	1.0	2.0	2.2	3.0	3.1	2.0	2.1
Micrinite	0.0	0.0	0.0	0.0	0.0	0.0	0.0	0.0	0.0	0.0	0.0	0.0	0.0	0.0	0.0	0.0	0.0	0.0
Macrinite	0.0	0.0	0.0	0.0	0.0	0.0	0.0	0.0	0.0	0.0	0.0	0.0	0.0	0.0	0.0	0.0	0.0	0.0
Secretinite	0.0	0.0	0.0	0.0	0.0	0.0	0.0	0.0	0.0	0.0	0.0	0.0	0.0	0.0	0.0	0.0	0.0	0.0
Funginite	0.0	0.0	0.0	0.0	0.0	0.0	0.0	0.0	0.0	0.0	0.0	0.0	0.0	0.0	0.0	0.0	0.0	0.0
Reactive inertodetrinite	0.0	0.0	0.0	0.0	0.0	0.0	0.0	0.0	0.0	0.0	0.0	0.0	0.0	0.0	0.0	0.0	0.0	0.0
Inert inertodetrinite	0.0	0.0	0.0	0.0	0.0	0.0	0.0	0.0	0.0	0.0	0.0	0.0	0.0	0.0	0.0	0.0	0.0	0.0
Total inertinite	**1.0**	**1.1**	**1.0**	**1.0**	**0.0**	**0.0**	**2.0**	**2.0**	**2.0**	**2.0**	**3.0**	**3.0**	**3.0**	**3.2**	**5.0**	**5.1**	**5.0**	**5.2**
Sporinite	0.0	0.0	0.0	0.0	0.0	0.0	0.0	0.0	0.0	0.0	0.0	0.0	0.0	0.0	0.0	0.0	0.0	0.0
Cutinite	0.0	0.0	0.0	0.0	0.0	0.0	0.0	0.0	0.0	0.0	0.0	0.0	0.0	0.0	0.0	0.0	0.0	0.0
Resinite	0.0	0.0	0.0	0.0	0.0	0.0	0.0	0.0	0.0	0.0	0.0	0.0	0.0	0.0	0.0	0.0	0.0	0.0
Alginite	0.0	0.0	0.0	0.0	0.0	0.0	0.0	0.0	0.0	0.0	0.0	0.0	0.0	0.0	0.0	0.0	0.0	0.0
Liptodetrinite	0.0	0.0	0.0	0.0	0.0	0.0	0.0	0.0	0.0	0.0	0.0	0.0	0.0	0.0	0.0	0.0	0.0	0.0
Suberinite	0.0	0.0	0.0	0.0	0.0	0.0	0.0	0.0	0.0	0.0	0.0	0.0	0.0	0.0	0.0	0.0	0.0	0.0
Exsudatinite	0.0	0.0	0.0	0.0	0.0	0.0	0.0	0.0	0.0	0.0	0.0	0.0	0.0	0.0	0.0	0.0	0.0	0.0
Total Liptinite	**0.0**	**0.0**	**0.0**	**0.0**	**0.0**	**0.0**	**0.0**	**0.0**	**0.0**	**0.0**	**0.0**	**0.0**	**0.0**	**0.0**	**0.0**	**0.0**	**0.0**	**0.0**
clays	4.0		1.0		1.0		1.0		1.0		0.0		5.0		2.0		1.0	
quartz	2.0		0.0		0.0		1.0		0.0		0.0		1.0		0.0		2.0	
sulphides	0.0		0.0		0.0		0.0		0.0		0.0		0.0		0.0		0.0	
carbonates	0.0		0.0		0.0		0.0		1.0		0.0		1.0		0.0		0.0	
other minerals	0.0		0.0		0.0		0.0		0.0		0.0		0.0		0.0		0.0	
Total minerals	**6.0**	**0.0**	**1.0**	**0.0**	**1.0**	**0.0**	**2.0**	**0.0**	**2.0**	**0.0**	**0.0**	**0.0**	**7.0**	**0.0**	**2.0**	**0.0**	**3.0**	**0.0**

Collotelinite is the major vitrinite maceral accounting for 72-89 vol% of the maceral composition. Collotelinite predominantly occurs as smooth homogeneous particles, typically ≥ 150 µm in diameter. Alternating bands of collotelinite were associated with collodetrinite up to 8 vol%, and minor vitrodetrinite of up to 1 vol%. Large particles (≥ 150 µm) of corpogelinite associated with telinite walls were also observed, each constituting up to 3 vol% and up to 2 vol% of the coal composition, respectively. These features are shown in Figure 8.3.

Pseudovitrinite was detected in all horizons, ranging between 2-20 vol%. Seam SML reported the highest count of 20.4 vol%. The pseudovitrinite particles are characterised by desiccation slits orientated perpendicular to bedding or sometimes randomly oriented (Figure 8.3F). Similar to collotelinite, pseudovitrinite particles are also large, typically ≥ 150 µm in diameter.

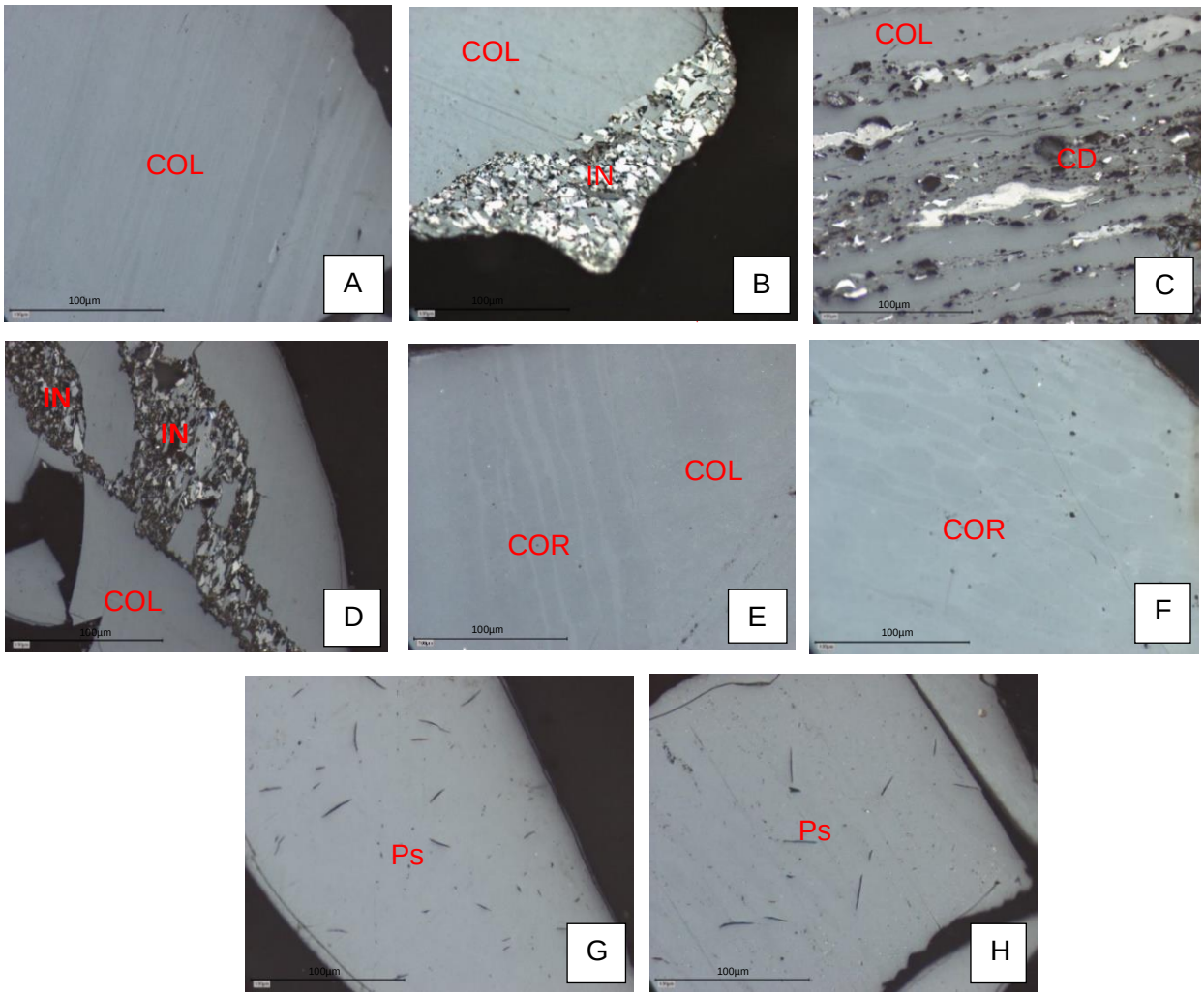

Figure 8.3. Vitrinite forms in the fine-float samples. (A) Alternating bands of collotelinite. (B) Inertodetrinite on the edge of a collotelinite particle. (C) Collodetrinite bands alternating with collotelinite (D) Collotelinite with fine minerals and fine inertodetrinite fragments. (E & F) Oval-oblong corpogelinite bodies associated with collodetrinite fine, minerals and inertinite fragments. (G & H) Massive pseudovitrinite particle showing randomly oriented slits. COL = collotelinite. CD = collodetrinite. VD = vitrodetrinite. Cl = clay minerals. COR = corpogelinite. IN = Inertodetrinite. Ps = Pseudovitrinite. Reflected light oil immersion at x500 µm magnification. Scale bar = 100 µm.

Inertinite is present as fusinite, semifusinite (inert and reactive) and secretinite (Figure 8.4). Large semifusinite particles typically ≥ 150 µm in diameter were observed. Small fusinite fragments ≤ 2 µm) commonly occur scattered within vitrinite. While larger fusinite forms occur as shards or bands alternating with vitrinite and/or semifusinite, others graded from reactive to inert forms. Reactive semifusinite was only counted in P3, albeit quite low at 1 vol%, whilst inert semifusinite was observed from P2 to SBL (1-3 vol%).

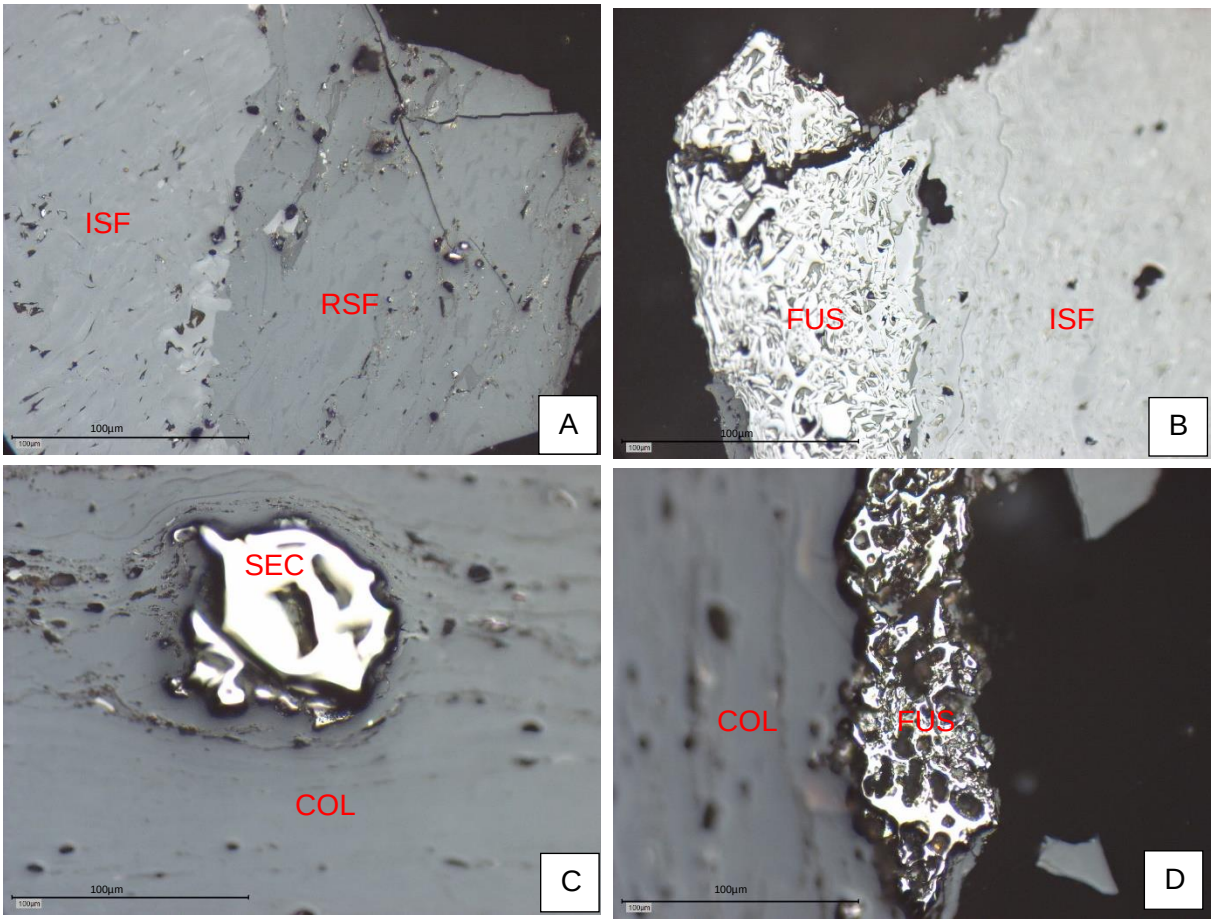

Figure 8.4. (A) Inert semifusinite and reactive semifusinite. (B) Fusinite displaying fragmented bogen structure grading into inert semifusinite. (C) Secretinite embedded in collotelinite. Note collotelinite wrapped around secretinite. (D) Fusinite char embedded in collotelinite. ISF = Inert semifusinite. RSF = reactive semifusinite. FUS = Fusinite. SEC = Secretinite. COL = collotelinite. Reflected light oil immersion at x500 µm magnification. Scale bar = 100 µm.

Mineral matter in all the horizons is minimal, only accounting for up to 7 vol% of the coal composition at a petrographic level (Table 8.2). Where present, the most frequently observed minerals are clay minerals and quartz. Less frequently observed minerals are carbonates such as siderite and calcite. SBU and SU reported the highest amount of mineral matter, specifically clay and quartz. Notably no mineral matter was counted for P3. The clay minerals are very finely dispersed or occur as flocculated lenses (Figure 8.5A-C) within vitrinite. Quartz grains occur as round to sub-spherical (< 5µm) and occur within the various maceral matrices or associated with clay minerals (Figure 8.5 D & E). Similarly, siderite nodules of varying sizes

(5-100µm) occur with the vitrinite and inertinite particles (Figure 8.4F-H). Calcite grains and laths were observed within vitrinite particles (Figure 8.4I).

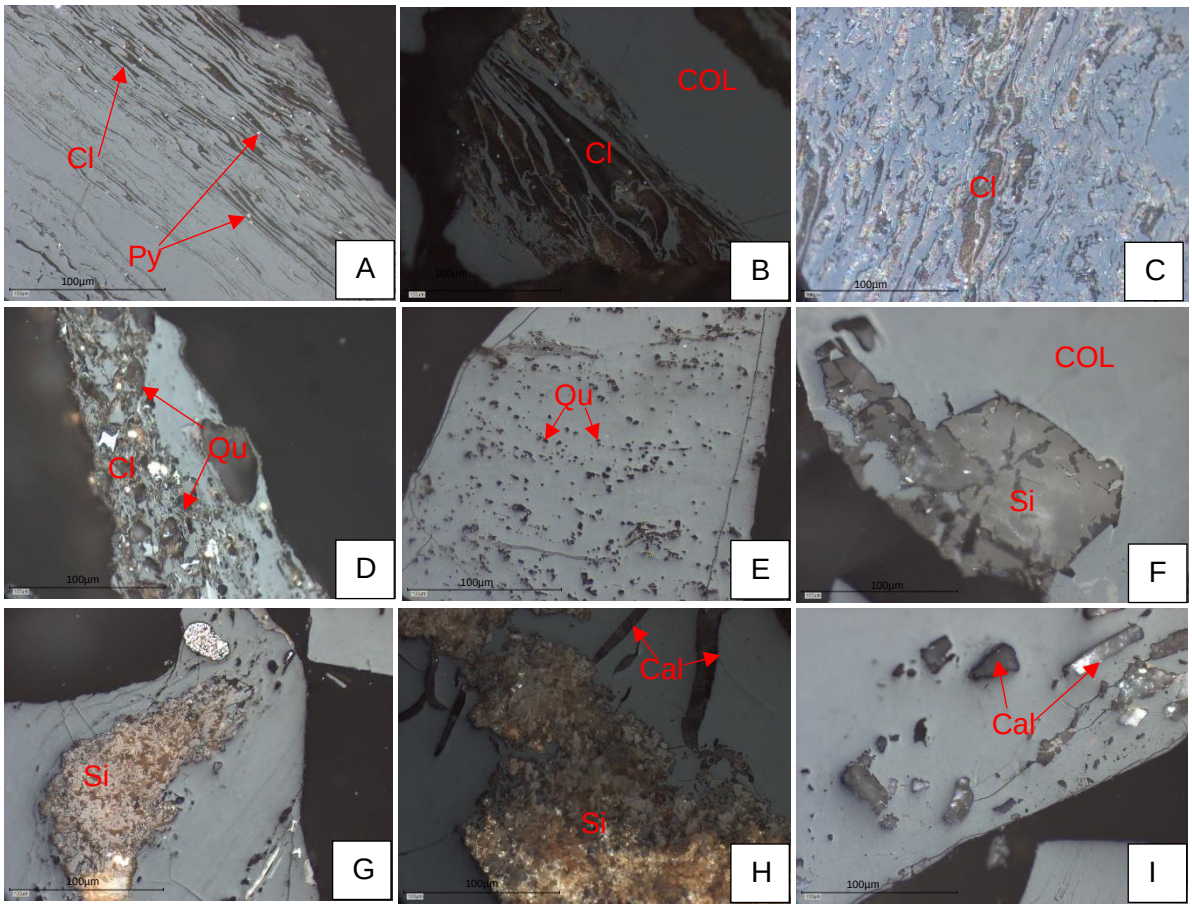

Figure 8.5. (A, B & C) Flocculated clay minerals infilling cell lumens in vitrinite particles. (D) Quartz particles of varying sizes associated with clay minerals. (E) Finely disseminated quartz grains within collotelinite. (F) Crystalline siderite infilling a cavity in collotelinite. (G) Siderite embedded within collotelinite. (H) Calcite cleats cross cutting siderite nodule. (I) Calcite within collotelinite. Cl = clay minerals. Py = Pyrite. Qu = Quartz. Si = Siderite. Cal = calcite. Reflected light oil immersion at x500 µm magnification. Scale bar = 100 µm.

Pyrite was observed as very fine particles and framboids. Due to the fractionated nature of the pyrite, it was not quantified during the maceral point count because it did not fall within the designated area of the cross hairs during the maceral count, despite being observed in the overall field of view. Figure 8.6 shows the fine nature of pyrite, occurring as dispersed granules (< 1µm) or as framboidal clusters. Rare pyrite cleats were also observed.

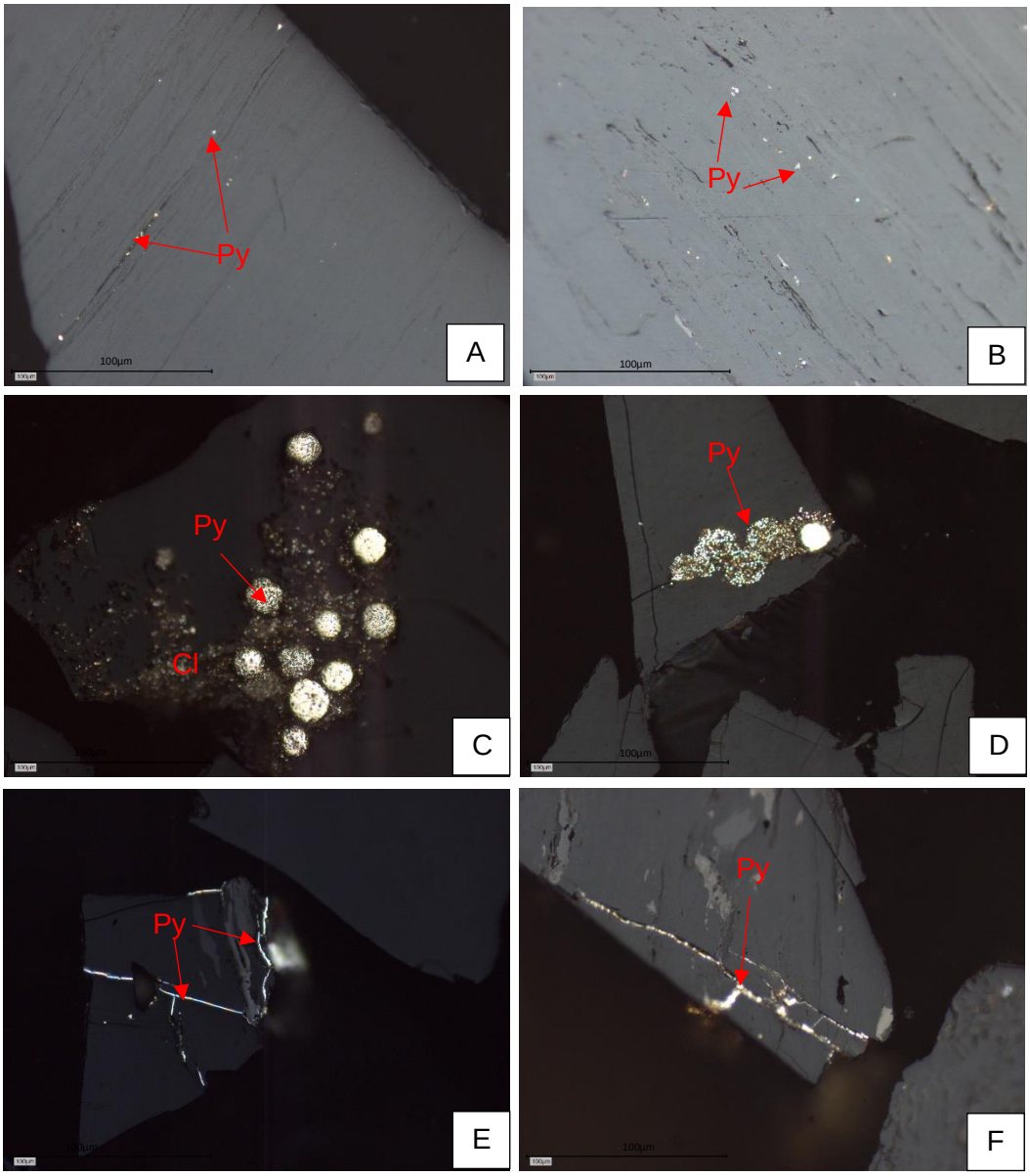

Figure 8.6. Rarely observed pyrite forms. (A & B) Micron-sized pyrite particles dispersed within collotelinite. (C & D) Clusters of framboidal pyrite occurring within clay minerals. (C) Fracture infilled with pyrite (E & F). Py = Pyrite. Cl = clay minerals. Quartz (Qu), Reflected light oil immersion at x500 µm magnification. Scale bar = 100 µm.

8.4. Microlithotype analysis

By virtue of the high vitrinite content, the fine-float samples predominantly consist of the monomaceral vitrite, averaging 86 vol% (Table 8.3). Inertite is less frequent, only constituting up to 5 vol%. Bimaceral microlithotypes observed are vitrinertite (13 vol%) and minor clarite (1 vol%). The latter was only reported in P3. The occurrence of carbominerites in order of abundance are: carbargilite > carbosilicate > carbankerite > carbopyrite. These carbominerites only constitute a maximum of up to 10 vol% of the coal composition. Figure 8.7 illustrates the microlithotype trends which correspond to those depicted in Figure 8.2.

Table 8.3. Microlithotype data for the fine-float samples (vol%).

Microlithotypes	Group	SU	P1	SMU	P2	SML	P3	SBU	SBM	SBL
	Vitrite	85.0	89.0	95.0	90.0	85.0	88.0	76.0	82.0	86.0
	Inertite	0.0	1.0	1.0	1.0	2.0	2.0	3.0	5.0	2.0
Monomaceral	Liptite	0.0	0.0	0.0	0.0	0.0	0.0	0.0	0.0	0.0
	Vitrinertite	0.0	2.0	1.0	2.0	4.0	4.0	13.0	9.0	7.0
	Durite	0.0	0.0	0.0	0.0	0.0	0.0	0.0	0.0	0.0
Bimaceral	Clarite	0.0	0.0	0.0	0.0	0.0	1.0	0.0	0.0	0.0
	Duroclarite	0.0	0.0	0.0	0.0	0.0	0.0	0.0	0.0	0.0
	Clarodurite	0.0	0.0	0.0	0.0	0.0	0.0	0.0	0.0	0.0
Trimaceral	Vitrinertoliptite	0.0	0.0	0.0	0.0	0.0	0.0	0.0	0.0	0.0
	Carbargillite	10.0	5.0	1.0	3.0	3.0	2.0	6.0	2.0	3.0
	Carbosilicate	3.0	1.0	1.0	3.0	4.0	2.0	2.0	2.0	1.0
	Carbankerite	0.0	0.0	0.0	0.0	1.0	0.0	0.0	0.0	1.0
	Carbopyrite	1.0	1.0	1.0	0.0	0.0	0.0	0.0	0.0	0.0
	Carbopolyminerite	1.0	1.0	0.0	1.0	1.0	1.0	0.0	0.0	0.0
Carbominerite	Minerite (rock)	0.0	0.0	0.0	0.0	0.0	0.0	0.0	0.0	0.0

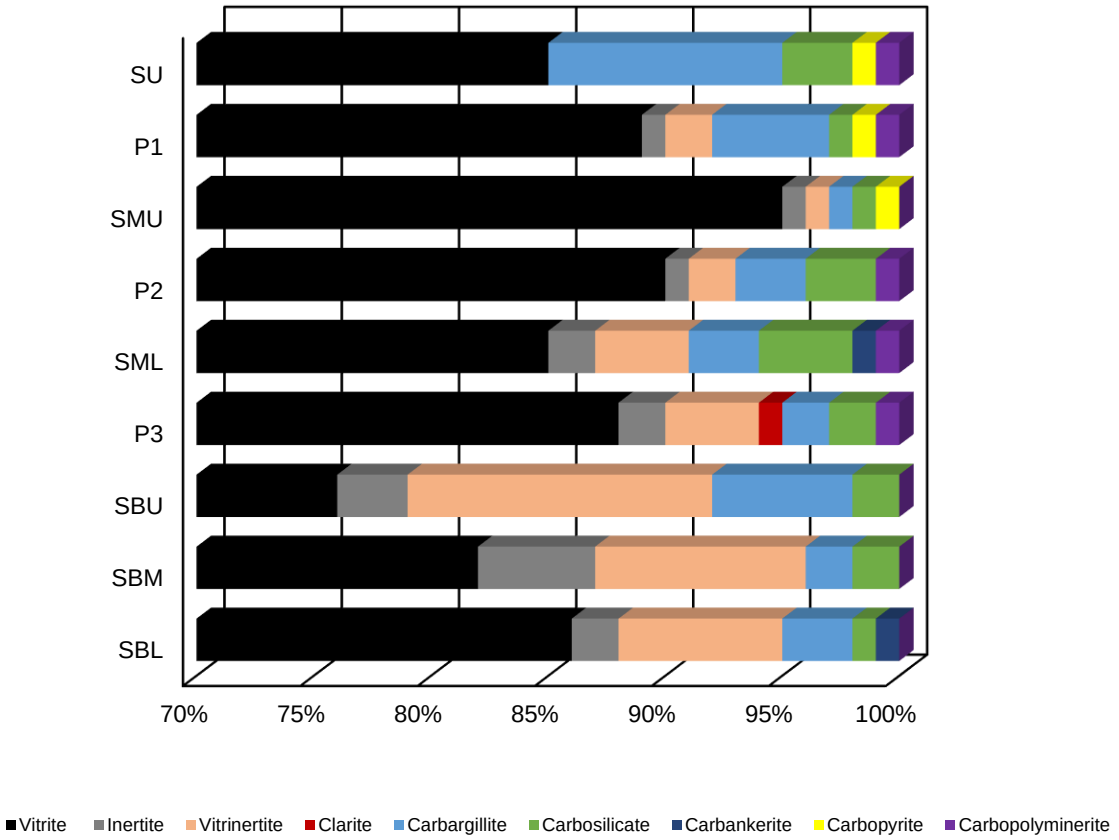

Figure 8.7. Microlithotypes in the fine-float samples (inc. mm vol%).

8.5. Discussion

Overall, the petrographic analyses show that the monomaceral vitrite is highly concentrated in the fine fraction (-1+0.25 mm) floats of the LD57 coals, with minimal associations of inertinite and syngenetic minerals. The dominance of vitrite is attributed to the inherently high amount of vitrinite occurring in Soutpansberg coals (Mphaphuli, 2017). Thus, vitrinite tends to report to the fine size fraction floats. This agrees with maceral and microlithotype partitioning trends published on other coals (Esterle, 2008, and the studies cited therein; Hower, 2008). From a utilisation point of view, the ratio of fusinite and other inertinites relative to vitrinite is favourable as inertinites in low amounts act to improve coke strength during carbonization (Suárez-Ruiz and Crelling, 2008). This is consistent with the high reactive versus inert maceral ratios for South African coking coals (Jordan, 2008; Powell, 2016). Pseudovitrinite was detected in all samples, on average 8 vol% (mmf). Only sample SML contains very high (20 vol% mmf) pseudovitrinite. Although pseudovitrinite is known to have a deleterious effect on the coking properties of metallurgical coal, studies have shown pseudovitrinite to be reactive under certain coking conditions (Kruszewska, 1998; Kyung Eun, 2012). Furthermore, the adverse effects of pseudovitrinite in the LD57 fine-floats may be negligible due to its low quantity relative to collotelinite, similar to the findings of Benedict and Thompson (1980).

Gravity separation by means of the float sink test has produced low mineral matter (≤ 7 vol%) in the fine fraction samples. This shows that much of the epigenetic minerals observed on the raw coal (LD57 lithology discussed in Chapter 4) such as void, cavity and cleat filling minerals, were successfully removed by crushing and gravity based separation. In contrast, the remaining mineral matter which is particularly fine grained and finely disseminated, is intricately bound and therefore indicative of syngenetic origins. This is in agreement with the high NGM calculated for the fine fraction as discussed in Chapter 6 because coals that are predominantly characterised by high proportions of syngenetic mineral matter (fixed ash) tend to generate more NGM. The syngenetic minerals are intricately bound to the organic carbonaceous material and are therefore difficult to separate by physical beneficiation (Bhattacharya *et al*., 2016; Subba Rao and Gouricharan, 2016). Therefore, further liberation of this form of mineral matter by physical methods will be ineffective for the LD57 coals.

It is important to note that the presence of pyrite may have been underestimated by the petrographic analysis due to its finely dispersed occurrence, i.e., pyrite not falling under the cross hairs during the maceral point count is not counted. The mineralogical analyses discussed in Chapter 9 will provide more insight into sulphur present in these samples.

In summary, the fine-float samples are ranked Medium Bituminous C coals (%RoV 0.88). The prime coking properties of the Makhado horizons have been proven through several industrial

tests including FSI, coke reactivity index with CO_2, coke strength after reaction (Sparrow, 2012; Matyjaszek *et al*., 2018; https://www.mcmining.co.za).

Chapter 9: Geochemistry

9.1. Introduction

The quality of the fine-float samples are characterised in this chapter with respect to their chemical composition (proximate analysis and total sulphur), FSI and mineralogy. Trace element and REE concentrations of the ashed fine-float samples are presented. The distribution and associations of the trace elements and REEs are determined. The implications of these properties on the production of metallurgical coal are discussed. This chapter addresses objectives for part two of the study.

9.2. Coal chemistry

The quality of the fine-float samples is reported in Table 9.1 in terms of the proximate data, total sulphur and FSI. On average, the fixed carbon content is 65% (daf), and volatile matter is 33% (daf). The coals contain low ash of 4% (db) and inherent moisture of 1%. These values show little variation with depth for all samples.

The total sulphur content varies from 0.98 to 1.47%, with the lowermost seams containing the least sulphur.

The FSI for all the fine samples is 9, and therefore all samples are classified with strongly caking properties.

Table 9.1. Coal quality of the fine-float samples.

Fine-float sample	Fixed Carbon% (daf)	Volatile Matter % (daf)	Ash % (db)	Moisture % (db)	Total sulphur %	FSI
SU	65.2	33.9	4.0	0.9	1.27	9
P1	65.7	33.2	3.2	1.1	1.38	9
SMU	65.8	33.3	3.0	0.9	1.47	9
P2	65.2	33.9	4.8	0.8	1.44	9
SML	65.8	33.3	4.8	0.8	1.27	9
P3	65.6	33.4	3.8	1.0	1.14	9
SBU	65.9	33.1	5.4	0.9	0.95	9
SBM	65.9	33.1	4.5	0.9	0.98	9
SBL	64.9	34.1	5.1	0.9	1.13	9

9.3. Mineral composition

The mineral composition as shown by the XRF data consists of quartz (≤ 3%), kaolinite (≤ 2.30%) and tridymite (≤ 0.90%). Moreover, the samples are characterised by high organic carbon of up to 96.60% (Table 9.2). Traces of additional minerals such as pyrite and siderite may be present but, were not detected above the detection limit of 0.5-3 wt% due to the

presence of high organic carbon. The XRD diffractogram for minerals identified in the fine-float samples is shown in Appendix H.

Table 9.2. Mineral species identified in the fine-float samples reported on weight percent basis (wt%).

Fine-float sample	Quartz (SiO_2)	Kaolinite ($Al_2Si_2O_5(OH)_4$)	Tridymite (SiO_2)	Organic C	LOI
SU	3.20	0.70	0.40	95.70	96.55
P1	2.00	1.00	0.40	96.60	97.14
SMU	1.60	1.20	0.40	96.80	97.25
P2	2.60	1.20	0.50	95.80	95.25
SML	2.20	1.50	0.80	95.50	96.16
P3	1.30	1.30	0.60	96.80	95.56
SBU	2.50	2.30	0.90	94.30	94.82
SBM	2.00	1.90	0.70	95.40	95.59
SBL	2.00	1.80	0.80	95.30	95.35

9.4. Major oxide composition

The major element oxides present in the ashes of fine-float samples are presented in Table 9.3 and are illustrated in Figure 9.1.

The dominant oxides occurring in the samples are silica (SiO_2: 42-67%), aluminium oxide (Al_2O_3: 14-27%), titanium dioxide (TiO_2: 5-14%), ferric oxide (Fe_2O_3: 2-7%), calcium oxide (CaO: 2-4%), and magnesium oxide (MgO: 1-2%). The remaining oxides generally occur in quantities less than 1%. Samples from the lower most seams appear to have higher amounts of Al_2O_3, CaO, Na_2O, K_2O and P_2O_5 compared to the upper most seams and partings, i.e., the aforementioned oxides increased with depth (Table 9.3). While SiO_2, Fe_2O_3 and NiO are highest in the samples from the uppermost seams and partings and tend to decrease with depth.

Table 9.3. Major oxides in the fine-float samples (wt %).

Fine-float Sample	SiO_2	Al_2O_3	Fe_2O_3	MnO	MgO	CaO	Na_2O	K_2O	TiO_2	P_2O_5	Cr_2O_3	NiO	LOI	Total	Ash
SU	66.91	13.96	2.83	0.02	1.28	2.15	0.30	0.91	4.59	0.06	0.08	0.05	0.64	93.79	3.96
P1	51.15	12.58	3.98	0.03	1.28	2.04	0.34	0.90	13.70	0.60	0.29	0.12	1.65	88.66	3.37
SMU	53.48	18.54	7.45	0.05	1.20	2.28	0.51	1.01	9.08	0.10	0.15	0.09	0.75	94.70	2.97
P2	55.28	18.01	4.31	0.04	1.39	1.90	0.39	1.20	7.43	0.26	0.20	0.09	1.39	91.90	5.20
SML	55.45	24.69	2.99	0.03	1.06	1.78	0.64	1.17	5.88	0.21	0.14	0.07	1.67	95.77	4.72
P3	46.15	22.05	1.93	0.00	1.81	3.25	1.15	0.80	10.26	0.36	0.27	0.05	2.10	90.15	4.44
SBU	46.67	24.24	2.81	0.03	1.02	2.16	0.75	0.94	6.39	1.78	0.15	0.05	5.63	92.61	5.58
SBM	49.18	27.24	3.08	0.03	1.15	2.55	0.94	1.04	6.37	1.99	0.14	0.06	0.69	94.46	4.70
SBL	42.10	23.75	3.12	0.03	1.26	3.53	0.80	1.15	10.16	2.93	0.23	0.07	0.96	90.08	4.88

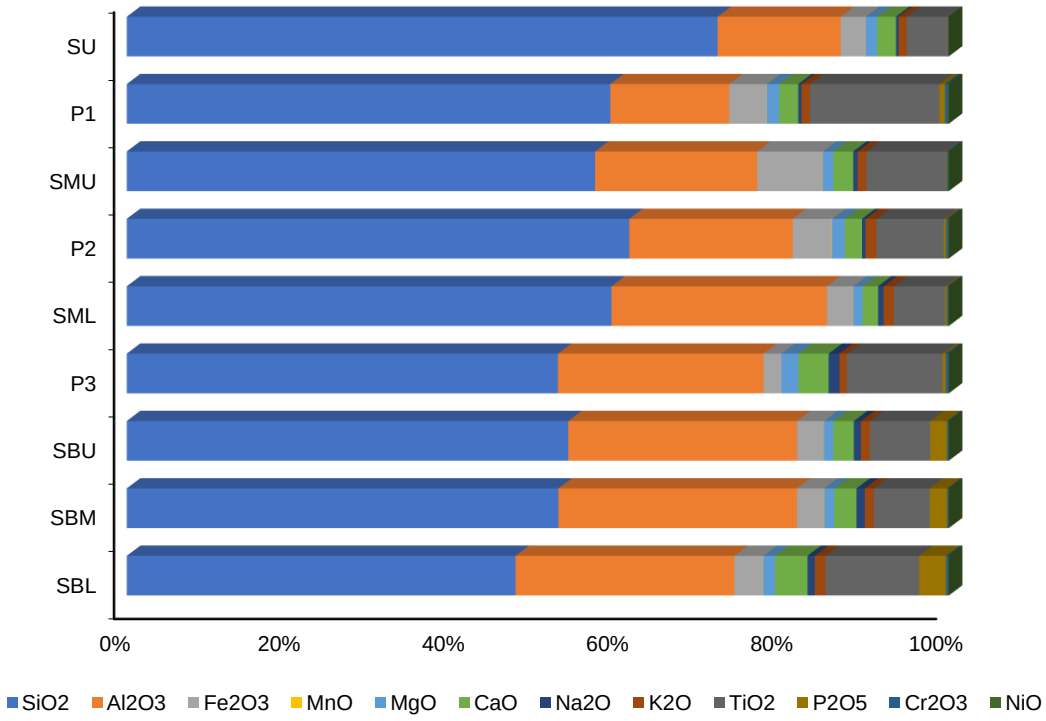

Figure 9.1. Major oxide composition of the fine-float samples (wt%).

The alkali content for the fine-float was determined by adding the Na_2O and K_2O content for each sample (Schernikau, 2017). The alkali values for the fine-float samples are in the range 1.21-1.95% and show an increase with depth as illustrated in Figure 9.2.

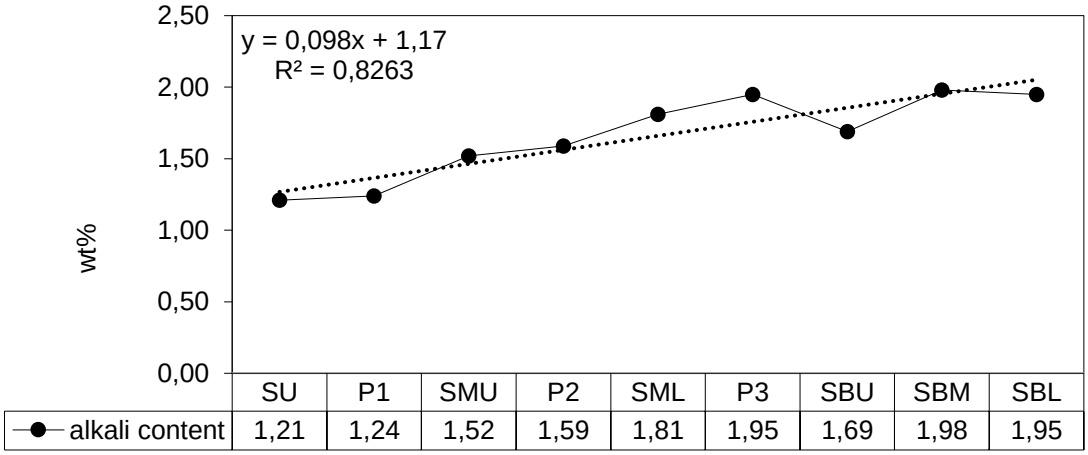

Figure 9.2. Alkali content in the fine-float samples calculated from Na_2O and K_2O.

The amount of phosphorus present in the coal ash of the fine-float samples was calculated from the P_2O_5 values (Table 9.3) using the following formula from Schernikau (2017):

$$\%P = \frac{0.43642\ (\ P_2O_5 \times Ash\%)}{100}$$

The results in Figure 9.3 show that the phosphorus content is in the range 0.001- 0.065%. Furthermore, the phosphorus content of the samples from the uppermost seams and partings is significantly lower compared to the samples from the lowermost seams. Hence, the phosphorus content shows an increase with depth.

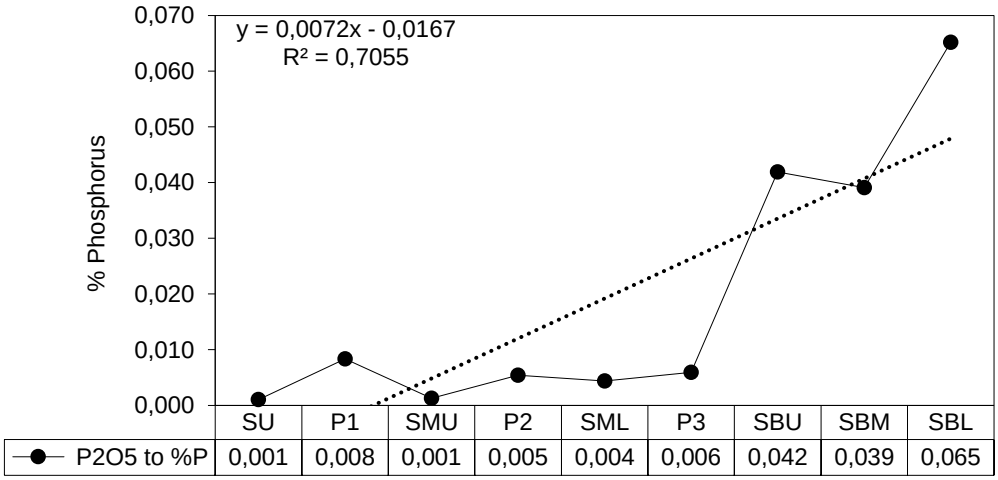

	SU	P1	SMU	P2	SML	P3	SBU	SBM	SBL
P2O5 to %P	0,001	0,008	0,001	0,005	0,004	0,006	0,042	0,039	0,065

Figure 9.3. Phosphorus content in the fine-float samples reported as %P in coal ash (ad) calculated from P_20_5.

9.5. Trace element composition

The major trace element composition for the fine-float samples discussed herein refer to the 25 elements illustrated on Figure 9.4 and listed in Table 9.4. Trace elements in terms of REE composition are discussed separately in Section 9.6. It is important to note that the trace element and REE concentrations determined for the LD57 fine-float samples are on ash-basis.

The data in Figure 9.4 is grouped into trace elements occurring in concentrations up to 47412 ppm (Ti, Zr, V, Sr, P), 1200 ppm (Ga, Ni, Nb, Cu, Pb, Co, Hf), and 146 ppm (Li, U, Th, Rb, Sb, W, Sn, Cs, Ta), respectively. Only Tl occurs in concentrations below 1.5 ppm. Overall, the trace element concentrations vary with depth but the samples from the lowermost seams show higher concentrations of Ba, Sr, P, Cu, U, Th, Cs and Tl, i.e., these concentrations show an increase with depth. Notably, sample P3 frequently contains the highest trace element concentrations, similarly SBL and, to a lesser extent P1 and SMU. The phosphorus content varies between 81-7444 ppm (or 0.0081-0.744%), which are higher than those reported for phosphorus calculated from P_2O_5 in the preceding Section 9.5 (Figure 9.3).

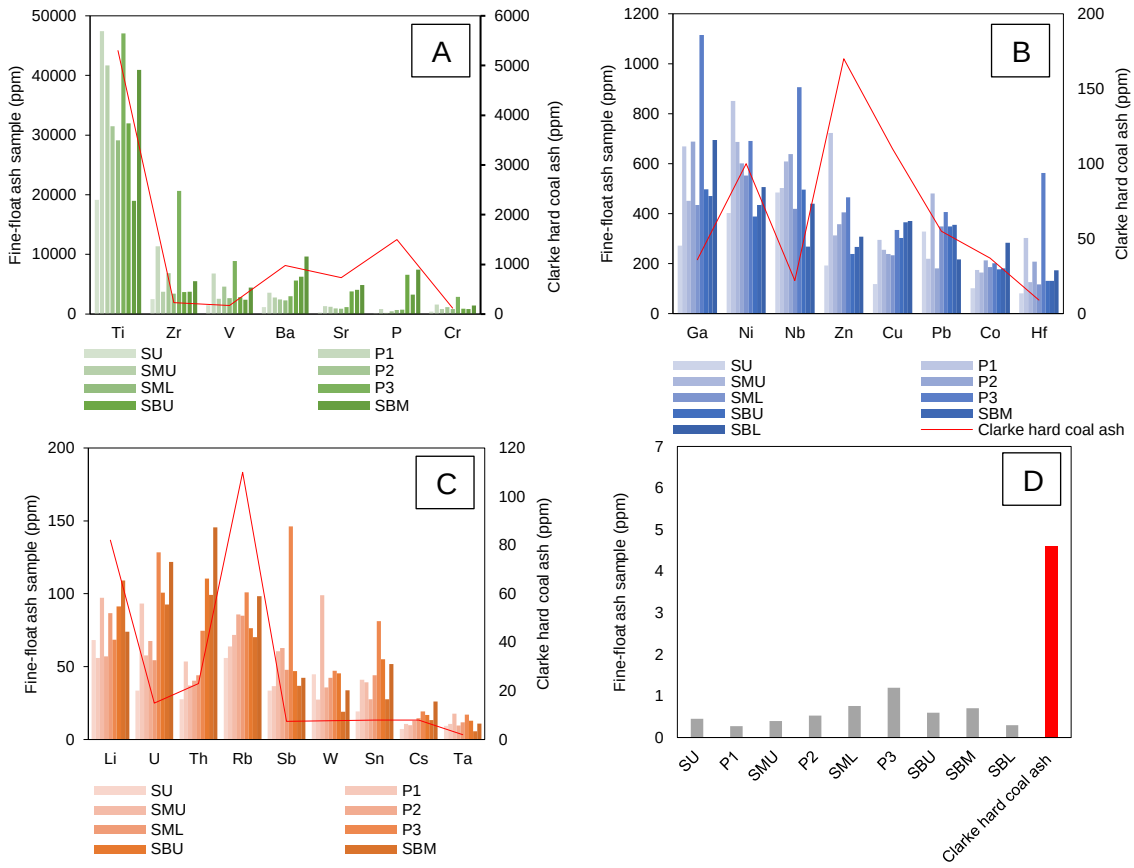

Figure 9.4. Trace elements concentrations in the -1+0.25mm ash samples relative to the Clarke hard coal ash values are grouped as, A) Ti, Zr, V, Ba, Sr, P and Cr ≤ 47412ppm. B) Ga, Ni, Zn, Nb, Cu, Pb, Co and Hf ≤ 1200ppm. C) Li, U, Th, Rb, Sb, W, Sn, Cs and Ta ≤ 146ppm. D) Tl ≤ 1ppm.

Trace elements considered to be of environmental and health concern include As, B, Cd, Hg, Mo, Pb, Se, Cr, F, Cl, Cu, Ni, V, Zn, Ba, Co, Ge, Li, Mn, Sb, Sr, Rn, Th, U, Be, I, Ra, Sn, Te and Tl (Finkelman, 1999; Swaine, 2000; Vejahati *et al*., 2010). In the present study, hazardous trace elements determined were limited Pb, Cr, Cu, Ni, V, Zn, Ba, Co, Li, Sb, Th, U, Sn and Tl due to instrument limitations (Table 9.4).

Table 9.4. Trace element concentrations in the fine-float samples (ppm)

Trace element	SU	P1	SMU	P2	SML	P3	SBU	SBM	SBL	World Hard Coal	World Hard Coal Ash
Li	68	56	97	57	87	69	91	109	74	14	82
P	81	833	206	445	668	731	6575	3289	7444	250	1500
Ti	19159	47412	41674	31480	29152	47056	31954	18961	40914	890	5300
V	1465	6802	2588	4584	2659	8898	2830	2402	4433	28	170
Cr	428	1592	857	1143	844	2908	921	844	1462	17	120
Co	101	175	164	213	186	202	178	181	284	6	37
Ni	403	851	687	601	552	691	389	435	507	17	100
Cu	119	295	256	239	233	335	302	365	370	16	110
Zn	193	723	312	358	405	466	239	267	308	28	170
Ga	272	669	452	689	434	1115	498	471	695	6	36
Rb	56	64	72	86	85	101	76	70	98	18	110
Sr	265	1323	1209	970	890	1176	3784	4062	4869	100	730
Zr	2508	11354	3762	6853	3410	20627	3685	3762	5533	36	230
Nb	484	503	609	639	420	906	496	267	439	4	22
Sn	19	41	39	28	44	81	55	28	52	1.4	8
Sb	33	37	61	63	48	146	47	37	42	1	7,5
Cs	7	11	10	13	15	19	17	13	26	1.1	8
Ba	1187	3595	2771	2478	2286	2979	5640	6265	9650	150	980
Hf	81	303	125	208	118	563	131	130	174	1.2	9
Ta	9	11	18	10	12	17	13	6	11	0.3	2
W	45	27	99	36	42	47	45	19	34	0.99	7,8
Tl	0.45	0.27	0.40	0.53	0.76	1.20	0.59	0.71	0.30	0.58	4,6
Pb	329	219	481	181	349	407	349	355	217	9	55
Th	28	54	37	40	44	75	110	99	146	3.2	23
U	34	93	58	67	54	129	101	93	122	1.9	15
Total	**27374**	**77041**	**56644**	**51480**	**43037**	**89745**	**58527**	**42532**	**77905**	**1601**	**9837**

9.6. Rare earth element (REE) composition

The distribution plots of rare earths in the ashed fine-float samples are illustrated in Figure 9.5. The rare earth concentrations are compared to the Earth`s UCC values determined by Taylor and McLennan (1985), as well as the Clarke values for world hard coals on ash-basis determined by Ketris and Yudovich (2009). The data is summarized in Table 9.5 and includes totals for the rare earths by geochemical class.

Figure 9.5 shows that the rare earths in the fine-float samples generally follow a similar distribution pattern to the crustal abundance (UCC) and Clarke trend. Although, the REY+Sc concentrations of the fine-size samples greatly exceed the UCC values, they are comparable to the Clarke coal ash concentrations.

Overall, the total REY+Sc (ΣREY+Sc) concentrations in the fine-float ash samples show an increase with depth (Figure 9.5), with sample SBL containing the highest amount of ΣREY+ Sc, 3193 ppm (Table 9.5). Sample P3 contains comparable ΣREY+Sc concentrations (2604 ppm) to the lowermost seams, i.e., 2521-3193 ppm (Table 9.5). The geochemical classes for the fine-float samples show that the ΣLREE +Sc concentrations (300-2618 ppm) are higher compared to ΣMREE+Y (213-1454 ppm) and ΣHREE (57-178 ppm), respectively. The order of decreasing abundance observed in the samples for the LREE+Sc follows the general trend:

Ce>La>Nd>Sc>Pr>Sm. While the MREE+Y trend generally follows Y>Dy>Gd>Eu>Tb. The HREE generally follow a trend of Yb>Er>Ho>Tm>Lu.

The total concentration of critical rare earths, i.e., rare earths considered to be of high economic value and in undersupply (Y, Nd, Dy, Er, Eu and Tb) as discussed in Seredin, (2010), are in the range 268-979 ppm, generally reaching their maximum in P3 and the lowermost seams (Table 9.5). Yttrium and Nd have the highest concentration in the samples (159-537 ppm and 53-510 ppm, respectively) compared to the other critical rare earths which generally occur in concentrations <91 ppm. Pr, which is also in high demand only occurs above 100 ppm in the lowermost seams.

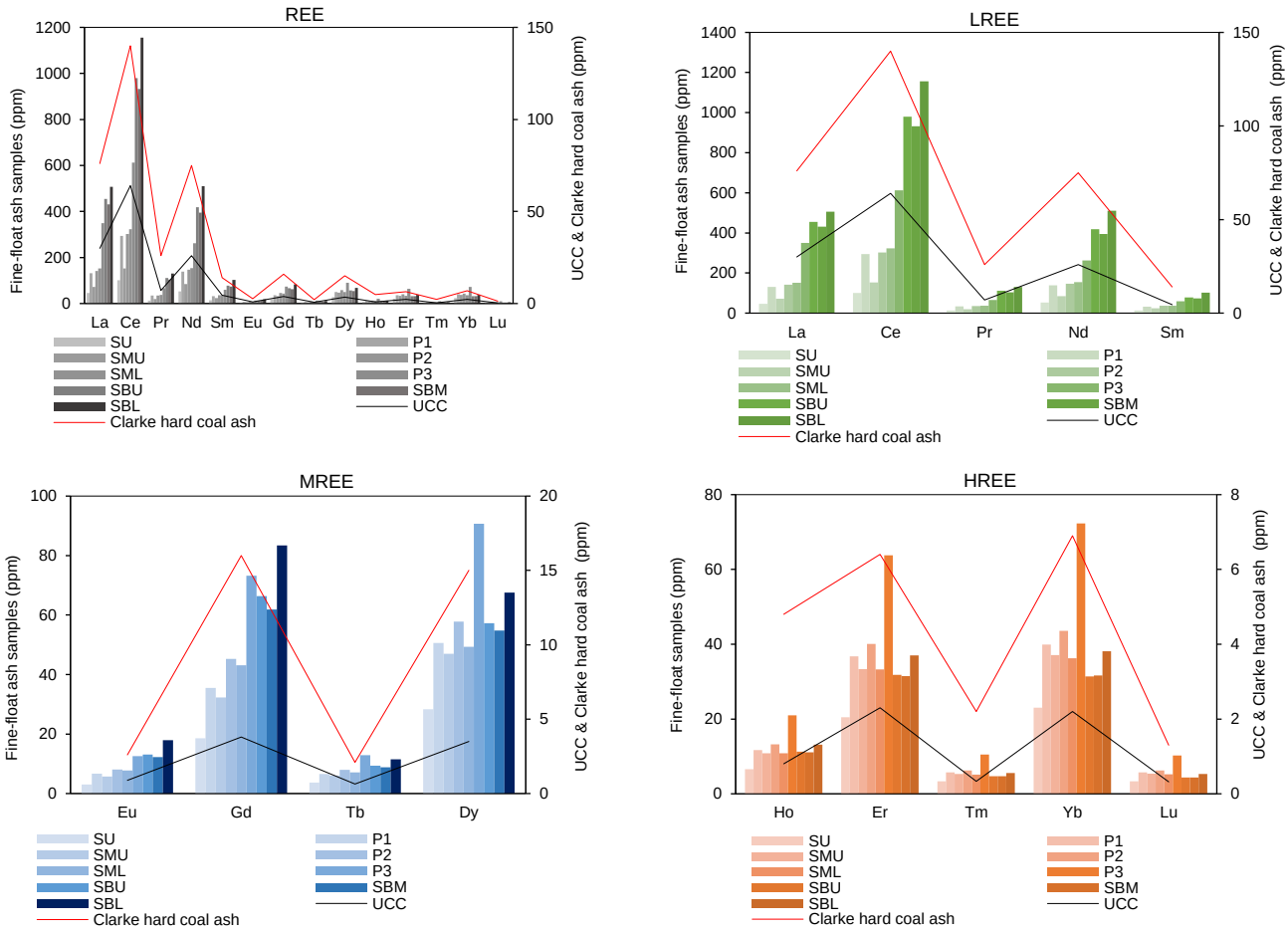

Figure 9.5 Rare earth concentrations in the -1+0.25mm samples relative to the UCC (Taylor and McLennan, 1985) and the Clarke values on coal ash basis (Ketris and Yudovich, 2009)

Table 9.5. REY+ Sc concentration (ppm) in the fine-float samples.

Geochemical class	REE	SU	P1	SMU	P2	SML	P3	SBU	SBM	SBL
LREE	Sc	74.61	169.16	131.78	205.26	166.84	349.04	136.47	113.99	211.99
	La	46.01	131.35	71.59	141.91	152.09	349.51	454.59	431.54	506.56
	Ce	100.63	294.30	152.83	302.64	322.88	612.59	979.07	932.12	1155.79
	Pr	12.33	34.14	19.20	35.15	37.62	66.09	110.86	104.07	130.90
	Nd	52.90	138.45	85.12	146.61	154.04	261.91	418.00	394.39	510.39
	Sm	13.43	31.48	23.61	36.46	36.24	59.56	77.45	73.97	102.51
MREE	Y	159.47	293.57	268.43	320.05	274.67	537.46	270.41	249.90	295.62
	Eu	3.08	6.72	5.71	8.12	7.72	12.60	13.10	12.20	17.98
	Gd	18.60	35.54	32.30	45.30	43.11	73.26	66.37	61.90	83.38
	Tb	3.64	6.59	6.09	7.92	7.07	12.95	9.42	8.88	11.51
	Dy	28.28	50.57	47.02	57.83	49.35	90.70	57.24	54.77	67.58
HREE	Ho	6.58	11.66	10.84	13.24	10.87	20.97	11.26	11.07	13.17
	Er	20.51	36.75	33.36	40.09	33.26	63.81	31.81	31.51	37.04
	Tm	3.30	5.74	5.29	6.27	5.16	10.51	4.72	4.67	5.55
	Yb	23.07	39.87	37.10	43.59	36.25	72.30	31.42	31.64	38.12
	Lu	3.33	5.73	5.39	6.24	5.26	10.26	4.34	4.38	5.29
ΣLREE +Sc		**300**	**799**	**484**	**868**	**870**	**1699**	**2176**	**2050**	**2618**
ΣMREE		**213**	**786**	**719**	**878**	**764**	**1454**	**833**	**775**	**952**
ΣHREE		**57**	**100**	**92**	**109**	**91**	**178**	**84**	**83**	**99**
ΣREY+ Sc		**570**	**1292**	**936**	**1417**	**1342**	**2604**	**2677**	**2521**	**3193**
ΣREY		**495**	**1122**	**804**	**1211**	**1176**	**2254**	**2540**	**2407**	**2981**
ΣREE		**336**	**829**	**535**	**891**	**901**	**1717**	**2270**	**2157**	**2686**
***LREE/HREE**		**1.11**	**1.62**	**1.07**	**1.58**	**1.84**	**1.88**	**4.35**	**4.35**	**4.55**

*The LREE/HREE ratio was calculated on the basis of HREE = Eu + Gd + Tb + Dy + Ho + Er + Tm + Yb + Lu + Y. LREE = La + Ce + Sc + Pr + Nd + Sm.

The normalized values plotted in Figure 9.6 for the fine-float samples exceed the Earth`s UCC as well as the Clarke values. This observation is especially true for sample P3 and the lowermost seams which are overall more REE enriched compared to samples from the uppermost seams and partings. Furthermore, the UCC and Clarke normalized curves are generally smooth however, a zig zag pattern is observed between Nd and Dy on the UCC normalized curves (Figure 9.6A). The zig zag pattern is also apparent for the HREEs (Ho-Lu) on the Clarke normalized curves (Figure 9.6B). The anomalies likely arise due to incomplete digestion during sample preparation, or spectral interferences (Dai *et al*., 2016). Moreover, the overall smoothness of the graphs give confidence in the REY+Sc data.

Enrichment relative to the UCC varies between 2 and 20 times in samples from the uppermost seams and partings, compared to 9 to 33 times enrichment in sample P3. Enrichment in the lowermost seams is in the range of 10 to 23. Sc and Y show enrichment factors of 32 and 24 in sample P3, respectively. In contrast, the enrichment of the fine-float samples relative to the Clarke values on ash basis is comparatively lower. The uppermost and lowermost seams only show up to 5- and 8-times enrichment, respectively. The partings show up to 10 times enrichment. Examination of the geochemical classes for the rare earths shows that the UCC normalized REEs in the lowermost seams are almost uniform, with LREEs being slightly more enriched than the MREEs and HREEs, respectively (Figure 9.6B). The opposite is true for the uppermost seams whereby HREEs are more enriched compared to MREEs and LREEs, respectively.

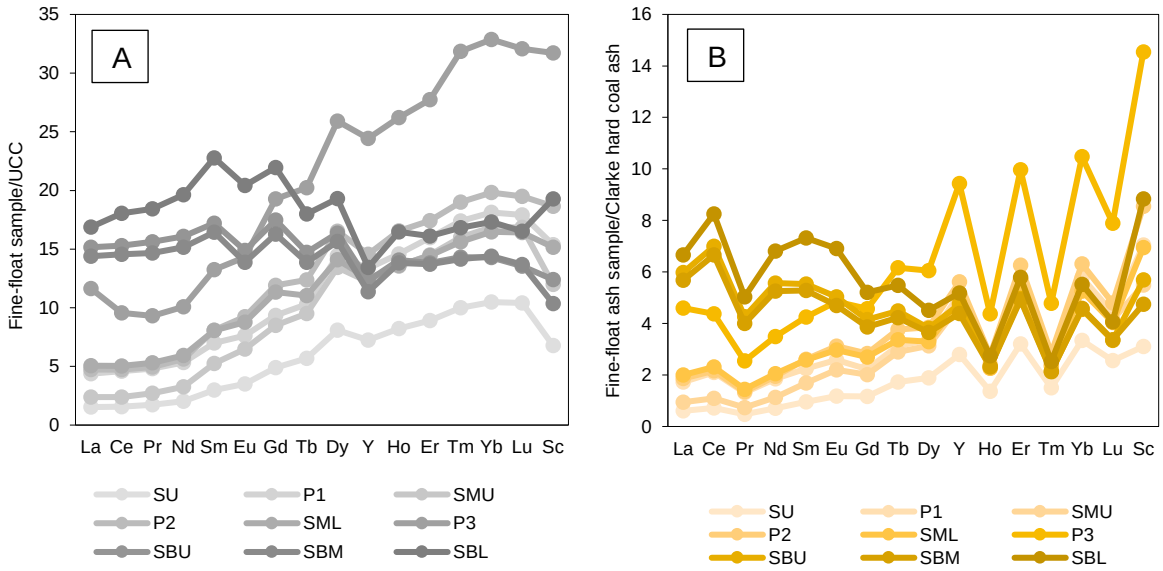

Figure 9.6. REY+Sc concentration in the -1+0.25 mm samples normalized to the A) the Earths UCC values (Taylor and McLennan, 1985). B) Clarke values on ash-basis (Ketris and Yudovich, 2009).

Table 9.6. UCC normalized REY+Sc concentrations for the fine-float samples.

REY+Sc	SU	P1	SMU	P2	SML	P3	SBU	SBM	SBL
La	1.53	4.38	2.39	4.73	5.07	11.65	15.15	14.38	16.89
Ce	1.57	4.60	2.39	4.73	5.05	9.57	15.30	14.56	18.06
Pr	1.74	4.81	2.70	4.95	5.30	9.31	15.61	14.66	18.44
Nd	2.03	5.32	3.27	5.64	5.92	10.07	16.08	15.17	19.63
Sm	2.99	6.99	5.25	8.10	8.05	13.23	17.21	16.44	22.78
Eu	3.50	7.64	6.49	9.23	8.77	14.32	14.89	13.87	20.43
Gd	4.90	9.35	8.50	11.92	11.34	19.28	17.47	16.29	21.94
Tb	5.68	10.29	9.52	12.37	11.05	20.23	14.71	13.88	17.99
Dy	8.08	14.45	13.44	16.52	14.10	25.91	16.35	15.65	19.31
Ho	8.23	14.58	13.55	16.55	13.59	26.22	14.08	13.83	16.47
Er	8.92	15.98	14.50	17.43	14.46	27.74	13.83	13.70	16.10
Tm	10.00	17.40	16.02	18.99	15.62	31.86	14.32	14.15	16.83
Yb	10.48	18.12	16.86	19.81	16.48	32.87	14.28	14.38	17.33
Lu	10.42	17.91	16.84	19.48	16.42	32.08	13.56	13.70	16.52
Sc	6.78	15.38	11.98	18.66	15.17	31.73	12.41	10.36	19.27
Y	7.25	13.34	12.20	14.55	12.48	24.43	12.29	11.36	13.44
ΣREY+ Sc	**94**	**181**	**156**	**204**	**179**	**341**	**238**	**226**	**291**
ΣREY	**86**	**161**	**142**	**180**	**159**	**297**	**210**	**202**	**255**
ΣREE	**80**	**152**	**132**	**170**	**151**	**284**	**213**	**205**	**259**

9.7. Evaluation of Makhado LD57 coal ash samples as economic raw materials

The C_{outl} for the LD57 fine-size samples vary from 0.8 to 2.0, with samples from the uppermost seams and partings showing higher C_{outl} values. Preliminary assessment of the fine-float samples based on the C_{outl} plot (Figure 9.7) revised by Dai *et al*. (2017) shows that the ashes of the fine-float samples are a promising REY source as all but samples SU and SMU fall into the 'promising area'. The ashes of samples SU and SMU do not qualify as promising REE sources because their ΣREY content is below 1000 ppm as per the updated requisites by Dai *et al*. (2017).

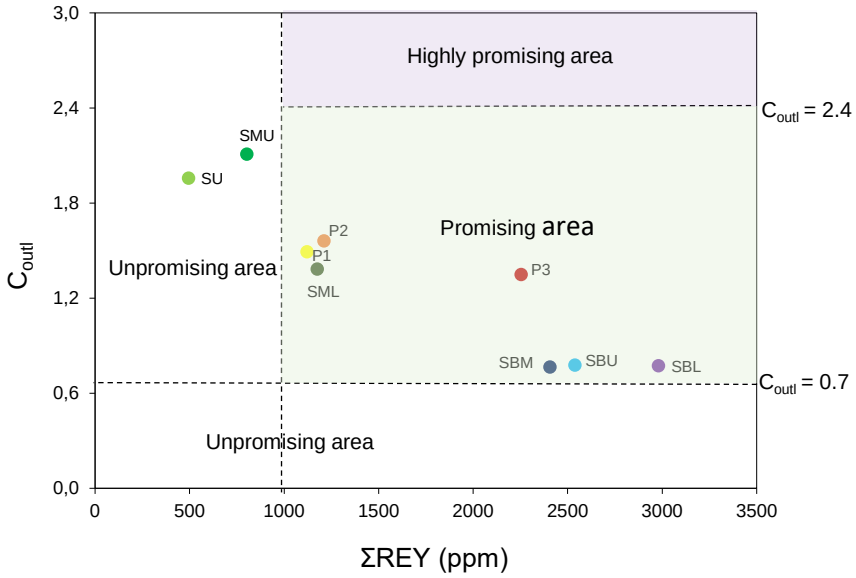

Figure 9.7. Revised C_{outl} graph by Dai *et al*. (2017). All the fine-float samples excluding SU and SMU fall in the promising area. Total REY concentrations in samples SU and SMU are < 1000 ppm.

9.8. Modes of association for trace elements and REEs

The regression and correlation analyses are widely used to give a likely indication into the of association of trace elements and REY+Sc in coals (Davidson, 1998; Wang *et al*., 2006; Wagner and Tlotleng, 2012; Kolker *et al*., 2017; Qin *et al*., 2018; Dai *et al*., 2021). In the present study the regression and correlation analyses were performed with respect to the vitrinite content, ash content and major oxides (Appendix I) to determine organic, inorganic or mixed associations between the coal constituents. Most trace elements and rare earths showed weak/no correlation ($R^2 \leq 1$) with the vitrinite content, ash and/or major oxides, respectively. Samples showing statistically significant correlations are reported below.

Correlations with vitrinite indicate that strong and negative correlations exist with P_2O_5, Sr, Th, Eu and all LREE excluding Sc. However, moderately negative associations exist with Al_2O_3, Na_2O, P, Cu, and Ba (Appendix J). The ash content shows moderately positive correlations with P and Ni.

The associations for the various oxides with trace elements and REY+Sc are presented in Appendix K and are summarized as follows:

- SiO_2 shows strong negative correlations with Cu, Cs, Th, U, all LREE excluding Sc, Eu, Gd and Tb. However, SiO_2 shows a moderate negative correlation with Co, P, Sn, Sr, Ba and Dy.
- Al_2O_3 shows moderate positive correlations with Li, Eu, Gd, and all LREE excluding Sc.

- Fe_2O_3 shows a moderately positive correlation with W.
- MnO shows moderately negative correlations with Zr, Hf and Tl.
- MgO shows moderately positive correlations with V, Sc, Y, and Ho. Strong positive correlations with Cr, Ga, Zr, Nb, Sb
- CaO shows moderately positive correlations with Cs, Th, U, La, Sm, and all MREE excluding Y.
- Na_2O shows moderately positive correlations with Cu, Sn, Tl, U, Ho, all LREE and MREE excluding Sc and Y.
- K_2O shows weak/no correlation with all trace elements and rare earths.
- Ti_2O shows strong positive correlations with Ti, Ni and Zn. Moderately positive with V.
- P_2O_5 shows a perfect positive correlation to Ba. Strong positive correlations with P, Th, Eu and all LREE excluding Sc. Moderately positive with Cu, Cs and Gd.
- Cr_2O_3 shows strong positive correlations with Ti, V, Cr and Ga. While, Ni, Zr, Hf, U, Sc, Y, Dy and all HREE show moderately positive correlations.
- NiO shows moderately positive correlations with Ni and Zn.

Correlation analysis between total sulphur and vitrinite content, ash content and major oxides are tabulated in Appendix L. The statistically significant total sulphur associations are as follows:

- Perfect positive correlations with Ce, Pr, Nd, Sm, Gd, Er, Tm, Yb and Lu.
- Strong positive correlations with MnO, Cr, Tb and Dy.
- Moderate positive correlation with vitrinite, Na_2O, V, Rb, Sb, Ba, W and U.

9.9. Discussion

The coal quality of the fine-float samples is characterised by low ash (≤5% db), high fixed carbon content (≈ 65% daf), high organic carbon (≈ 95%), and high volatile matter (≈ 34% daf). The total sulphur content is on average 1.2 %. The FSI of 9 for all the fine-float samples is comparable to G9+ on the Gray-King Index, >140 on a dilatometer and >45 on the Roga Index (Speight, 2005, Kruger, 2013; Mazumder, 2012). While the FSI values of the fine-float samples are promising, the above-mentioned parameters must be tested on the samples to verify their carbonization properties. Previous testing by MC Mining on the No.6 coal seams have proven HCC properties as reported by Sparrow (2012) and others (de Klerk and Sparrow, 2015; Mostert, 2016).

The XRD and XRF data are in agreement as the measured high silica (SiO_2) and aluminium (Al_2O_3) which correspond to the dominance of quartz and kaolinite reported in the samples. The alkali content of the fine-float samples, excluding SU and P1, exceed the recommended 1.5% limit (Schernikau, 2017). Similarly, the phosphorus content (calculated from P_2O_5 in ash) in the lowermost seams exceed the limit for coking coals used in the South African steel industry which must be ≤ 0.010% (Xaba, 2004). Likewise, the lowermost seams, samples P1, SML and P3 exceed the limit of %P ≤ 0.006% for coking coals used in the South African ferro-alloy industry (Xaba, 2004). Comparatively, the phosphorus content determined by ICPMS reported in Table 9.4 is much higher, ranging between 0.081-0.833% for the uppermost seams and partings, and 3.289-7.444% for the lowermost seams. The correlations observed for elemental P and P_2O_5 with the ash and vitrinite, respectively, indicate phosphorus has an inorganic association. It therefore remains to be determined whether the proposed froth floatation step by MC Mining will reduce the alkali and phosphorus content to acceptable industry levels.

The major trace elements and REY+Sc reported for the fine-float samples (on ash basis) are highly enriched relative to the UCC. However, the enrichment is more comparable to the Clarke values on ash-basis. The REY+Sc enrichment is particularly pronounced in sample P3, as well as the lowermost seams. The enrichment is notably highest for the HREEs. The concentration of trace elements and REY+Sc in the fine-float samples is considered to be abnormally high given the fact that they are low ash clean coals. Furthermore, high concentrations of trace elements and REY+Sc are generally expected in the sink fractions because they contain high amounts of mineral matter which host the trace elements and REY+Sc (Wang *et al*., 2006; Wen-feng *et al*., 2009; Dai *et al*.,2017; Lin *et al*., 2017; Zhang *et al*., 2017; Duan *et al*., 2019). The enrichment is particularly of concern for hazardous trace elements identified in the samples namely: V, Cr. Co, Ni, Cu, Zn, Ba, Pb, Th and Sn. Studies

including Davidson, (1998); Wen-feng *et al.*, (2009); Park *et al.*, (2021), and others have shown that reduction of trace elements by froth floatation in fine coal is achievable.

Of economic interest, the ΣREY for the lowermost seams as well as P2, SML and P3 exceeds 2000 ppm compared to the uppermost seams SU, P1 and SMU where ΣREY > 1000 ppm (Table 9.4). The samples from the lowermost seams and P3 exceed the suggested cut-off grade for REE of 1000 ppm discussed by Dai *et al.* (2017), albeit at laboratory scale and for the -1+0.25 mm particle size. Moreover, the critical trace elements in the fine-float samples that exceed the suggested cut-off grades (Dai and Finkelman, 2018), are Ga, Nb, Zr, Sc (all samples excluding SU) and Y (only samples P2 and P3).

Preliminary assessment for potential economic development based on the revised C_{outl} by Dai *et al.* (2017), shows that all the fine-float ash samples excluding SU and SMU qualify as promising REY sources due to their ΣREY concentrations being less than the required 1000 ppm cut-off grade. Similar findings were reported by Wagner and Matiane (2018) for South African coal ash samples obtained from power stations in the MKB which could not be considered as potential sources of REY due to the low ΣREY content, despite being classified in cluster II. Overall, the trace element and REY+Sc data for the LD57 fine-float samples are interesting and indicate further study is necessary on the coals. The preliminary finding on the promising nature of the fine-float ash samples necessitates further research into the origin of REE in fine-float samples with respect to the genetic types proposed by Seredin and Dai. (2012).

According to Dai *et al*. (2020) the association of trace elements in coal can be classified as organic, mineral, and intimate organic associations. Given that the ashed fine-float samples are carbon rich (Table 9.1 and 9.2) and consist of low mineral matter (Table 9.2) and ash (Table 9.2), suggests that the trace elements and rare earths occurring in these coals are predominantly organically bound to the coal matrices (Finkelman *et al*., 2019). However, correlation with the ash, oxides and vitrinite content predominantly showed an overlap between the inorganic association, and the mixed organic association categories hence, the mode of occurrence for the oxides, trace elements and rare earths in the fine-float samples can be classified as an intimate association whereby some elements are adsorbed onto the surface of the vitrinite particles or are associated with the finely dispersed mineral matter such as kaolinite reported in the samples (Table 9.7). Kaolinite in particular is known to host variety of trace elements (Qin *et al*., 2018; Finkelman *et al*., 2019). Correlation between Fe_2O_3 and CaO likely indicates association with siderite and pyrite, albeit these minerals were not detected above the XRD detection limit. Moreover, correlations with SiO_2, Al_2O_3, TiO_2, Na_2O, K_2O, and MgO indicates associations with aluminosilicate minerals in the coal, i.e., kaolinite

since negative relationships were observed between many of the trace elements and REY+Sc with SiO_2 (Quartz). Hence, kaolinite is a likely host of Li, Ti, Ni, Zn, Cr, Ga, Zr, Nb, Sb, V, Cu, Sn, Tl, U, all LREE, all MREE, Sc, Y, and Ho in the fine-float samples.

Notably the lowermost seams have higher total REY+Sc concentrations, particularly LREE as well as, higher phosphorus content. This may indicate an association with phosphate bearing minerals such as monazite since P_2O_5 was found to show significant positive affinities with La, Ce, Pr, Nd, Sm, Eu and Gd.

Organic sulphur affinity in the fine-float samples is indicated by the positive correlation between vitrinite and the total sulphur content, which corresponds to observations made in Chapter 7, regarding organic sulphur being the major sulphur form in the clean fraction of the LD57 samples. Hence, organic sulphur affinity in the fine-float samples is observed for MnO, Na_2O, Cr, V, Rb, Sb, Ba, W, U, all LREE excluding Sc and La, all MREE excluding Y and Eu, and all HREE excluding Ho.

Table 9.7. Classification of trace element and rare earth association for the LD57 samples.

Mode of occurrence	Criteria	*Oxide/Element*
Organic association	• Perfect/moderate/strong positive correlation with vitrinite • Perfect/moderate/strong positive correlation with total sulphur (predominantly organic as per Chapter 7 discussion)	• None • Ce, Pr, Nd, Sm, Gd, Er, Tm, Yb and Lu Cr, Tb, Dy, V, Rb, Sb, Ba, W, U, MnO and Na2O.
Inorganic/mineral association	• Perfect/moderate/strong positive correlation with ash and or oxides	• Li, Cu, P, Ba, Cs, Sn, Eu, Gd, W, Zr, Hf, Tl, V, Sc, Y, Ho, Cr, Ga, Nb, Sb, Hf, Th, U, Sm, Ti, Ni, Zn, LREE, MREE, HREE.
Mixed organic-inorganic association	• Perfect/moderate/strong negative correlation with vitrinite • no or weak correlation with vitrinite, ash and oxides	• P_2O_5, Al_2O_3, Na_2O, Sr, Th, Eu, P, Cu, Ba & all LREE excluding Sc. • All other oxides, major trace elements, MREY & HREE

*Some constituents overlap both inorganic and mixed organic categories as reported in Section 9.7

Notably, the negative Ti association with vitrinite observed for the sample's contrasts with the positive Ti correlation with vitrinite reported in the literature for South African coals by Snyman *et al*., (1983), Van Alphen (2005), Matjie *et al*., (2016), Rautenbach *et al*., (2019). The positive correlation between Ti and TiO_2 in the present study therefore suggests Ti occurs as finely dispersed rutile or anatase within the vitrinite-rich coal. Affinity of Ti with clay minerals is ruled out due to the fact that poor correlation exists between Ti and Al_2O_3. Uranium universally shows an organic association with vitrinite (Dai *et al*., 2021). However, in the present study, uranium showed a strong positive correlation to Cr_2O_3 and CaO, and moderately positive with Na_2O. Fe_2O_3 in coal commonly shows association with pyritic sulphur and less frequently with

carbonates (Dai *et al*., 2021). In line with the literature (Dai *et al*., 2021), tungsten in the fine-float samples shows an organic association because of the positive affinity with total sulphur content, which was inferred to be predominately organic. In contrast, Fe_2O_3 in the fine-float samples shows a moderately positive correlation with tungsten. To conclude, the inferences made on the trace elements and REY+Sc associations discussed hereto are tentative on the basis of the data presented herein. As such, further study using advanced methods are required to verify the associations and host minerals.

Since trace elements and REY+Sc are known to have a greater inorganic affinity and are therefore hosted in mineral matter occurring in the coal, most of which reports to the sinks/discards during coal cleaning (Huggins *et al*., 2009; Ward, 2016; Zhang *et al*., 2017; Finkelman *et al*., 2018; Kolker *et al*., 2021). It is therefore likely that the sink samples of LD57 contain higher concentrations of trace elements and rare earths, especially since no/weak correlations were reported with the ash. Hence, further study into the mode of occurrence and association of the trace elements and rare earths in the corresponding sink fractions of the Makhado samples analysed in this study will be beneficial as it will allow a better understanding of the partitioning behaviour between coal products and discard fraction during coal beneficiation. Moreover, the economic potential of these discards for REE extraction is of interest.

Chapter 10: Conclusion and Recommendations

10.1. Summary

This study investigated the impact of beneficiation on metallurgical coals from the Makhado Project in the Soutpansberg Coalfield, South Africa. The first part of the study characterised the breakage and washability properties of the coal horizons with the primary objective of producing a 10% ash metallurgical coal product. The second part of the study characterised the petrographic and geochemical properties of the 10% ash metallurgical product i.e., the fine size float fraction (-1+0.25 mm). The coals were obtained from a large diameter drill core intercepting the No. 6 seam of the Madzaringwe Formation.

10.2. Conclusions

The aim and objectives of the study were met as follows:

Part 1 objectives: The influence of coal properties on the breakage and washability characteristics of metallurgical coal

- Characterisation of the physical properties of the coal horizons through strength and friability test indicate that predominantly coarse particles (45%) will be generated during transportation, handling and processing of the coals. The partings will generate higher proportions of coarse particles owing to their relatively high stone lithologies (Figure 4.3). It is estimated that up to 19% of ultrafine material will be generated. The highest amounts of fine and ultrafine particles will be produced from the seams, particularly the lowermost seams SBU, SBM and SBL. Hence, effective measures must be implemented by the mine for the handling of fine and ultrafine particles to avoid loss of product, clogging of equipment and to mitigate against dust.

- Characterisation of the washability properties by float-sink testing indicate that the desired metallurgical product (10% ash) can be achieved at a particle size of -1+0.25 mm, in the density interval of 1.55-1.70 g/cm^3. Maximum yields of 78% are achievable at these specifications, under simple to moderate separation conditions at ± 0.10 NGM, or simple separation conditions at ± 0.05 NGM. On average, the coal quality at this particle size and density is characterised by average moisture of 1.4%, ash content of 10.6%, volatile matter of 29.5%, CV of 31.6MJ/kg and total sulphur of 1.1%. These washability parameters are applicable to all the No. 6 seam horizons excluding the partings P1 and P3, which were found to have low yields.

Part 2 objectives: Assessment of the petrographic and geochemical properties of the fine size float fraction

- Characterisation of the -1+0.25 mm float fractions (metallurgical product) indicate these fine-float samples are highly vitrinitic (97 vol% mmf), hence dominated by the monomaceral vitrite (86%). The samples are classified as Medium Rank Bituminous C coals (0.88% RoV) and show average maximum reflectance readings of 0.92%R_{max}. Moreover, the petrographically observable mineral matter were found to be minimal in the samples, on average 3%. The minerals petrographically identified were limited to clay minerals, quartz, siderite, calcite and pyrite. These minerals occurred finely disseminated within the macerals and are of syngenetic origin, thus contributing to the relatively high NGM and therefore difficult separation conditions at smaller particle sizes.

- Coal quality based on the proximate analysis and total sulphur test indicate that the fine-float samples contain average fixed carbon content of 65% (daf), volatile matter of 33% (daf), ash of 4% (db), inherent moisture of 1% and total sulphur of 1.2 %. Correlation and regression analysis confirmed the dominance of organic sulphur in the fine-float samples, which shows pyritic sulphur forms were successfully reduced from the coals by means of gravity based separation.

- Coking coal properties were inferred from observations of the high vitrinite content, 0.92%R_{max}, and FSI of 9. However, reduction of the alkali content in sample SU and P1, as well as reduction of the phosphorus content in the lowermost seams is necessary in order to meet coking coal quality parameters as discussed in Chapter 9, Sections 9.4 and 9.9.

- The trace element and REE concentrations in the ashed fine-float samples were found to be highly enriched relative to the UCC and Clarke coal ash values, respectively. This includes hazardous trace elements such as V, Cr. Co, Ni, Cu, Zn and Pb. Moreover, trace elements and REE are more enriched in samples from the uppermost seams and P3. Preliminary analysis following Seredin and Dai. (2012) and Dai *et al*. (2017) shows that the fine-float ash samples (excluding SU and SMU) are a promising source for REE extraction. Correlation analysis suggests many of the trace elements and REE in the fine-float ash samples have mixed associations with both the macerals and minerals despite the samples being carbon rich and low in ash. However, selected trace elements (Li, Ti, Ni, Zn, Cr, Ga, Zr, Nb, Sb, V, Cu, Sn, Tl, U, all LREE, all MREE, Sc, Y, and Ho) distinctly show associations with kaolinite detected in the samples. Correlation analysis

indicates the total sulphur content has an affinity with vitrinite, hence the dominant sulphur form in the fine-float samples is organic (see section 7.3, Chapter 7, and section 9.9, Chapter 9). Consequently, selected trace elements and REE (Ce, Pr, Nd, Sm, Gd, Tm, Yb, Lu, Cr, Tb, Dy, V, Rb, Sb, Ba, W and U) showing positive correlations with the total sulphur have an organic sulphur affinity.

This study has assessed the properties of beneficiated metallurgical coals from the Makhado Project and their amenability to gravity-based beneficiation for the production of a primary 10% ash metallurgical coal product at -1+0.25 mm. These float products require further minor reductions of their sulphur, alkali and phosphorus contents, pending further processing by froth floatation. The -1+0.25 mm floats showed strongly caking properties which are attributed to their highly vitrinitic composition and very low ash content. A predominantly coarse particle size distribution (+63-31.5+20 mm) is expected during the initial handling of the coals, with caution advised for downstream beneficiation involving the handling of fine and ultrafine particles to avoid material loss.

The novel trace element and REE data assessed for the LD57 fine-float samples (on ash basis) indicated all but two samples to be promising REY sources due to their enriched REY concentrations. This major finding further highlights the value of the Soutpansberg Coalfield not only as South Africa's metallurgical coal reservoir, but also a potential unconventional REE source pending further research. While the enriched trace element and REY concentrations are promising at laboratory level, their mode of occurrence and associations have yet to be fully understood and will be a topic for ongoing research for the further advancement of knowledge on the Soutpansberg coals.

10.3. Recommendations

While this thesis has presented the findings on the petrographic and geochemical characteristics of the LD57 coals, the following recommendations are suggested for further insight as they were beyond the scope of this research:

- The partitioning behavior of coal constituents from the perspective of a parent coal compared to clean and sink/discard fractions.

- Detailed investigation into the coking properties of the Makhado samples entailing, advanced characterisation of the coking/plasticity properties by means of Gray-King

Index and Giseler plastometer test would further contribute to the knowledge pool of the Soutpansberg coals.

- Investigation into froth floatation for the final stage preparation of metallurgical products. This is especially critical for the reduction of the sulphur, alkali content and phosphorus, and hazardous trace elements.

- Assess the coals and ashes in terms of trace elements and REE, including advanced determination of the mode of occurrence and associations of REE and identification of REE host minerals by direct methods such as SEM-EDX, XAFS, FTIR etc.

- Economic feasibility study into the extraction of REE, especially in the sink fractions, which may host higher concentrations of critical elements. Additionally, the genetic origin of trace element and REE enrichment should be looked into using parent samples.

References

Akdogan, G., Bradshaw, S., Dorfling, C., Bergmann, C., Ghosh, T., Campbell, Q. (2019). Characterization of rare earth elements by XRT sorting products of a South African coal seam. International Journal of Coal Preparation and Utilization, 1-17.

Akinyemi, S.A., Gitari, W.M., Akinlua, A., Petrik, L.F. (2012). Mineralogy and geochemistry of sub-bituminous coal and its combustion products from Mpumalanga Province, South Africa, Chapter 2. In: Krull, I.S. (Ed.), Analytical Chemistry. InTechOpen.

Anderson, W. (2020). Anthracite Market Review-SAMANCOR. HISLOP Anderson Commodities (HAC) presentation, 41pp.

ArcelorMittal (2021). https://arcelormittalsa.com. [Accessed 10 August 2021].

AS 1038.21.1.1. Coal and coke - Analysis and testing Higher rank coal and coke - Relative density - Analysis sample/density bottle method.

AS 4156.1 1994. Coal preparation Part 1.1: Higher rank coal—Float and sink testing (Appendix E).

AS 4156.8 2007. Coal preparation - Sample pre-treatment - Drop-shatter. Australian Standard (AS).

ASTM D2639 / D2639M-21, Standard Test Method for Plastic Properties of Coal by the Constant-Torque Gieseler Plastometer, ASTM International, West Conshohocken, PA, 2021, www.astm.org.

ASTM D4239-14: 2015. Standard Test Method for Sulphur in the Analysis Sample of Coal and Coke Using High-Temperature Tube Furnace Combustion. American Society for Testing and Materials (ASTM).

Barker, O.B., (1999). A Techno-economic and historical review of the South African Coal Industry in the 19th and 20th centuries, in: Pinheiro, H.J. (Ed). A Techno-economic and historical review of the South African Coal Industry in the 19th and 20th centuries and analyses of coal product samples of South African collieries 1998-1999. Part 1. Bulletin 113 South African Bureau of Standards, pp. 1–63.

Bergh, J. P., Falcon, R. M. S., Falcon, L. M. (2013). Techno-economic impact of optimized low-grade thermal coal export production through beneficiation modelling. Journal of the Southern African Institute of Mining and Metallurgy, 113, 817-824.

Bertling, H. (1999). Coal and coke for blast furnaces. ISIJ international, 39, 617-624.

Benedict, L.G., and Thompson, R.R. (1980).Coke/carbon reactions in the study of factors affecting coke quality, International Journal of Coal Geology, 1, 19-34.

Bhattacharya, S., Maheshwari, A., Panda, M. (2016). Coal Cleaning Operations: The Question of Near Gravity Material. Transactions of the Indian Institute of Metals, 69, 157-172.

BHP (2021). Metallurgical coal Properties, facts, uses and production. https://www.bhp.com/our-businesses/our-commodities/metallurgical-coal , [Accessed 11 May 2021].

Bird, B. M. BHP (1931). Interpretation of float and sink data. Proceedings of the Third International Conference on Bituminous' Coal (Pittsburgh), November 16 to 21 1931, 721.

Bordy, E. M. (2018). Lithostratigraphy of the Tshidzi Formation (Dwyka Group, Karoo Supergroup), South Africa. South African Journal of Geology 2018, 121, 109-118.

Bordy, E. M., and Head, H. V. (2018). Lithostratigraphy of the Clarens Formation (Stormberg Group, Karoo Supergroup), South Africa. South African Journal of Geology 2018, 121, 119-130.

Brandl, G. (1981). The geology of the Messina area. Explanation, Sheet 2230, Messina, Geological Survey of South Africa, 35 pp.

Brandl, G., (2002). The geology of the Alldays area. Explanation sheet 2228, Alldays, Geological Survey South Africa, 71 pp.

Bunt, J. R. (1997). Development of a fine coal beneficiation circuit for the Twistdraai Colliery. Doctoral dissertation (unpubl). University of Cape Town, Cape Town, 283pp.

Bytnar, K., and Burmistrz, P. (2013). Alkalis in coal and coal cleaning products. Archives of Mining Sciences, 58, 913-924.

Cadle, A.B., Cairncross, B., Christie, A.D.M., Roberts, D.L. (1993). The Karoo Basin of South Africa: type basin for coal-bearing deposits of southern Africa. International Journal of Coal Geology. 23, 117–157.

Cairncross, B. (2001). An overview of the Permian (Karoo) coal deposits of southern Africa. Journal of African Earth Sciences, 33, 529-562.

Catuneanu, O., Wopfner, H., Eriksson, P. G., Cairncross, B., Rubidge, B. S., Smith, R. M. H., Hancox, P. J. (2005). The Karoo basins of south-central Africa. Journal of African Earth Sciences, 43, 211-253.

Chakravarty, K., Mishra, V., Chakravarty, S., Chakladar, S., Saxena, V. K., Bhattacharya, S. (2020). Mineralogical study of beneficiated and carbonized indian coking coal for better utilization: A case study. Natural Resources Research, 29, 2431-2450.

Cindi, B. (2014), Detailed petrographic and palynological study of the Soutpansberg Coal, Unpublished Honours Research Report, University of the Witwatersrand, Johannesburg, 88pp.

CoAL (2016). Unlocking the Musina-Makhado Special Economic Zone through the Makhado Hard Coking Coal Project. Coal of Africa Limited (MC Mining). https://www.mcmining.co.za/downloads/send/31-2016/238-unlocking-musina-15-november-2016. [Accessed 14 October 2018].

Coe, G.D. (1938). An explanation of washability curves for the interpretation of float-sink data on coal. Department of the interior Bureau of mines, 10 pp.

Cooke, A.B. (1994). Coal and progress: The South African Story. The Journal of the South African Institute of Mining and Metallurgy,94, 329-336.

da Silva, G. L. R., Moura, L. C. A., de Oliveira, I. P. V., Carlos, A., Quintas, B., Dornelas, P. H. G., Assis, P. S. (2017). Use of free swelling index for determining rate of desulphurization of coking process. In: AISTech Proceedings, 2016.

Dai, S., and Finkelman, R. B. (2018). Coal as a promising source of critical elements: Progress and future prospects. International Journal of Coal Geology, 186, 155-164

Dai, S., Hower, J. C., Finkelman, R. B., Graham, I. T., French, D., Ward, C. R., Eskenazy, G. Wei, Q., Zhao, L. (2020). Organic associations of non-mineral elements in coal: A review. International Journal of Coal Geology, 218, 103347.

Dai, S., Graham, I. T., Ward, C. R. (2016). A review of anomalous rare earth elements and yttrium in coal. International journal of coal geology, 159, 82-95.

Dai, S., Xie, P., Jia, S., Ward, C.R., Hower, J.C, Yan, X., French, D. (2017). Enrichment of URe-V-Cr-Se and rare earth elements in the Late Permian coals of the Moxinpo Coalfield, Chongqing, China: Genetic implications from geochemical and mineralogical data. Ore Geology Reviews, 80, 1-17.

Dai, S., Finkelman, R. B., French, D., Hower, J. C., Graham, I. T., Zhao, F. (2021). Modes of occurrence of elements in coal: A critical evaluation. Earth-Science Reviews, 103815.

Das, T. K. (2001). Thermogravimetric characterisation of maceral concentrates of Russian coking coals. Fuel, 80, 97-106.

Davidson, R.M. (1998). Coal Cleaning to Remove Trace Elements – A Review. Coal Preparation, 19, 159-176.

Davis, A. (1978). The measurement of reflectance of coal macerals: its automation and significance. Technical Report 10, U.S. Department of Energy, 98pp.

De Jager, F.S.J. (1986). Coal occurrences of the central, north-western, northern and eastern Transvaal. In: Anhaeusser, C.R., Maske, S. (Eds.), Mineral Deposits of Southern Africa. Geological Society of South Africa, pp. 2047–2055.

de Klerk, E., and Sparrow, J. (2015). Independent Competent Persons Report on Coal of Africa Limited's Greater Soutpansberg Projects Prepared for Coal of Africa Limited and Peel Hunt LL. Unpublished Report by Venmyn Deloitte for Coal of Africa Limited, 290 pp.

de Korte, G. J. (2001). Beneficiation of Fine Coal: Froth Flotation Efficiency. CoalTech Project 4.11.1, 25pp.

de Korte, G. J. (2008). The influence of near-dense material on the separation efficiency of dense-medium processes. International Journal of Coal Preparation and Utilization, 28, 69-93.

de Korte, G. J. (2010). Coal preparation research in South Africa. Journal of the Southern African Institute of Mining and Metallurgy, 110, 361-364.

de Korte, G. J. (2013). Dry processing versus dense medium processing for preparing thermal coal. CSIR - Council for Scientific and Industrial Research.

de Korte, G. J. (2014). Dry Processing of Coal–Status Update. Report CSIR/NRE/MMR/ER/2014/0040/B, COALTECH, 18pp.

de Korte, G. J. (2015). Processing low-grade coal to produce high-grade products. Journal of the Southern African Institute of Mining and Metallurgy, 115, 569-572.

de Korte, G. J. (2016). Low relative density processing of fine coal. In XVIII International Coal Preparation Congress, Springer, Cham. pp. 555-560. Litvinenko, V. (Ed.). (2016). XVIII International Coal Preparation Congress: 28 June—01 July 2016 Saint-Petersburg, Russia. Springer.

de Souza, K. F., Sampaio, C. H., Kussler, J. T. (2012). Washability curves for the lower coal seams in Candiota Mine-Brazil. Fuel processing technology, 96, 140-149.

Diessel, C.F.K. (1992). Coal-Bearing Depositional Systems. Springer-Verlag, Berlin, 721pp.

Diez, M. A., Alvarez, R., Barriocanal, C. (2002). Coal for metallurgical coke production: predictions of coke quality and future requirements for coke making. International Journal of Coal Geology, 50, 389-412.

Dikgwatlhe, P. (2018). Coal as a strategic resource in South Africa. Society of Mining Professors 6th Regional Conference 2018, Birchwood Hotel and Conference Centre, Johannesburg, South Africa, 12-13 March 2018, 8pp.

DOE (2001). National Inventory Discard and Duff Coal – 2001.Department of Energy (DOE), Republic of South Africa, Pretoria, 31pp.

DOE (2019). The South African Energy Sector Report. Department of Energy (DOE), Republic of South Africa, Pretoria, 38pp.

Duan, P., Wang, W., Liu, X., Sang, S., Ma, M., Zhang, W. (2019). Differentiation of rare earth elements and yttrium in different size and density fractions of the Reshuihe coal, Yunnan Province, China. International Journal of Coal Geology, 207, 1-11.

Duda, A., and Fidalgo Valverde, G. (2021). The Economics of Coking Coal Mining: A Fossil Fuel Still Needed for Steel Production. Energies, 14, 7682.

Duncan, R. A., Hooper, P. R., Rehacek, J., Marsh, J. S., Duncan, A. R. (1997). The timing and duration of the Karoo igneous event, southern Gondwana. Journal of Geophysical Research, 102, 18127-18138.

Eberhard, A. (2011). The future of South African coal: Market, investment and policy challenges. Program on energy and sustainable development, 44pp.

ECE-UN (Economic Commission for Europe – United Nations) (1998). International classification of in-seam coals. (Energy/1998/19). In: Geneva.

Ekmann, J. M., and Le, P. H. (2004). Coal storage and transportation. Encyclopaedia of Energy. Elsevier, New York, 551-580.

England, T., Hand, P.E., Michael, D.C., Falcon, L.M., Yell, A.D. (2002). Coal Preparation in South Africa, South African Coal Processing Society, 120–121pp.

Enslin, F. H., and Bekker, E. (2019). Taking care of your plant's cyclones in order to take care of your plant. In Southern African Coal Society's 2019 Biennial Conference: Coal processing–extracting value from low grade reserves, Secunda, South Africa (Vol. 19).

Esterle, J. S. (2008). Mining and Beneficiation. In: Suárez-Ruiz, I., and Crelling, J. C. (Eds.). Applied coal petrology: the role of petrology in coal utilization. Academic Press, 61-83.

Esterle, J. S., Kolatschek, Y., O'Brien, G. (2002). Relationship between *in situ* coal stratigraphy and particle size and composition after breakage in bituminous coals. International Journal of Coal Geology, 49, 195-214.

Eterigho-Ikelegbe, O., Harrar, H., Bada, S. (2021). Rare earth elements from coal and coal discard–A review. Minerals Engineering, 173, 107187.

European Commission (2020). Study on the EU's list of Critical Raw Materials-Final Report 2020. http://www.europa.eu. [Accessed 11 May 2021].

Exxaro (2019). From ex-mining community to eco-village, transforming Tshikondeni. https://www.exxaro.com/media-centre/2019/from-ex-mining-community-to-eco-village-transforming-tshikondeni. [Accessed 11 January 2022].

Eze, C.P., Fatoba, O., Madzivire, G., Ostrovnaya, T.M., Petrik, L.F., Frontasyeva, M.V., Nechaev, A.N. (2013). Elemental composition of fly ash: a comparative study using nuclear and related analytical techniques. Chem. Didact. Ecol. Metrol. 18, 19–29.

Falcon, L.M, and Falcon, R. (1987). The petrographic composition of Southern African coals in relation to friability, hardness, and abrasive indices. Journal of the Southern African Institute of Mining and Metallurgy, 87, 323-336.

Falcon, R.M.S, and Ham, A. J. (1988). The characteristics of Southern African coals. Journal of the South African Institute of Mining and Metallurgy, 88, 145-161.

Falcon, R.M.S. and Snyman, C.P. (1986). An Introduction to Coal Petrography: Atlas of Petrographic Constituents in the Bituminous Coals of Southern Africa. Geological Society of Southern Africa, Johannesburg. 27pp.

Falcon. R. (2013). Coal petrography. In The coal handbook: towards cleaner production (pp. 53-79). Woodhead Publishing. Osborne. D. (Ed.). (2013). The Coal Handbook: Towards Cleaner Production: Volume 2: Coal Utilisation. Elsevier.

Franus, W., Wiatros-Motyka, M. M., Wdowin, M. (2015). Coal fly ash as a resource for rare earth elements. Environmental Science and Pollution Research, 22, 9464-9474.

Finkelman, R. B. (1999). Trace elements in coal. Biological trace element research, 67, 197-204.

Finkelman, R. B., Dai, S., French, D. (2019). The importance of minerals in coal as the hosts of chemical elements: A review. International Journal of Coal Geology, 212, 103251.

Finkelman, R.B., Palmer, C.A., Wang, P.P. (2018). Quantification of the modes of occurrence of 42 elements in coal. International Journal of Coal Geology. 185, 138–160.

Franzidis, J. P. (1992). Developments in fine coal beneficiation in South Africa. Coal Preparation, 11, 103-114.

Fu, B., Hower, J. C., Zhang, W., Luo, G., Hu, H., Yao, H. (2022). A review of rare earth elements and yttrium in coal ash: Content, modes of occurrences, combustion behaviour, and extraction methods. Progress in Energy and Combustion Science, 88, 100954.

Galileoresources (2021). Glenover Rare Earth Project - Limpopo Province, South Africa. https://galileoresources.com/glenover-rare-earth-project/ [Accessed 3 December 2021]

Ghosh, B., Sahoo, B. K., Jha, P. K., Manjhi, K. K., Sahu, J. N., Varma, A. K. (2020). Effect of Microlithotype Maceral Distribution on Coke Quality. Coke and Chemistry, 63, 294-302.

Gluskoter, H. J. (1975). Mineral matter and trace elements in coal. ACS Symposium Series, Vol. 141, Trace Elements in Fuel; Babu, S, Ed.; American Chemical Society: Washington, DC, 1975; Chapter 1, pp 1-22.

GOVZA, (2017). National Infrastructure Plan. Government of South Africa, http://www.gov.za/issues/national-infrastructure-plan. [Accessed 6 September 2018].

Granda, M., Blanco, C., Alvarez, P., Patrick, J. W., Menendez, R. (2014). Chemicals from coal coking. Chemical Reviews, 114, 1608-1636.

Grigore, M., Sakurovs, R., French, D., Sahajwalla, V. (2008). Mineral matter in coals and their reactions during coking. International Journal of Coal Geology, 76, 301-308.

Guerrero, A., Diez, M. A., Borrego, A. G. (2013). Effect of volatile matter release on optical properties of macerals from different rank coals. Fuel, 114, 21-30.

Hancox, P. J., and Götz, A. E. (2014). South Africa's coalfields-A 2014 perspective. International Journal of Coal Geology, 132, 170-254.

Hand, P. E. (2014). Sampling the coal chain. Journal of the Southern African Institute of Mining and Metallurgy, 114, 39-46.

Harmer, R. E., and Nex, P. A. M. (2016). Rare earth deposits of Africa. Episodes, 39, 381-406.

Harrar, H., Eterigho-Ikelegbe, O., Modiga, A., Bada, S. (2022). Mineralogy and distribution of rare earth elements in the Waterberg coalfield high ash coals. Minerals Engineering, 183, 107611.

Holuszko, M. E., and Grieve, D. A. (1990). Washability characteristics of British Columbia coals. Province of British Columbia, Ministry of Energy, Mines and Petroleum Resources. Geological Fieldwork, 1990, 371-379.

Hower, J. C. (2008). Maceral/microlithotype partitioning with particle size of pulverized coal: Examples from power plants burning Central Appalachian and Illinois basin coals. International Journal of Coal Geology, 73, 213-218.

Huggins, F.E., Seidu, L.B.A., Shah, N., Huffman, G.P., Honaker, R.Q., Kyger, J.R., Higgins, B.L., Robertson, J.D., Pal, S., Seehra, M.S., (2009). Elemental modes of occurrence in an Illinois #6 coal and fractions prepared by physical separation techniques at a coal preparation plant. International Journal of Coal Geology, 78, 65-76.

ICCP (2001). The new inertinite classification (ICCP System 1994). International Committee for Coal and Organic Petrology (ICCP). Fuel, 80, 459-471.

ICCP (1998). The new vitrinite classification (ICCP system 1994). International Committee for Coal and Organic Petrology (ICCP). Fuel 77, 349–358.

IEA (2017). Coal 2017-Analysis and forecast to 2022, IEA, Paris. https://www.iea.org/reports/coal-2017. [Accessed 13 August 2022].

IEA (2019). Coal 2019, IEA, Paris. https://www.iea.org/reports/coal-2019. [Accessed 13 June 2021].

IEA (2020). Coal 2020-Analysis and forecast to 2025. IEA, Paris. https://www.iea.org/reports/coal-2020. [Accessed 13 June 2021].

IEA (2021), Coal 2021- Analysis and forecast to 2024. IEA, Paris. https://www.iea.org/reports/coal-2021. [Accessed 25 February 2022].

IEA (2022), Coal 2022- Analysis and forecast to 2025. IEA, Paris. https://www.iea.org/reports/coal-2022. [Accessed 11 March 2023].

ISO 335:1974. Hard coal — Determination of caking power — Roga test. . International Organization for Standardization (ISO), Geneva, Switzerland.

ISO 7936:1992. Hard coal — Determination and presentation of float and sink characteristics — General directions for apparatus and procedures. International Organization for Standardization (ISO), Geneva, Switzerland.

ISO 1171: 2003. Determination of Ash. International Organization for Standardization (ISO), Geneva, Switzerland.

ISO 501: 2012. Hard Coal-Determination of the crucible swelling number. International Organization for Standardization (ISO), Geneva, Switzerland.

ISO 502:2015 Coal — Determination of caking power — Gray-King coke test. International Organization for Standardization (ISO), Geneva, Switzerland.

ISO 562: 2010. Hard coal and coke-Determination of volatile matter. International Organization for Standardization (ISO), Geneva, Switzerland.

ISO 1928:2020. Coal and coke — Determination of gross calorific value. International Organization for Standardization (ISO), Geneva, Switzerland.

Jeffrey, L.S. (2005a). Characterization of the coal resources of South Africa. Journal of the Southern African Institute of Mining and Metallurgy, 105, 95-102.

Jeffrey, L.S. (2005b). Challenges associated with further development of the Waterberg Coalfield. Journal of the Southern African Institute of Mining and Metallurgy, 105, 453-457.

Jellico, B. (2019). The relevance of rare earths to South Africa. NSTF presentation. 51pp.

Johnson, M.R., Van Vuuren, C.J., Visser, J.N.J., Cole, D.I., Wickens, H., de, V., Christie, A.D.M., Roberts, D.L., Brandl, G. (2006). Sedimentary rocks of the Karoo Supergroup. In: Johnson, M.R., Anhaeusser, C.R., Thomas, R.J. (Eds.), The Geology of South Africa, Geological Society of South Africa, Johannesburg/Council for Geoscience, Pretoria, pp. 461–499.

Jordan, P. (2008). Characterising coals for coke production and assessing coke: predicting coke quality based on coal petrography, rheology and coke petrography. Unpublished MSc Thesis. University of Witwatersrand. 121pp.

Kataka, M. O., Matiane, A. R., Odhiambo, B. D. O. (2018). Chemical and mineralogical characterization of highly and less reactive coal from Northern Natal and Venda-Pafuri coalfields in South Africa. Journal of African Earth Sciences, 137, 278-285.

Kernot, C. (2000). The coal industry. Elsevier, England. 354pp.

Kershaw, J. R., and Taylor, G. H. (1992). Properties of Gondwana coals with emphasis on the Permian coals of Australia and South Africa. Fuel Processing Technology, 31, 127-168.

Ketris, M., and Yudovich, Y. (2009). Estimations of Clarkes for Carbonaceous Biolithes: world averages for trace element contents in black shales and coals. International Journal of Coal Geology, 78, 135-148.

King, R.P., and Birtek, N. (1990). The washability of fine South African coals. Journal of the Southern African Institute of Mining and Metallurgy, 90, 289-301.

Kolker, A., Scott, C., Lefticariu, L., Mastalerz, M., Drobniak, A., Scott, A. (2021). Trace element partitioning during coal preparation: Insights from US Illinois Basin coals. International Journal of Coal Geology, 243, 103781.

Kolker, A., Senior, C., van Alphen, C., Koenig, A., Geboy, N. (2017). Mercury and trace element distribution in density separates of a South African Highveld (# 4) coal: Implications for mercury reduction and preparation of export coal. International Journal of Coal Geology, 170, 7-13.

Kruger, H. (2013). Coking Coal. ArcelorMittal presentation for Fossil Fuel Foundation Coal Coke and Carbon in the Metallurgical Industry, 32 pp.

Kruszewska, K. J. (1998). The reactivity of pseudovitrinite in some coals. Fuel, 77, 1655-1661.

Kumar, D., and Kumar, D. (2018). Sustainable management of coal preparation. Woodhead Publishing, New York, USA, 421pp.

Kumar, P. P., Barman, S. C., Singh, S., Ranjan, M. (2008). Influence of coal fluidity on coal blend and coke quality. Ironmaking & Steelmaking, 35, 416-420.

Kundu, T., Das, S. K., Biswal, D. K., Angadi, S. I. (2021). Mineral Beneficiation and Processing of Coal. In Clean Coal Technologies, Springer, Cham, 1-38.

Kus, J., and Misz-Kennan, M., ICCP (2017). Coal weathering and laboratory (artificial) coal oxidation. International Journal of Coal Geology, 171, 12-36.

Kyung Eun, J (2012). The effect of coal properties on carbonization behaviour and strength of coke blends. Unpublished PhD Thesis, The University of New South Wales, 152pp.

Laskowski, J. (2001). Coal flotation and fine coal utilization. Elsevier, Amsterdam, 371 pp.

Lett, R.G. and Ruppel, T.C. (2004). Coal, Chemical and Physical Properties. In Encyclopaedia of Energy. Eds C.J., Cleveland Elsevier, New York, 411-423. 5376pp.

Li, K., Khanna, R., Zhang, J., Liu, Z., Sahajwalla, V., Yang, T., Kong, D. (2014). The evolution of structural order, microstructure and mineral matter of metallurgical coke in a blast furnace: A review. Fuel, 133, 194-215.

Lin, C. L., Miller, J. D., Nguyen, T., Nguyen, A. (2019). Characterization of breakage and washability of ROM coal using X-ray computed tomography. International Journal of Coal Preparation and Utilization, 39, 145-158.

Lloyd, P. J. (2000). The potential of coal wastes in South Africa. Journal of the Southern African Institute of Mining and Metallurgy, 100, 69-72.

Lu, L., Devasahayam, S., Sahajwalla, V. (2013). Evaluation of coal for metallurgical applications. The coal handbook: towards cleaner production, 352-386.

Luyt, J. P. (2017). The tectono-sedimentary history of the coal-bearing Tshipise Karoo basin. Unpublished MSc dissertation, University of Pretoria. 190pp.

Mackinnon, W. L. A. and Swanson, A. R. (2010). Strategies for Washing Australian Coals, International Journal of Coal Preparation and Utilization, 30, 69-82.

Magwai, M. K., and Claassen, J. O. (2013). Near-Gravity material experience at Leeuwpan coal mine. In SACPS Bi-annual Conference, Secunda. Exxaro Resources, 18pp.

Malaza, N. (2013). Basin Analysis of the Soutpansberg and Tuli Coalfields, Limpopo Province of South Africa. Unpublished PhD Thesis, University of Fort Hare. 270 pp.

Malaza, N., Liu, K., Zhao, B. (2013). Facies analysis and depositional environments of the Late Palaeozoic coal-bearing Madzaringwe Formation in the Tshipise-Pafuri Basin, South Africa. ISRN Geology, 2013.

Maroto-Valer, M. M., Taulbee, D. N., Andrésen, J. M., Hower, J. C., Snape, C. E. (1998). The role of semifusinite in plasticity development for a coking coal. Energy and fuels, 12, 1040-1046.

Matjie, R. H., Li, Z., Ward, C. R., Bunt, J. R., Strydom, C. A. (2016). Determination of mineral matter and elemental composition of individual macerals in coals from Highveld mines. Journal of the Southern African Institute of Mining and Metallurgy, 116, 169-180.

Matyjaszek, M., Wodarski, K., Krzemień, A., García-Miranda, C. E., Sánchez, A. S. (2018). Coking coal mining investment: Boosting European Union's raw materials initiative. Resources Policy, 57, 88-97.

Mawila, E. E. T. (2019). Variation of the coal stratigraphy and characterization of the Soutpansberg Coalfield, Limpopo Province, South Africa. Unpublished MSc Thesis, University of Venda, 145 pp.

Mazumder, B. (2012). Coal Science and Engineering, WPI Publishing, New York, 450pp.

Mazurek, I., Skawińska, A., and Sajdak, M. (2021). Analysis of chlorine forms in hard coal and the impact of leaching conditions on chlorine removal. Journal of the Energy Institute, 94, 337-351.

MC Mining (2018). Makhado Project. http://www.mcmining.co.za/ourbusiness/projects/makhado. [Accessed 28 September 2018].

MC Mining (2019). Announcement: Additional Makhado Project Phase 1 Information, 8pp.

MC Mining, (2021). https://www.mcmining.co.za. [Accessed 18 January 2021]

McCourt, S., and Brandl, G. (1980). A lithostratigraphic subdivision of the Karoo Sequence in the north-eastern Transvaal. Annals Geological Survey of South Africa, 14, 51-56.

Mdungazi, N. (2019). Musina-Makhado special economic zone development ledet REF: 12/1/9/2-V79 Final scoping report, Delta Built Environment Consultants (Pty) Ltd, 246 pp.

Mikhail, M. W., and Patching, T. H. (1981). Methods for predicting size degradation of Western Canadian coals. Fuel, 60, 1073-1078.

Minerals Council South Africa (2018). National Coal Strategy for South Africa report, 30pp.

Minerals Council, (2021). https://www.mineralscouncil.org.za/sa-mining/coal [Accessed 13 April 2021].

Mir, F. (2014). Washability characteristics of low volatile Pakistani coking coal by crushing. Journal of Minerals and Materials Characterization and Engineering, 2, 502-506.

Mochizuki, Y., Ono, Y., Uebo, K., Tsubouchi, N. (2013). The fate of sulfur in coal during carbonization and its effect on coal fluidity. International Journal of Coal Geology, 120, 50-56.

Mostert, P. (2016). Independent Competent Person's Report on the Makhado Coal Project of Coal of Africa Limited. Report prepared by The MSA Group (Pty) Ltd on behalf of: Coal of Africa Limited and their nominated advisor Peel Hunt LLP, 120pp.

Mphaphuli. M. (2017). Petrographic consideration of the impact of the Tshipise Fault on coal quality in the Soutpansberg Coalfield. South Africa. Unpublished MSc Thesis. University of Johannesburg. 160pp.

Mukatuni, S. (2019). Geology and characterization of coal at the Mushithe Coal Occurrence, Soutpansberg Coalfield, Limpopo Province, South Africa. Unpublished MSc Thesis, University of Venda, 154 pp.

Nasir, S., Kucerik, J., Mahmood, Z. (2012). A study on the washability of the Azad Kashmir (Pakistan) coalfield. Fuel processing technology, 99, 75-81.

Noble, A., Luttrell, G.H. (2015) A review of state-of-the-art processing operations in coal preparation. International Journal of Mining Science and Technology. 25, 511–521.

Nomura, S. (2010). Behaviour of coal chlorine in coke making process. International Journal of coal geology, 83, 423-429.

Norrish, K. and Hutton, J. T. (1969). An accurate X-ray spectrographic method for the analysis of geologic samples. Geochemica et Cosmochimica Acta 33, 431-454.

O'Keefe, J. M., Bechtel, A., Christanis, K., Dai, S., DiMichele, W. A., Eble, C. F., Esterle, J.S., Mastalerz, M., Raymond, A.L., Valentim, B.V., Wagner, N.J., Ward C.R., Hower, J.C. (2013). On the fundamental difference between coal rank and coal type. International Journal of Coal Geology, 118, 58-87.

Ozbayoglu, G. (2018). Energy production from coal. Comprehensive Energy Systems3, 788-821.

Ozga-Blashke, U. (2020). Coking coal in the European green deal strategy. Inżynieria Mineralna 2, pp. 87–93.

Park, H., Wang, L., Yun, J. H. (2021). Coal beneficiation technology to reduce hazardous heavy metals in fly ash. Journal of Hazardous Materials, 416, 125853.

Peatfield, D. (2003). Coal and coal preparation in South Africa-A 2002 review. Journal of the Southern African Institute of Mining and Metallurgy, 103, 355-372.

Pickel, W., Kus, J., Flores, D., Kalaitzidis, S., Christanis, K., Cardott, B. J., M. Misz-Kennan, S. Rodrigues, A. Henschel, M. Hamor-Vido, Crosdale, P. Wagner, N.J., ICCP. (2017). Classification of liptinite–ICCP System 1994. International Journal of Coal Geology, 169, 40-61.

Powell, D. M. (2016). A techno-economic evaluation of the production of hard coking coal from Tshikondeni coal discards. Unpublished MSc dissertation, North-West University (South Africa), 409 pp.

Pretorius, G. J. (2010). Coal beneficiation by means of conventional flotation treating the size range of+ 0.5 mm-1.4 mm. Unpublished MSc dissertation, University of the Witwatersrand, 135pp.

Prévost, X. (2013). Review of the South African coal mining industry. Unpublished Report, 12pp.

Prévost, X. (2017). Coal's powerful role. Inside Mining, 10, 12-13.

PWC (2017). SA Mine -Highlighting trends in the South African mining industry, 9th edition, 45pp.

Qin, S., Lu, Q., Li, Y., Wang, J., Zhao, Q., Gao, K. (2018). Relationships between trace elements and organic matter in coals. Journal of Geochemical Exploration, 188, 101-110.

Raaness, O., and Gray, R. (1995). Coal in the production of silicon rich alloys. Infacon, 7, 201-219.

Ramudzwagi, M., Tshiongo-Makgwe, N., Nheta, W. (2020). Recent developments in beneficiation of fine and ultra-fine coal-review paper. Journal of Cleaner Production, 276, 122693.

Rautenbach, R., Strydom, C. A., Bunt, J. R., Matjie, R. H., Campbell, Q. P., Van Alphen, C. (2019). Mineralogical, chemical, and petrographic properties of selected South African power stations' feed coals and their corresponding density separated fractions using float-sink and reflux classification methods. International Journal of Coal Preparation and Utilization, 39, 421-446.

Ribeiro, J., da Silva, E. F., Flores, D. (2010). Burning of coal waste piles from Douro Coalfield (Portugal): petrological, geochemical and mineralogical characterization. International Journal of Coal Geology, 81, 359-372.

Roux, L. (2011). Optimal yield and cut density prediction of semi soft coking coal and power station coal in the Waterberg Coalfield, Limpopo Province, Unpublished MSc dissertation, University of the Witwatersrand, 228 pp.

SACAA (2021). Ash Benefits & Uses. South African Coal Ash Association. https://www.sacaa.co.za/about-us/ash-benefits-uses. [Accessed 3 December 2021].

Sahajwalla, V., Hilding, T., Oelreich, A. V., Gupta, S. K., Björkman, B., Wikström, J. O., Fredriksson, P Seetharaman, S. (2004). Structure and alkali content of coke in an experimental blast furnace and their gasification reaction. In AISTech 2004: 15/09/2004-17/09/2004. 491-500, Iron and Steel Society.

Sahoo, R., and Roach, D. (2005). Quantification of the lump coal breakage during handling operation at the Gladstone port. Chemical Engineering and Processing: Process Intensification, 44, 797-804.

SAISI (2013). South African Iron and Steel Institute (SAISI), https://saisi.co.za/index.php/our-members/arcelormittal-south-africa. [Accessed 10 August 2021].

SAISI (2022). South African Iron and Steel Institute (SAISI), https://www.saisi.org/steel-statistics/overview-of-the-primary-steel-industry-in-south-africa/. [Accessed 10 August 2022].

Sana, H., Kanwal, S., Akhtar, J., Sheikh, N., Munir, S. (2017). Evaluation of the washability characteristics of Khushab coal (Pakistani) by heavy media separation process. Energy and Environment, 28, 598-607.

SANS 5925: 2007. Moisture Content of coal samples intended for general analysis (Air-Oven Method): second edition; South African National Standard (SANS).

SANS 7404-2: 2015. Methods for the petrographic analysis of coals Part 2: Methods of preparing coal samples. South African National Standard, Pretoria (2015).

SANS 7404-3: 2016. Methods for the petrographic analysis of coals Part 3: Method of determining maceral group composition. South African National Standard, Pretoria (2016).

SANS 7404-4: 2020. Methods for the petrographic analysis of coals Part 4: Method of determining microlithotype, carbominerite and minerite composition. South African National Standard, Pretoria (2020).

SANS 7404-5: 2016. Methods for the petrographic analysis of coals Part 5: Method of determining microscopically the reflectance of vitrinite. South African National Standard, Pretoria (2016).

Saurabh S., Arnold B., Carter D. (2017). Future Coal Processing Strategies for India, Conference Proceedings of Coal Washing 2017, Coal Preparation Society of India (CPSI) Journal, 9, 28-33.

Schernikau, L. (2017). Economics of the international coal trade: why coal continues to power the World. Second edition, Springer, Berlin, 463 pp.

Schobert, H. H., and Song, C. (2002). Chemicals and materials from coal in the 21st century. Fuel, 81, 15-32.

Schweinfurth, S. P. (2009). An introduction to coal quality. The National Coal Resource Assessment Overview: US Geological Survey Professional Paper, 20pp.

Sebola, M. J. T. (2015). The effects of weathering on coal quality in the Limpopo and Soutpansberg Coalfields. Unpublished Honours dissertation, University of the Witwatersrand, 61 pp.

Sebola, M. J. T. (2018). Weathering of coals from the Waterberg and Limpopo Coalfields, South Africa. Unpublished MSc dissertation, University of the Witwatersrand, 178pp.

Seredin, V. V., and Dai, S. (2012). Coal deposits as potential alternative sources for lanthanides and yttrium. International Journal of Coal Geology, 94, 67-93.

Seredin, V.V. (2010). A new method for primary evaluation of the outlook for rare earth element ores. Geol. Ore Deposits 52, 428–433.

Shi, F., Liu, H., Rodrigues, S., Esterle, J., Nguyen, A. K., Manlapig, E. (2018). Lithotype-based modelling and simulations of coal degradation conditioned by both high and low energy breakage. Fuel, 232, 405-414.

Singh, S. (1987). Coal beneficiation. Energy, 12, 805-812.

Snyman, C.P. (1989). The role of coal petrography in understanding the properties of South African coal. International Journal of Coal Geology. 14, 83–101.

Snyman, C. P., and Barclay, J. (1989). The coalification of South African coal. International Journal of Coal Geology, 13, 375-390.

Snyman, C.P. (1998). Coal. In: Wilson, M.G.C., Anhaeusser, C.R. (Eds.), The Mineral Resources of South Africa. Handbook, 16. Council for Geoscience, South Africa, pp. 136–205. South African Committee.

Snyman, C.P., Van Vuuren, M.C.J., and Barnard, J.M. (1983). Chemical and physical characteristics of South African coal and a suggested classification system. National Institute for Coal Research, Coal 8306,1–63.

Sparrow, J. (2012). The Soutpansberg Coalfield “The Forgotten Basin”. Presentation at the Inaugural FFF Limpopo Conference, October 2012, 45pp.

Speight, J. G. (2005). Handbook of coal analysis. John Wiley and Sons, New Jersey, 212pp.

Steenkampskraal (2021). Steenkampskraal Monazite Mine https://www.steenkampskraal.com [Accessed 3 December 2021]

Suárez-Ruiz, I., and Crelling, J. C. (2008). Applied coal petrology: the role of petrology in coal utilization. Academic press, 301pp.

Subba-Rao, D. V., and Gouricharan, T. (2016). Constituents of coal. Coal Processing and Utilization, CRS Press, 536.

Sullivan, J.H. (1995). The Geology of the Coal-bearing Rocks of the Karoo Sequence in the Tshikondeni Mine Area, Northern Transvaal. Unpublished MSc Thesis, University of Pretoria.

Swaine, D. J. (2000). Why trace elements are important. Fuel Processing Technology, 65, 21-33.

Swanson, A. (2001). Australian coal preparation-a 2000 review. Journal of the Southern African Institute of Mining and Metallurgy, 101, 107-113.

Swanson, A., Fletcher, I., and Partridge, A. (1993). Improved prediction of size distributions and their effects in materials handling and coal preparation systems. Final Report for NERDDC, Project 1290.

Tankard, A., Welsink, H., Aukes, P., Newton, R., Stettler, E. (2009). Tectonic evolution of the Cape and Karoo basins of South Africa. Marine and Petroleum Geology, 26, 1379-1412.

Taylor, S.R., and McLennan, S.M. (1985). The continental crust: its composition and evolution. Blackwell, Oxford. pp 312.

Teichmüller, M. (1989). The genesis of coal from the viewpoint of coal petrology. International Journal of Coal Geology, 12, 1-87.

Teo, C. S., Waters, A. G., Nicol, S. K. (1990). Quantification of the breakage of lump materials during handling operations. International Journal of Mineral Processing, 30, 159-184.

Thabo, F. E., and Sullivan, J. H. (2000). The geotechnical aspects of Tshikondeni coal mine. Journal of African Earth Sciences, 31, 78-78.

Thomas, L. (2012). Coal Geology- second edition John. Wiley and Sons Ltd, 444pp.

Trollip, H., McCall, B., Bataille, C. (2022). How green primary iron production in South Africa could help global decarbonization. Climate Policy, 22, 236-247.

Tsubouchi, N., Mochizuki, Y., Wang, Y., Ohtsuka, Y. (2018). Fate of the chlorine in coal in the heating process. ISIJ International, 58, 227-235.

Vale (2021). Coal.http://www.vale.com/brasil/PT/business/mining/coal/Paginas/default.aspx. [Accessed 7 May 2021].

Van Gosen, B.S., Verplanck, P.L., Long, K.R., Gambogi, J., Seal II, R.R. (2014). The Rare-Earth Elements-Vital to modern technologies and lifestyles. USGS Mineral Resources Program, Fact Sheet 2014-3078.

Van Alphen, C. (2005). Factors influencing fly ash formation and slag deposit formation (slagging) on combusting a South African pulverised fuel in a 200 MWe boiler. Unpublished Doctoral dissertation, University of the Witwatersrand, 354pp.

Van der Berg, H.J. (1980). Die sedimentologie van die Soutpansberg-steenkoolveld met spesiale verwysing na steenkoolvorming. Unpublished MSc Thesis, University of Orange Free State, Bloemfontein, 127 pp.

Vassilev, S. V., and Vassileva, C. G. (1996). Occurrence, abundance and origin of minerals in coals and coal ashes. Fuel processing technology, 48, 85-106.

Voges, H. C. (1991). Tests on the beneficiation of coal fines. Journal of the Southern African Institute of Mining and Metallurgy, 91, 41-51.

Von Ketelhodt, L., and Bergmann, C. (2010). Dual energy X-ray transmission sorting of coal. Journal of the South African Institute of Mining & Metallurgy, 110, 371.

Wagner, N. J., and Tlotleng, M. T. (2012). Distribution of selected trace elements in density fractionated Waterberg coals from South Africa. International Journal of Coal Geology, 94, 225-237.

Wagner, N. J., and Matiane, A. (2018). Rare earth elements in select Main Karoo Basin (South Africa) coal and coal ash samples. International Journal of Coal Geology, 196, 82-92.

Wagner. N., Malumbazo. N., Falcon. R. (2018). Southern African Coals and Carbons; definitions and applications of organic petrology. Struik Nature. Cape Town. 248pp.

Wang, H., Dlugogorski, B. Z., Kennedy, E. M. (2003). Analysis of the mechanism of the low-temperature oxidation of coal. Combustion and Flame, 134, 107-117.

Wang, W., Qin, Y., Sang, S., Jiang, B., Guo, Y., Zhu, Y., Fu, X. (2006). Partitioning of minerals and elements during preparation of Taixi coal, China. Fuel, 85, 57-67.

Ward, C. R. (2002). Analysis and significance of mineral matter in coal seams. International Journal of Coal Geology, 50, 135-168.

Ward, C. R. (2016). Analysis, origin and significance of mineral matter in coal: An updated review. International Journal of Coal Geology, 165, 1-27.

Ward, C. R., Corcoran, J. F., Saxby, J. D., Read, H. W. (1996). Occurrence of phosphorus minerals in Australian coal seams. International Journal of Coal Geology, 30(3), 185-210.

Wen-feng, W., Yong, Q., Jun-yi, W., Jian, L. (2009). Partitioning of hazardous trace elements during coal preparation. Procedia Earth and Planetary Science, 1, 838-844.

World Steel Association (2021). 2021 World steel in Figures. Report, 32 pp.

World Steel Association (2022). 2022 World steel in Figures. Report, 17 pp.

Xaba, D.S. (2004). Evaluate the remaining resources of low phosphorus coal in Mpumalanga Province. Coaltech 2020 Task 1.2.1 report. CSIR Miningtek, Johannesburg, 32 pp.

York, R., and Bell, S. E. (2019). Energy transitions or additions?: Why a transition from fossil fuels requires more than the growth of renewable energy. Energy Research & Social Science, 51, 40-43.

Yudovich, Y. E., and Ketris, M. P. (2006). Chlorine in coal: A review. International Journal of Coal Geology, 67, 127-144.

Zhang, W., Honaker, R. Groppo, J. (2017). Concentration of rare earth minerals from coal by froth flotation. Mining, Metallurgy & Exploration, 34**,** 132–137.

Appendices

Appendice A. Drop Shatter

Drop shatter particle size distribution after 20 drops from a height of 2 m.

Seam	Start Mass (g)	Mass	+63 mm	-63+50 mm	-50+31.5 mm	-31.5+20 mm	-20+16 mm	-16+12.5 mm	-12.5+8 mm	-8+6 mm	-6+4 mm	-4+2 mm	-2+1 mm	-1+0.5 mm	-0.5 mm
SU	35490	**Mass (g)**	15960	1570	3880	2970	1110	1390	1670	670	1090	1590	1290	920	1380
		Mass (%)	45	4	11	8	3	4	5	2	3	5	4	3	4
		Mass cumulative (%)	45	49	60	69	72	76	80	82	85	90	94	96	100
P1	202200	**Mass (g)**	148610	7920	11470	9250	2840	3150	4780	1240	2520	2960	2430	2000	3030
		Mass (%)	74	4	6	5	1	2	2	1	1	2	1	1	2
		Mass cumulative (%)	74	77	83	88	89	91	93	94	95	96	98	99	100
SMU	173110	**Mass (g)**	91490	7390	11740	11710	3880	4860	7770	2850	4740	6830	6290	5070	8490
		Mass (%)	53	4	7	7	2	3	5	2	3	4	4	3	5
		Mass cumulative (%)	53	57	64	71	73	76	80	82	85	89	92	95	100
P2	238710	**Mass (g)**	157080	6990	16700	12050	4120	5880	7550	2020	4660	6410	6040	3800	5410
		Mass (%)	66	3	7	5	2	3	3	1	2	3	3	2	2
		Mass cumulative (%)	66	69	76	81	83	85	88	89	91	94	96	98	100
SML	108150	**Mass (g)**	54030	6580	5880	7090	2840	3200	5930	1930	3680	5080	4470	3090	4350
		Mass (%)	50	6	5	7	3	3	6	2	3	5	4	3	4
		Mass cumulative (%)	50	56	62	68	71	74	79	81	84	89	93	96	100
P3	107680	**Mass (g)**	43940	11480	15380	10680	3460	4360	5710	960	2510	2820	2100	1590	2690
		Mass (%)	41	11	14	10	3	4	5	1	2	3	2	2	3
		Mass cumulative (%)	41	52	66	76	79	83	88	89	92	94	96	98	100
SBU	124480	**Mass (g)**	29690	14260	15740	13230	4500	5040	7840	2300	4570	6640	5550	3750	11370
		Mass (%)	24	12	13	11	4	4	6	2	4	5	5	3	9
		Mass cumulative (%)	24	35	48	59	62	66	73	74	78	83	88	91	100
SBM	114840	**Mass (g)**	37170	7030	12250	11710	4460	5070	7450	1880	3850	5430	4840	3520	10180
		Mass (%)	32	6	11	10	4	4	7	2	3	5	4	3	9
		Mass cumulative (%)	32	39	49	59	63	68	74	76	79	84	88	91	100
SBL	87850	**Mass (g)**	39850	3710	9130	6470	2760	2950	5160	1620	2820	3830	3300	2420	3830
		Mass (%)	45	4	10	7	3	3	6	2	3	4	4	3	4
		Mass cumulative (%)	45	50	60	67	71	74	80	82	85	89	93	96	100

Appendice B. Dry tumbling

Particle size distribution for dry tumbling (5 MIN)

Seam	Start Mass (g)	Mass	-63+50 mm	-50+31.5 mm	-31.5+20 mm	-20+16 mm	-16+12.5 mm	-12.5+8 mm	-8+6 mm	-6+4 mm	-4+2 mm	-2+1 mm	-1+0.5 mm	-0.5 mm
SU	**35380**	**Mass (g)**	2160	11380	5140	1520	1640	2280	740	1260	1490	1550	2310	3860
		Mass (%)	6	32	15	4	5	7	2	4	4	4	7	11
		Mass cumulative (%)	6	38	53	57	62	68	70	74	78	83	89	100
P1	**202150**	**Mass (g)**	41290	68560	27300	7380	7460	10330	2280	3830	6660	4980	5470	16320
		Mass (%)	21	34	14	4	4	5	1	2	3	3	3	8
		Mass cumulative (%)	21	54	68	72	75	80	82	83	87	89	92	100
SMU	**170690**	**Mass (g)**	5600	55730	27490	7130	7780	11760	2910	5960	7270	8110	9620	21040
		Mass (%)	3	33	16	4	5	7	2	3	4	5	6	12
		Mass cumulative (%)	3	36	52	56	61	68	69	73	77	82	88	100
P2	**237720**	**Mass (g)**	40680	76200	30110	8680	9600	13830	2960	5350	10130	8140	10180	21710
		Mass (%)	17	32	13	4	4	6	1	2	4	3	4	9
		Mass cumulative (%)	17	49	62	66	70	75	77	79	83	87	91	100
SML	**107260**	**Mass (g)**	6820	33450	12810	3800	4110	7230	1750	3880	6090	7300	6440	13490
		Mass (%)	6	31	12	4	4	7	2	4	6	7	6	13
		Mass cumulative (%)	6	38	50	53	57	64	65	69	75	81	87	100
P3	**107310**	**Mass (g)**	27430	28470	12860	4150	5040	7030	1510	2540	4300	2970	3040	7910
		Mass (%)	26	27	12	4	5	7	1	2	4	3	3	7
		Mass cumulative (%)	26	52	64	68	73	79	81	83	87	90	93	100
SBU	**117330**	**Mass cumulative (%)**	26	52	64	68	73	79	81	83	87	90	93	100
		Mass (%)	13	22	13	4	4	7	2	4	5	7	6	13
		Mass cumulative (%)	13	35	48	52	57	63	65	68	74	81	87	100
SBM	**108210**	**Mass (g)**	7930	30950	14500	5030	5530	8400	1820	3850	5690	5850	6300	12220
		Mass (%)	7	29	13	5	5	8	2	4	5	5	6	11
		Mass cumulative (%)	7	36	49	54	59	67	69	72	77	83	89	100
SBL	**87370**	**Mass (g)**	8180	23900	11930	3690	3680	6550	1640	3290	4230	4380	6210	9510
		Mass (%)	9	27	14	4	4	8	2	4	5	5	7	11
		Mass cumulative (%)	9	37	51	55	59	66	68	72	77	82	89	100

Appendice C. Wet Tumbling

Particle size distribution fore wet tumbling with cubes (5 MIN)

No. 6 Seam horizons	Start Mass (g)	Mass	-63+50 mm	-50+31.5 mm	-31.5+20 mm	-20+16 mm	-16+12.5 mm	-12.5+8 mm	-8+6 mm	-6+4 mm	-4+2 mm	-2+1 mm	-1+0.5 mm	-0.5 mm
SU	35240	Mass (g)	1410	11110	5200	1610	1640	2250	590	1140	1360	1420	1600	2310
		Mass (%)	4	32	15	5	5	6	2	3	4	4	5	7
		Mass cumulative (%)	4	36	50	55	60	66	68	71	75	79	83	90
P1	200760	Mass (g)	34900	69040	28770	9700	5630	9750	2370	4950	5270	6490	3800	7960
		Mass (%)	17	34	14	5	3	5	1	3	3	3	2	4
		Mass cumulative (%)	17	52	66	71	74	79	80	82	85	88	90	94
SMU	169570	Mass (g)	4190	54450	27800	6220	7730	9930	2780	5130	7030	6180	8910	12700
		Mass (%)	3	32	16	4	5	6	2	3	4	4	5	8
		Mass cumulative (%)	3	35	51	55	59	65	67	70	74	78	83	90
P2	236320	Mass (g)	36160	76780	30730	10040	7030	11910	3290	6570	8060	9630	6300	11480
		Mass (%)	15	33	13	4	3	5	1	3	3	4	3	5
		Mass cumulative (%)	15	48	61	65	68	73	74	77	81	85	87	92
SML	106580	Mass (g)	6540	33050	11720	3330	3860	6370	1610	3880	5880	7250	5550	7640
		Mass (%)	6	31	11	3	4	6	2	4	6	7	5	7
		Mass cumulative (%)	6	37	48	51	55	61	62	66	72	78	84	91
P3	107060	Mass (g)	15180	33430	16780	5600	3970	6730	1570	3570	3510	2800	2700	4170
		Mass (%)	14	31	16	5	4	6	2	3	3	3	3	4
		Mass cumulative (%)	14	45	61	66	70	76	78	81	84	87	90	93
SBU	116650	Mass (g)	11540	26810	14590	4780	4920	6330	2870	3460	5640	6740	7230	10510
		Mass (%)	10	23	13	4	4	5	3	3	5	6	6	9
		Mass cumulative (%)	10	33	45	50	54	59	62	65	69	75	81	90
SBM	107780	Mass (g)	6880	30900	13810	4510	5560	6710	3020	3360	4980	5180	4070	10940
		Mass (%)	6	29	13	4	5	6	3	3	5	5	4	10
		Mass cumulative (%)	6	35	48	52	57	63	66	69	74	79	83	93
SBL	86800	Mass (g)	6470	24420	11270	3410	3520	5280	2530	2920	3910	4220	4090	6690
		Mass (%)	8	28	13	4	4	6	3	3	5	5	5	8
		Mass cumulative (%)	8	36	49	53	57	63	66	69	73	78	83	91

Appendice D. Vitrinite Reflectance Histograms

SU

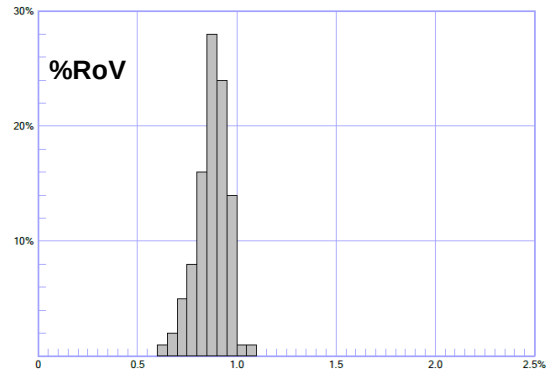

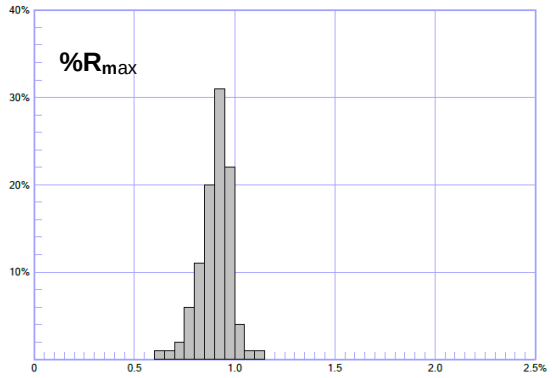

P1

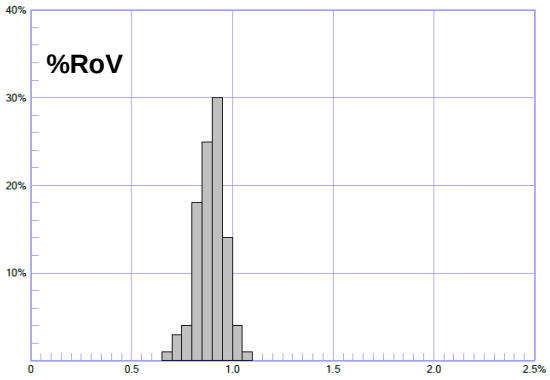

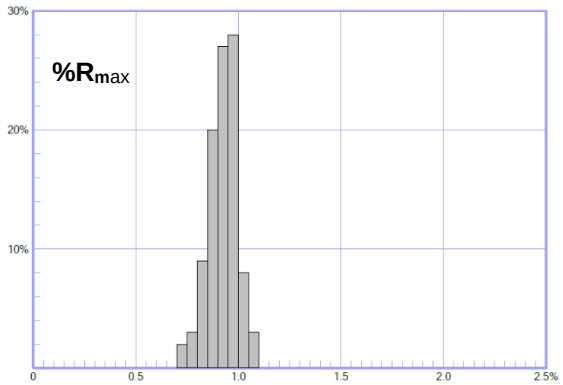

SMU

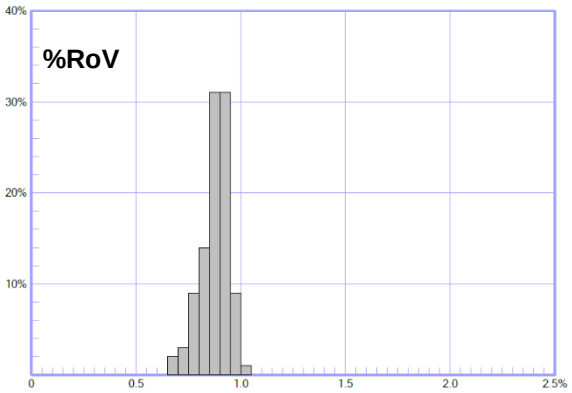

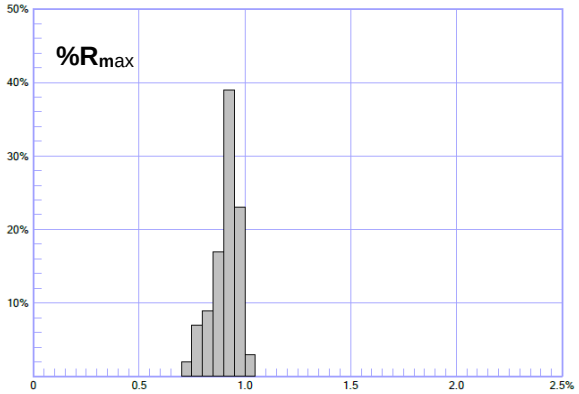

P2

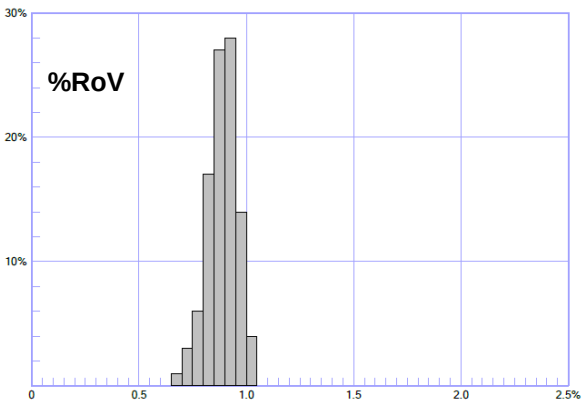

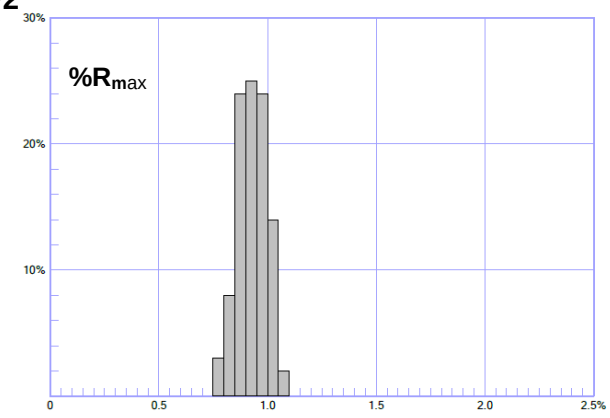

SML

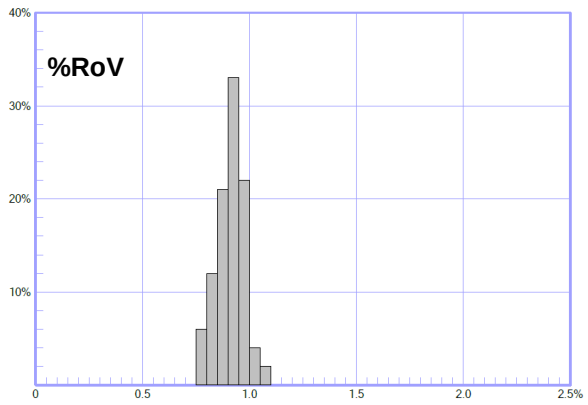
%RoV
40%
30%
20%
10%
0
0.5
1.0
1.5
2.0
2.5%

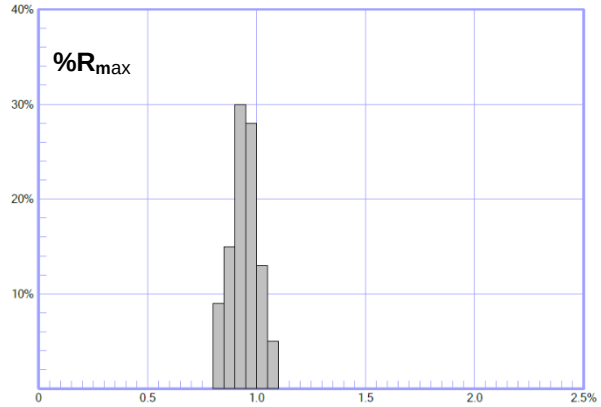
%Rmax
40%
30%
20%
10%
0
0.5
1.0
1.5
2.0
2.5%

P3

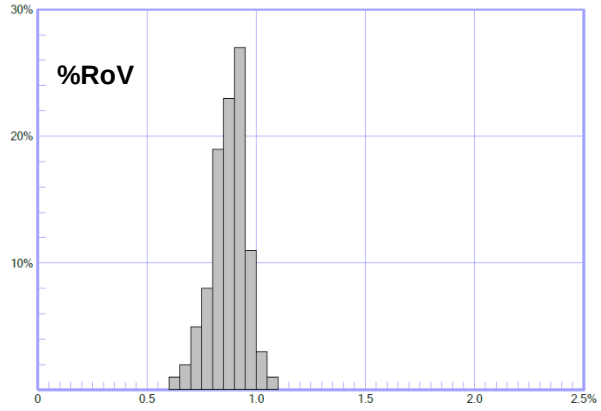
%RoV
30%
20%
10%
0
0.5
1.0
1.5
2.0
2.5%

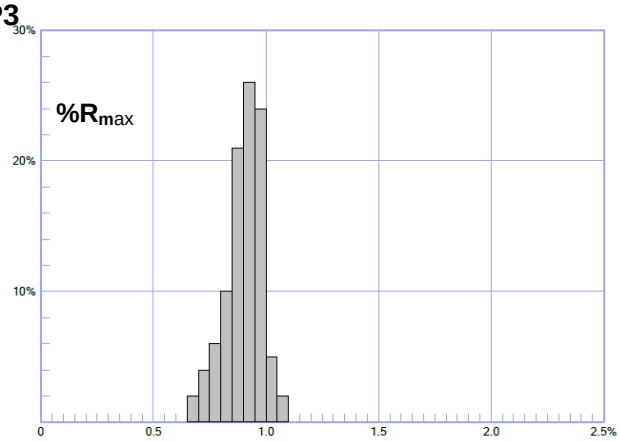
%Rmax
30%
20%
10%
0
0.5
1.0
1.5
2.0
2.5%

SBU

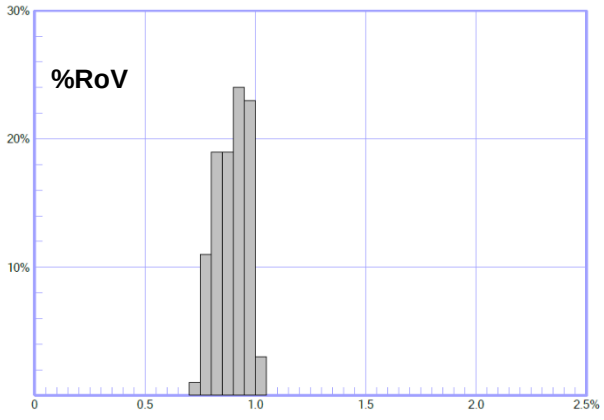
%RoV
30%
20%
10%
0
0.5
1.0
1.5
2.0
2.5%

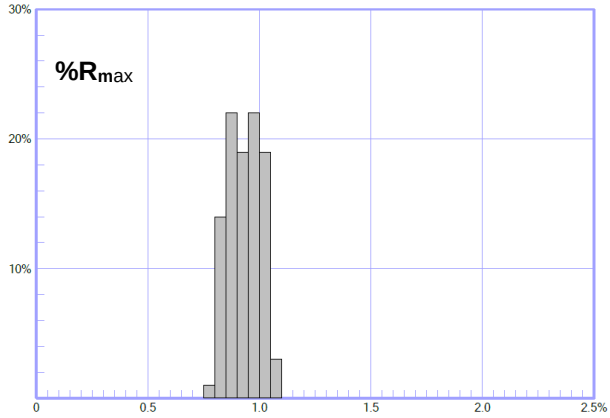
%Rmax
30%
20%
10%
0
0.5
1.0
1.5
2.0
2.5%

SBM

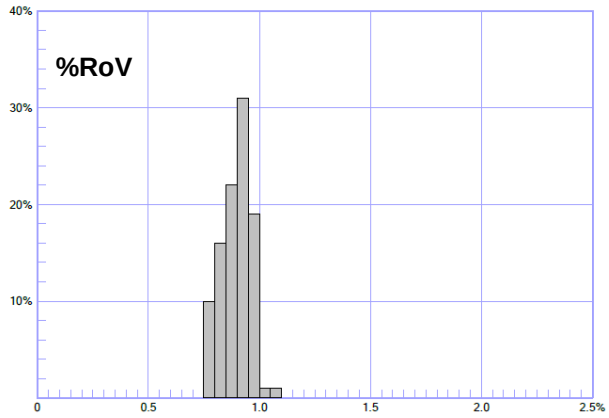
%RoV
40%
30%
20%
10%
0
0.5
1.0
1.5
2.0
2.5%

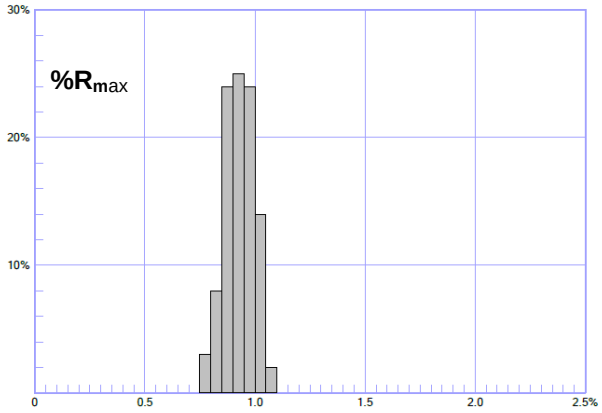
%Rmax
30%
20%
10%
0
0.5
1.0
1.5
2.0
2.5%

SBL

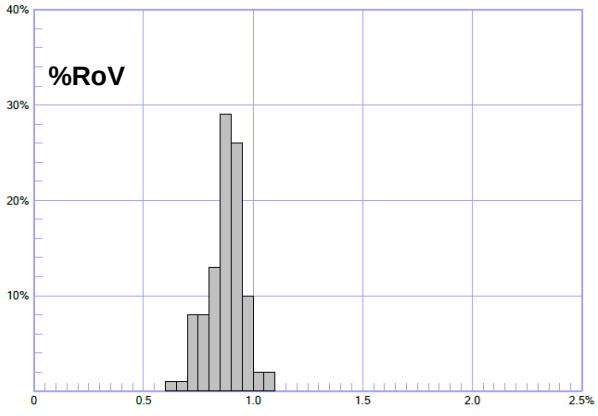
%RoV
40%
30%
20%
10%
0
0.5
1.0
1.5
2.0
2.5%

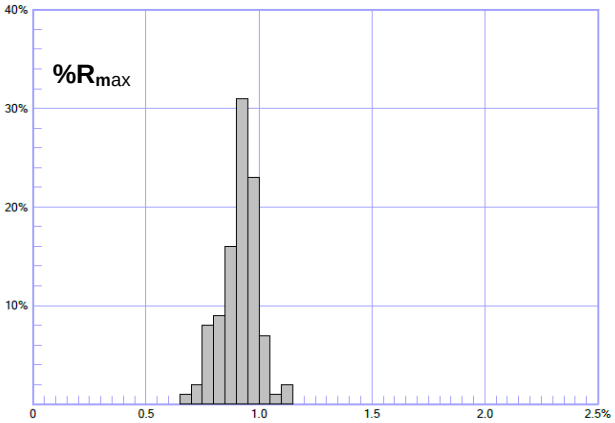
%Rmax
40%
30%
20%
10%
0
0.5
1.0
1.5
2.0
2.5%

Appendice E. Standards for XRF testing

Standard	SiO_2	Al_2O_3	Fe_2O_3	FeO	MnO	MgO	CaO	Na_2O	K_2O	TiO_2	P_2O_5	Cr_2O_3	NiO	TOTAL	LOI
NIM-P	51.17	4.29	1.28	10.34	0.23	25.36	2.64	0.35	0.10	0.19	0.03	3.54	0.08	99.60	-0.23
NIM-D	39.08	0.32	1.72	13.92	0.22	44.10	0.31	0.03	0.01	0.03	0.02	0.43	0.26	100.45	-0.51
W2	53.17	15.62	1.09	8.85	0.17	6.43	10.96	2.22	0.65	1.09	0.13	0.02	0.01	100.42	0.19
NIM-S	64.13	17.37	0.14	1.13	0.01	0.49	0.63	0.37	15.40	0.05	0.12	0.00	0.00	99.84	0.42
GSP2	67.75	15.14	0.50	4.05	0.05	1.01	2.12	2.81	5.48	0.68	0.29	0.00	0.00	99.87	0.87
BCR2	54.59	13.67	1.40	11.30	0.20	3.64	7.18	3.19	1.79	2.30	0.36	0.01	0.00	99.62	0.10
NIM-N	53.39	16.79	0.91	7.35	0.17	7.54	11.55	2.48	0.25	0.20	0.02	0.01	0.02	100.68	0.04
NIM-G	76.66	12.28	0.20	1.60	0.02	0.08	0.78	3.35	5.06	0.10	0.01	0.00	0.00	100.15	0.73
PCC1	44.61	0.75	0.87	7.06	0.12	45.81	0.61	0.07	0.00	0.01	0.01	0.43	0.33	100.69	5.09
BHVO2	50.42	13.76	1.25	10.15	0.17	7.33	11.52	2.26	0.52	2.80	0.27	0.05	0.02	100.52	-0.48
AGV2	60.68	17.34	0.69	5.56	0.10	1.85	5.31	4.30	2.94	1.07	0.48	0.00	0.00	100.31	1.80
G2	69.54	15.41	0.27	2.15	0.04	0.79	1.93	4.11	4.48	0.49	0.14	0.00	0.00	99.34	0.64
DTS1	40.82	0.27	0.87	7.06	0.13	49.98	0.17	0.07	0.00	0.01	0.01	0.59	0.31	100.28	-0.02

Appendice F. Trace element and REE Standards for ICPMS analysis

	Measured			Recommended		
ppm	**BCR2**	**BHVO2**	**BIR1**	**BCR2**	**BHVO2**	**BIR1**
Li	9.55	5.19	3.73	9.90	5.00	3.40
P	1541.31	1201.16	83.80	1571.00	1178.00	100.00
Sc	31.98	31.02	42.18	32.00	31.00	44.00
Ti	12869.03	15787.84	5509.64	13005.00	15621.00	5755.00
V	421.51	323.24	323.36	414.00	329.00	313.00
Cr	15.51	315.37	419.66	17.00	285.00	382.00
Co	37.43	45.04	52.70	35.80	47.00	51.40
Ni	11.77	121.57	173.41	12.70	112.00	166.00
Cu	18.99	145.11	136.30	19.40	142.00	126.00
Zn	143.63	109.57	73.56	147.00	107.00	71.00
Ga	22.46	21.23	13.52	22.70	21.00	-
Rb	49.96	9.91	0.23	49.00	10.10	0.25
Sr	323.50	379.07	103.99	321.00	382.00	108.00
Y	31.42	22.70	13.01	31.00	23.00	16.00
Zr	183.19	170.04	12.69	194.00	160.00	15.50
Nb	11.86	17.82	0.54	12.80	16.40	0.60
Sn	2.10	1.43	0.42	2.10	2.70	0.65
Sb	0.62	0.15	0.79	0.62	0.16	0.58
Cs	1.24	0.10	0.01	1.17	0.11	-
Ba	639.44	129.02	6.29	641.00	128.70	7.00
La	25.21	15.18	0.62	24.50	15.60	0.62
Ce	51.20	36.50	1.80	50.50	37.00	1.95
Pr	6.34	4.97	0.35	6.30	5.00	0.38
Nd	27.53	23.55	2.27	27.00	24.00	2.50
Sm	6.29	5.81	1.02	6.30	5.80	1.10
Eu	1.91	2.00	0.49	1.91	2.00	0.54
Gd	6.48	5.92	1.64	6.50	5.90	1.85
Tb	0.96	0.85	0.31	0.95	0.86	0.36
Dy	5.99	4.91	2.29	6.00	4.90	2.50
Ho	1.21	0.91	0.51	1.20	0.91	0.57
Er	3.33	2.28	1.48	3.30	2.30	1.70
Tm	0.47	0.29	0.21	0.46	0.30	0.26
Yb	3.33	1.94	1.57	3.20	2.02	1.65
Lu	0.47	0.26	0.22	0.47	0.26	0.26
Hf	4.79	4.29	0.54	5.00	4.10	0.60
Ta	0.71	1.04	0.06	0.78	0.94	0.04
W	0.44	0.30	0.26	0.44	0.27	0.01
Tl	0.30	0.02	0.00	0.30	0.06	0.01
Pb	10.67	1.43	2.79	10.90	1.40	3.00
Th	5.65	1.15	0.03	5.50	1.18	0.03
U	1.75	0.44	0.01	1.73	0.44	0.01

Appendice G. Proximate correlations with ash for Makhado float yields

Sample	SU			P1			SMU		
Coefficient	Volatile matter	Calorific value	Total sulphur	Volatile matter	Calorific value	Total sulphur	Volatile matter	Calorific value	Total sulphur
R	0.8723	0.9985	0.2667	0.6750	0.9993	0.4725	0.9558	0.9986	0.4772
r	-0.9340	-0.9993	-0.5164	-0.8216	-0.9996	-0.6874	-0.9777	-0.9993	-0.6908
Sample	P2			SML			P3		
Coefficient	Volatile matter	Calorific value	Total sulphur	Volatile matter	Calorific value	Total sulphur	Volatile matter	Calorific value	Total sulphur
R	0.8795	0.9985	0.9102	0.8280	0.9981	0.9491	0.8593	0.9992	0.9806
r	-0.9378	-0.9993	-0.9541	-0.9099	-0.9990	-0.9742	-0.9270	-0.9996	-0.9903
Sample	SBU			SBM			SBL		
Coefficient	Volatile matter	Calorific value	Total sulphur	Volatile matter	Calorific value	Total sulphur	Volatile matter	Calorific value	Total sulphur
R	0.9532	0.9990	0.9515	0.8657	0.9977	0.9059	0.4306	0.9980	0.8868
r	-0.9763	-0.9995	-0.9754	-0.9304	-0.9988	-0.9518	-0.6562	-0.9990	-0.9417

The Table of critical values of the correlation coefficients from Speight (2005) was used. Degree of freedom = sample size -2 = 9-2 =. Two-sided hypothesis at probability level of 0.025% = 0.6664 critical value

Appendice H. XRD diffractogram for minerals identified in the fine-float samples.

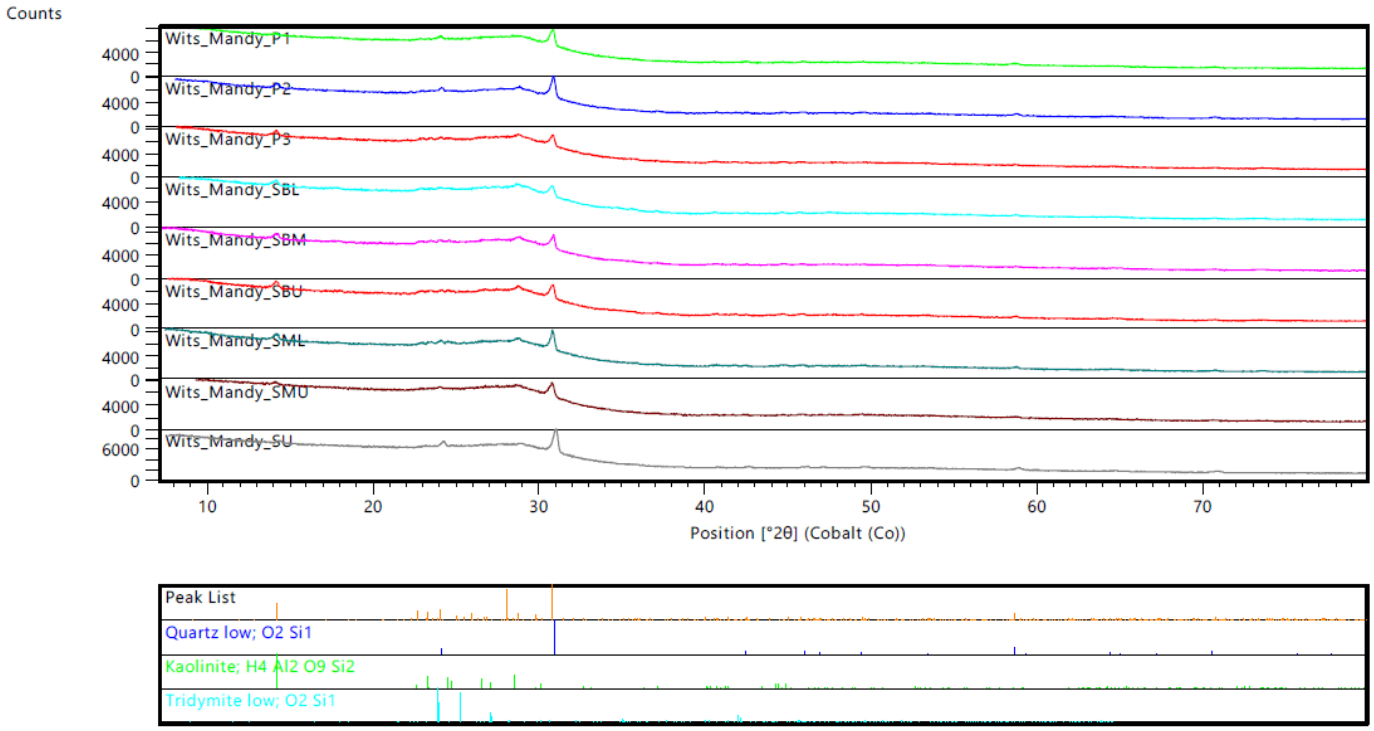

Appendice I. Vitrinite association with oxides, trace elements and REY+Sc

Vitrinite (mmf) association with major oxides (wt%)												
Coefficient	SiO_2	Al_2O_3	Fe_2O_3	MnO	MgO	CaO	Na_2O	K_2O	TiO_2	P_2O_5	Cr_2O_3	NiO
R^2	0.3743	0.5851	0.2935	0.0626	0.0024	0.3295	0.4848	0.0452	0.0144	0.7076	0.0046	0.1967
r	0.6118	-0.7649	0.5418	0.2501	0.0491	-0.5740	-0.6963	-0.2126	0.1198	-0.8412	-0.0676	0.4435

Vitrinite (mmf) association with trace elements													
Coefficient	Li	P	Ti	V	Cr	Co	Ni	Cu	Zn	Ga	Rb	Sr	Zr
R^2	0.1393	0.4899	0.0685	0.0001	0.0203	0.3103	0.2378	0.5179	0.0797	0.0394	0.1667	0.6953	0.0001
r	-0.3732	-0.6999	0.2617	-0.0085	-0.1423	-0.5570	0.4876	-0.7196	0.2822	-0.1986	-0.4083	-0.8338	0.0115

Coefficient	Nb	Sn	Sb	Cs	Ba	Hf	Ta	W	Tl	Pb	Th	U
R^2	0.1534	0.0287	0.0010	0.4399	0.6199	0.0004	0.2477	0.3840	0.0542	0.0365	0.6925	0.3778
r	0.3916	-0.1695	0.0314	-0.6633	-0.7873	-0.0205	0.4977	0.6197	-0.2328	0.1910	-0.8322	-0.6146

Vitrinite (mmf) association with LREE +Sc (ppm)						
Coefficient	Sc	La	Ce	Pr	Nd	Sm
R^2	0.0238	0.7895	0.7975	0.7877	0.7852	0.7658
r	-0.1543	-0.8886	-0.8930	-0.8875	-0.8861	-0.8751

Vitrinite (mmf) association with MREE+Y (ppm)					
Coefficient	Y	Eu	Gd	Tb	Dy
R^2	0.0163	0.6852	0.6384	0.4244	0.1935
r	-0.1275	-0.8278	-0.7990	-0.6514	-0.4399

Vitrinite (mmf) association with HREE (ppm)					
Coefficient	Ho	Er	Tm	Yb	Lu
R^2	0.0589	0.0173	0.0042	0.0013	0.0001
r	-0.2428	-0.1317	-0.0651	-0.0359	0.0089

Appendice J. Ash association with oxides, trace elements and REY+Sc

Ash (ad%) association with major oxides (wt%)												
Coefficient	SiO_2	Al_2O_3	Fe_2O_3	MnO	MgO	CaO	Na_2O	K_2O	TiO_2	P_2O_5	Cr_2O_3	NiO
R^2	0.0782	0.3947	0.2800	0.0092	0.1220	0.0059	0.0744	0.2587	0.2463	0.3334	0.0542	0.2420
r	-0.2797	0.6283	-0.5291	0.0959	-0.3493	0.0771	0.2728	0.5086	-0.4963	0.5774	-0.2328	-0.4920

Ash (ad%) association with trace elements (ppm)													
Coefficient	Li	P	Ti	V	Cr	Co	Ni	Cu	Zn	Ga	Rb	Sr	Zr
R^2	0.0222	0.4606	0.1729	0.0797	0.0408	0.1899	0.5105	0.0398	0.2314	0.0080	0.1504	0.3118	0.1174
r	0.1489	0.6787	-0.4158	-0.2823	-0.2021	0.4358	-0.7145	0.1994	-0.4810	-0.0892	0.3878	0.5584	-0.3427

Coefficient	Nb	Sn	Sb	Cs	Ba	Hf	Ta	W	Tl	Pb	Th	U
R^2	0.1187	0.0018	0.0424	0.3079	0.2347	0.0949	0.1655	0.2214	0.0086	0.1367	0.3276	0.0424
r	-0.3445	0.0419	-0.2059	0.5549	0.4844	-0.3081	-0.4068	-0.4706	0.0929	-0.3697	0.5724	0.2059

Ash (ad%) association with LREE +Sc (ppm)						
Coefficient	Sc	La	Ce	Pr	Nd	Sm
R^2	0.0003	0.3732	0.4128	0.4222	0.4193	0.3963
r	-0.0159	0.6109	0.6425	0.6498	0.6475	0.6295

Ash (ad%) association with MREE+Y (ppm)					
Coefficient	Y	Eu	Gd	Tb	Dy
R^2	0.0131	0.3420	0.2984	0.1320	0.0215
r	-0.1144	0.5848	0.5463	0.3633	0.1467

Ash (ad%) association with HREE (ppm)					
Coefficient	Ho	Er	Tm	Yb	Lu
R^2	0.0014	0.0185	0.0373	0.0468	0.0617
r	-0.0377	-0.1359	-0.1931	-0.2163	-0.2484

Appendice K. Major oxide (wt%) association with trace elements and REY+Sc.

SiO_2 (wt%) association with trace elements (ppm)													
Coefficient	Li	P	Ti	V	Cr	Co	Ni	Cu	Zn	Ga	Rb	Sr	Zr
R^2	0.0351	0.4756	0.2921	0.2326	0.3261	0.6313	0.0200	0.9056	0.0437	0.3705	0.4406	0.5560	0.1427
r	-0.1875	-0.6897	-0.5404	-0.4823	-0.5710	-0.7946	-0.1413	-0.9517	-0.2091	-0.6087	-0.6638	-0.7457	-0.3778
Coefficient	Nb	Sn	Sb	Cs	Ba	Hf	Ta	W	Tl	Pb	Th	U	
R^2	0.0085	0.4750	0.0903	0.6816	0.6152	0.1662	0.0399	0.0282	0.0271	0.0038	0.6890	0.8476	
r	-0.0925	-0.6892	-0.3005	-0.8256	-0.7844	-0.4077	-0.1998	0.1678	-0.1647	0.0616	-0.8301	-0.9207	

SiO_2 (wt%) association with LREE +Sc (ppm)						
Coefficient	Sc	La	Ce	Pr	Nd	Sm
R^2	0.3002	0.6880	0.6580	0.6526	0.6683	0.7288
r	-0.5479	-0.8295	-0.8112	-0.8079	-0.8175	-0.8537

SiO_2 (wt%) association with MREE+Y (ppm)					
Coefficient	Y	Eu	Gd	Tb	Dy
R^2	0.3038	0.8028	0.8104	0.7654	0.6118
r	-0.5512	-0.8960	-0.9002	-0.8749	-0.7821

SiO_2 (wt%) association with HREE (ppm)					
Coefficient	Ho	Er	Tm	Yb	Lu
R^2	0.3997	0.3020	0.2293	0.2066	0.1760
r	-0.6322	-0.5495	-0.4789	-0.4545	-0.4196

Al_2O_3 (wt%) association with trace elements (ppm)													
Coefficient	Li	P	Ti	V	Cr	Co	Ni	Cu	Zn	Ga	Rb	Sr	Zr
R^2	0.4863	0.3128	0.0569	0.0272	0.0020	0.2128	0.2466	0.3642	0.1612	0.0072	0.2757	0.4295	0.0175
r	0.6974	0.5593	-0.2385	-0.1648	0.0449	0.4613	-0.4966	0.6035	-0.4014	0.0848	0.5250	0.6554	-0.1321

Coefficient	Nb	Sn	Sb	Cs	Ba	Hf	Ta	W	Tl	Pb	Th	U
R^2	0.0757	0.1116	0.0146	0.3619	0.3024	0.0071	0.0095	0.0300	0.2217	0.0691	0.4055	0.1716
r	-0.2751	0.3341	0.1209	0.6015	0.5499	-0.0840	-0.0975	-0.1731	0.4709	0.2628	0.6368	0.4143

Al_2O_3 (wt%) association with LREE +Sc (ppm)						
Coefficient	Sc	La	Ce	Pr	Nd	Sm
R^2	0.0258	0.5592	0.5345	0.5301	0.5277	0.5236
r	0.1606	0.7478	0.7311	0.7281	0.7265	0.7236

Al_2O_3 (wt%) association with MREE+Y (ppm)					
Coefficient	Y	Eu	Gd	Tb	Dy
R^2	0.0366	0.4941	0.5197	0.3685	0.1897
r	0.1914	0.7029	0.7209	0.6071	0.4356

Al_2O_3 (wt%) association with HREE (ppm)					
Coefficient	Ho	Er	Tm	Yb	Lu
R^2	0.0706	0.0282	0.0120	0.0077	0.0032
r	0.2658	0.1679	0.1096	0.0876	0.0563

Fe_2O_3 (wt%) association with trace elements (ppm)													
Coefficient	Li	P	Ti	V	Cr	Co	Ni	Cu	Zn	Ga	Rb	Sr	Zr
R^2	0.0348	0.0899	0.0521	0.0648	0.1041	0.0129	0.1491	0.0257	0.0005	0.0818	0.0796	0.0440	0.0957
r	0.1866	-0.2999	0.2283	-0.2546	-0.3226	-0.1138	0.3861	-0.1604	0.0230	-0.2859	-0.2822	-0.2098	-0.3094

Coefficient	Nb	Sn	Sb	Cs	Ba	Hf	Ta	W	Tl	Pb	Th	U
R^2	0.0005	0.1105	0.0403	0.1676	0.0345	0.1003	0.1216	0.5363	0.2513	0.0660	0.1474	0.1589
r	0.0232	-0.3325	-0.2008	-0.4094	-0.1857	-0.3167	0.3487	0.7323	-0.5013	0.2570	-0.3840	-0.3987

Fe_2O_3 (wt%) association with LREE +Sc (ppm)						
Coefficient	Sc	La	Ce	Pr	Nd	Sm
R^2	0.0954	0.2454	0.2009	0.1874	0.1823	0.1751
r	-0.3089	-0.4954	-0.4482	-0.4329	-0.4269	-0.4185

Fe_2O_3 (wt%) association with MREE+Y (ppm)					
Coefficient	Y	Eu	Gd	Tb	Dy
R^2	0.0660	0.1683	0.2037	0.1840	0.1179
r	-0.2568	-0.4103	-0.4513	-0.4290	-0.3434

Fe_2O_3 (wt%) association with HREE (ppm)					
Coefficient	Ho	Er	Tm	Yb	Lu
R^2	0.0752	0.0548	0.0495	0.0403	0.0305
r	-0.2742	-0.2340	-0.2225	-0.2008	-0.1747

MnO (wt%) association with trace elements (ppm)													
Coefficient	Li	P	Ti	V	Cr	Co	Ni	Cu	Zn	Ga	Rb	Sr	Zr
R^2	0.0780	0.0007	0.0092	0.2967	0.4134	0.0015	0.0017	0.0121	0.0198	0.2950	0.0958	0.0081	0.4611
r	0.2793	0.0267	-0.0957	-0.5447	-0.6429	0.0387	0.0411	-0.1100	-0.1408	-0.5431	-0.3096	0.0901	-0.6790
Coefficient	Nb	Sn	Sb	Cs	Ba	Hf	Ta	W	Tl	Pb	Th	U	
R^2	0.1771	0.3191	0.3663	0.0799	0.0048	0.4605	0.0079	0.1374	0.4674	0.0065	0.0230	0.1912	
r	-0.4209	-0.5649	-0.6053	-0.2827	0.0692	-0.6786	-0.0888	0.3707	-0.6837	-0.0809	-0.1518	-0.4373	

MnO (wt%) association with LREE +Sc (ppm)						
Coefficient	Sc	La	Ce	Pr	Nd	Sm
R^2	0.3103	0.0800	0.0339	0.0253	0.0248	0.0325
r	-0.5571	-0.2828	-0.1842	-0.1590	-0.1576	-0.1804

MnO (wt%) association with MREE+Y (ppm)					
Coefficient	Y	Eu	Gd	Tb	Dy
R^2	0.3150	0.0537	0.1108	0.2079	0.2539
r	-0.5612	-0.2318	-0.3328	-0.4560	-0.5039

MnO (wt%) association with HREE (ppm)					
Coefficient	Ho	Er	Tm	Yb	Lu
R^2	0.2889	0.2927	0.3206	0.3063	0.2915
r	-0.5375	-0.5410	-0.5662	-0.5535	-0.5399

MgO (wt%) association with trace elements (ppm)													
Coefficient	Li	P	Ti	V	Cr	Co	Ni	Cu	Zn	Ga	Rb	Sr	Zr
R^2	0.2802	0.1212	0.2209	0.6370	0.6936	0.0251	0.1970	0.0156	0.1027	0.6803	0.2146	0.1077	0.7779
r	-0.5293	-0.3481	0.4700	0.7981	0.8328	0.1586	0.4438	0.1248	0.3205	0.8248	0.4633	-0.3282	0.8820

Coefficient	Nb	Sn	Sb	Cs	Ba	Hf	Ta	W	Tl	Pb	Th	U
R^2	0.6875	0.2518	0.7203	0.0340	0.0468	0.7772	0.1373	0.0000	0.2771	0.0001	0.0124	0.1632
r	0.8292	0.5018	0.8487	0.1843	-0.2164	0.8816	0.3705	-0.0051	0.5264	0.0087	-0.1114	0.4040

MgO (wt%) association with trace elements (ppm)						
Coefficient	Sc	La	Ce	Pr	Nd	Sm
R^2	0.6460	0.0002	0.0140	0.0204	0.0165	0.0022
r	0.8037	-0.0149	-0.1181	-0.1428	-0.1284	-0.0467

MgO (wt%) association with MREE+Y (ppm)					
Coefficient	Y	Eu	Gd	Tb	Dy
R^2	0.6405	0.0076	0.0444	0.2119	0.4237
r	0.8003	0.0870	0.2107	0.4603	0.6509

MgO (wt%) association with HREE (ppm)					
Coefficient	Ho	Er	Tm	Yb	Lu
R^2	0.6080	0.6691	0.7261	0.7345	0.7377
r	0.7798	0.8180	0.8521	0.8570	0.8589

CaO (wt%) association with trace elements (ppm)

Coefficient	Li	P	Ti	V	Cr	Co	Ni	Cu	Zn	Ga	Rb	Sr	Zr
R^2	0.0005	0.2464	0.1370	0.1861	0.3621	0.3628	0.0010	0.4095	0.0069	0.3404	0.3764	0.2915	0.1965
r	0.0233	0.4964	0.3702	0.4314	0.6017	0.6023	-0.0312	0.6399	-0.0833	0.5835	0.6135	0.5399	0.4433

Coefficient	Nb	Sn	Sb	Cs	Ba	Hf	Ta	W	Tl	Pb	Th	U
R^2	0.0608	0.3288	0.1919	0.5788	0.4227	0.2130	0.0380	0.0061	0.0460	0.0024	0.4849	0.5681
r	0.2466	0.5734	0.4380	0.7608	0.6501	0.4615	0.1951	-0.0780	0.2145	0.0491	0.6964	0.7537

CaO (wt%) association with LREE +Sc (ppm)

Coefficient	Sc	La	Ce	Pr	Nd	Sm
R^2	0.3097	0.4480	0.4044	0.3903	0.4095	0.4821
r	0.5565	0.6694	0.6359	0.6247	0.6399	0.6943

CaO (wt%) association with MREE+Y (ppm)

Coefficient	Y	Eu	Gd	Tb	Dy
R^2	0.2491	0.5563	0.5605	0.5733	0.4614
r	0.4991	0.7459	0.7487	0.7572	0.6792

CaO (wt%) association with HREE (ppm)

Coefficient	Ho	Er	Tm	Yb	Lu
R^2	0.3347	0.2607	0.2375	0.2228	0.1945
r	0.5785	0.5106	0.4873	0.4721	0.4410

Na_2O (wt%) association with trace elements (ppm)													
Coefficient	Li	P	Ti	V	Cr	Co	Ni	Cu	Zn	Ga	Rb	Sr	Zr
R^2	0.1772	0.1678	0.0214	0.1298	0.3402	0.1994	0.0272	0.5416	0.0125	0.3169	0.4315	0.2629	0.2016
r	0.4210	0.4097	0.1462	0.3603	0.5832	0.4465	-0.1648	0.7360	-0.1120	0.5630	0.6569	0.5127	0.4490
Coefficient	Nb	Sn	Sb	Cs	Ba	Hf	Ta	W	Tl	Pb	Th	U	
R^2	0.0387	0.5094	0.3520	0.4484	0.2183	0.2384	0.0373	0.0218	0.5260	0.1338	0.3956	0.5497	
r	0.1966	0.7137	0.5933	0.6696	0.4673	0.4883	0.1932	-0.1475	0.7253	0.3658	0.6289	0.7414	

Na_2O (wt%) association with LREE +Sc (ppm)						
Coefficient	Sc	La	Ce	Pr	Nd	Sm
R^2	0.3367	0.6012	0.4834	0.4583	0.4610	0.5003
r	0.5803	0.7754	0.6953	0.6770	0.6790	0.7073

$N_{a2}O$ (wt%) association with MREE+Y (ppm)					
Coefficient	Y	Eu	Gd	Tb	Dy
R^2	0.4167	0.5586	0.6883	0.7388	0.6338
r	0.6455	0.7474	0.8296	0.8595	0.7961

Na_2O (wt%) association with HREE (ppm)					
Coefficient	Ho	Er	Tm	Yb	Lu
R^2	0.4864	0.3914	0.3490	0.3211	0.2855
r	0.6974	0.6256	0.5908	0.5666	0.5343

K_2O (wt%) association with trace elements (ppm)													
Coefficient	Li	P	Ti	V	Cr	Co	Ni	Cu	Zn	Ga	Rb	Sr	Zr
R^2	0.0116	0.0302	0.0774	0.1683	0.1885	0.2311	0.0458	0.0002	0.0526	0.0798	0.0638	0.0425	0.3044
r	0.1079	0.1737	-0.2782	-0.4103	-0.4342	0.4807	-0.2140	0.0139	-0.2293	-0.2824	0.2526	0.2062	-0.5518
Coefficient	Nb	Sn	Sb	Cs	Ba	Hf	Ta	W	Tl	Pb	Th	U	
R^2	0.1934	0.1646	0.1807	0.0452	0.0606	0.2844	0.1401	0.0141	0.1017	0.1748	0.0078	0.0614	
r	-0.4398	-0.4057	-0.4251	0.2125	0.2462	-0.5333	-0.3744	-0.1188	-0.3188	-0.4181	0.0884	-0.2479	

K_2O (wt%) association with LREE +Sc (ppm)						
Coefficient	Sc	La	Ce	Pr	Nd	Sm
R^2	0.0308	0.0003	0.0098	0.0138	0.0172	0.0240
r	-0.1755	0.0164	0.0991	0.1174	0.1313	0.1550

K_2O (wt%) association with MREE+Y (ppm)					
Coefficient	Y	Eu	Gd	Tb	Dy
R^2	0.0997	0.0222	0.0052	0.0040	0.0283
r	-0.3158	0.1489	0.0722	-0.0633	-0.1682

K_2O (wt%) association with HREE (ppm)					
Coefficient	Ho	Er	Tm	Yb	Lu
R^2	0.0638	0.0846	0.1119	0.1033	0.1024
r	-0.2526	-0.2909	-0.3345	-0.3214	-0.3200

Ti_2O (wt%) association with trace elements (ppm)													
Coefficient	Li	P	Ti	V	Cr	Co	Ni	Cu	Zn	Ga	Rb	Sr	Zr
R^2	0.1876	0.0001	0.7901	0.5852	0.4225	0.1714	0.7115	0.2396	0.6731	0.3845	0.0505	0.0031	0.3907
r	-0.4331	0.0095	0.8889	0.7650	0.6500	0.4140	0.8435	0.4895	0.8204	0.6201	0.2248	0.0555	0.6251

Coefficient	Nb	Sn	Sb	Cs	Ba	Hf	Ta	W	Tl	Pb	Th	U
R^2	0.1195	0.1881	0.0653	0.0641	0.0533	0.3666	0.1073	0.0001	0.0397	0.0594	0.0260	0.3161
r	0.3457	0.4337	0.2554	0.2533	0.2309	0.6055	0.3276	-0.0114	-0.1992	-0.2437	0.1611	0.5622

Ti_2O (wt%) association with LREE +Sc (ppm)						
Coefficient	Sc	La	Ce	Pr	Nd	Sm
R^2	0.2514	0.0035	0.0023	0.0019	0.0036	0.0137
r	0.5014	0.0592	0.0474	0.0440	0.0597	0.1169

Ti_2O (wt%) association with MREE+Y (ppm)					
Coefficient	Y	Eu	Gd	Tb	Dy
R^2	0.2349	0.0412	0.0423	0.1094	0.1981
r	0.4847	0.2030	0.2056	0.3308	0.4450

Ti_2O (wt%) association with HREE (ppm)					
Coefficient	Ho	Er	Tm	Yb	Lu
R^2	0.2355	0.2642	0.2494	0.2542	0.2561
r	0.4852	0.5140	0.4994	0.5041	0.5061

P_2O_5 (wt%) association with trace elements (ppm)													
Coefficient	Li	P	Ti	V	Cr	Co	Ni	Cu	Zn	Ga	Rb	Sr	Zr
R^2	0.1029	0.8807	0.0019	0.0062	0.0001	0.3953	0.1780	0.5220	0.0626	0.0033	0.0858	0.9643	0.0352
r	0.3208	0.9385	-0.0441	-0.0787	0.0099	0.6287	-0.4219	0.7225	-0.2502	0.0576	0.2929	0.9820	-0.1877

Coefficient	Nb	Sn	Sb	Cs	Ba	Hf	Ta	W	Tl	Pb	Th	U
R^2	0.2316	0.0239	0.0819	0.5154	0.9609	0.0273	0.1319	0.1856	0.0444	0.0777	0.9239	0.3976
r	-0.4813	0.1544	-0.2861	0.7179	0.9802	-0.1652	-0.3631	-0.4309	-0.2108	-0.2788	0.9612	0.6306

P_2O_5 (wt%) association with LREE +Sc (ppm)						
Coefficient	Sc	La	Ce	Pr	Nd	Sm
R^2	0.0003	0.7859	0.8811	0.8947	0.8959	0.8575
r	-0.0183	0.8865	0.9387	0.9459	0.9465	0.9260

P_2O_5 (wt%) association with MREE+Y (ppm)					
Coefficient	Y	Eu	Gd	Tb	Dy
R^2	0.0064	0.7372	0.5773	0.2975	0.0813
r	-0.0799	0.8586	0.7598	0.5454	0.2852

P_2O_5 (wt%) association with HREE (ppm)					
Coefficient	Ho	Er	Tm	Yb	Lu
R^2	0.0019	0.0058	0.0232	0.0334	0.0521
r	0.0440	-0.0764	-0.1524	-0.1827	-0.2282

Cr_2O_3 (wt%) association with trace elements (ppm)													
Coefficient	Li	P	Ti	V	Cr	Co	Ni	Cu	Zn	Ga	Rb	Sr	Zr
R^2	0.2944	0.0041	0.7163	0.8551	0.6953	0.3291	0.5637	0.3305	0.6483	0.7146	0.2431	0.0070	0.6315
r	-0.5426	0.0640	0.8463	0.9247	0.8338	0.5737	0.7508	0.5749	0.8052	0.8454	0.4930	0.0839	0.7947
Coefficient	Nb	Sn	Sb	Cs	Ba	Hf	Ta	W	Tl	Pb	Th	U	
R^2	0.2271	0.3501	0.2130	0.1998	0.0613	0.6207	0.0688	0.0546	0.0059	0.1420	0.0652	0.5209	
r	0.4766	0.5917	0.4616	0.4470	0.2476	0.7879	0.2624	-0.2337	0.0771	-0.3769	0.2554	0.7217	

Cr_2O_3 (wt%) association with LREE +Sc (ppm)						
Coefficient	Sc	La	Ce	Pr	Nd	Sm
R^2	0.5680	0.0524	0.0357	0.0320	0.0385	0.0728
r	0.7537	0.2290	0.1888	0.1789	0.1963	0.2699

Cr_2O_3 (wt%) association with MREE+Y (ppm)					
Coefficient	Y	Eu	Gd	Tb	Dy
R^2	0.5127	0.1473	0.1829	0.3368	0.4848
r	0.7160	0.3838	0.4277	0.5804	0.6962

Cr_2O_3 (wt%) association with HREE (ppm)					
Coefficient	Ho	Er	Tm	Yb	Lu
R^2	0.5280	0.5484	0.5132	0.5117	0.5029
r	0.7266	0.7406	0.7164	0.7153	0.7092

NiO (wt%) association with trace elements (ppm)													
Coefficient	Li	P	Ti	V	Cr	Co	Ni	Cu	Zn	Ga	Rb	Sr	Zr
R^2	0.1462	0.0977	0.2327	0.0616	0.0001	0.0143	0.6037	0.0003	0.5128	0.0021	0.0443	0.0568	0.0039
r	-0.3824	-0.3125	0.4824	0.2482	0.0113	0.1196	0.7770	0.0184	0.7161	0.0456	-0.2106	-0.2383	0.0623

Coefficient	Nb	Sn	Sb	Cs	Ba	Hf	Ta	W	Tl	Pb	Th	U
R^2	0.0007	0.0600	0.0677	0.0752	0.0124	0.0010	0.0001	0.0034	0.3265	0.1602	0.0997	0.0126
r	-0.0257	-0.2449	-0.2603	-0.2743	-0.1112	0.0323	0.0094	0.0586	-0.5714	-0.4002	-0.3157	-0.1123

NiO (wt%) association with LREE +Sc (ppm)						
Coefficient	Sc	La	Ce	Pr	Nd	Sm
R^2	0.0016	0.2050	0.1610	0.1520	0.1436	0.1248
r	-0.0404	-0.4528	-0.4012	-0.3898	-0.3790	-0.3532

NiO (wt%) association with MREE+Y (ppm)					
Coefficient	Y	Eu	Gd	Tb	Dy
R^2	0.0048	0.1005	0.1317	0.0912	0.0309
r	-0.0690	-0.3170	-0.3629	-0.3020	-0.1758

NiO (wt%) association with HREE (ppm)					
Coefficient	Ho	Er	Tm	Yb	Lu
R^2	0.008	0.001	0.001	0.000	0.000
r	-0.091	-0.027	-0.034	-0.012	0.013

Appendice L. Total sulphur association with oxides, trace elements and REY+Sc.

Total sulphur association with oxides, trace elements and REY+Sc

Total sulphur association with major oxides (wt%)

Coefficient	SiO_2	Al_2O_3	Fe_2O_3	MnO	MgO	CaO	Na_2O	K_2O	TiO_2	P_2O_5	Cr_2O_3	NiO
R	0,2	0,3	0,1	0,7	0,4	0,3	0,5	0,0	0,1	0,0	0,0	0,2
r	0,4909	-0,5727	-0,3164	0,8159	-0,6496	0,5004	0,6895	-0,1997	-0,2693	0,0864	0,1254	0,4890

Total sulphur association with trace elements

Coefficient	Li	P	Ti	V	Cr	Co	Ni	Cu	Zn	Ga	Rb	Sr	Zr
R	0,2	0,1	0,0	0,6	0,9	0,2	0,0	0,0	0,0	0,2	0,5	0,1	0,0
r	-0,480	0,285	0,005	0,779	0,957	0,447	0,121	0,137	0,221	0,500	0,738	0,281	-0,209

Coefficient	Nb	Sn	Sb	Cs	Ba	Hf	Ta	W	Tl	Pb	Th	U
R	0,6	0,4	0,6	0,1	0,6	0,0	0,2	0,6	0,0	0,2	0,0	0,6
r	0,7765	0,6163	0,7633	0,2943	0,7739	-0,0885	0,4429	0,7883	-0,0620	0,4515	-0,1838	0,7854

Total sulphur association with LREE +Sc (ppm)

Coefficient	Sc	La	Ce	Pr	Nd	Sm
R	0,0	0,1	1,0	1,0	1,0	1,0
r	-0,0220	0,3021	0,9905	0,9995	0,9994	0,9925

Total sulphur association with MREE+Y (ppm)

Coefficient	Y	Eu	Gd	Tb	Dy
R	0,0	0,2	1,0	0,9	0,9
r	-0,0735	0,4086	0,9829	0,9528	0,9530

Total sulphur association with HREE (ppm)

Coefficient	Ho	Er	Tm	Yb	Lu
R	0,0	1,0	1,0	1,0	1,0
r	-0,1399	0,9914	0,9958	0,9990	0,9987

Total sulphur association with vitrinite (mmf)	
Coefficient	
R	0,6
r	0,7998